Evaluation of Shear Tab Connections as Supplemental Energy Dissipators

by

Hongyang Wu

A dissertation submitted to the Graduate Faculty of
Auburn University
in partial fulfillment of the
requirements for the Degree of
Doctor of Philosophy

Auburn, Alabama
Dec 10, 2022

Keywords: shear tab connection, bottom flange friction device (BFFD),
nonlinear analysis, earthquake engineering

Approved by

Justin D. Marshall, Committee Chair, Associate Professor of Civil and Environmental Engineering
Andrzej S. Nowak, Professor and Chair of Civil and Environmental Engineering
Robert W. Barnes, Associate Professor of Civil and Environmental Engineering
James S. Davidson, Professor of Civil Engineering
Nedret Billor, Professor of Mathematics and Statistics

Abstract

As structural engineering practice moves from life-safety to functional recovery after a significant seismic event, taking advantage of structural components to enhance the energy dissipation of a structure will be important. Based on current design criteria, lateral loads are resisted only by the lateral force resisting system. The energy generated by seismic events is designed to be dissipated through plastic deformation in specific ductile components to meet life-safety requirements. Shear tab connections designed as part of gravity load system are assumed as pinned and ignored as contributors to the lateral load resisting system. However, previous research shows that the shear tab connections in the gravity load system can carry moment and dissipate energy as rotation occurs at the end of beam. Including the shear tab connections in the model improves the performance of structure in the seismic analysis as supplemental dissipators. Two modifications to the shear tab connections, adding a Bottom Flange Friction Device (BFFD) and increasing the connection depth (wider bolt spacing), were proposed to improve the performance of shear tab connections. Both modifications provide larger moment strength and stiffness of connection and dissipate more energy.

This dissertation is divided into three phases (manuscripts). The first phase of the research project is to experimentally evaluate the shear tab connection with different configurations. The second phase of the research project is to evaluate the shear tab connection with different configurations numerically at the component level. A simplified method of modelling the shear tab connection was proposed for use in numerical building models. The third project phase is to investigate the impact of shear tab connections on the seismic response of steel structures.

The findings of the work presented in this dissertation are expected to be useful for performance-based design and seismic analysis of steel structures.

Acknowledgment

This is the ninth year for me at Auburn university. I still remember myself as an ambitious and aspiring young man with big smiles when I first stepped into Auburn (Figure 0). I was curious about everything here. Nine years passed and here comes the graduation. Now, I'm 31 years old. My view of Auburn University is still the same, but my mindset and understanding have significantly changed. Like the other Ph.D. students (I guess), I experienced ups and downs in my research and my mindset. I even thought about giving up multiple times last year when I had some bad health issues. However, when I am writing the acknowledgment now, these negative feelings seem to have disappeared completely. During my graduate studies at Auburn, I have slowly learned how to become a good researcher and understand how to compromise with myself. This personal growth cannot happen without my advisor Dr. Marshall and other colleagues and friends.

I would like to thank my advisor Dr. Marshall for his help in my courses and research throughout my nine years at Auburn University. I really appreciate his vast knowledge, guidance and assistance in writing this dissertation. I really would like to thank him for giving me the unique opportunity to pursue a Ph.D. degree as his last student at Auburn University. I would like to thank him for keeping in touch with via zoom every week for the last whole year even though he has already become the CEO of a company. His patience and passion have encouraged me greatly.

I would like to thank the rest of my committee, Dr. Nowak, Dr. Davidson, and Dr. Barnes for all the help they have provided. I would like to give a special thanks to Dr. Billor, who gave me a lot of statistical knowledge which was used in this dissertation as well.

I also would like to thank my parents for their support and understanding in my entire life. Even though they don't want me to be too far away from them, they still respect all my choices and decisions.

I also appreciate my friends for their friendship and help, especially Aravind Tankasala, Victor Aguilar and Connor Halbrooks, who helped me a lot in my life at Auburn.

I would also thank my officemates and all the other fellow graduate students and faculty members. They have offered me a great experience at Auburn University, which I will never forget.

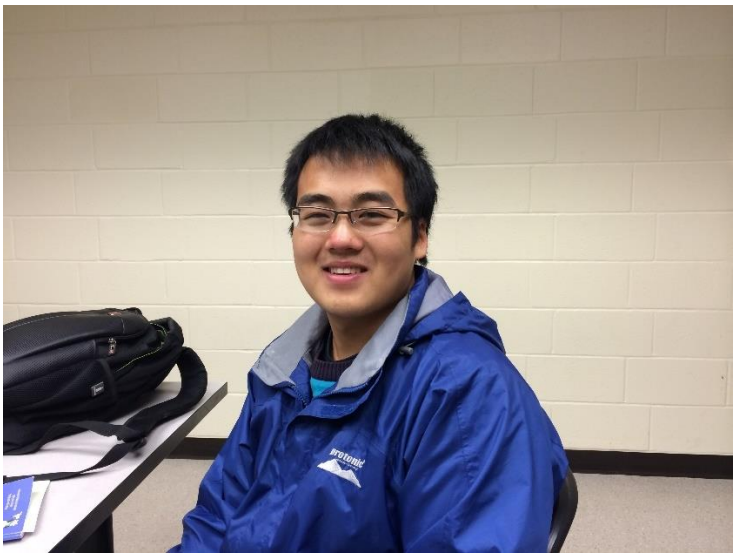

Figure 0: First Photo in Auburn University taken by Aravind Tankasala

Table of Contents

List of Tables

List of Figures

Chapter 1 Introduction

1.1 Motivation for the Research

In structural steel design, the lateral load-resisting system and gravity load system are normally designed independently. The lateral load-resisting system is controlled by lateral force demands while gravity load frames are controlled by gravity demands. Well-detailed and designed structural steel frames are generally considered to have very good ductility and hence are able to meet and exceed the life safety demands specified by current building codes for seismic events. Gravity load frames are typically not included in the lateral load design and subsequent performance assessment. The reason the gravity systems are typically neglected in the lateral load design and assessment is the difficulty of modelling the beam-to-column connection and lack of information regarding the expected behavior of connections (Flores, Charney, & Lopez-Garcia, 2016). Simple shear tab connections are widely used in the gravity load system in steel structures. Experimental tests on simple shear connections with and without the concrete slab conducted by Liu and Astaneh (2000) show that energy can be dissipated by the simple shear tab connection. The primary objective of this research effort is to identify ways in which the analytical performance of structural steel frames could be improved by including the effects of energy dissipation from the gravity system. In addition, enhancing the energy dissipation of these connections could provide significant performance improvement for seismic and wind events for steel structures. Several modifications of the shear tabs are considered to increase the positive effect of the gravity system on dynamic response. These modifications include adding a Bottom Flange Friction Device (BFFD) and increasing the bolt spacing on the shear tab. Both these methods increase the connection slip moment and energy dissipation capacity. Neither of these modifications have been previously assessed analytically or experimentally.

1.2 Scope of Work

The overall research objective is to improve the energy dissipation capacity of steel frames by supplementing the lateral system with the gravity system. The energy dissipation from the gravity system can be activated in small and moderate earthquakes which would result in energy dissipation without damage to the structure. Enhancing energy dissipation would serve to decrease demands on the structure and improve performance of steel structures in small, moderate and severe earthquakes as well as significant wind events.

This dissertation is divided into three phases (manuscripts). The first phase of the research project is to experimentally evaluate the shear tab connection with different configurations. It is the first stage of this effort and includes the experimental testing needed to assess the hysteretic response of shear tab connections and shear tab connections with the proposed modifications. The second phase of the research project is to evaluate the shear tab connection with different configurations numerically at the component level. It continues the research effort by utilizing the experimental test results in rigorous numerical models that investigate the important parameters of baseline shear tab models as well as shear tabs with a BFFD and with wider bolt spacing. A simplified method of modelling the shear tab connection was proposed to be used in numerical building models. The third research phase is to investigate the impact of shear tab connections on the seismic response of steel structures. Shear tab connections were included in numerical building models to investigate the overall influence of shear tab connections and the proposed modifications on the response of steel structures.

1.3 Organization of Dissertation

Chapter 1 is the introduction to define the problem in this dissertation. The motivation of the research and scope of the work are also discussed in this chapter.

Chapter 2 provides the literature review on shear tab connections and friction devices used in beam-column joints.

Chapter 3 describes the first phase of this research project which is titled “Experimental Evaluation of a Shear Tab Connection with a Bottom Flange Friction Device”.

Chapter 4 describes the second phase of this research project which is “Numerical Evaluation of Strength and Energy Dissipation of Modified Shear Tab”.

Chapter 5 describes the third phase of this research project which is “Impact of Shear Tab connection on the Seismic Response of Steel Structures”.

Chapter 6 is the conclusion of this dissertation. This chapter will summarize the entire research project and present the important outcomes and conclusions.

Chapter 2 Literature Review

Steel structures typically contain both of gravity load and lateral load resisting system which are designed separately. The lateral load resisting system is designed to resist the effects of wind and seismic loads as well as providing stability to the gravity system. The gravity load system is designed to carry the dead and live loads with beams and columns and a concrete filled steel deck. Therefore, in structural analysis, the gravity load system is often idealized as pinned connections with negligible participation in the resistance of lateral loads. However, based on previous research, the gravity load system can also provide considerable lateral stiffness and dissipate energy through the continuous column effect and the rotational resistance of simple connections. In structural steel design, certain levels of damage happen in lateral resisting system under significant earthquakes. This damage as well as the other energy dissipation mechanisms make sure structures that meet life safety criteria during earthquakes. However, this damage might result in permanent (residual) displacement in the system even after a small earthquake. Detecting and repairing damage can be difficult and expensive. Friction damping, provided by devices like the slotted bolted friction damper, is an effective source of energy dissipation in structures. The behavior of shear tab connections and the use of slotted bolted friction dampers or friction energy dissipation are key elements of the low slip force connection concept. These low slip force connections present a low damage solution in the early stage of earthquakes.

2.1 Shear Tab Connections

Shear Tab Connections (STC) are the most common connections for gravity load systems in steel frame structures in North America (Astaneh-Asl, Liu, & McMullin, 2002). Although these connections are not designed for resisting seismic load, they are frequently used in steel frame structures in seismic zones. This type of connection consists of a steel shear tab which is fillet

welded to a column or girder and bolted to the web of a beam or girder. Unlike the design of connections in moment frame which moment capacity will dominate the design, the design of shear tab connections are dominated by the shear strength to support the beams as well as ensure the occurrence of ductile failure modes before the fracture of welds and bolts (Astaneh-Asl, Liu, & McMullin, 2002). Several examples of STCs are shown in Figure 2-1.

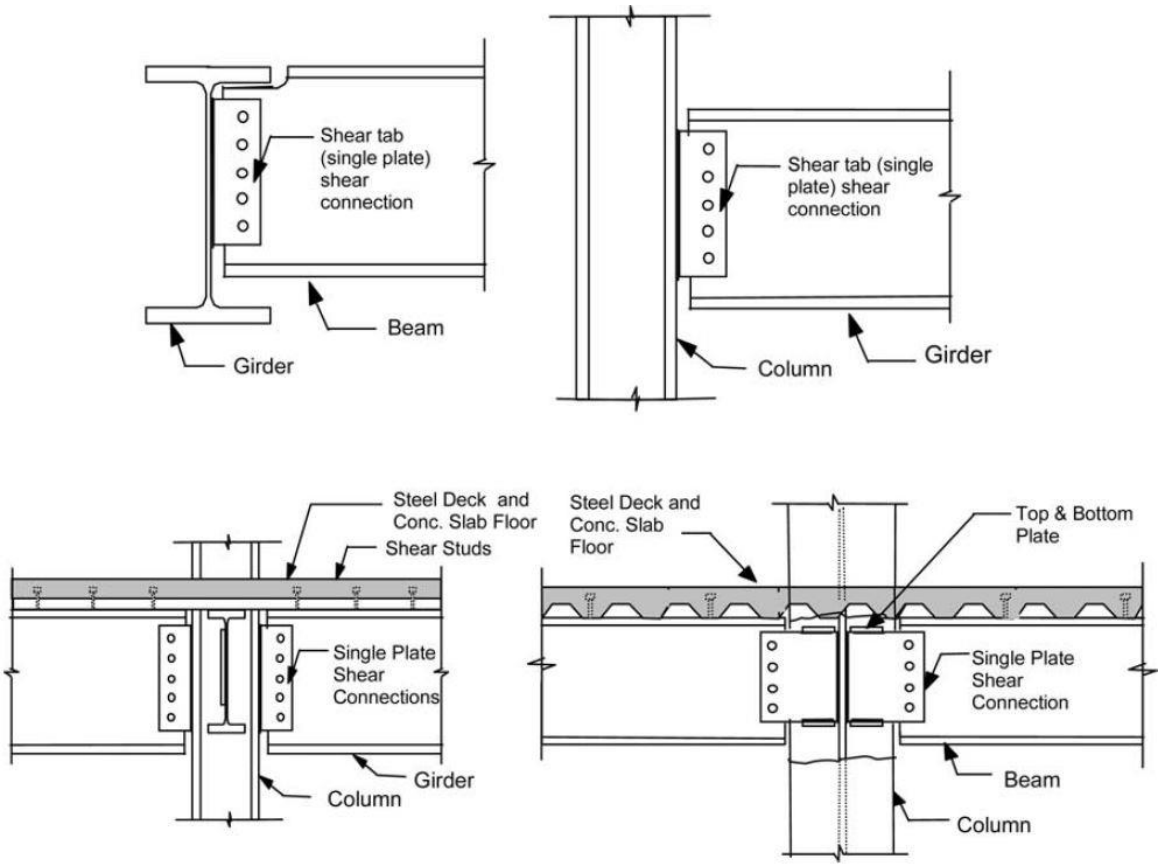

Figure 2-1. Single Plate Shear Tab Connections (Astaneh-Asl, Liu, & McMullin, 2002)

In steel frame structures, beams in the gravity load system are designed (idealized) as simply supported with STCs which can be modeled with moment releases at both ends (Crocker & Chambers, 2004). In addition, the shear connections must allow the beams to reach their rotational demands with little resistance (Astaneh-Asl, Liu, & McMullin, 2002) which means shear tab connections typically are not considered in the lateral load resisting system.

During an earthquake, lateral displacement occurs in both gravity load frames and lateral resisting frames. The rotational demand on the shear tab connections due to lateral load is much larger than that due to shear force which is created by gravity load which means the response of shear tab connection will be different during a seismic event as compared with a gravity load only situation. If there is only gravity load on the structure, the moment generated at the connection is a result of a rather small eccentricity relatively to the bolt line. Based on previous research, if the shear force is far away from the bolt line, which means the distance between shear force and bolt line is larger than the height of bolt line, the relationship between rotation and moment is insensitive to connection shear (Richard R. G., 1980). The connection plate is experiencing the rigid body plate rotation under cyclic load. Therefore, predicting the behavior of these shear tab connections is important in predicting the structure seismic performance (Crocker & Chambers, 2004).

In structural design, the assumption of beam-to-column connections are typically considered as rigid or pinned. Rigid connections provide full restraint and do not allow any relative rotational movement while pinned connections provide zero restraint and are able to rotate freely. However, these assumptions are not consistent with standard construction due to the actual conditions. According to previous research, both the shear tab connections without slab and shear tab connections combined with slab system (Liu & Astaneh-Asl, 2000) have been shown to have significant rotational stiffness and resistance to lateral load.

For shear tab connections without a slab, yield lines began to appear at the top and bottom bolts of the shear tabs during loading followed by slip between the shear tab and the beam webs, bolt hole deformation and other mechanisms leading to connection failure (Liu & Astaneh-Asl, 2000). Typically, the first of these mechanisms is yielding of the shear tab followed by bearing of

the bolt holes and out-of-plane warping of the plate and beam web. Limit states observed in STCs include yielding of the shear tab, fracture of the net section of shear tab, bearing failure of the bolt holes, bolt fracture, and fracture of the weld. Figure 2-2 shows the progression of slip, yielding, and fracture of a shear tab connection.

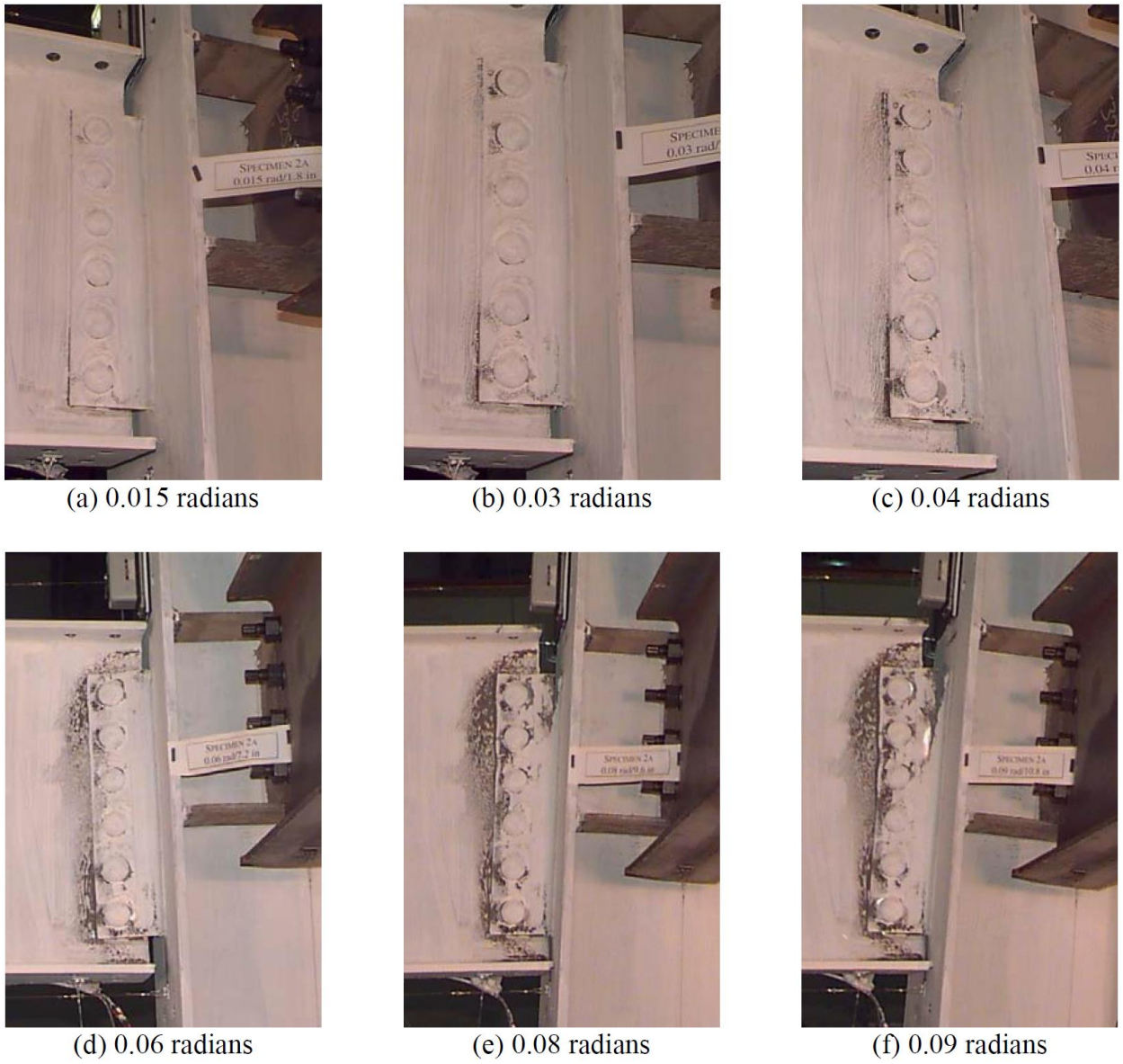

(a) 0.015 radians (b) 0.03 radians (c) 0.04 radians

(d) 0.06 radians (e) 0.08 radians (f) 0.09 radians

Figure 2-2. STC Failure Progression (Liu & Astaneh-Asl, 2000)

For shear tab connection with a slab, the connection behavior in the cyclic tests is like the behavior of simple connections without slab. In general, it starts with slip followed by yielding in

the shear tab and beam web, deterioration of concrete slab, bolt deformation and other mechanisms leading to connection failure. The contribution of composite behavior of simple beam connection and slab is proved to be significant tests. In Liu & Astaneh_Asl's tests, it showed that the lateral resistance capability was literally doubled based on the connections which were tested. The slab also had the effect of limiting rotation, as expected, because of the restraint from the concrete floor. In detail, the shear tab connection with a slab were acting like semi-rigid connections rather than simple connections which means the moment capacity was significantly increased. However, after the concrete of slab crushed, the connection began to behave like a bare shear tab connection.

The maximum moment capacity of shear tab connection is related with the connection's neutral axis location. For shear tab connections without a slab, when the beam flange bears on the column at large rotations, the neutral axis moves close to this point of contact (Crocker & Chambers, 2004). Figure 2-3 shows a shear tab connection with the bottom flange of the beam bearing against the column. Similarly, by adding a concrete floor system on the bare shear tab connection can also move neutral axis.

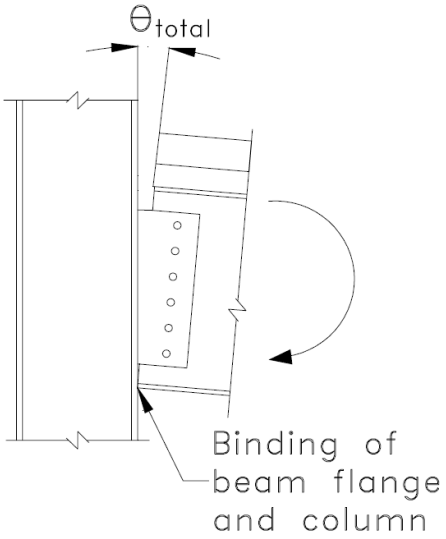

Figure 2-3. STC Rotation (Liu & Astaneh-Asl, 2000)

This stiffness increases shear tab connections, especially the beam flange contacting the column flange, will cause yielding in column panel zones and lead to fracture of the shear tab (Liu & Astaneh-Asl, 2000). Some shear tab connections are designed with angle plates fixing the bottom of the beams to the columns which can be considered as semi-rigid connection. These types of shear tab connection have significantly higher moment capacity as well as rotational stiffness which also put a high demand on the column which can induce yielding in column panel zones, followed by yielding and fracture of angle plates and shear tab plates (Liu & Astaneh-Asl, 2000). Fig 2-4 shows a failed of shear tab connection with a seat angle plate.

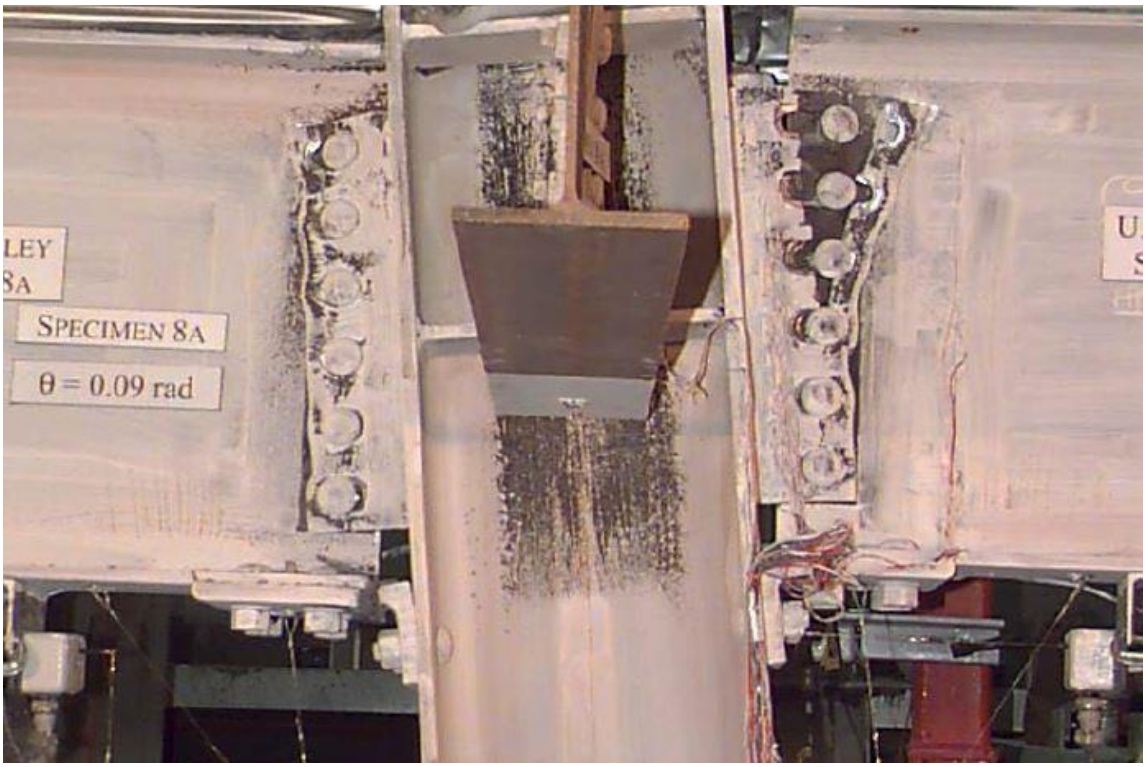

Figure 2-4. STC with Seat Angle Failure (Liu & Astaneh-Asl, 2000)

Extensive laboratory testing of simple shear tab connections was also performed at the University of California at Berkley as part of Subtask 7.04 of Phase II of the SAC Steel Project. The testing was performed to determine if shear tab connections in the gravity frame could provide

decent lateral resistance. A variety of shear tab connections were put into cyclic tests with simulated gravity load (Liu & Astaneh-Asl, 2000).

A typical shear tab moment rotation model was developed from Liu & Astaneh-Asl's research as well. Figure 2-5 shows the general behavior of the model presented in the SAC Steel Project Report.

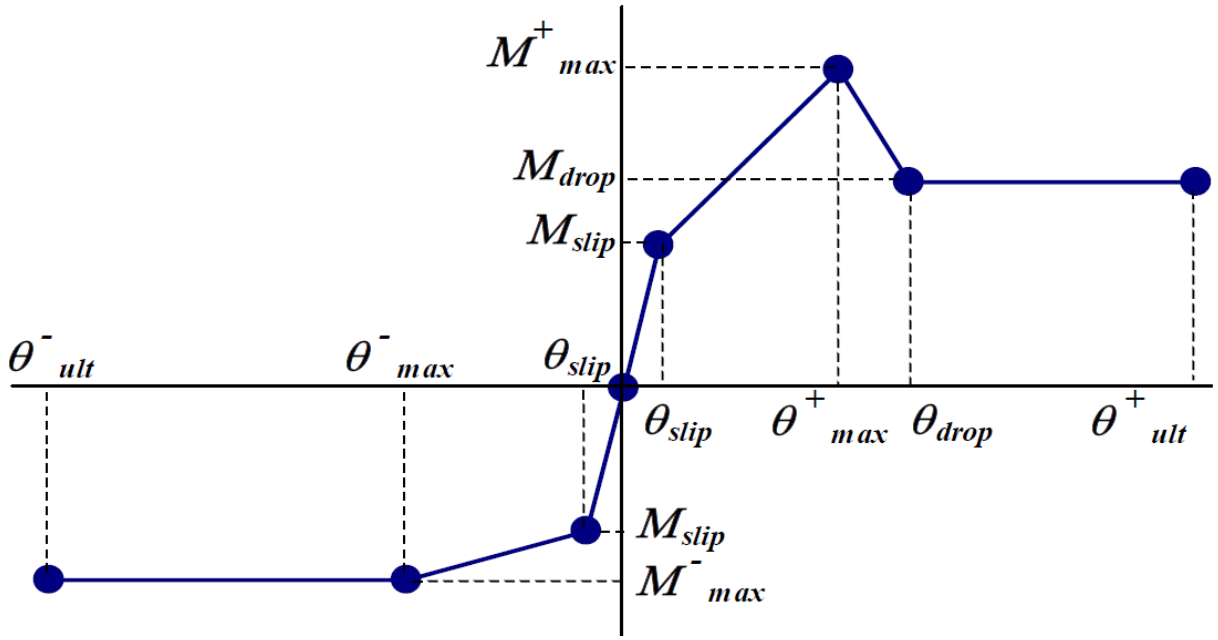

Figure 2-5. STC Moment-Rotation Model (Liu & Astaneh-Asl, 2000)

The initial stiffness of the connection is established by determining the moment and rotation required to overcome the static friction restraining the connection (Liu & Astaneh-Asl, 2000). This friction is caused by the bolt tension, and the moment required to overcome it is referred to as the "slip moment" (M_{slip}). Calculated estimates of the slip moment begin with identifying the frictional force of one bolt. This assumes the minimum bolt tension defined and the coefficient of static friction for a class A faying surface. An estimate of the slip moment (M^*_{slip}) is then calculated from the resultant force couple needed to overcome the static friction of each bolt. Figure 2-6 shows the assumed force distribution on shear tab connections without and with a slab system. The SAC experiments found that underestimates and overestimates of slip moments happened consistently

on the shear tab bare connection and shear tab connection with a slab, respectively. Therefore, two adjustment factors which were 1.5 and 1.67 were developed and with them an accurate estimate of the slip moment can be made (Liu & Astaneh-Asl, 2000). In addition, the corresponding slip rotation is determined empirically from the SAC experiments which is 0.0044 rad.

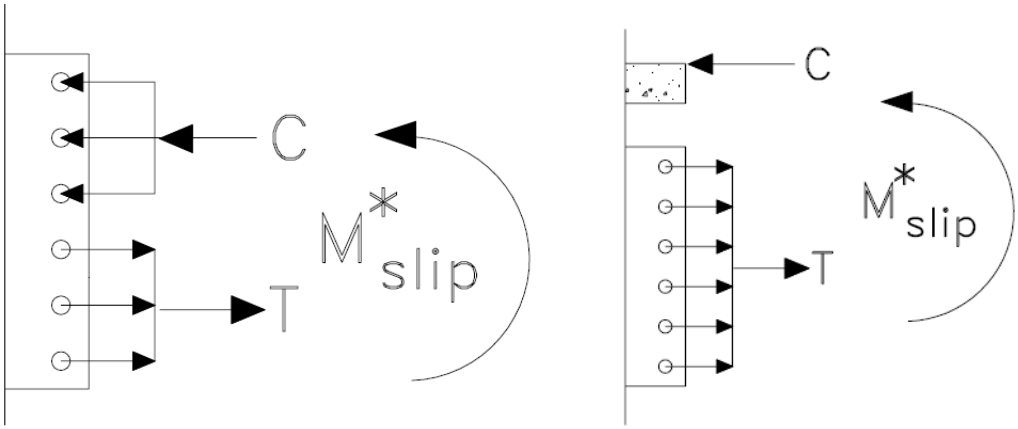

Figure 2-6. Force Distribution on STC without and with Slab (Liu & Astaneh-Asl, 2000)

Once the shear tab connection slips, the stiffness of shear tab connection decreases. The reduced resistance of subsequent cycles comes from kinetic friction in the connection. Therefore, it may be more accurate to use the secant stiffness model (Liu & Astaneh-Asl, 2000). The secant stiffness model neglects the initial stiffness based on the initial slip behavior. The secant stiffness is established by the maximum positive and negative moment capacity and corresponding rotation. This secant stiffness is roughly 15% of the initial stiffness for bare shear tab connections and roughly 50% of the initial stiffness for shear tab connections with a slab system (Liu & Astaneh-Asl, 2000). Figure 2-7 outlines the behavior of a shear tab connection showing the secant stiffness for positive moment. Though not depicted, the secant stiffness would also apply to the negative moment-rotation relationship.

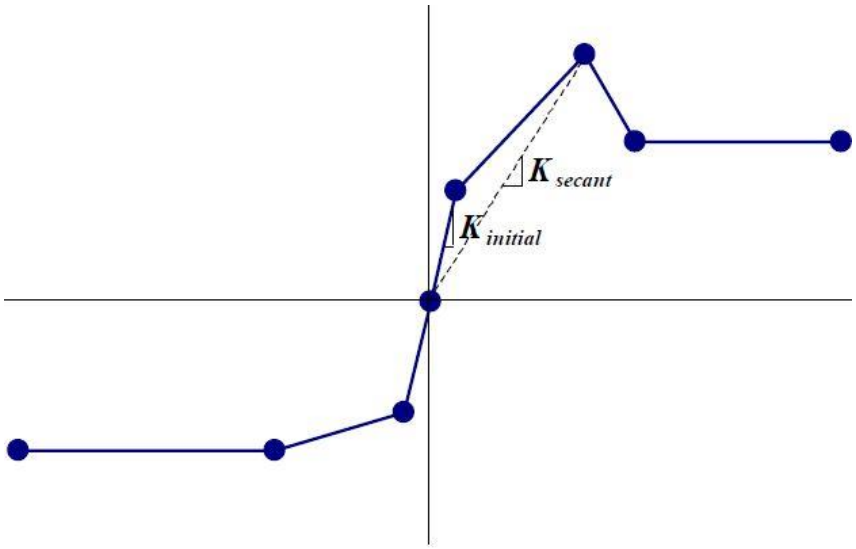

Figure 2-7. STC Secant Stiffness (Liu & Astaneh-Asl, 2000)

Design equations for calculating the maximum moment capacity of shear tab connection have been developed and verified through cyclic testing as part of the SAC Steel Project. The rotation at which the maximum capacity first occurs is defined empirically. The ultimate rotation (θ_{ult}) is defined as the rotation at which the beam flange bears against the column. This is purely a function of the connection geometry.

The drop in the positive moment-rotation relationship of Figure 2-6 signifies the failure of the concrete slab. The rotation at which the slab is no longer effective (θ_{drop}) is an empirical value. The slab only participates when bending of the connection puts the concrete in compression. Thus, the negative portion of the STC moment-ration curve has no drop in capacity. The positive moment-rotation relationship mirrors this portion of the curve for bare shear tab connections and shear tab connections with composite slabs following the failure of the concrete. The shear tab connection moment-rotation models are a basis for incorporating simple connections in structures subjected to lateral loadings (Liu & Astaneh-Asl, 2000).

A more complicated finite element model was established by Rou Wen et al. (2013). The finite element simulation provides more information related with shear tab connection with and

without slab in the micro level including stress distribution in the shear tab connection zone, change of the neutral axis along the beam sections and the distribution of normal stress along the shear tab connection. Figure 2-8 shows the 3D Global view and local view close to shear tab connection.

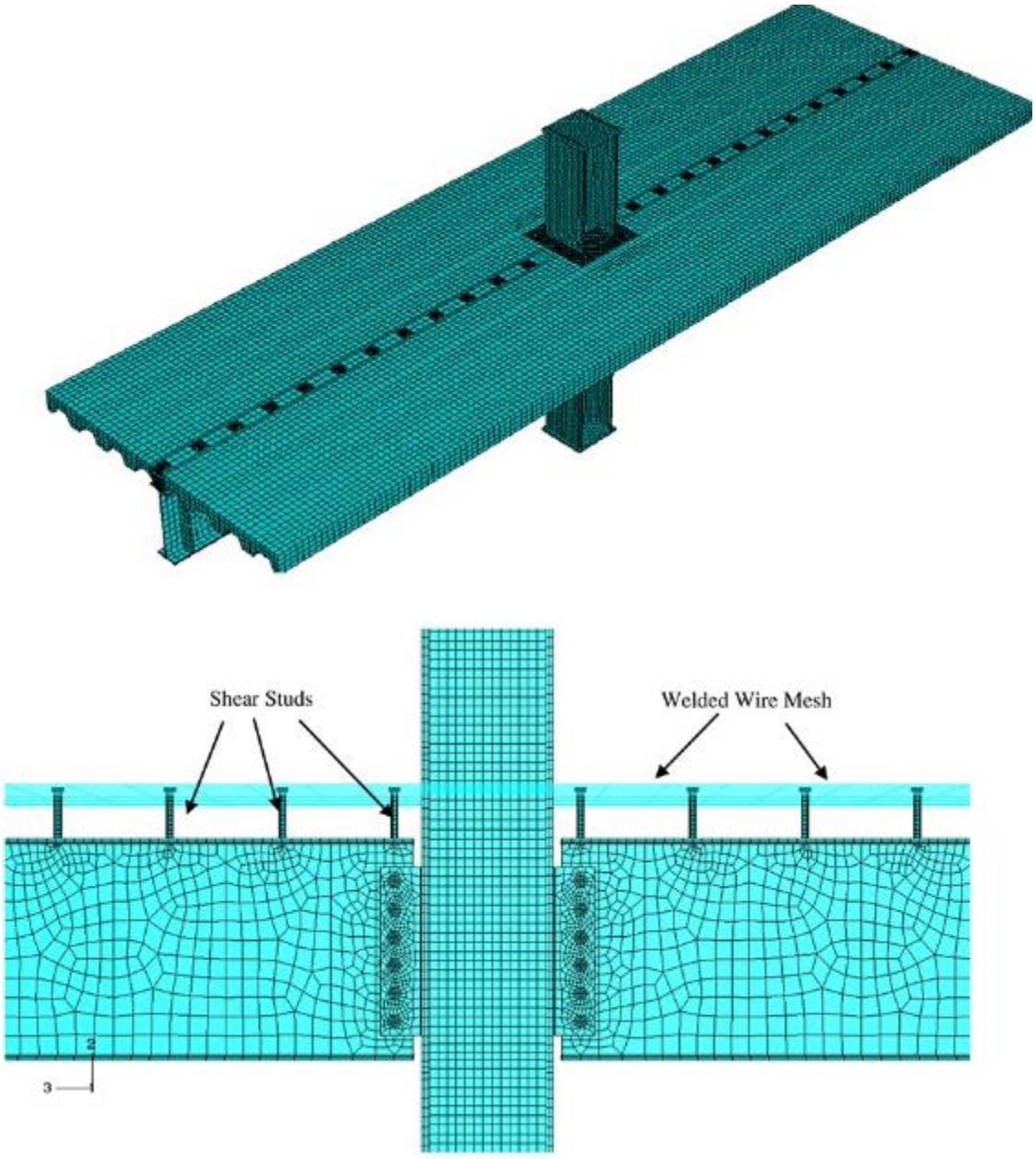

Figure 2-8. 3D Global and Local View of Finite Element Model of STC (Wen, Akbas, Sutchiewcharn, & Shen, 2013)

These finite element simulations found that for shear tab connection with a slab system, Liu & Astaneh-Asl's moment-rotation model of shear tab connection performs well while significant differences happened between the results of Astaneh-Asl's model and finite element model. The Astaneh-Asl model is underestimating moment capacity and rotation limitation for the shear tab connection with a floor system. Figure 2-9 and 2-10 shows the comparsion of results between experiment and numerical simulation on shear tab connection without slab and shear tab connection with slab, respectively.

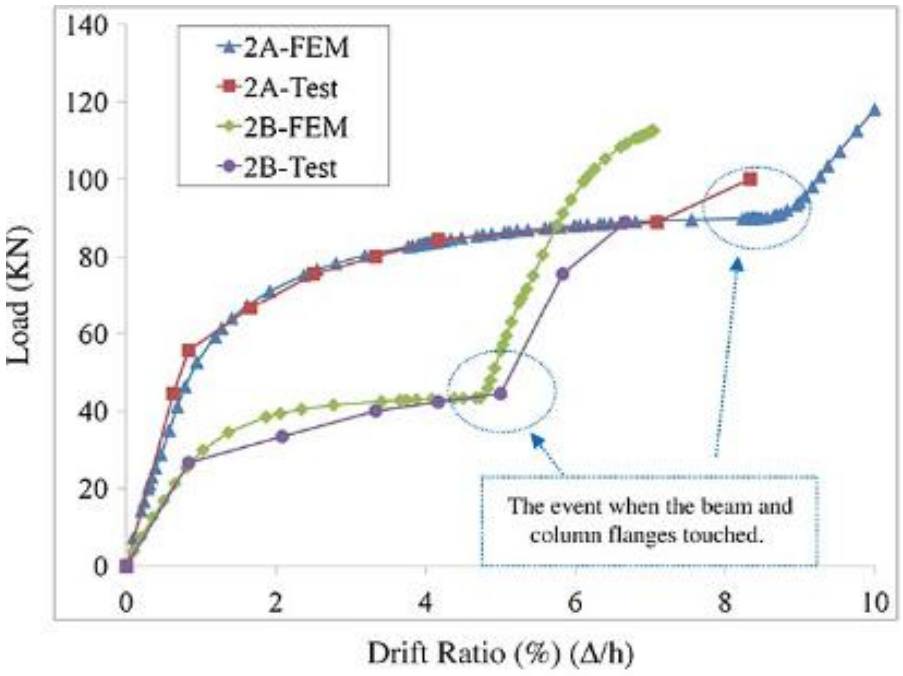

Figure 2-9. Comparison of Result between Experiment and Finite Element Simulation on Bare STC (Wen, Akbas, Sutchiewcharn, & Shen, 2013)

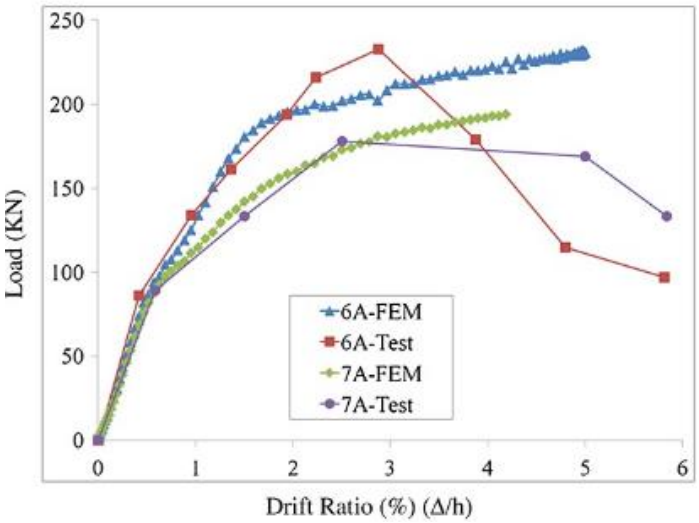

Figure 2-10. Comparison of Result between Experiment and Finite Element Simulation on STC with Slab System (Wen, Akbas, Sutchiewcharn, & Shen, 2013)

Another finite element model verified by experiment results (Rahman A. , Mahamid, Amro, & Ghorbanpoor, 2010) using and unstiffened extended shear tab connection, the shear tab was welded on the column web (weak axis), was accomplished by Abou-zidan & Liu (2015). Figure 2-11 shows the extended shear tab connection meshing in this finite element simulation.

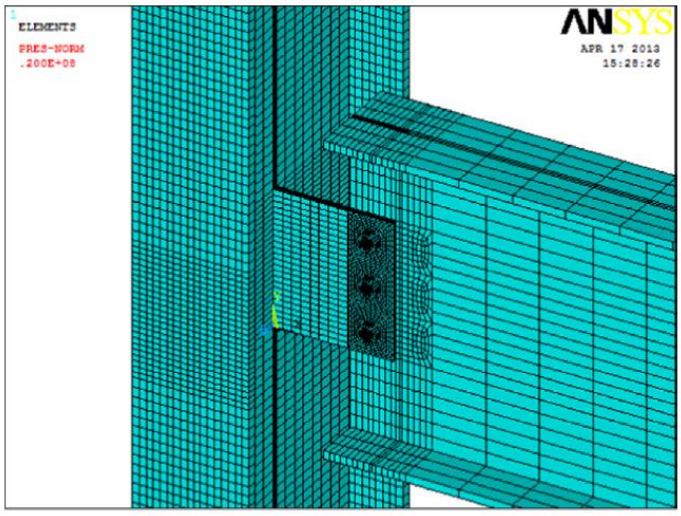

Figure 2-11. Extended STC Meshing (Abou-zidan & Liu, 2015)

A parametric study was conducted based on the finite element model which shows that the extended shear tab connection can also dissipate energy during the tests. Figure 2-12 shows the comparison of experimental and finite element shear versus beam end rotation response for all four connections: (a) 3-bolt shear tab connection; (b) 5-bolt shear tab connection; (c) 3-bolt extended shear tab connection and (d) 6-bolt extended shear tab connection (Abou-zidan & Liu, 2015).

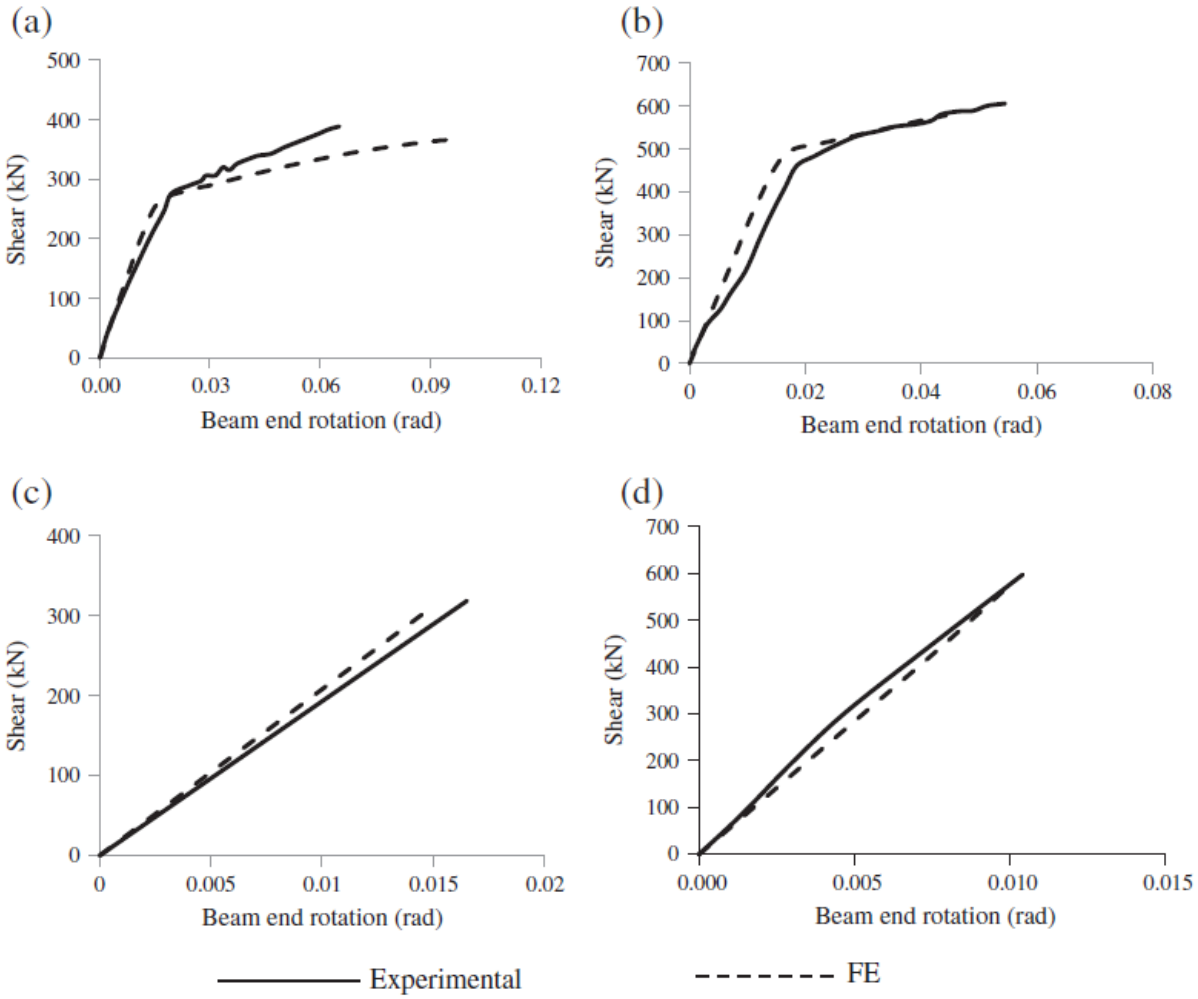

Figure 2-12. Comparsion of Result between Experiment and Numerical Simulation on Different STC (Abou-zidan & Liu, 2015)

More recent examples of shear tab connection studies have related to other types of demands. For example, the effect of column removal scenario on shear tab connection

(Daneshvar & Driver, 2017) and effect of thermal creep on shear tab connection due to fire (Jabotian & Hantouche, 2018). Therefore, considering the behavior of simple shear tab connections on system behavior is important in structural design and analysis.

2.2 Slotted Bolted Friction Dampers

The Slotted Bolted Friction Damper (SBFD) is a commonly used device for dissipating energy. The device is a simple and inexpensive design that can be installed in many arrangements throughout a structure. A typical configuration for a slotted bolted friction device is shown in Figure 2-13. Generally, these devices are composed of three steel plates separated by two "shims" of a selected friction material with high strength bolts clamping all five layers together. Spring washers maintain bolt tension during loading cycles. The center plate contains slotted holes allowing it to move relative to the rest of the device. Energy dissipation occurs as the slotted plate slides past the shims above and below it. A detailed depiction of an assembled SBFD is shown in Figure 2-14.

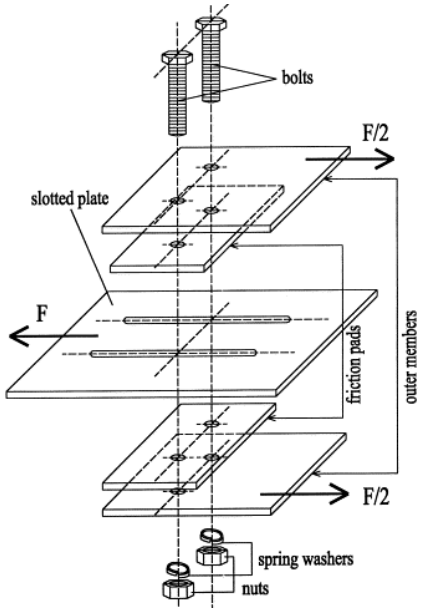

Figure 2-13. Typical SBFD Configuration (Balendra, Yu, & Lee, 2001)

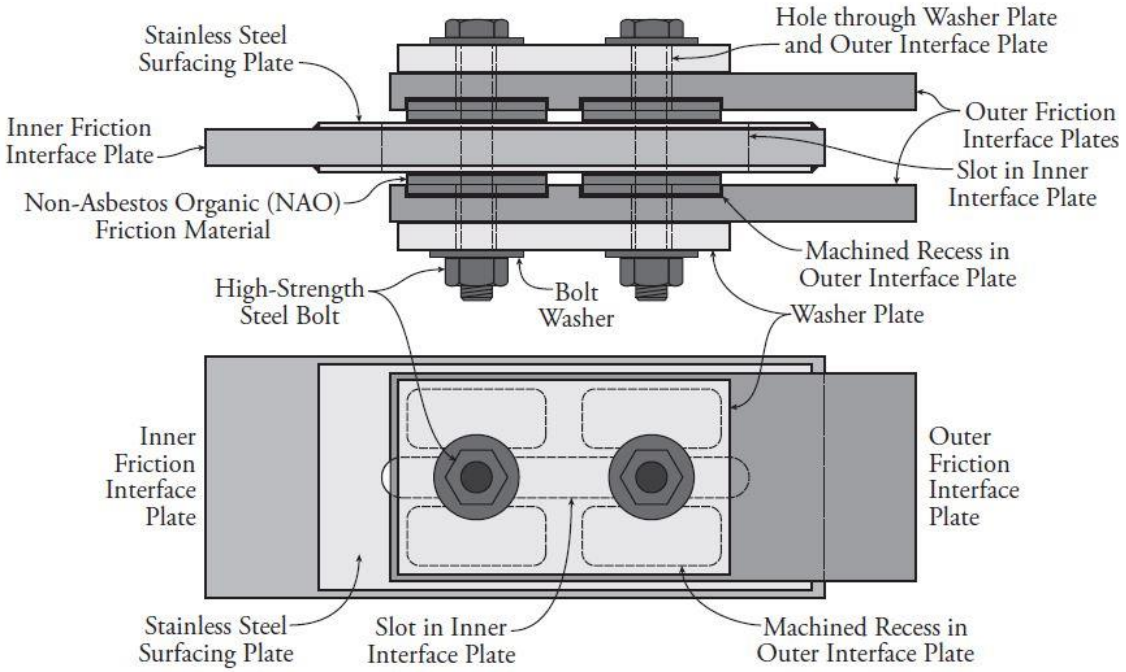

Figure 2-14. Slotted Bolted Friction Damper (Erochko, 2013)

Friction dampers resist motion as kinetic energy converts to thermal energy by the abrasion of one surface against another. Friction dampers behave according to the Coulomb friction model (Erochko, 2013). The Coulomb friction model is an empirical description of dry friction behavior (Bhavikatti & Rajashekarappa, 1998). It assumes that only a small portion of the friction surfaces are in atomically close contact thus the friction force is independent of the contact area. The model assumes the friction force is linearly proportional to the normal force compressing the surfaces together (Bhavikatti & Rajashekarappa, 1998). A coefficient of friction is an empirical multiplier that equates the normal force to the frictional force. A coefficient of friction is unique to the two contacting surfaces as well as the mode of friction. This classic model describes friction in two modes: static and dynamic. Static friction can occur when friction surfaces are stationary relative to one another. Dynamic friction occurs when friction surfaces are in relative motion. Friction is a

more complicated physical interaction, but the Coulomb model is a simple and adequately accurate approximation of friction damper behavior (Bhavikatti & Rajashekarappa, 1998).

The SBFD activates through axial deformation. A minimum of two bolts assures the device deforms in a straight line. As the device is loaded, there is an initial elastic stiffness (Golondrino, et al., 2013). The axial load on the device builds until the force exceeds the static friction and the surfaces begin to slide. The load at which this occurs is called the slip force. After the SBFD slips, there is a constant force of kinetic friction resisting deformation. This resistance is referred to as the sliding force. The SBFD behaves similarly under tensile or compressive loads. Figure 2-15 shows the SBFD sliding mechanics.

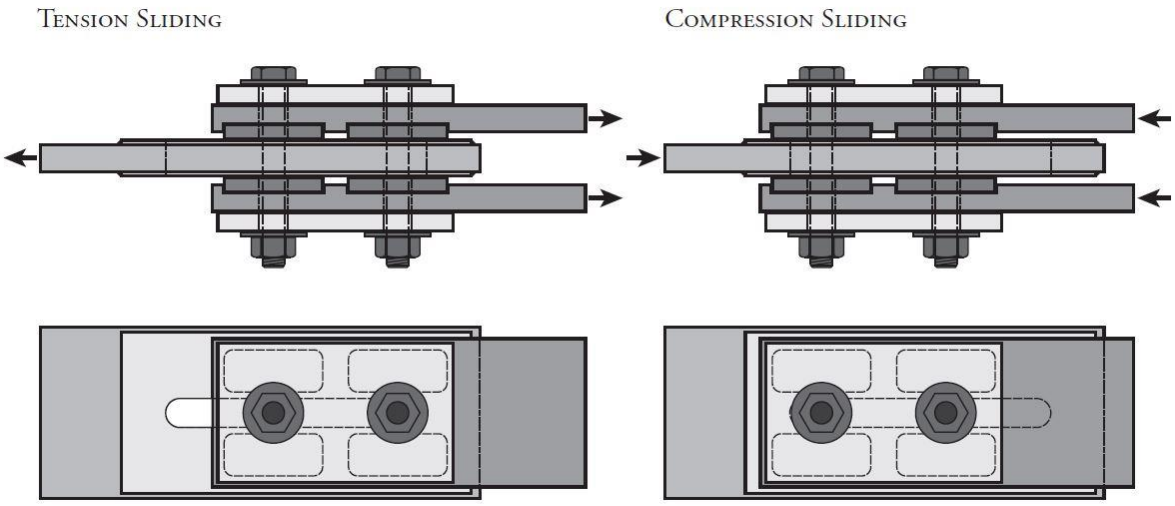

Figure 2-15. SBFD Mechanics (Erochko, 2013)

The friction force is a function of the normal force provided by the tension in the bolts and the friction coefficient for the sliding surfaces (Golondrino, et al., 2013). This relationship is described for a SBFD by Equation 2-1. In this equation, F_f represents the sliding force, μ_e is the effective coefficient of friction, n is the number of bolts, η is the number of friction planes, and T is the bolt tension. The sliding force is set by adjusting the bolt tension. The other variables generally remain reasonably constant (Golondrino, et al., 2013).

$$F_f = \mu_e * n * \eta * T \qquad \textbf{Equation 2-1}$$

Energy dissipates in moving the SBFD as a constant force is exerted through the sliding distance. The energy required to deform the device is shown in a plot of the applied force versus the resulting deformation. This plot is called a hysteresis. The area enclosed by the hysteresis loop represents the energy dissipated. This hysteretic behavior of SBFDs changes for different friction shim materials. Common materials used in SBFDs include aluminum, brass, mild steel, and Non-Asbestos Organic (NAO) friction composites (Golondrino, et al., 2013). Figure 2-16 shows the hysteresis of a SBFD with an NAO. Hysteresis of SBFDs using different metals as friction shims is shown in Figure 2-17. A friction device with a constant and repeatable slip force is desirable for design and reliable performance. These characteristics are evident in a stable hysteresis.

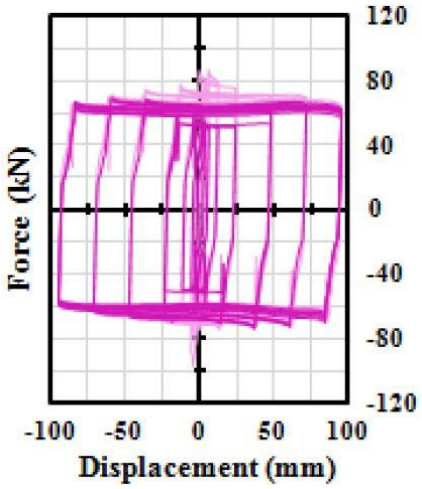

Figure 2-16. SBFD Hysteresis for NAO Friction Shims (Golondrino, et al., 2013)

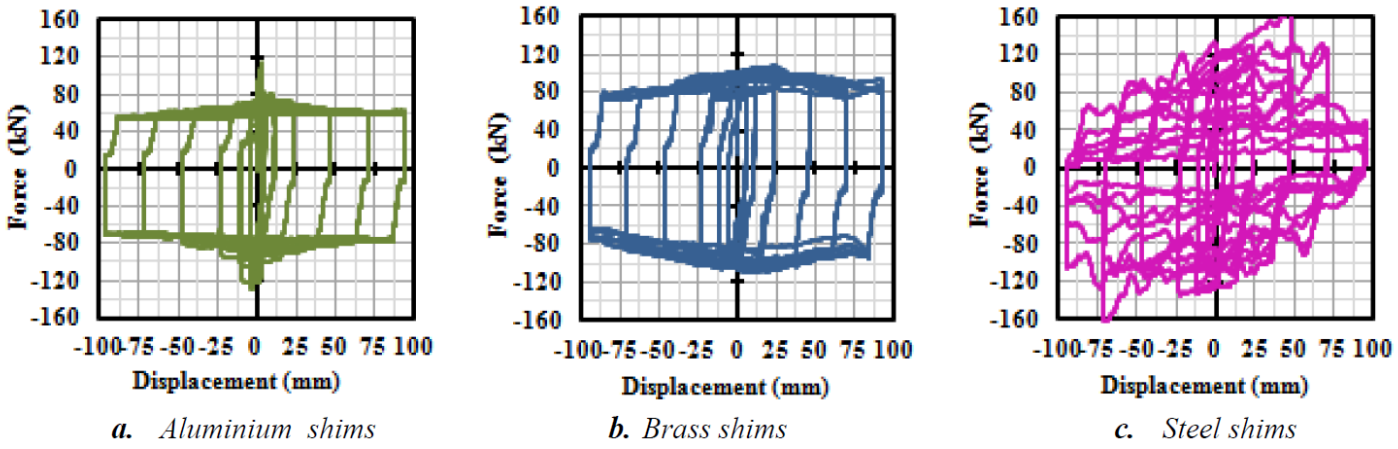

Figure 2-17. SBFD Hystereses for Different Metallic Shims (Golondrino, et al., 2012)

Certain metallic friction surfaces exhibit irregular hysteretic behavior like the mild steel to mild steel contact shown in Figure 2-17 (c). This is caused by particles that wear off one surface and interfere with the friction contact. These wear particles can have an adhesive effect, and their physical presence between the two sliding surfaces can create more physical damage. The adhesive effect of these particles creates a "stick-slip" behavior resulting in erratic spikes in the sliding force (Khoo, et al., 2012). An upper and lower bound design approach is recommended for the friction coefficient to deal with uncertainty in the slip force (Erochko, 2013).

SBFDs with brass and aluminum shims have moderately stable hysteresis, but still suffer some surface wear effects (Golondrino, et al., 2012). Ensuring a difference in hardness between the friction surfaces results in a more stable sliding performance and less wear. This allows the softer material to conform to the harder material and absorb wear particles (Khoo, et al., 2012). SBFDs with NAO composite shims provide a more stable hysteretic behavior than metallic friction surfaces (Golondrino, et al., 2013). This is visible when comparing the smooth hysteresis loops of a SBFD with NAO composite shims in Figure 2-16 to the sporadic hysteresis of SBFDs with metallic shims in Figure 2-17. The components of a SBFD with NAO composite shims can be seen

in Figure 2-18. The NAO material is bonded to machined recesses in the outer plates of the SBFD with epoxy (Erochko, 2013).

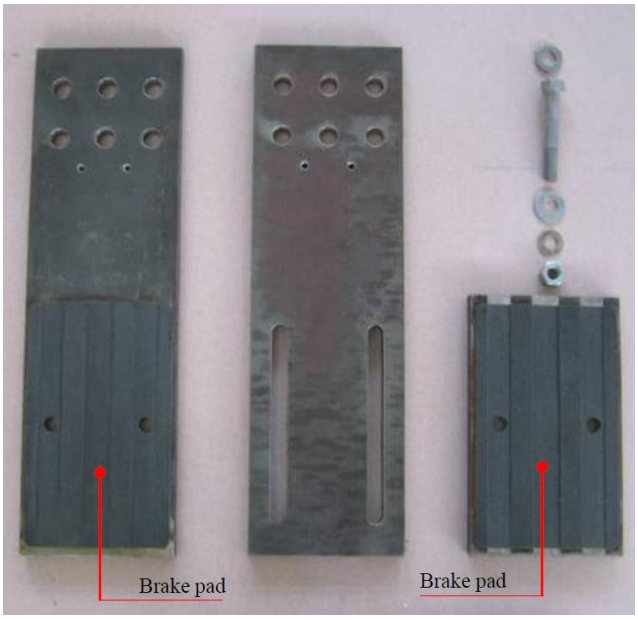

Figure 2-18. NAO Composite SBFD (Golondrino, et al., 2013)

NAO composite shims produce a constant friction force through the sliding length once a "steady wear" state occurs. A steady wear state occurs when the wear resistant segments of the heterogeneous NAO composite carry the bolt load and the softer filler material is worn and receded. Wear continues after the system reaches steady state, but the damage to the friction surfaces and adverse effects on friction behavior are considerably less than devices with metallic shims (Golondrino, et al., 2013). The stable and repeatable behavior of NAO composite friction pads and steel has led this to become a popular combination in friction applications (Erochko, 2013). However, the long-term performance of SBFDs with NAO composite shims is not well documented. Issues with creep of the NAO material may lead to bolt relaxation and a reduced slip force (Erochko, 2013).

SBFDs have been used in a variety of structural applications. A prestressed concrete rocking wall with SBFDs is shown in Figure 2-19. These devices are commonly installed in beam-column

connections of moment resisting frames and brace connections of braced frames (Golondrino, et al., 2013). Figure 2-20 shows a beam-column joint with a SBFD. In this connection, the FDs are activated by lateral displacement of the column as well as in-plane rotation at the end of the beam.

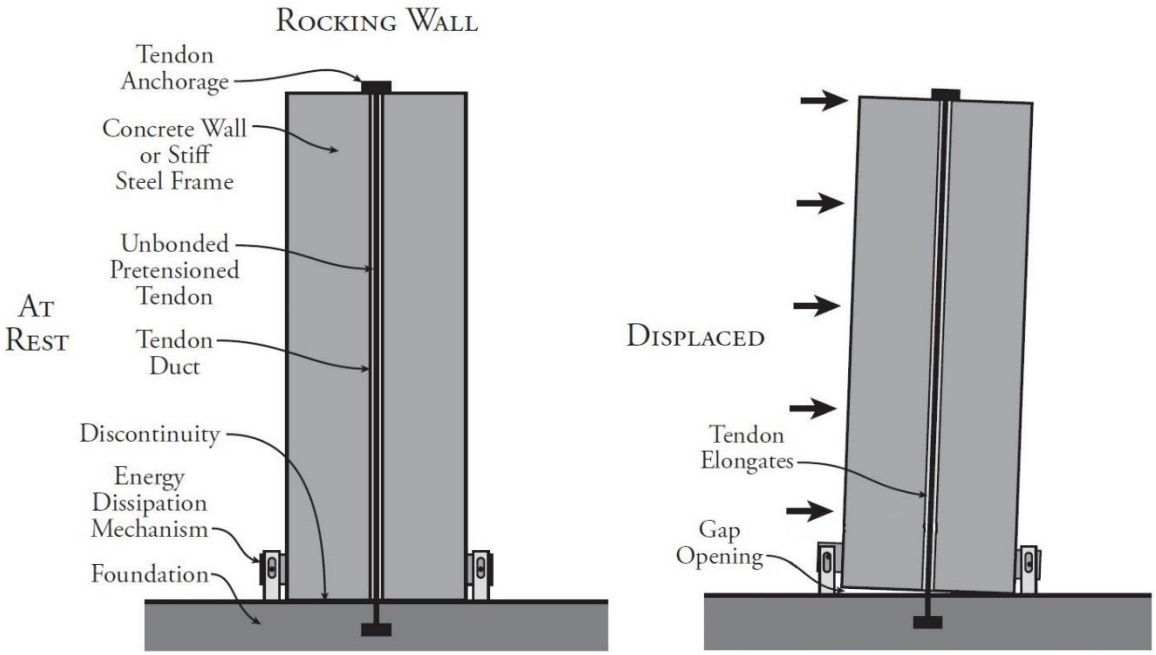

Figure 2-19. Rocking Wall with SBFD (Erochko, 2013)

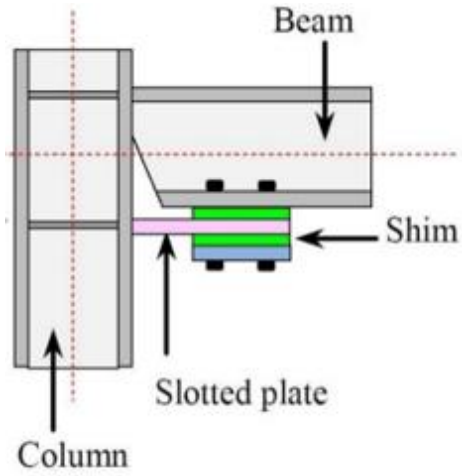

Figure 2-20. Beam-Column Connection with SBFD (Golondrino, et al., 2013)

The Sliding Hinge Joint (SHJ) is a moment resisting frame connection currently in use that contains bottom flange SBFDs. The SHJ utilizes NAO composite and stainless-steel sliding

surfaces. While the SHJ does not have a self-centering mechanism, residual drifts of structures with bottom flange friction devices (BFFD) are typically less than structures that rely on beam hinging in the moment resisting frame (Khoo, et al., 2012). A post-tension friction damped connection for steel moment frames is introduced by P.Rojas at el (2005). The friction device was installed on the top and bottom of beam flange while the post-tension high strength strands were installed parallel to the corresponding beams. Figure 2-21 shows the frame with post-tensioned friction damped connections (PFDC).

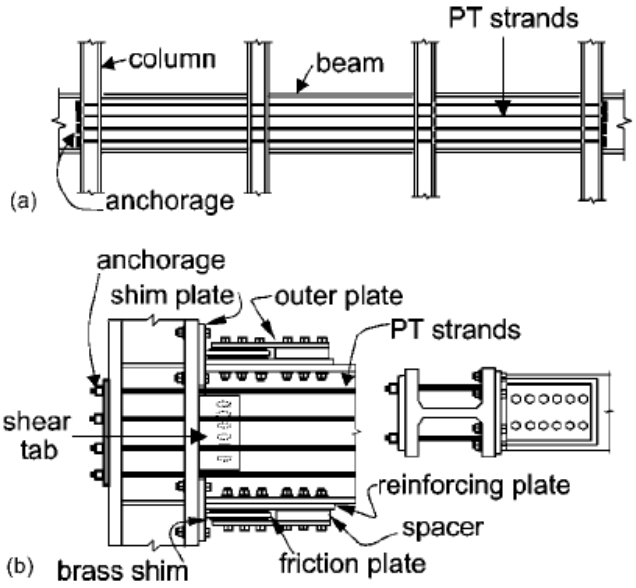

Figure 2-21. Overview of Frame with Post-Tensioned Friction Damped Connections(top and bottom of beam flange) and Details of Post-Tensioned Friction Damped Connections (Rojas, Ricles, & Sause, 2005)

Inelastic analysis was performed on four-story and six-story moment frames to evaluate the effect of using this type of post-tension friction damped connection on the seismic behavior of steel moment frames. Figure 2-22 shows the comparison of residual floor displacements of a six-story steel frame between moment frame with post-tensioned friction damped connections and moment frames without post-tensioned friction damped connections.

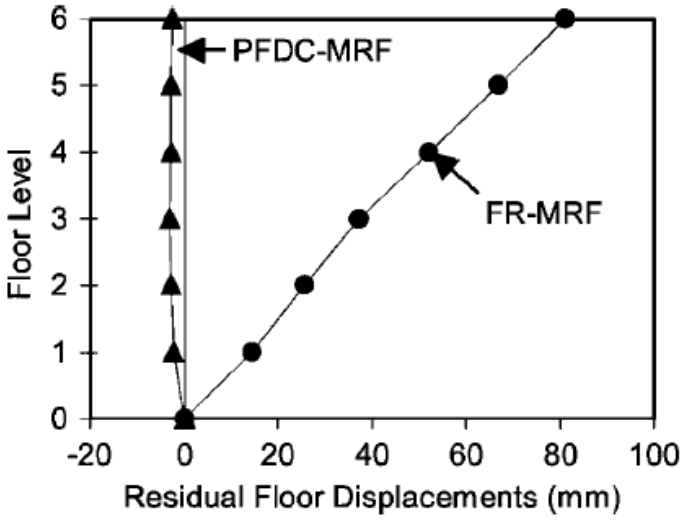

Figure 2-22. Comparsion of Residual Floor Displacement between Moment Frame with PFDC and without PFDC (Rojas, Ricles, & Sause, 2005)

The result shows the post-tension friction damped connections have a significant effect on the moment frame while the change of maximum friction force in the friction device did not have significant effect on seismic behavior of steel moment frames (Rojas, Ricles, & Sause, 2005).

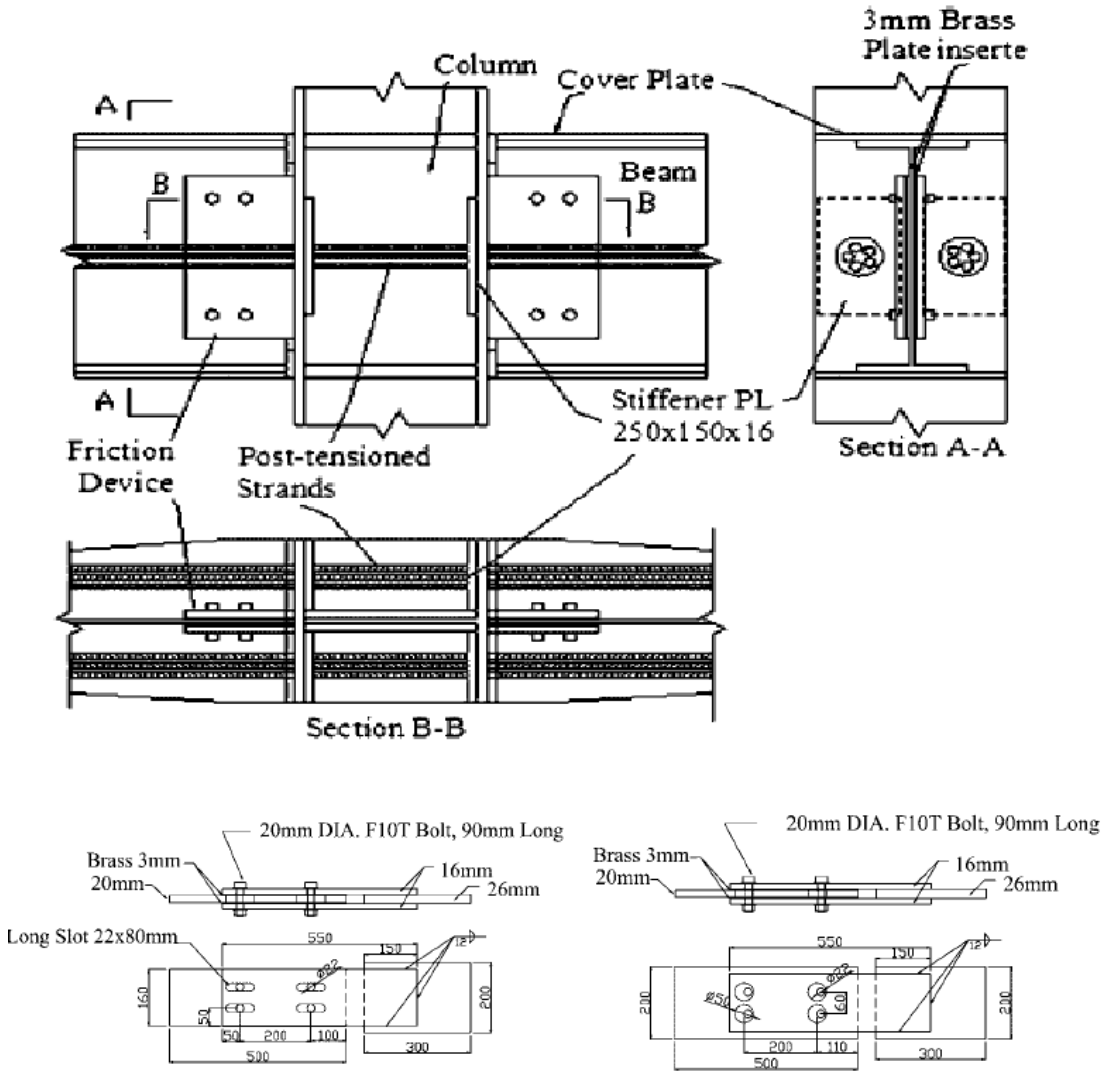

Figure 2-23. Overview of Frame with Post-Tension Friction Damped Connections(both sides of beam web) and Details of Post-Tension Friction Damped Connections (Tsai K.-C. , Chou, Lin, Chen, & Jhang, 2008)

Another self-centering post-tension friction damped connection was introduced by Tsai et al. (Tsai K.-C. , Chou, Lin, Chen, & Jhang, 2008). The friction device was installed on both sides of beam web while the post-tension high strength strands were installed parallel to the corresponding beams through the column flange. Both slot holes and oversized holes were used in these tests. Figure 2-23 shows the frame with post-tensioned friction damped connections and the details of post-tensioned friction damped connections in this research.

Since the floor system is on the top of the moment frame in steel structure, installing friction devices interferes with the slab system. Therefore, a new type of post-tensioned friction damped connection was introduced by Wolski et al. (2009). The friction device was installed on the bottom beam flange while the post-tensioned high strength strands were installed parallel to the corresponding beams through the column flange. A 22-degree slotted hole was adopted in the friction device to have a better fit of the rotational behavior in the test. The test results show that the BFFD provides reliable energy dissipation, and that the connection remains damage-free under the design earthquake (Wolski, Ricles, & Sause, 2009). The result was also validated by the numerical analysis using OpenSees (Guo, Song, & Zhang, 2011). Figures 2-24 and 2-25 show sketches of experimental details for self-centering connections with BFFD and the corresponding numerical model, respectively.

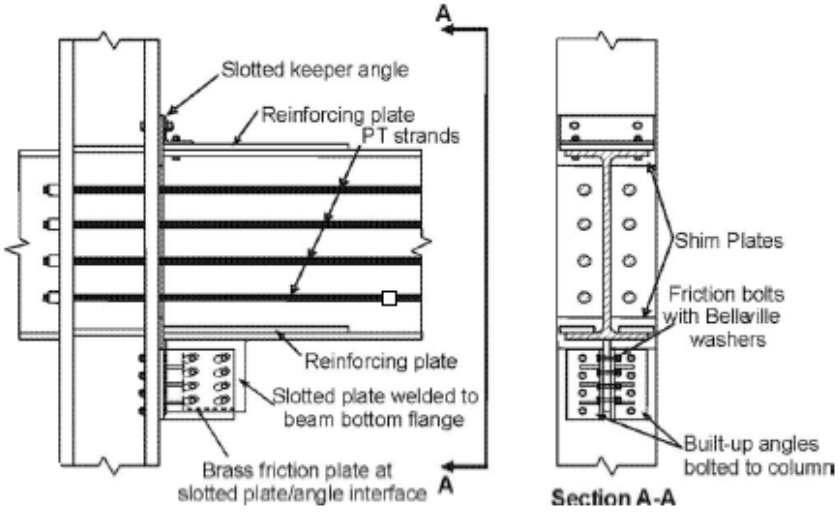

Figure 2-24. Details for Self-Centering Connection with BFFD (Wolski, Ricles, & Sause, 2009)

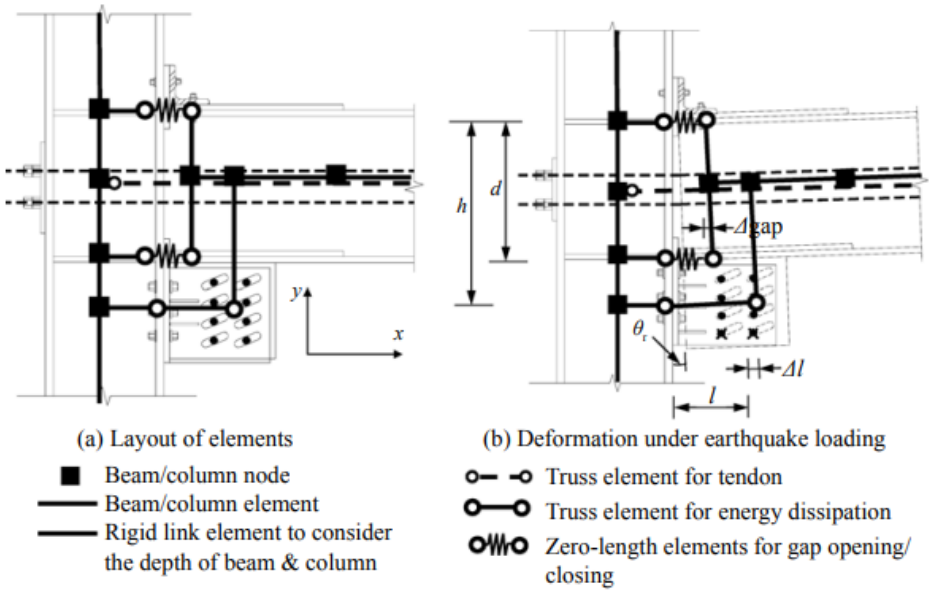

Figure 2-25. Numerical Model for Self-Centering Connection with BFFD (Guo, Song, & Zhang, 2011)

Based on the previous literature review, friction devices have been proved to be effective to dissipate energy during earthquake event. If the friction device is combined with the self-centering beam column system, the chances for damage in the designed earthquake is low. However, the friction device might be damaged even in a small earthquake if the friction device is not combined with a self-centering beam column system. A new removable friction device for low damage steel beam-column joints was introduced (Latour, et al., 2018). Figure 2-26 shows the detail of beam column joint with BFFD with two different configurations. The result was also validated through numerical analysis by using Abaqus. Figure 2-27 shows the mesh detail of the beam-column joint with BFFD with two different configurations. Figure 2-28 shows the result of moment versus rotation for the beam-column joint with a BFFD for two different configurations with small assemblies and large assemblies. The results show that even without the self-centering system, the beam-column joint with a friction device can still be efficient to dissipate energy. These two different configurations have almost the same effect on the behavior of beam-column joint. A

design criterion for beam column joint with BFFD was proposed (Francavilla A. B., Latour, Piluso, & Rizzano, 2020) based these tests and the numerical analysis results.

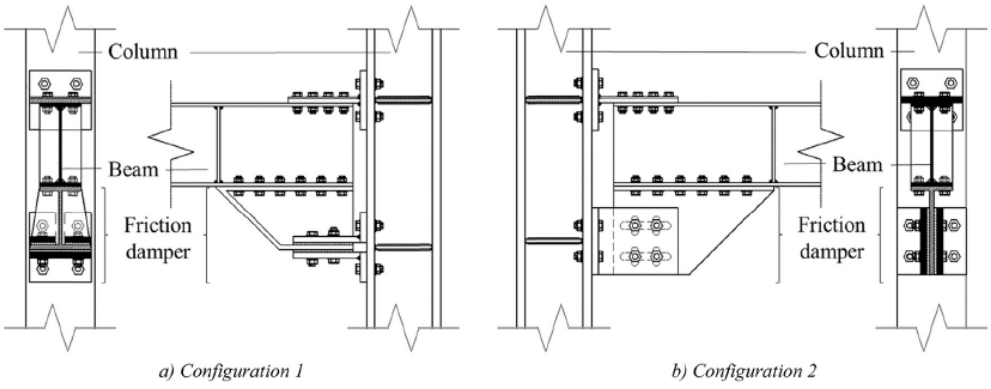

Figure 2-26. Detail of Beam Column Joint with BFFD with Two Different Configurations (Latour, et al., 2018).

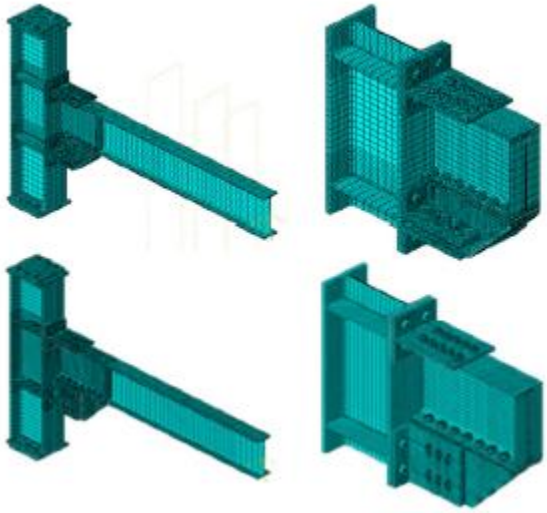

Figure 2-27. Abaqus Model of Beam Column Joint with BFFD with Two Different Configurations (Latour, et al., 2018).

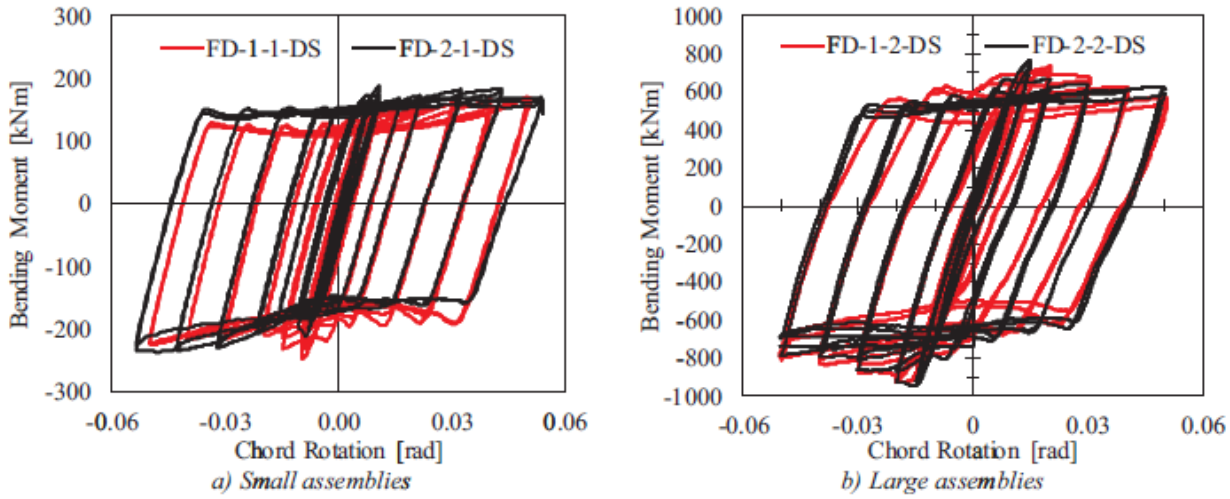

Figure 2-28. Moment versus Rotation for Beam Column Joint with BFFD with Two Different Configurations a) Small Assemblies and b) Large Assemblies (Latour, et al., 2018).

SBFDs are also employed in braces. A typical use of a SBFD can be seen in Figure 2-29. Here, an SBFD has been incorporated into one of the brace connections. The Self-Centering Energy Dissipative (SCED) brace is a brace design with an internal friction damper. The SCED brace has internal pretensioned tendons that provide a self-centering mechanism (Erochko, 2013). Figure 2-30 shows an idealized SCED brace as it undergoes its full range of motion. The brace must first overcome the pretension force before the SBFD begins to take load and slip. The flag-shaped hysteresis seen in Figure 2-30 is typical of self-centering devices with energy dissipation. The friction damping braces decrease drifts while increasing accelerations when compared to conventionally braced structures (Erochko, 2013).

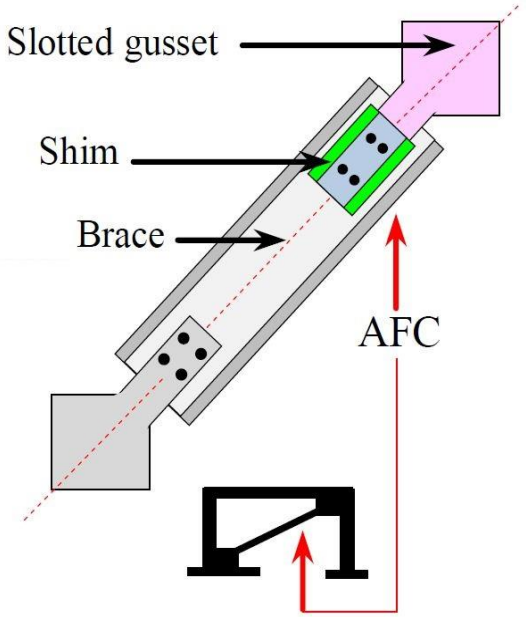

Figure 2-29. Brace with SBFD (Golondrino, et al., 2013)

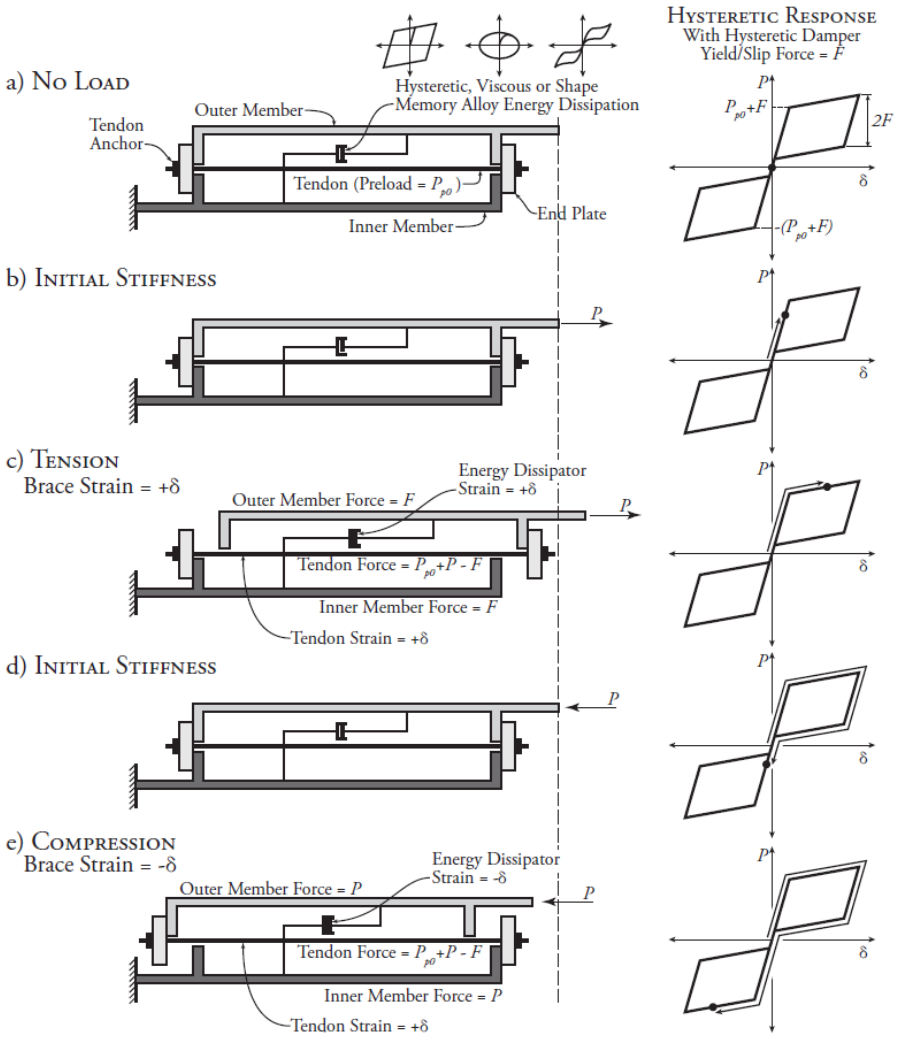

Figure 2-30. SCED Brace (Erochko, 2013)

2.3 Summary

This chapter provides a review of literature pertaining to shear tab gravity frame connections and slotted bolted friction devices in structural applications. The design, application, and performance of these structural elements are necessary in understanding the connections investigated in this thesis. The reviewed literature suggests slotted bolted friction dampers with NAO composite shims provide a simple and reliable source of energy dissipation in a wide variety of structural applications. A scarce selection of literature exists on the effect the gravity frame during lateral loading and how those effects should be accounted for in structural modeling.

References

Abou-zidan, A., & Liu, Y. (2015). Numerical study of unstiffened extended shear tab connections. *Journal of Constructional Steel Research Volume 107*, 70-80.

Astaneh-Asl, A., Liu, J., & McMullin, K. M. (2002). Behavior and Design of Single Plate Shear Connections. *Journal of Constructional Steel Research*, 1121-1141.

Balendra, T., Yu, C., & Lee, F. L. (2001). An Economical Structural System for Wind and Earthquake Loads. *Engineering Structures, 23*(5), 491-501.

Bhavikatti, S. S., & Rajashekarappa, K. G. (1998). *Engineering Mechanics.* New Delhi: New Age International.

Crocker, J. P., & Chambers, J. J. (2004). Single Plate Shear Connection Response to Rotation Demands Imposed by Frames Undergoing Cyclic Lateral Displacements. *Journal of Structural Engineering*, 934-941.

Daneshvar, H., & Driver, R. G. (2017). Behaviour of shear tab connections in column removal scenario. *Journal of Constructional Steel Research*, 580-593.

Erochko, J. A. (2013). *Improvements to the Design and Use of Post-Tensioned Self-Centering Energy-Dissipative (SCED) Braces.* Toronto, Canada: University of Toronto.

Francavilla, A. B., Latour, M., Piluso, V., & Rizzano, G. (2020). Design criteria for beam-to-column connections equipped with friction devices. *Journal of Constructional Steel Research.*

Golondrino, J. C., MacRae, G. A., Chase, J. G., Rodgers, G. W., & Clifton, C. G. (2012). Behavior of Asymmetrical Friction Connections Using Different Shim Materials. Christchurch, New Zealand: New Zealand Society for Earthquake Engineering.

Golondrino, J. C., MacRae, G. A., Chase, J. G., Rodgers, G. W., & Clifton, C. G. (2013). Application of Brake Pads on Asymmetrical Friction Connection. Wellington, New Zealand: New Zealand Society for Earthquake Engineering.

Guo, T., Song, L., & Zhang, G. (2011). Numerical simulation of the seismic behavior of self-centering steel beam-column connections with bottom fl ange friction devices. *EARTHQUAKE ENGINEERING AND ENGINEERING VIBRATION*, 229-238.

Jabotian, H. V., & Hantouche, E. G. (2018). Thermal creep effect on the behavior of shear tab connections due to fire temperatures. *Fire Safety Journal*, 74-92.

Khoo, H.-H., Clifton, C., Butterworth, J., MacRae, G., Ferguson, G., & . (2012). Influence of Steel Shim Hardness on the Sliding Hinge Joint Performance. *Journal of Construction Steel Research*, 119-129.

Latour, M., Aniello, M. D., Zimbru, M., Rizzano, G., Piluso, V., & Landolfo, R. (2018). Removable friction dampers for low-damage steel beam-to-column joints. *Soil Dynamics and Earthquake Engineering*, 66-81.

Liu, J., & Astaneh-Asl, A. (2000). *Cylclic Tests on Simple Connections Including Effects of the Slab.* Sacramento.

Rahman, A., Mahamid, A., Amro, A., & Ghorbanpoor, A. (2010). The analyses of extended shear tab steel connections-Part I: The unstiffened connections. *Eng J Am Inst Steel Constr*, Vol. 44(No. 2).

Richard, R. G. (1980). The analysis and design of single plate framing connections. *Engineering Journal*, Quarter 2, 38-52.

Rojas, P., Ricles, J. M., & Sause, R. (2005). Seismic Performance of Post-tensioned Steel Moment Resisting Frames With Friction Devices. *Journal of Structural Engineering*, 529-540.

Tsai, K.-C., Chou, C.-C., Lin, C.-L., Chen, P.-C., & Jhang, S.-J. (2008). Seismic self-centering steel beam-to-column moment connections. *EARTHQUAKE ENGINEERING AND STRUCTURAL DYNAMICS*, 627-644.

Wen, R., Akbas, B., Sutchiewcharn, N., & Shen, J. (2013). Inelastic behaviors of steel shear tab connections. *Structural Design of Tall and Special Buildings Volume 23, Issue 12*, 929-946.

Wolski, M., Ricles, J. M., & Sause, R. (2009). Experimental Study of a Self-Centering Beam–Column Connection with Bottom Flange Friction Device. *Journal of Structural Engineering*, 479-488.

Chapter 3 Experimental Evaluation of a Shear Tab Connection with a Bottom Flange Friction Device

Hongyang Wu, Graduate Research Assistant, Department of Civil and Environmental Engineering, 238 Harbert Engineering Center, Auburn University, Auburn, AL 36849, hzw0035@auburn.edu

Justin D. Marshall, Associate Professor of Civil and Environmental Engineering, 238 Harbert Engineering Center, Auburn University, Auburn, AL 36849, jdmarshall@auburn.edu

Abstract

As structural engineering practice moves from life-safety to functional recovery after a significant seismic event, taking advantage of structural components to enhance the energy dissipation of a structure will be important. This paper is the first phase of a research effort to assess the impact of enhancing the energy dissipation of the gravity system to improve the response of steel frames. One of the proposed connection modifications is a Bottom Flange Friction Device (BFFD). Increasing energy dissipation in simple gravity connections provides an economical mechanism for increasing energy dissipation for moderate to severe earthquakes and severe windstorms. In order to provide the experimental data to assess the impact of the gravity connections on a frame, a series of 27 small-scale tests were used to investigate the performance of a Slotted Bolted Friction Device. Then, a series of 18 large-scale tests were performed to investigate the performance of a Bottom Flange Friction Device on a shear tab beam-column connection. The hysteretic response, energy dissipation, bolt tension, friction coefficient and initial connection stiffness are presented and discussed in this paper. The experimental testing of the shear tab connection with a bottom flange friction device showed improved energy dissipation and

capacity over the simple connections without any adverse impacts on the performance and deformation capacity of the shear tab alone.

Keywords: early phase energy dissipation, slotted bolted friction device, Bottom Flange Friction Device

3.1 Introduction

In structural steel design, the lateral load-resisting system and gravity load system are normally designed independently. The lateral load-resisting system is controlled by lateral force demands while gravity load frames are controlled by gravity demands. Well-detailed and designed structural steel frames are generally considered to have very good ductility and hence are able to meet and exceed the life safety demands specified by current building codes for seismic events. Gravity load frames are typically not included in the lateral load design and subsequent performance assessment. The reason the gravity systems are typically neglected in the lateral load design and assessment is the difficulty of modelling the beam-to-column connection and lack of information regarding the expected behavior of connections (Flores, Charney, & Lopez-Garcia, 2016). Simple shear tab connections are widely used in the gravity load system in steel structures. Experimental tests on simple shear connections with and without the concrete slab conducted by Liu and Astaneh (2000) showed that energy can be dissipated by the simple shear tab connection. The primary objective of this research effort is to identify ways in which the analytical performance of structural steel frames could be improved by including the effects of energy dissipation from the gravity system. In addition, enhancing the energy dissipation of these connections could provide significant performance improvement for seismic and wind events for steel structures. Several modifications of the shear tabs are considered to increase the positive effect of the gravity system on dynamic response. These modifications include adding a Bottom

Flange Friction Device (BFFD) and increasing the bolt spacing on the shear tab. Both these methods increase the connection slip moment and energy dissipation capacity. Neither of these modifications have been assessed analytically or experimentally.

The overall research objective is to improve the energy dissipation capacity of steel frames by supplementing the lateral system with the gravity system. The energy dissipation from the gravity system can be activated in small and moderated earthquakes which would result in energy dissipation without damage to the structure. Enhancing energy dissipation would serve to decrease demands on the structure and improve performance of steel structures in small, moderate and severe earthquakes. This paper is the first stage of this effort and includes the experimental testing needed to assess the hysteretic response of shear tab connections and shear tab connections with the proposed modifications. The simplest modification to increase the slip moment of the shear tabs is to widen the bolt spacing. The second modification is the addition of a BFFD which is a Slotted Bolted Friction Device (SBFD) attached between the bottom flange of a beam and the supporting column flange (See Figure 3-1). It is paramount that the BFFD be able to activate consistently and subsequently work to dissipate energy in a stable manner while also maintaining the gravity load path. Equally important is that upon activation of the main lateral force resisting system, the BFFD acts to supplement energy dissipation. The supplemental energy dissipation would be engaged before the seismic force resisting system yields providing a mechanism to dissipate energy without damage to the frame and throughout the event. This supplemental friction device would be effective when the structure is experiencing a minor earthquake or under wind load when the lateral system is still elastic. In order to evaluate this concept, this paper provides a description of and then reports on a series of experimental tests that characterize the simple connection without and with a BFFD. The simple shear tab connection itself is considered as a

baseline model in this experimental test. The concrete floor system is an important component of the system which can significantly affect the behavior of the simple shear connection, especially in a composite floor system. However, it was not considered in this research. A similar effect of the BFFD is expected whether the shear tab connection is bare or has a concrete slab. Including the floor system in the test is considered to increase the effect of BFFD more than for a bare shear tab since the center of rotation of the connection is moved up which means the distance between center of rotation and BFFD will increase which could provide lager moment strength and dissipate more energy.

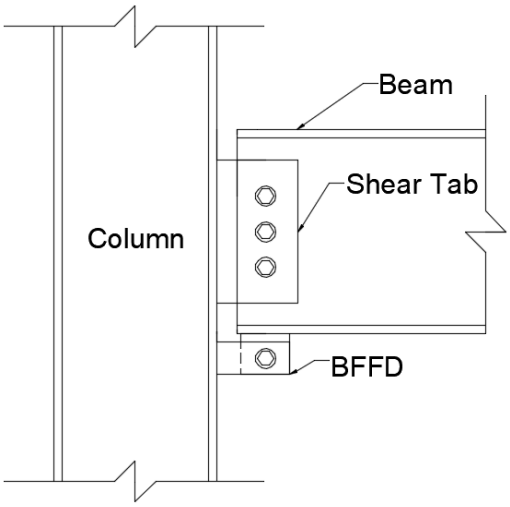

Figure 3-1. Sketch of Simple Shear Connection with BFFD

This paper represents the first stage of the research with experimental testing. The data generated from these tests will be critical to future efforts related to the overall research objective. The next phase will be validating high fidelity finite element analysis models of the connections with and without the proposed modifications. These validated models will be used to identify important parameters and develop numerical models (i.e., backbone curves) that can be used in structural analysis models. The last research phase will assess the impact of including the gravity

system with enhanced shear tabs on the response of case study steel frame buildings. The research presented in this paper provides the foundation for these future efforts.

3.2 Literature Review

At the core of the BFFD is the slotted bolted connection that is referred to as a Slotted Bolted Friction Device (SBFD) in this work. According to Grigorian and Popov (1994), the original design (see Figure 3-2) consisted of a steel plate interposed between two external steel plates and clamped together by a steel bolt with Belleville washers to maintain clamping force. The connection succeeded in dissipating energy through friction but was plagued with an unstable hysteretic response stemming from the tribological effects of steel sliding across steel. Subsequent research by Grigorian and Popov (1994) found that these shortcomings could be resolved by installing brass shims into the friction planes, resulting in a consistent friction force and stable hysteretic response. A great deal of research involving the use of materials other than brass for shims and the effect on friction device response, as well as new methods of implementing sliding friction devices into traditional lateral force resisting frames followed these research efforts (Guo, Song, & Zhang, 2011; Tsai K. , Chou, Lin, Chen, & Jhang, 2008; Zhang A. , Zhang, Li, & Wang, 2016).

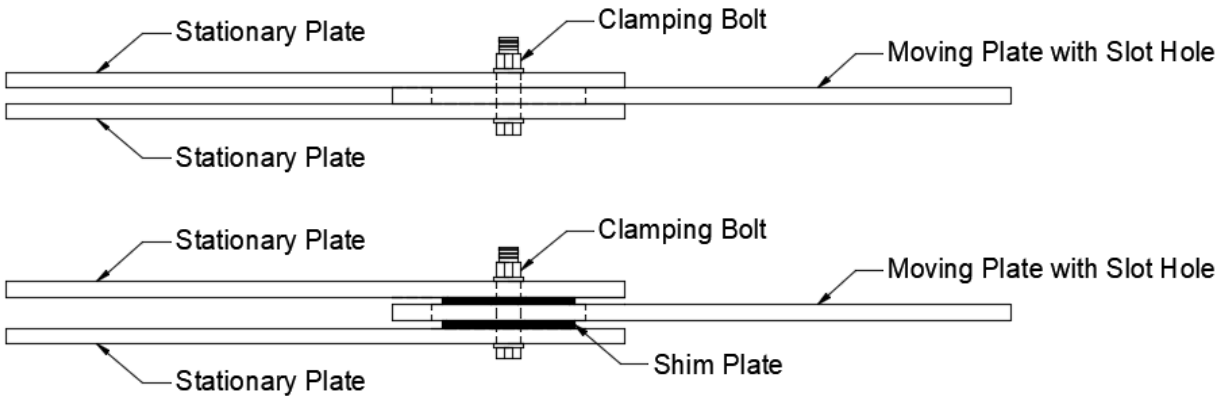

Figure 3-2. Slotted Bolted Friction Connection without Shims (top) and with Shims (bottom)

Research undertaken by Clifton (2005) resulted in additional SBFD design options through a classification into Symmetric Friction Connections (SFCs) and Asymmetric Friction Connections (AFCs). SFCs are the traditional designs which provide a symmetric load path by transferring force through two external plates to a single interior plate, or vice versa. An altered version of this, the AFC, was introduced as a component of a joint developed by Clifton (2005) for steel moment resisting frames. Noticeably different when comparing AFCs with SFCs is the asymmetrical load path introduced by a backing plate clamping the connection together and replacing the previously present external plate that provided both clamping action and continuity between connection elements. This modification enables the AFC to be applied at beam-column joints in a manner that results in both the internal plate and its friction plane adjoining the beam flange while allowing sliding upon joint rotation (Clifton, 2005).

Research by Golondrino, et al. (2013) found that hysteretic behavior of SBFDs changes based on different shim materials. Common materials used as shims include aluminum, brass, mild steel, and Non-Asbestos Organic (NAO) composites. Golondrino, et al. (2012) and Khoo, et al. (2012) showed that high hardness steel shims with low wear rates were more conducive to achieve consistent and stable hysteretic behavior. Ensuring a difference in hardness between the friction surfaces also results in more stable sliding performance and less wear. This allows the softer material to conform to the harder material and absorb wear particles (Khoo, Clifton, Butterworth, MacRae, & Ferguson, Influence of Steel Shim Hardness on the Sliding Hinge Joint Performance, 2012). SBFDs with NAO composite shims (e.g., Ferotec Friction Inc. D3923) provide a more stable hysteretic behavior than metallic friction surfaces (Golondrino, et al., 2013). NAO composite shims produce a constant friction force through the sliding length once a “steady wear” state occurs. A steady wear state occurs when the wear resistant segments of the NAO composite

carry the bolt load and the softer filler material is worn and receded. Wear continues after the system reaches steady state, but the damage to the friction surfaces and adverse effects on friction behavior are considerably less than devices with metallic shims (Golondrino, et al., 2013). The stable and repeatable behavior of NAO composite friction pads and steel has led this to become a popular combination in friction applications. However, the long-term performance of SBFDs with NAO composite shims is not well documented. Issues with creep of the NAO material may lead to bolt relaxation and a reduced slip force (Erochko, 2013).

A Bottom Flange Friction Device was developed by Wolski M. (2006) as a method of incorporating an energy dissipating friction device into Self-Centering (SC) Moment Resisting Frames (MRF) with Post-Tensioned (PT) steel moment connections or PT SC-MRF systems. The device was placed at the bottom of the beam-column interface to enable energy dissipation through friction without conflicting with the concrete slab or the other connection components (Wolski, Ricles, & Sause, 2009). The test results show that the Bottom Flange Friction Device provides reliable energy dissipation, and the connection remains damage-free under the design earthquake. A removable friction device for low damage steel beam-column joints was introduced by Latour et al. (2018). The results show that even without the self-centering system, the beam-column joint with a friction device can still dissipate energy efficiently (Francavilla A. , Latour, Piluso, & Rizzano, 2020).

The previous research efforts have focused on the friction components as the primary energy dissipation component. In this research the BFFD are incorporated into the gravity system and are supplemental to the primary lateral system. The impact of BFFDs in the gravity system can be taken into account using performance-based design. Adding the shear tab connection with BFFDs in the structural models can help engineers to have a better understanding of the behavior of

structures under lateral loading. The concept of the BFFD in the gravity load system is meant to provide energy dissipation distributed through the structure that initiates at lower deformation levels. This early initiation serves to provide energy dissipation prior to inelastic response of the primary lateral system which can serve to dissipate energy for a wider array of lateral demands.

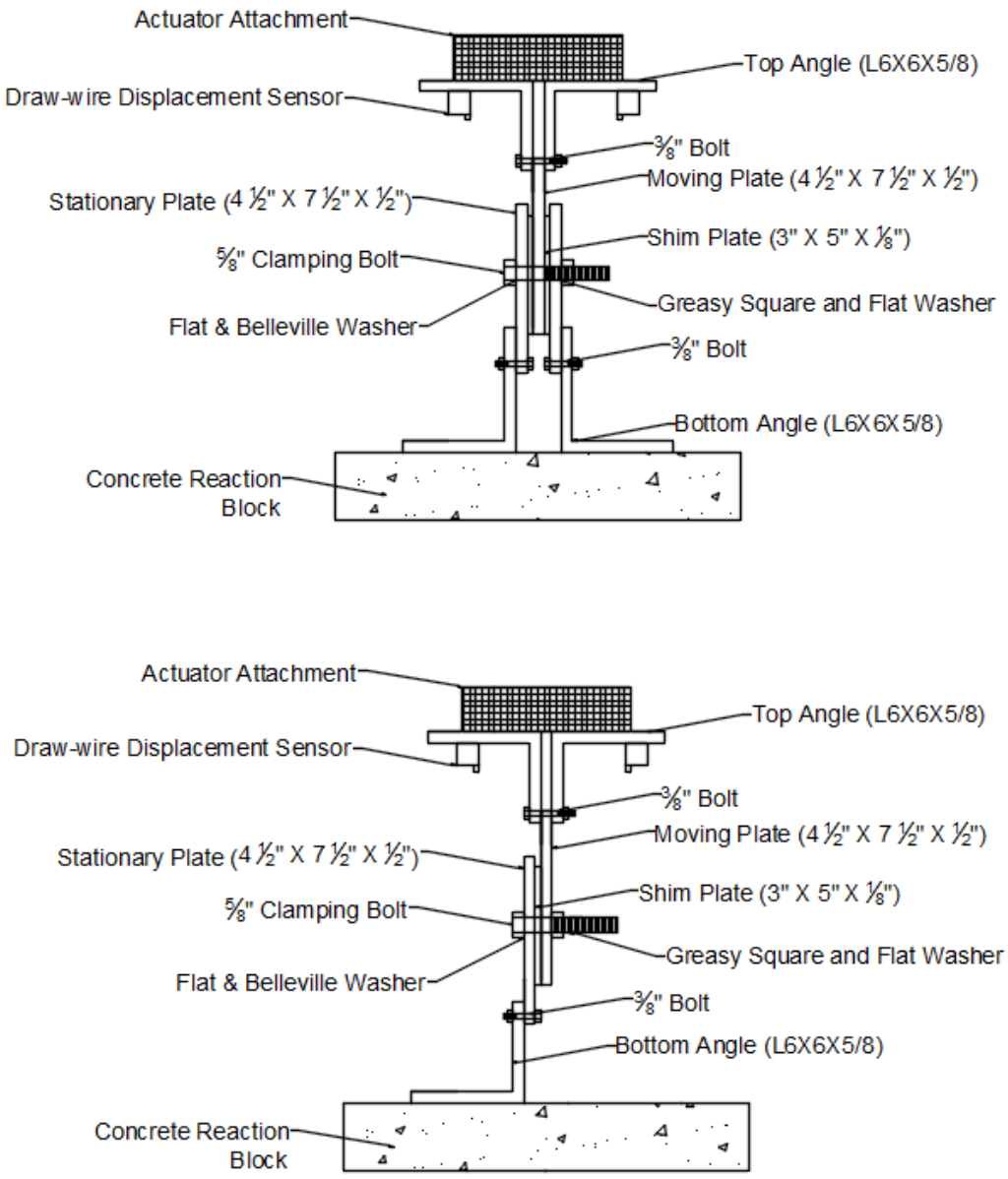

Figure 3-3. Sketch of SFC-Type (top) and AFC-Type (bottom) SBFD

3.3 Development and Description of the SBFD

Experimentally characterizing the configuration and performance of the different materials in the BFFD is more easily completed by assessing a simpler Slotted Bolted Friction Device. Two types of SBFDs were tested including an Asymmetric Friction Connection and a Symmetric Friction Connection. An AFC-type SBFD is beneficial since it allows for connection at the beam-column joint with fewer plates while an SFC−type SBFD is expected to have more stable performance.

3.3.1 SBFD Description

This section includes a part-by-part review of the design and fabrication of both the AFC and SFC SBFDs. The assembled connections can be seen in Figure 3-3.

The stationary and moving plates measured 7.5 x 4.5 x 0.5 in. and were fabricated using 0.5 in. thick AISI 1018 cold-drawn low-carbon steel. An extra-wide long-slotted hole exists through the thickness of the moving plate that allows the SBFD to have vertical displacement and horizontal movement caused by imperfection of the test set up. For AFC-type SBFDs, two recessed channels were machined on one side of the moving plate that allow the friction material to be embedded 1/16 in. deep. For the SFC-type SBFD, recesses were machined on both sides of the moving plate. It is intended for the friction material to project 1/16 in. above the steel surface and create an elevated friction plane for the shim to slide across. The stationary plate has a single 5/8 in. through-hole for the clamping bolt. Two 3/8 in. through-holes were made near the edge of the moving plate for a bolted connection with top angles which were also connected to the actuator. Similarly, two 3/8 in. through-holes were made near the edge of the stationary plates for a bolted connection with the bottom angle. The bottom angles were connected to a concrete reaction block on the strong floor.

Following fabrication of the SBFD plates, NAO friction material was attached in the recesses of the moving plate. D2017, a NAO friction material manufactured by Ferotec Friction Inc., was used. Notable improved features of the D2017 material include increased shear and compressive force capacities and added oil resistance. The friction material was affixed to the steel moving plate using Loctite EA E-120HP adhesive. The process consisted of applying a thin layer of adhesive to the friction material and the degreased moving plate, clamping the two components together, and then curing the assembled piece at 150°F for 12 hours.

Different steel shims were used to assess the effects of shim hardness and surface treatment on SBFD performance. Both shim types have dimensions of 3 x 5 x 1/8 in. The shims were fabricated from 1/8 in. thick sheets of both AISI 1018 cold-rolled steel with a precision ground finish and 304 stainless steel with a mirror-like (#8) finish. Both materials were listed as being compliant with the appropriate ASTM standards as well as having Rockwell hardness scale B (HRB) values of 71 and 80 for the 1018 carbon and the 304-stainless steel, respectively.

Clamping bolt tension provides the normal force in the Coulomb friction model. A method for measuring tension in SBFD clamping bolts is necessary for controlling slip criteria. Several methods, each with a differing level of accuracy, exist for approximating bolt tension. The options ordered by accuracy are strain gauge instrumented bolts, Direct Tension Indicator (DTI) washers, turn control methods, and torque control methods. Of the four methods, strain gauge instrumented bolts are most fitting for initiating and measuring bolt tension during experimental evaluation.

Once initial tensioning of the clamping bolt is complete, maintaining tension throughout service life is crucial for proper performance. Though difficult to predict, the potential exists for stress relaxation and creep to progressively decrease bolt tension. Furthermore, surface wear resulting from the interaction between the shim and friction material during slipping could reduce

component thicknesses enough to have a noticeable effect on bolt tension. The most common method for maintaining bolt tension in SBFDs is Belleville washers on the clamping bolt. A Belleville washer is a washer-shaped conical spring that flattens elastically when compressed and maintains bolt tension by exerting an opposing force on the bolt that allows for the compensation of lost bolt tension which reduces variability in both the slip and sliding forces (Grigorian & Popov, 1994; Khoo, 2013). Belleville washers can be combined through stacking to increase spring force. The washers can be stacked in parallel, in series, or other combinations. However, care must be taken in selecting a stacking configuration on account of the impact on elastic properties (Schnorr Corporation, 2003). Belleville washers are a simple, readily available, and economical method of maintaining SBFD bolt tension.

Bolt strain gauges were installed in all clamping bolts in order to capture the bolt tension during testing. A 0.07 in. diameter hole with an approximate 1.4 in. length was drilled at the center of the head and then a BTM-6C bolt strain gauge manufactured by Tokyo Measuring Instruments Lab was inserted. The remaining void was filled by A-2 adhesive manufactured by Tokyo Measuring Instruments Lab or AE-10 which is made by Micro-Measurement. Following installation, the bolt strain gauge was calibrated in a universal testing machine to determine the stress versus strain relationship. Figure 3-4 shows two ASTM F3125 A325 bolts with installed bolt strain gauges.

Figure 3-4. ASTM F3125 A325 5/8 in. Diameter Bolts with Bolt Strain Gauge

Once calibration was completed, all SBFD components were clamped by the single, strain-gauged 5/8 in. ASTM F3125 A325 bolt. The clamping bolts could be tightened to a precise tension value to better control SBFD slip force and limit performance variability. In addition, both Belleville and flat structural steel washers were installed on the clamping bolt to maintain bolt tension and distribute clamping force.

3.3.2 Experimental Testing of SBFD

The goal of the testing was to assess the friction coefficient between the friction material (D2017) and shim plates, the friction coefficient between the washer and steel moving plate, energy dissipated, and loss of bolt tension. SFC-Type SBFD tests provided the friction coefficient between friction material (D2017) and shim plates while AFC-Type SBFD test provided the friction coefficient between washer and steel moving plates. Loss of bolt tension was captured by measurement of bolt strain gauges. The simple design of the test setup allowed for energy dissipated to be easily calculated alongside other performance variables.

3.3.3 Experimental Setup

The setup shown in Figure 3-5 was devised to experimentally evaluate the SBFD. The moving plate was bolted between two pieces of L6×6×5/8 angle which connected with an aluminum block on the MTS 243.35 hydraulic actuator attached to a reaction frame. The stationary plate assembly was bolted to L6×6×5/8 angles which were connected to a concrete reaction block attached to the strong floor. Four safety straps were used to prevent movement of the actuator which might cause bending behavior of connection. Lastly, two draw-wire sensors were clamped on the two top angles separately to measure the displacement of the top angle.

Figure 3-5. SBFD Test Configuration

Once the SBFD plates were in place, installation of the clamping bolt was performed with great care as the bolt strain gauges proved to be particularly sensitive. The bolt was inserted into the SBFD with the proper washer arrangement prior to the installation of the nut. For AFC-type SBFD, grease was applied between moving plate and flat washer to avoid significant damage of the surface of the moving plate during tests. Installation of the nut consisted of hand tightening it onto the bolt until the slightest amount of resistance was felt, zeroing the strain gauge, and then tightening the bolt to the desired tension (clamping force). Once tightened, bolt strain gauge values were monitored to ensure no significant changes in strain gauge readings occurred prior to testing. Lastly, following each experimental trial, the instrumented clamping bolt was removed, and the installation process repeated prior to testing the next specimen. An image of the fully installed clamping bolt is shown in Figure 3-6.

Figure 3-6. Installed Clamping Bolt in AFC SBFD

3.3.4 Calibration of Instrumented Clamping Bolt

Measurement of tension present in the clamping bolts first required calibration of bolt strain gauge readings to a series of known tensile forces applied to the bolts. Each instrumented bolt was subjected to three cycles of incremental monotonic loading from 0 to 10 kips (1/3 of the yield strength) using a Tinius-Olsen universal testing machine and a strain indicator. The relationship between bolt tension and bolt strain is linear since all the tensile behavior during calibration is in the elastic range. A simple linear regression model without intercept was determined based on relating the two variables formulaically. With the relationship between the two variables determined, precise tightening of the clamping bolts to a predetermined tension is achievable and allows for control of SBFD slip force.

3.3.5 Equipment and Instrumentation

A variety of equipment was used to ensure the execution of a well-controlled and accurately measured experiment. Table 3-1 shows a detailed list of the equipment and instruments used during SFC-Type SBFD and AFC-Type SBFD tests.

Table 3-1. Equipment Used for Experimental Evaluation

Actuator		
Manufacturer	Model	Equipment
MTS Systems Corporation	243.35	Hydraulic Actuator
	FlexTest 60	Feedback Controller
Instrumentation		
Manufacturer	Model	Equipment
Micro-Epsilon	WDS-1000-P60	Draw-wire Displacement Sensor
Tokyo Instruments	BTM-6C	Bolt Strain Gauge
Pacific Instruments	6000	Data Acquisition System

The actuator was controlled using a closed-loop hydraulic system manufactured by MTS Systems Corporation. The actuator system had the capacity to apply forces up to 82 kips in compression or 54 kips in tension and a 10-in stroke length. An integrated load cell and Linear Variable Differential Transformer (LVDT) enabled measurement of force and displacement generated by the actuator, respectively, while an MTS FlexTest 60 feedback controller was responsible for control commands and actuator sensor data. User control of the system was achieved using MTS Multipurpose Elite software. Vertical displacement of the SBFD plates was measured using two analog Micro-Epsilon WDS-P60 wire potentiometers (draw-wire sensors). This configuration enabled the direct measurement of vertical displacement in the moving plate. The actuator LVDT served as a confirmation of the vertical displacement. A Pacific Instruments Data Acquisition System 6000 and accompanying software collected sensor data. The remaining tasks of calibrating and recording transducer output were handled using the PI660-6000

Acquisition & Control software. The force and displacement data generated during the experiment was used to calculate the response quantities of interest to assess SBFD performance.

3.3.6 Loading Protocol

Experimental evaluation of the SBFD was displacement controlled. The loading protocol was the interim protocol I-quasi-static cyclic testing from FEMA 461 (ATC, 2007). The initial amplitude, Δ_0, was defined as the smallest deformation amplitude during the test. After two cycles, the amplitude increased by 40% until the final target amplitude, Δ_m, is achieved. The initial amplitude is 0.0135 in. while the final target amplitude is 0.75 in. in this test (See Figure 3-7). The loading rate was 0.005 in./sec which was slow enough to minimize dynamic effects and fast enough to prevent unacceptable test duration. The range of the deformation for the SBFD tests is similar to the deformation range at the BFFD, which is controlled by the rotation at which the flange of the beam would come into contact with the adjacent column.

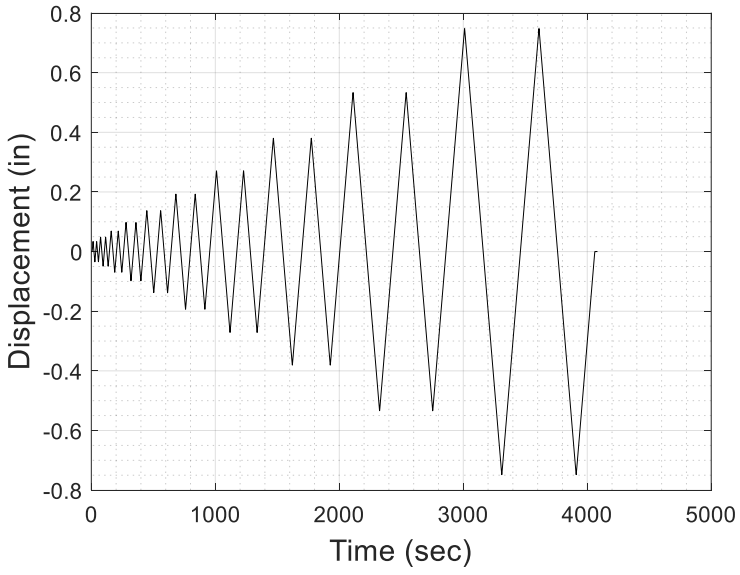

Figure 3-7. Displacement Protocol for SBFD

3.3.7 SBFD Test Cases

Several cases were tested to evaluate SBFD performance under varying configurations of shim material and bolt tension (See Table 3-2). SFC-type connections were tested first. Six test cases total were completed. Three repetitions of each test case were completed to assess repeatability. It was found that the coefficient between the NAO friction material and the 304-stainless shim plate is larger than that between the friction material and the 1018 low-carbon steel shim plate which will be discussed later. Therefore, for AFC-type SBFD connections, only 304-stainless shim plates were used in the tests which means three test cases with three repeated tests were completed for the AFC-type SBFD connection. The same loading protocol was used for all test cases. The differences were the connection type, shim material and targeted initial bolt tension.

Table 3-2. Test Cases for Experimentally Evaluating SBFD

Case	Test	Connection Type	Shim Type	Bolt Tension
1	1	SFC-Type	1018	3kips
	2			
	3			
2	4			5kips
	5			
	6			
3	7			7kips
	8			
	9			
4	10		304	3kips
	11			
	12			
5	13			5kips
	14			
	15			
6	16			7kips
	17			
	18			
7	19	AFC-Type	304	3kips
	20			
	21			
8	22			5kips
	23			
	24			
9	25			7kips
	26			
	27			

3.4 SBFD Experimental Results and Discussion

The focus of this section is the presentation and discussion of results obtained from experimentally evaluating the SBFD. The data presented includes hysteresis loops, energy dissipation, bolt tension and friction coefficient.

3.4.1 Hysteretic Data

Figure 3-8(a) shows hysteretic data from Test 01, 04 and 07 to represent Test cases 1, 2 and 3, which evaluated the SFC-type SBFD connections when configured with 1018 steel shim plates with initial bolt tension of 3 kips, 5 kips and 7 kips, respectively. The plotted data shows a high level of hysteretic stability occurring during individual tests. The sliding force increases as bolt tension increases. The SBFD configuration in Test cases 4, 5 and 6 also featured an SFC-type connection but used 304 stainless steel shim plates. Figure 3-8(b) depicts the plotted hysteretic data from Test 10, 13 and 16 to represent Test cases 4, 5 and 6 with initial bolt tension of 3 kips, 5 kips and 7 kips, respectively. Similar to results with 1018 steel shim plates, the results show a high level of stability and consistency. Even though the test specimen is symmetric, and the actuator was restrained by straps, small variation in sliding force was still observed in the tests based on Figure 8. The reason for these variations in the tests could be the insufficient restraint provided by the safety straps. It also could be the behavior of propagation of wear particles as they were either embedded into the wearing surface or pushed away from the sliding plane (Grigorian & Popov, 1994). Based on results of hysteresis from Test case 1 to 6, the sliding force of SFC-type SBFD with 304 stainless steel shim plates is slightly larger than that of SFC-type SBFD with 1018 steel shim plates. This conclusion was also proved by the coefficient of friction between friction material and shim plates. Therefore, for AFC-type SBFD tests, only 304 stainless steel was selected as the shim plates since it can dissipate more energy per cycle. Figure 3-8(c) shows the

AFC-type SBFD hysteretic data from Test 19, 22 and 25 to represent Test cases 7, 8 and 9 with initial bolt tension of 3 kips, 5 kips and 7 kips, respectively. Compared with SFC-type SBFD, the results were not stable at the beginning of the cyclic protocol while it became stable after the initial cycles. Larger variation of sliding force showed in the results of the AFC-type SBFD because of the inherent eccentricity of the AFC-type connections. The eccentricity of the friction device resulted in bending demands that resulted in prying of the bolt which caused greater variation in the friction coefficient. These nine individual tests were selected to represent the nine different SBFD Test cases. The results not shown are consistent with those provided.

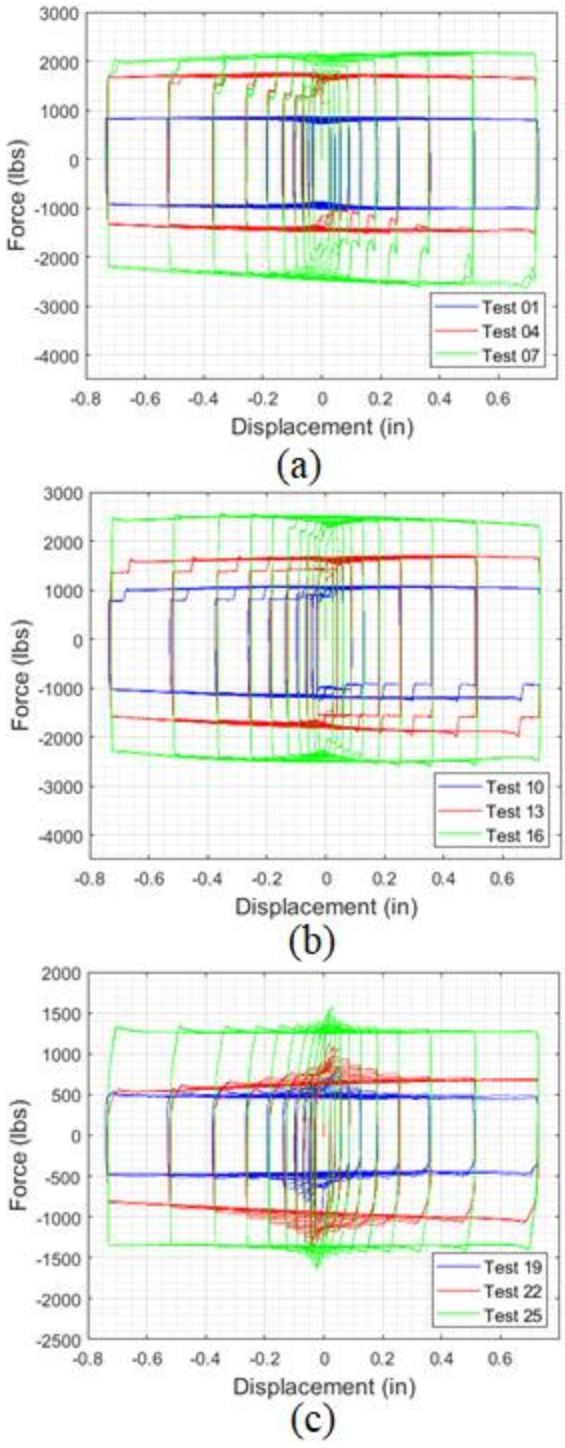

Figure 3-8. Hysteresis Plots of SBFD: a) SFC with 1018 Shim, b) SFC with 304 Shim, c) AFC with 304 Shim

3.4.2 Energy Dissipation

The energy dissipated by the SBFD, and its consistency varied depending on the type of shim plates and the type of SBFD. Figure 3-9 shows the energy dissipated per cycle from the selected test set. For the same configuration, the energy dissipated per cycle increases as bolt tension increases. The energy dissipated per cycle by the SFC with 1018 shim plate is slightly less than that by SFC with 304 shim plate. Noteworthy in data from all test cases are the linearity and stable growth of energy dissipated as displacement cycles progressed. All cases also show the elastic portion of the protocol for the smallest displacement cycles. Apparent increases in energy dissipated stems from a minor increase in bolt tension between tests which would increase the forces required to initiate sliding. The decrease in bolt tension during tests resulted in an insignificant decrease of energy dissipated. All the results of individual tests were consistent within the presented data.

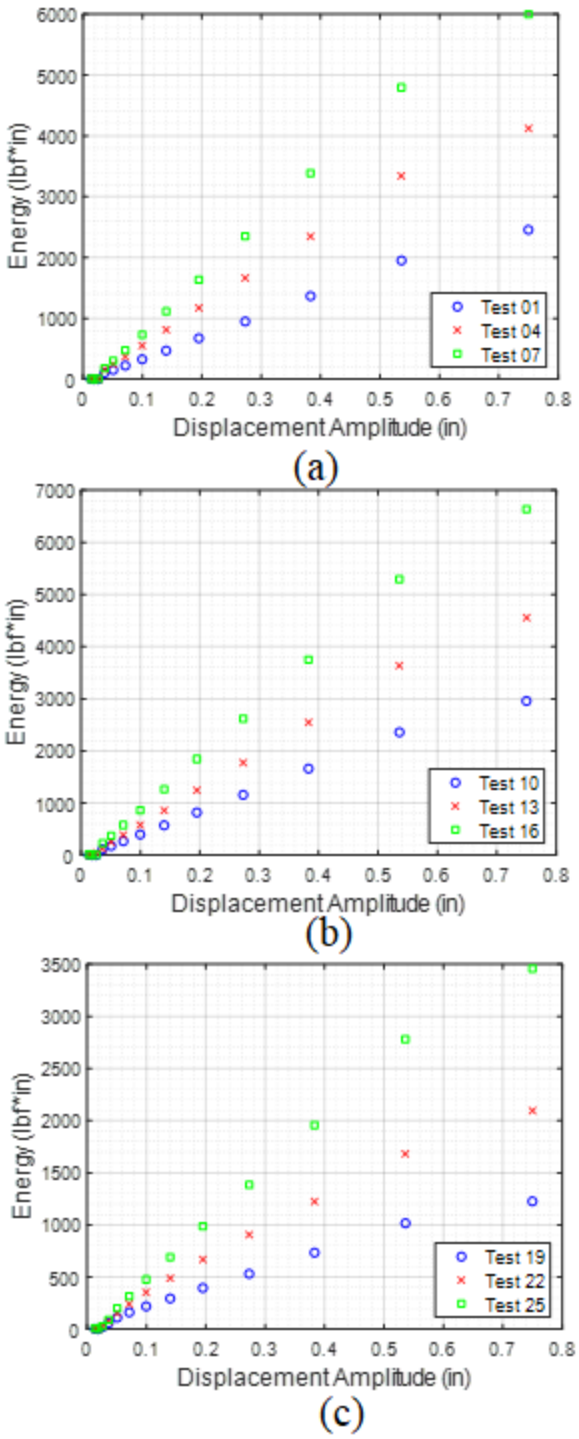

Figure 3-9. Energy Dissipated per Cycle: a) SFC with 1018 Shim, b) SFC with 304 Shim, c) AFC with 304 Shim

3.4.3 Bolt Tension

Due to the addition of Belleville washers, it was expected that the clamping force would be relatively constant. Selected clamping bolt tension histories (Figure 3-10) instead depict variation throughout testing. Table 3-3 shows initial and final bolt tension loss for each test. For the SFC-type connections with AISI 1018 steel, the variation of bolt tension was not significant. The modulation in bolt tension was greater when the bolt pretension was larger, and Test 08 was the worst test for bolt tension cycling due to loosening of one of the stationary plates during the test. For the SFC-type connections with 304 Stainless Steel, it was clear that the variation was greater than for the AISI 1018 steel but the trend on loss of bolt tension was similar. For AFC-type SBFD, the trending loss of bolt tension was greater than for either of the SFC-type connections. This deviation from anticipated behavior is due to the eccentric nature of the SBFD that attempted to disjoin the SBFD plates at the clamping bolt. The interaction of external forces on the clamping bolt during sliding that attempts to rotate the clamping bolt from its initial orientation also plays a role in this fluctuation of bolt tension. As a result, the deviation from initial clamping bolt force over the duration of testing falls out of the bounds of the Belleville washers which are intended to maintain the axial load of the clamping bolt during wear of the shim or minor translations of the bolt itself. Ultimately, this data exemplifies the effects of eccentric loading on SBFD behavior and the influence it has on maintaining clamping force. Additionally, discernable in the time histories is the increased influences of these effects as less area of the SBFD plates overlap during higher SBFD displacement amplitudes as shown by the elevated clamping bolt forces near the completion of experimental evaluation. An additional caveat remains that given the combination of forces experienced by the bolt, and the bolt being instrumented to measure axial forces solely, some of information on bolt bending is missing.

Table 3-3. Bolt Tension Results for SBFD

Case	Test	Initial Bolt Tension (kips)	Final Bolt Tension (kips)	Percentage Change
1	1	3.11	2.82	-9.2%
	2	3.00	2.90	-3.2%
	3	3.09	3.08	-0.3%
2	4	5.04	4.61	-8.4%
	5	5.12	4.83	-5.8%
	6	5.00	4.81	-3.8%
3	7	7.36	7.51	2.1%
	8	7.20	6.65	-7.7%
	9	7.04	6.80	-3.4%
4	10	2.97	2.59	-12.6%
	11	3.03	2.67	-12.0%
	12	3.00	2.75	-8.4%
5	13	5.00	4.65	-7.0%
	14	5.05	4.77	-5.6%
	15	4.96	4.70	-5.2%
6	16	6.94	6.76	-2.6%
	17	6.97	6.75	-3.2%
	18	7.07	6.68	-5.4%
7	19	3.17	1.59	-49.9%
	20	3.02	1.49	-50.8%
	21	3.04	1.69	-44.4%
8	22	5.08	2.64	-48.1%
	23	5.09	2.84	-44.3%
	24	5.12	3.37	-34.2%
9	25	7.00	4.65	-33.6%
	26	7.09	4.84	-31.8%
	27	7.03	4.29	-39.0%

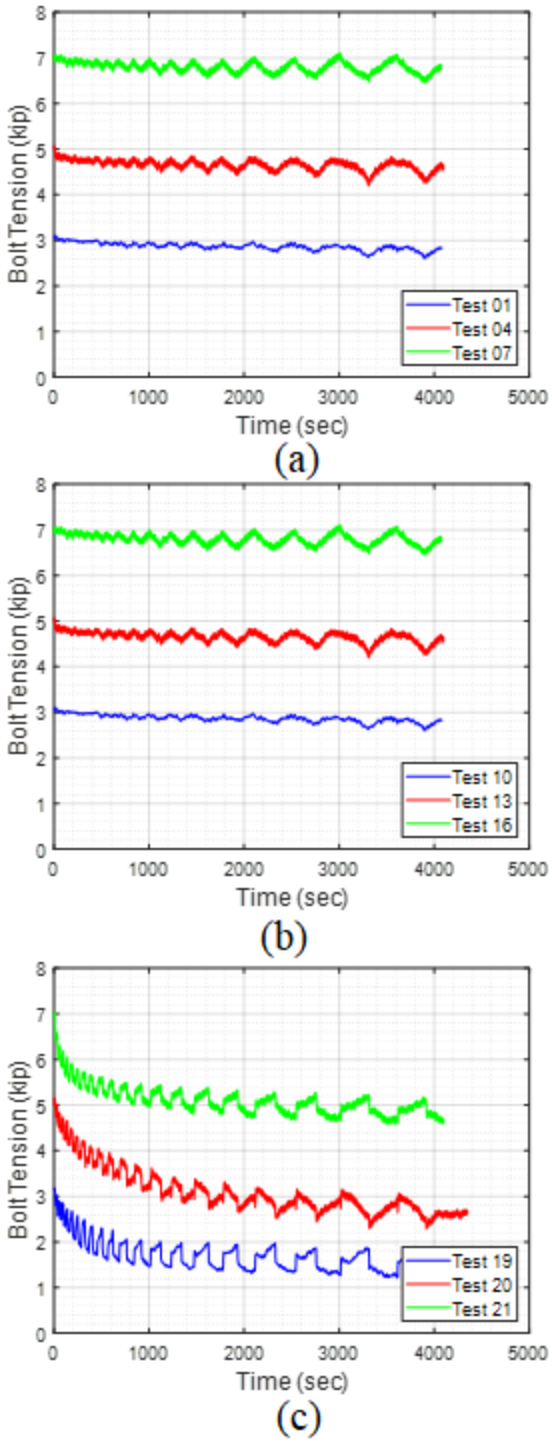

Figure 3-10. Bolt Tension History: a) SFC with 1018 Shim, b) SFC with 304 Shim, c) AFC with 304 Shim

3.4.4 Coefficient of Friction

The undulations and decrease present in clamping bolt time histories did not extend into friction coefficient calculations as evident by the uniformity of friction coefficient histories. The data processing was based on the standard Coulomb friction model, with time-based actuator load cell forces with correction factor and clamping bolt tension data used as the friction force and normal force, respectively. Figure 3-11 shows the friction coefficient of the selected test set. For the SFC-type connections with AISI 1018 steel, the variation of friction coefficient was not significant within individual tests. For the SFC-type connections with 304 Stainless Steel, the friction coefficient is also quite stable within individual tests. However, for tests with larger bolt tension (Test cases 3 and 4), there are some variations of friction coefficient between different tests which are in the same Test case. For AFC-type SBFD, the friction coefficient had more fluctuation than for either of the SFC-type connections due to the eccentricity of the test set up. The difference between individual tests within the same Test cases was also greater compared with SFC-type SBFD. Minor differences between up and down portions were found in all individual tests as well. It should be noted that the results are broken down into what is called up and down. For this case, up refers the moving plate displacing upward while down refers the moving plate displacing downward.

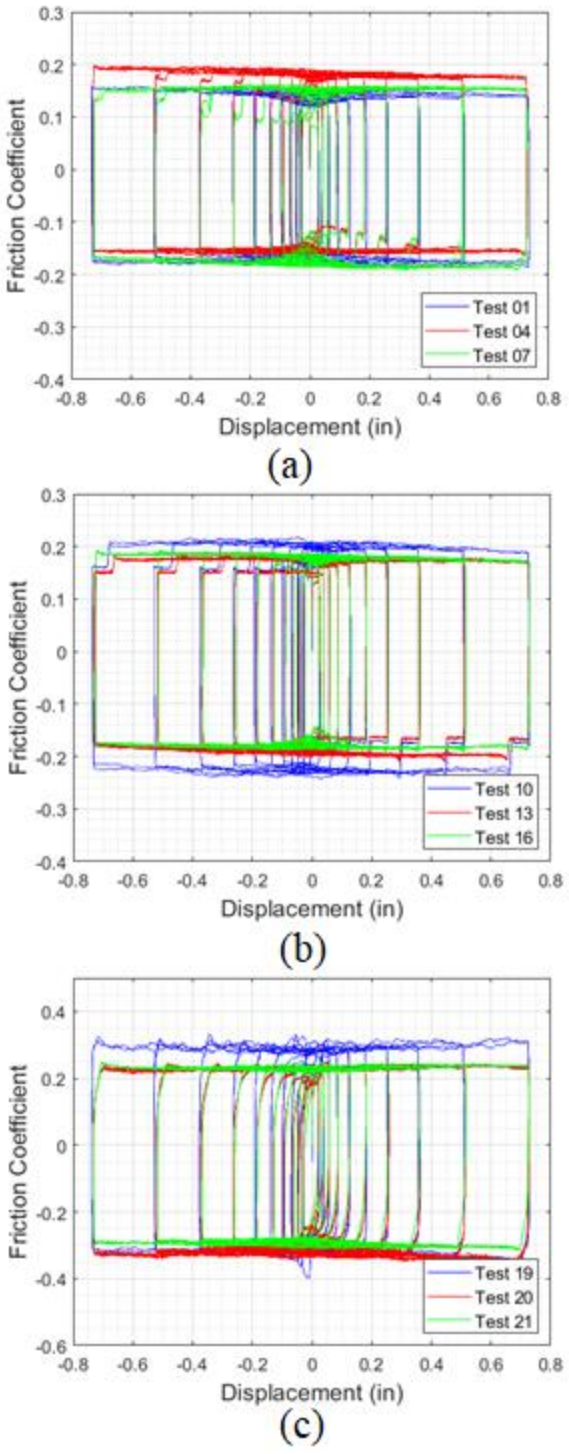

Figure 3-11. Friction Coefficient: a) SFC with 1018 Shim, b) SFC with 304 Shim, c) AFC with 304 Shim

The final tabulated values of average friction coefficient during up and down periods for SFC-type SBFD and AFC-type SBFD can be found in Tables 3-4 and 3-5. The friction coefficients in Table 4 represent the friction coefficient between friction material and shim plate only while the friction coefficients in Table 5 represents the friction coefficient between friction material and shim plate plus friction coefficient between greasy square washer and moving plate. Tabulated data shows the average coefficient of friction having only varied slightly between up and down portions of the cycle. The average friction coefficient for each individual test, each Test case and each type of SBFD were also calculated in Tables 4 and 5. The SFC-type connections with AISI 1018 steel had less fluctuation in the bolt tension as well as friction coefficient. However, the coefficient between friction material and 304 stainless steel is larger than that between friction material and 1018 steel. Therefore, 304 stainless steel was selected as shim material for the beam-column joint testing.

Table 3-4. Friction Coefficient for SFC-type SBFD

Case	Test	Up	Down	AVG (test)	AVG (Case)	AVG (Shim)
1	1	0.15	0.17	0.16	0.16	0.17
	2	0.16	0.17	0.17		
	3	0.15	0.16	0.16		
2	4	0.18	0.15	0.17	0.16	
	5	0.17	0.16	0.16		
	6	0.16	0.17	0.16		
3	7	0.18	0.18	0.18	0.18	
	8	0.18	0.18	0.18		
	9	0.15	0.18	0.17		
4	10	0.19	0.22	0.21	0.21	0.19
	11	0.20	0.22	0.21		
	12	0.20	0.24	0.22		
5	13	0.17	0.19	0.18	0.18	
	14	0.17	0.19	0.18		
	15	0.17	0.20	0.19		
6	16	0.18	0.18	0.18	0.18	
	17	0.17	0.19	0.18		
	18	0.18	0.21	0.20		

Table 3-5. Friction Coefficient for AFC-type SBFD

Case	Test	Up	Down	AVG (test)	AVG (Case)	AVG
7	19	0.33	0.27	0.30	0.28	0.26
	20	0.27	0.27	0.27		
	21	0.29	0.26	0.28		
8	22	0.22	0.31	0.26	0.26	
	23	0.20	0.29	0.24		
	24	0.22	0.31	0.26		
9	25	0.23	0.29	0.26	0.26	
	26	0.23	0.28	0.25		
	27	0.25	0.27	0.26		

Only minor degradation of the shims occurred over the duration of the experiments. The shim wear patterns are shown in Figure 3-12. The 1018 shim exhibited uniform wear throughout experimental evaluation while the friction material experienced difficulties in attempting to abrade the 304 stainless steel shims. Wear patterns also suggest that shims could have been rotating slightly during experimental evaluation because of the inconsistent clamping force. Notwithstanding, it is evident that discernable wear of the 1018 shim was taking place in contrast to the 304 stainless steel shims surfacing merely being “buffed”.

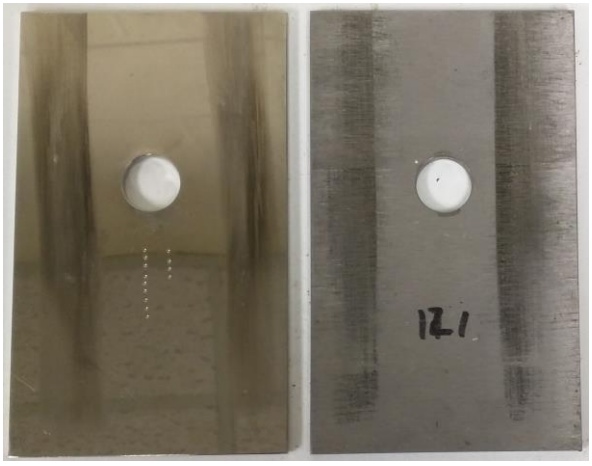

Figure 3-12. Wear Patterns on 304 Stainless Steel (left) and 1018 Steel (right) Shims Following Experimental Evaluation

3.4.5 Summary of SBFD Results

The test results for the SBFDs provide reliable and consistent behavior among all the test cases. The primary deviation of AFC-type SBFD occurs due to the connection eccentricity which resulted in prying apart of the plates and modulating the clamping force. The AFC-type SBFD were still used as BFFD in the simple shear tab connection test since an SFC-type SBFD would be much harder to erect. The eccentricity of the connection will be present in the Bottom Flange Friction Device (BFFD), however the constraint provided by the beam-column connection will limit the out-of-plane effects due to the eccentric nature of the AFC. The most important information from the tests is the friction coefficients. The friction force in the BFFD in the simple shear tab connection test will be estimated based on the friction coefficient in the SBFD tests. Although there are some variabilities in sliding forces due to effects of eccentricity, the results are still reliable since the friction coefficients were calculated as the average value of all the data points. The other important performance aspect is the energy dissipation and bolt tension which were within expectations based on theoretical calculations.

When the SBFD testing was conducted initially, only flat washers were used at the end of clamping bolts. The flat washers caused significant damage on the moving plates. In order to prevent the damage, square washer and grease was used throughout all the SBFD tests in this paper. It was later determined that negligible damage was found during the test when using a square washer even without grease. Therefore, grease was not used in the simple shear tab connection test due to the use of square washers. This is clearly preferable as using grease in the field would be problematic. In addition, 304 stainless steel shim plates will be used for beam-column tests of the Bottom Flange Friction Device.

3.5 Beam-Column Joint Tests with BFFD

The BFFD is to serve as an energy dissipating friction component with a structural steel simple shear connection to mitigate structural damage during seismic events through early phase energy dissipation. Given that the BFFD will be attached at the bottom of the beam-column interface, limiting rotational eccentricities and ensuring consistent behavior independent of direction of lateral motion is critical. Care must also be taken to prevent the BFFD from influencing existing shear tab design procedures and the rotational limits (e.g., beam flange contacting column flange).

3.5.1 Description of Specimens

An AFC-type SBFD was used as a BFFD. The slotted plate of the SBFD was attached to the bottom of the beam flange. A complementing plate with a single standard hole is attached to the column offset in a manner that would allow a steel shim to be interposed between the two plates. A single bolt with Belleville washers is used to provide bolt tension.

W14×26 and W16×31 steel sections were used during experimental evaluation. A standard three-bolt shear tab served as connection for the W14×26 section. The W16×31 beam was connected with a four-bolt shear tab.

Methodologies created by Crocker and Chambers (2004) enabled estimates of shear tab rotation up to beam binding and, correspondingly, determination of the minimum required BFFD dimensions and its optimal placement in conjunction with a shear tab. It was determined that center-to-center placement of the BFFD to the three- and four- bolt shear tabs be 9 and 10 in., respectively.

A 304 stainless steel shim was selected based on the SBFD test results. The same strain gauge instrumented bolt used in the experimental evaluation of the SBFD was used given its

efficiency in establishing and monitoring clamping bolt tension. Belleville washers were used on the clamping bolt as was done in previous tests. Lastly, use of D2017 friction material was utilized given its durability and performance in previous testing. Figure 3-13 shows a picture of simple shear tab connection in the test, a 3-D rendering of the BFFD and a picture of the device installed during experimental evaluation.

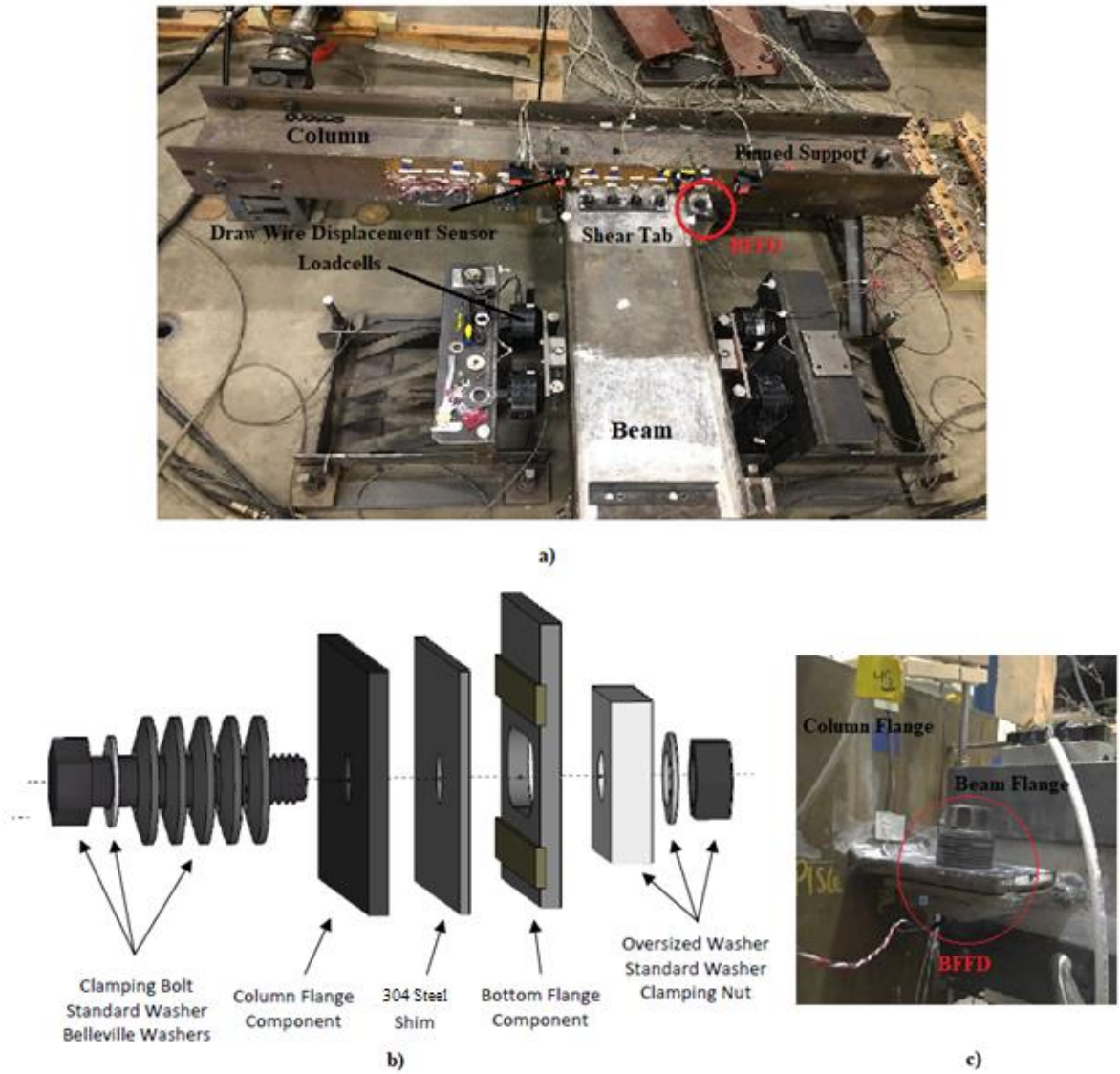

Figure 3-13. a) Photo of Simple Shear Tab Connection with BFFD, b) BFFD 3D Rendering, c) Photo of Installed BFFD

The beam bottom flange component was comprised of a 4 x 3.5 x 1/4 in. piece of 1018 cold-drawn low-carbon steel fabricated with two recesses and a slotted hole. Centered between the two recesses was an oversized slot measuring 2 in. long by 1 in. wide to provide adequate space for the clamping bolt to translate angularly in a rocking motion until binding of the beam occurred. Friction material 1/8 in. thick (Ferotec Friction D2017) was adhered in the recesses with 1/16 in. of friction material protruding above the plate surface. This provides an elevated friction surface at the interface of the steel shim and friction material on which the flange component can slide. The modulus of elasticity of D2017 is 1120 ksi and the compression strength is 18.5 ksi. The friction material was affixed in the recesses using Loctite EA E-120HP adhesive in a procedure that involved applying a thin layer of adhesive to contacting surfaces, before clamping the surfaces together to open-air cure a minimum of 24 hours as recommended by the manufacturer. The position of the recesses was primarily influenced by the necessity for even distribution of clamping forces, in addition to furnishing the clearance necessary for welds and the column flange component. The column flange component of the device was made from A36 steel plate dimensioned 5 x 3 x 1/4 in. A 5/8 in. through-hole located off-center along the horizontal centroidal axis allowed for BFFD components to be clamped together by a bolt. The selection of a standard size through-hole also served to restrain movement of the bolt during sliding of the beam flange component. The edges of the column flange component extended outward only a minor amount beyond the beam flange component. Steel shims measuring 3 x 4.5 x 1/8 in. were fabricated for the BFFD using 304 stainless steel. The shims were fabricated from the same piece of 304 steel purchased to fabricate shims for the SBFD. A 5/8 in. ASTM F3125 A325 structural steel bolt instrumented with a strain gauge, was used again to join components of the BFFD with the desired bolt tension.

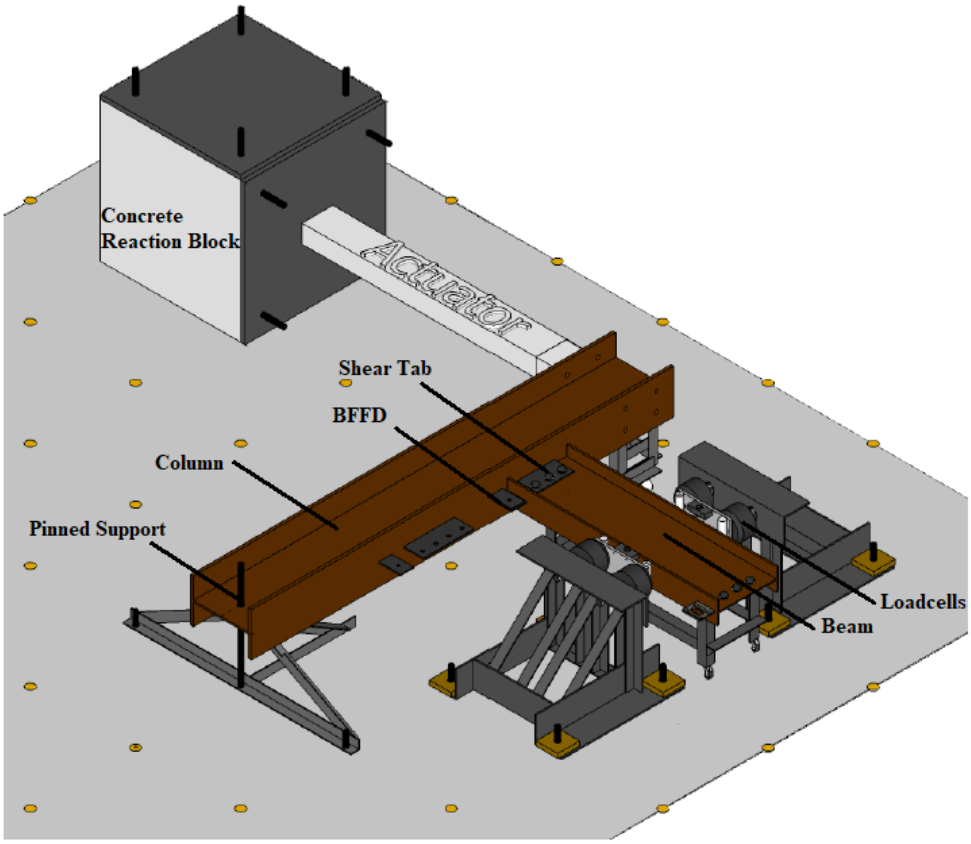

Figure 3-14. Experimental Setup to Evaluate BFFD

3.5.2 Test Set-up

The experimental setup for BFFD evaluation (Figure 3-14) was designed with the capability to test the BFFD in multiple configurations through use of a single column and two beams. Featured in this setup was a reusable eight-foot long W14×61 steel column with two shear tabs welded on the outside of both column flanges. Three-bolt shear tabs were located on the column flange faces opposing each other, while the four-bolt shear tabs were located below in an identical manner. In addition to the shear tabs, the column flange components of the BFFD were welded 9 and 10 in. below the center of the three-bolt and four-bolt shear tabs, respectively. A hole near the bottom of the column in the web allowed a rod to be inserted to establish the center of rotation, while holes in both flanges near the top allowed for actuator attachment and a rolling

vertical support. A W14×26 and W16×31 steel section, both 4 ft. in length, served as beams to be connected to the three-bolt and four-bolt shear tabs, respectively. Located on both ends of the two beams were bolt holes arranged in a configuration appropriate for connection to the corresponding shear tab. An actuator mounted to the top of the column was used to induce rotation about a fixed-point located at the bottom of the column. At this fixed point, a rod secured to the strong floor would project through a hole at the bottom of the beam, where thrust and sleeve bearings present at the interface would enable rotation. Motion of the beam would be permitted exclusively in the horizontal direction through restraint imposed by reaction frames. This would result in the rotation of the column and connection, while the beam would slide horizontally along rollers anchored to the reaction apparatuses. Rolling carts were also placed underneath the top and midpoint of the column, in addition to underneath the beam, to maintain the height of the test setup components and provide support during testing.

3.5.3 Monitored Parameters and Instrumentation Details

Multiple response parameters were monitored during the tests. The prime variables which need to be measured accurately were the rotation of the beam-column connection and the applied forces due to the imposed deformation. The moment on the beam-column connection can be calculated using the force in the load cells and the distance between load cells and the column flange. Four load cells were placed in groups of two and attached to reaction frames. This allowed for the measurement of forces imparted by the beam as it alternated between bearing on reaction frames on the two sides of the beam during bi-directional displacement. This configuration allowed simple calculations to determine the forces and moments required in quantifying energy dissipation through use of elementary engineering mechanics. The loadcells were attached using threaded rods fed through slotted holes on the side of the reaction frame, with nuts used to clamp

the rods to the frame. Through this method, location of the loadcells and attached roller could be adjusted in accordance with the dimensional requirements imposed by the beam to be tested. The rollers minimized the axial force in the beam while allowing for bearing to generate moments. The roller was a polished 4140 steel rod with ends drawn down for press into pillow block bearings with a steel plate backing which allowed for attachment to loadcells. The rotation of frame components was measured through measuring gap distance between beam top flange and column surface and gap distance between beam bottom flange and column surface using analog Micro-Epsilon WDS-P60 draw-wire potentiometers (draw-wire sensors). Draw-wire sensors were located on both sides of the beam top and bottom flanges to measure gap distance between beam and column flanges during tests. Figure 3-15 shows the layout of draw-wire sensors and loadcells and the corresponding picture in the experiment. Bolt tension on both the shear tab and BFFD were monitored during testing. The bolt tension on the shear tab started around 30 kips which corresponds with minimum full pretension of the 3/4 in diameter ASTM F3125 A325 bolts. The initial bolt tension of the BFFD varied based on different test cases.

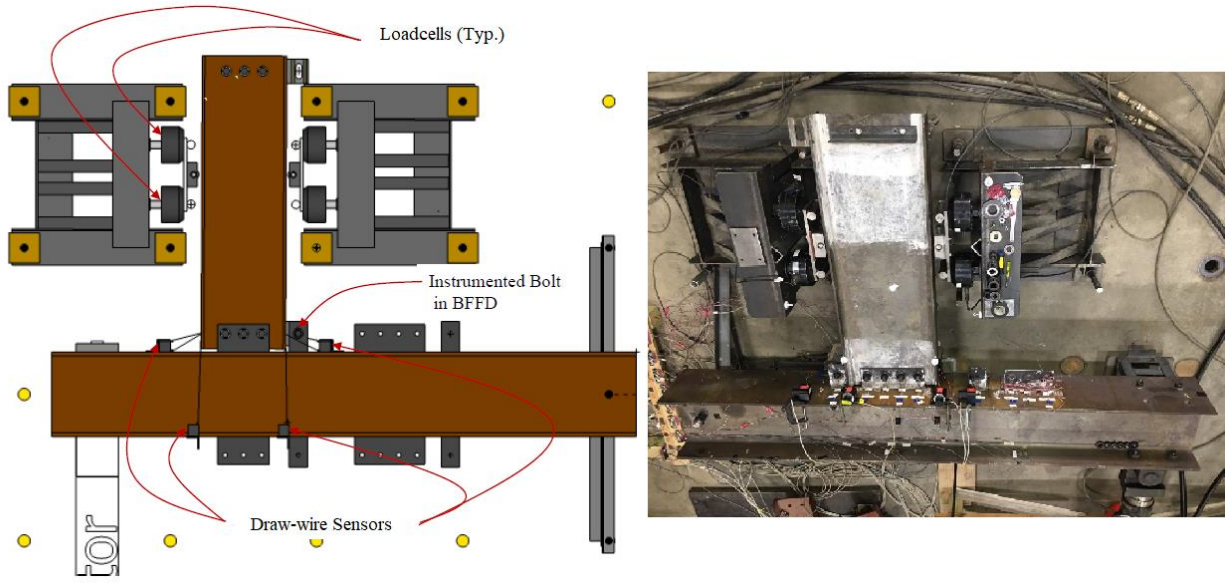

Figure 3-15. Sketch and Photo of Layout of Experimental Set-up

3.5.4 Loading Protocol

Similar to the SBFD tests, the loading protocol was the interim protocol I-quasi-static cyclic testing from FEMA 461 (ATC, 2007) standard. For the three-bolt shear tab, the initial amplitude is 0.05 in., and the final target amplitude is 3 in. while initial amplitude is 0.04 in., and the final target amplitude is 2.5 in. for four-bolt shear tab (Figure 3-16). The loading rate was 0.02 in./sec which was slow enough to minimize dynamic effects and capture the monitored variables.

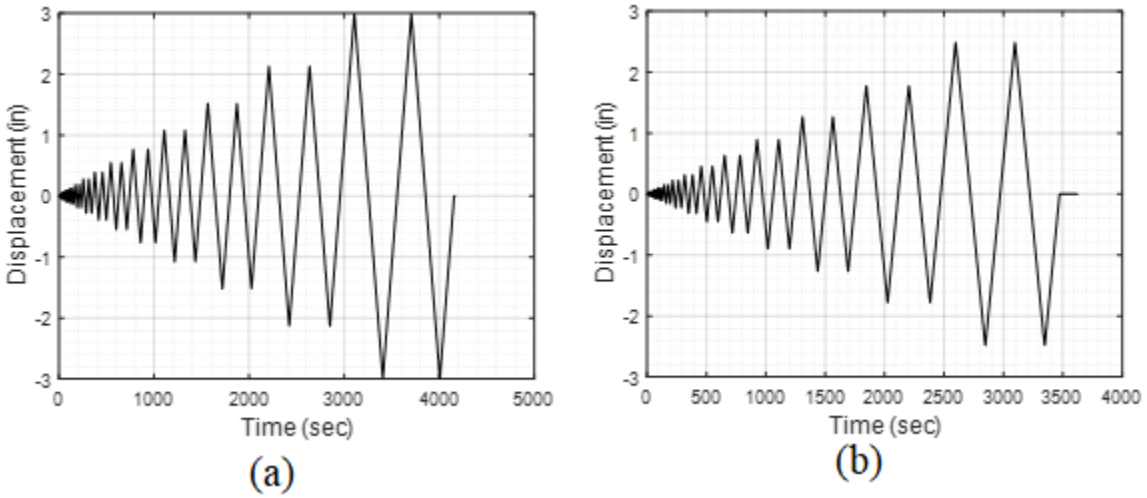

Figure 3-16. Displacement Protocol for BFFD a) Three-Bolt Connection, b) Four-Bolt Connection

3.5.5 BFFD Test Cases

Three-bolt and four-bolt connections with and without a BFFD were tested. Six test cases total were completed for the beam-column joint. Three repetitions were done for each test case to assess repeatability. Table 3-6 shows all test cases with detailed test configurations. Test cases were ordered in a manner such that connections were first evaluated without contribution of the BFFD so that baseline shear tab measurements could be obtained. Succeeding cases were performed with the inclusion of the BFFD configured to activate at the preliminary friction forces of 5 and 9 kips. The preliminary activation force which was the slip force of the BFFD can be calculated through friction coefficient and bolt tension which was monitored by the bolt strain

gauge. The friction coefficient between friction material and shim plate is assumed as 0.19 while the friction coefficient between square washer and moving plate connected with beam flange is assumed as 0.3. Therefore, the corresponding bolt pretension load is 10.2 kips and 18.4 kips for 5-kip BFFD and 9-kip BFFD, respectively.

Table 3-6. BFFD Test cases

Case	Test	Connection	Targeted Slip
B1	1	Three-Bolt	without BFFD
	2		
	3		
B2	4		5-kip
	5		
	6		
B3	7		9-kip
	8		
	9		
B4	10	Four-Bolt	without BFFD
	11		
	12		
B5	13		5-kip
	14		
	15		
B6	16		9-kip
	17		
	18		

3.6 BFFD Experimental Results and Discussion

The focus of this section is the presentation and discussion of results obtained from experimentally evaluating the BFFD. Firstly, plotted hysteretic data will be introduced that provides a general overview of BFFD behavior. Following this general overview, plotted data is used in quantifying properties of the BFFD related to energy dissipation. In addition, results involving initial stiffness of the beam-column connection, and loss of bolt tension are discussed.

3.6.1 Hysteretic Data

Moment-rotation data from Test cases B1, B2 and B3 is shown in Figure 3-17, which evaluated the beam-column joint when configured as a three-bolt shear tab with BFFD activation force of 0 kip (without BFFD), 5 kips and 9 kips. One common characteristic in the plot occurs prior to significant slipping of the connection. A cluster of loops form at the center of all the hysteresis plots because the connection is subjected to lower displacement amplitudes. Slip at these lower displacement amplitudes is minor, if occurring at all, and difficult to discern from elastic deformation of components within both the connection and experimental setup. Then slip becomes more pronounced. The progression from slip to sliding occurs throughout testing marked by a decrease in slope of the moment-rotation curve. There are also many occurrences of increases in slope after slipping has occurred. This is primarily due to bolts in the shear tab connection coming into bearing with the edge of the holes at higher levels of deformation. This type of behavior is seen in all the plots in the bottom left quadrant. Non-symmetric behavior can also be seen throughout the results. The connection should theoretically behave in a symmetric fashion, however much of the data shows slight non-symmetry in the response. This lack of symmetry results from several potential sources. The variation in rotation often stemmed from the initial gap between the beam and load cells between test cases following reconfiguration. Furthermore, fabrication defects, such as the shear tab not being welded plum with the column, and positioning of bolts during erection are present in the tests. Figure 3-17 shows very good agreement between the different tests within same Test case. Tests 02, 05, and 08 were selected to represent Test cases B1, B2 and B3, respectively. Figure 3-17(d) shows the comparison among three different configurations for the three-bolt shear tab connection. The moment strength of shear tab connection with 5-kip BFFD was about 40 kip-in larger (36% increase) compared with bare shear

tab connection while the moment strength of shear tab connection with 9-kip BFFD was about 60 kip-in larger (54% increase) compared with the bare shear tab. The increase in joint stiffness between the bare shear tab and those with a BFFD is also discernible in Figure 3-17(d). The increase in moment strength is approximately equal to 75% of the friction force in BFFD times the distance between the center of shear tab and the BFFD clamping bolt (9 in.).

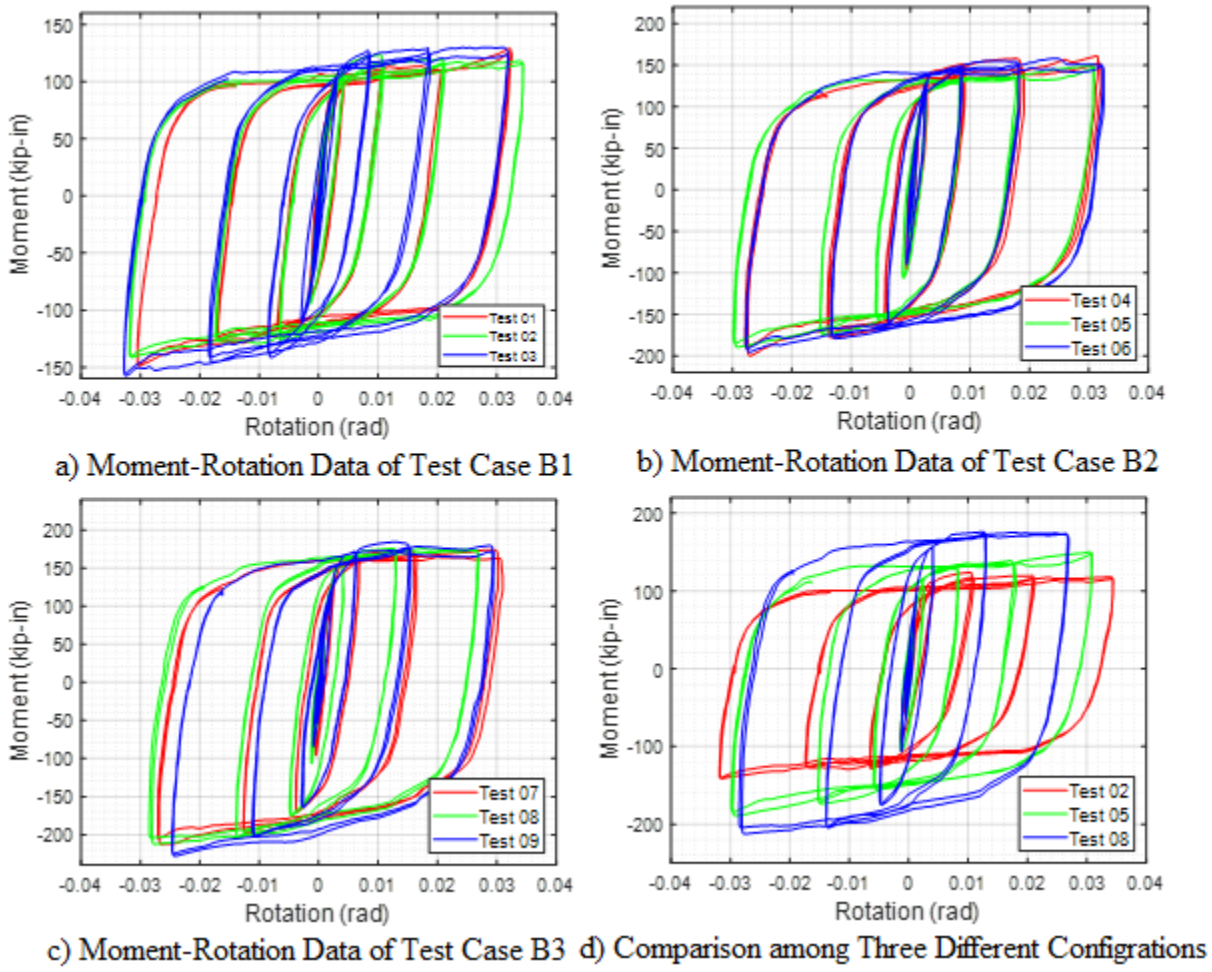

Figure 3-17. Moment-Rotation Response of Three-Bolt Shear Tab Connection

The results of the four-bolt shear tab testing with and without the BFFD is shown in Figure 3-18. Tests 11, 15, and 17 were selected to represent Test cases B4, B5 and B6, respectively. Figure 3-18(d) shows the comparison among three different configurations for the four-bolt shear tab

connection. The result of Test 10 (Figure 3-18(a)) and Test 13 (Figure 3-18(b)) shifted to the left compared with two other repeated tests. That's because the initial position of beam in these two tests are not perfectly perpendicular to the column and the gap between beam and loadcells were too big. The moment strength of the shear tab connection with a 5-kip BFFD was 40 kip-in larger (15% increase) than the bare shear tab connection. This behavior is consistent with the results of the three-bolt tests as the single BFFD bolt represents a smaller percentage of the four-bolt strength. The increase in moment strength is also approximately equal to 75% the friction force in BFFD times the distance between the center of shear tab and the BFFD clamping bolt (10 in.). However, the increase in strength from 5-kip BFFD shear tab connection to the 9-kip BFFD is insignificant. The reason the difference is insignificant is because when the activation force is 9 kips, the corresponding clamping force is about 18 kips. This high clamping force caused the shim plate in BFFD to bend slightly during the test which reduced the normal force between the friction material and shim plate significantly which reduced the strength of the 9-kip BFFD connection from what it should have been. Once the connection was disassembled the damage to the shim plate was identified and the reason behind the inconsistency was clear. The shim plate bending which caused results between the 5kip and 9kip BFFD to be insignificant was a local effect on the shim plate in the BFFD during the tests. A thicker shim plate should be used to carry high bolt tension. The moment strength provided by all the connections were less than 20% of the fully plastic moment of the beam at a rotation of 0.02 rad which means the simple shear tab connections with BFFD can be still considered as simple connections.

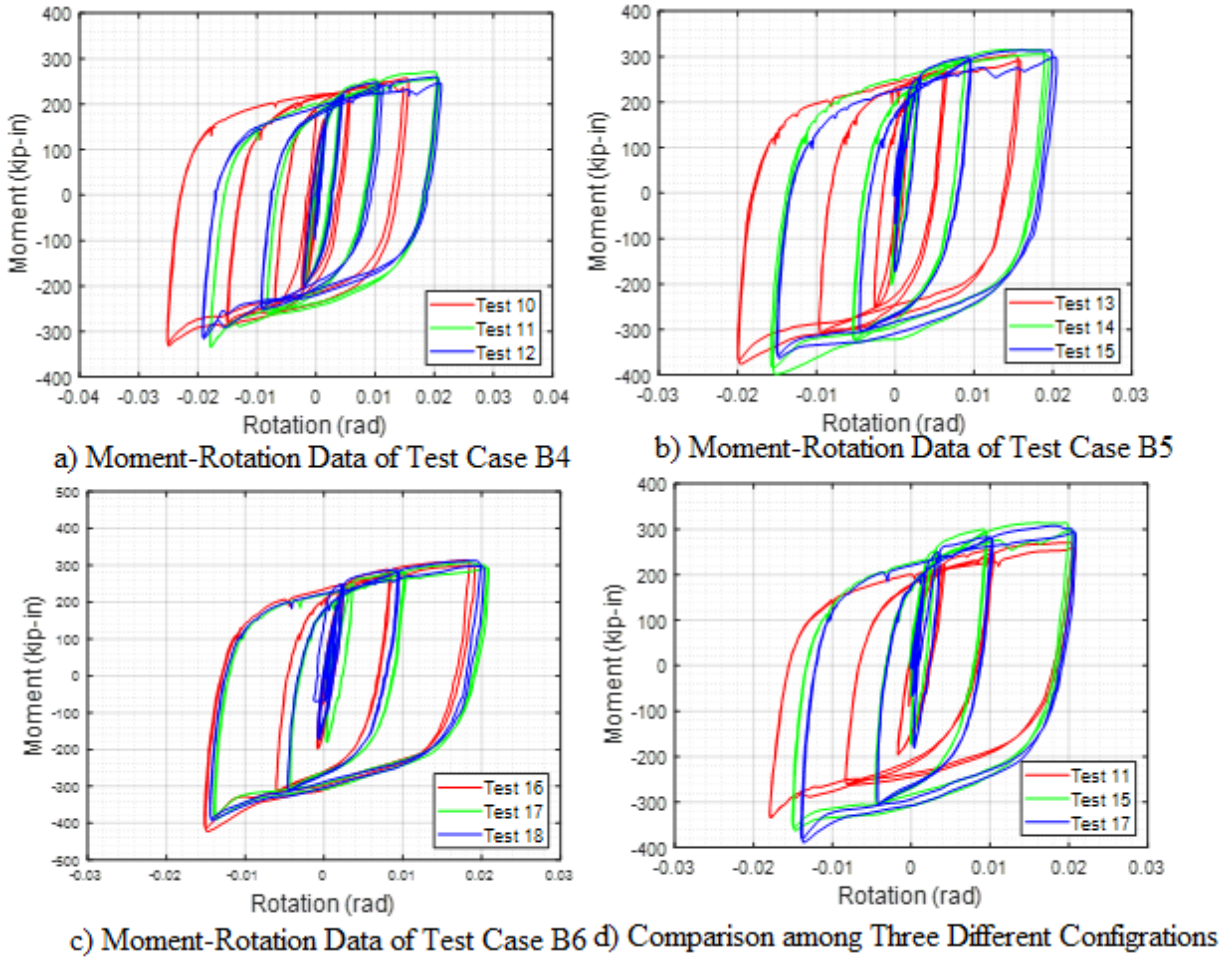

Figure 3-18. Moment-Rotation Data of Four-Bolt Shear Tab Connection

3.6.2 Initial Stiffness

With the experimental moment rotation results of three-bolt and four-bolt shear tab connections with and without BFFD, initial stiffness can be calculated to help understand the performance. Due to the fact that there is not a well-defined yield point, calculation of the initial stiffness and the slip rotation was not trivial. For each time increment of response, both previous stiffness and current stiffness were calculated. If the current stiffness is less than half of previous stiffness, the corresponding moment and rotation was defined as slip moment and slip rotation. The initial stiffness was calculated as slip moment divided by slip rotation (secant stiffness). Table 3-7 shows the initial stiffness for all the tests. The initial stiffness of BFFD shear tab

connections was larger than the bare shear tab connection. Initial stiffness of the 9-kip BFFD connection was slightly larger than that of the 5-kip BFFD connection. The lower slip rotation means the BFFD was activated earlier than the bare shear tab in the displacement protocol. The higher slip force in the BFFD (i.e., 9-kip vs 5-kip) resulted in a larger slip rotation. The trend of initial stiffness and slip rotation is the same for three-bolt and four-bolt shear tab connections. The data has demonstrated that these tests have a reasonable amount of variability. This is due to several different effects. Unlike a fully resistant moment connection or a yielding brace, the limit states for these simple connections are relying on friction initially until slip occurs. Friction has more uncertainty in general than material properties as it depends on the clamping force and the surface conditions. It can also depend on the tolerances related to the connection fit-up.

Table 3-7. Slip Moment, Slip Rotation and Initial Stiffness for Beam-Column Tests

Case	Test	Slip Moment (kip-in)	Slip Rotation (rad)	Initial Stiffness (10^4*kip-in/rad)	AVG Initial Stiffness (10^4*kip-in/rad)
B1	1	65	0.0011	5.87	4.99
	2	72	0.0015	4.81	
	3	51	0.0012	4.28	
B2	4	42	0.00055	7.68	7.25
	5	58	0.00088	6.61	
	6	35	0.00047	7.46	
B3	7	66	0.00096	6.91	7.41
	8	93	0.0012	7.76	
	9	75	0.00099	7.56	
B4	10	52	0.00064	8.18	9.22
	11	53	0.00057	9.34	
	12	46	0.00045	10.1	
B5	13	45	0.00033	13.6	14.6
	14	45	0.00031	14.4	
	15	59	0.00037	15.8	
B6	16	63	0.00034	18.4	17.0
	17	55	0.00037	14.9	
	18	48	0.00027	17.6	

3.6.3 Energy Dissipation

Figure 3-19 depicts the energy dissipated versus accumulated rotation for test cases including and excluding the BFFD. The same set of tests selected previously were used to represent six different test cases. A significant increase in energy dissipation was evident with the addition of the BFFD to shear tab connections. For the three-bolt shear connection, the choice of BFFD

activation force has similar significant effect on the overall energy dissipated by the connection. For the four-bolt shear connection, only the bare shear tab and the 5-kip BFFD data are presented and show a similar pattern to the three-bolt test. The result of 9-kip BFFD data was not shown due to the damage of shim plate which caused inconsistent results.

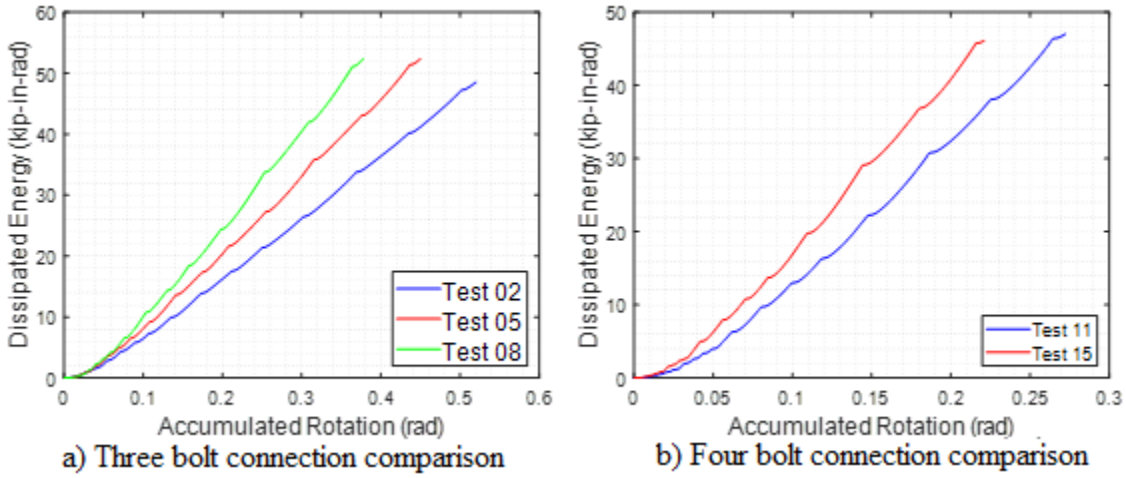

Figure 3-19. Energy Dissipation for Shear Tab Connection with and without BFFD

3.6.4 Loss of Bolt Tension

The tension in the BFFD clamping bolt and the shear tab bolts were monitored during the tests. The difficulties experienced in maintaining consistent clamping bolt tension for the AFC-type SBFD did not continue with the BFFD clamping bolt. Data in Table 3-8 portrays an average decrease of 11.6% between initial and final clamping bolt tension in all test cases. The decline of clamping bolt tension throughout experimental evaluation likely stems from a combination of events occurring. Previous findings (Yeung, Zhou, Khoo, Clifton, & MacRae, 2013) show the complex combination of moment, shear, and axial forces experienced by the bolt as it meets surrounding edges significantly affects bolt tension throughout the duration of sliding. Likely responsible for most of the losses in clamping bolt tension was subtle wearing of the steel shims and the propagation of wearing surface particles. The degradation of steel shims during evaluation

of individual test case instances remained small. Nonetheless, the occurrence of any loss or propagation of wear particles across wearing surfaces would result in noticeable decreases of clamping bolt tension. Additional factors potentially contributing to this effect include the undulations present in the concrete floor over which the beam rolled causing an uneven distribution of forces across the bolt. Lastly, imperfections in the positioning of components during fabrication presumably resulted in uneven surface pressure throughout rotation.

Table 3-8. BFFD Clamping Bolt Tension

Case	Test	Initial Bolt Tension (kips)	Final Bolt Tension (kips)	Percentage Change
B2	4	11.6	11.0	-5.6%
	5	11.1	9.9	-10.8%
	6	11.3	10.1	-10.8%
B3	7	18.9	15.7	-16.9%
	8	18.2	15.2	-16.6%
	9	18.5	16.4	-11.2%
B5	13	10.7	9.8	-8.0%
	14	10.9	9.9	-9.4%
	15	11.2	10.0	-11.3%
B6	16	18.1	15.4	-14.6%
	17	17.7	15.9	-10.3%
	18	18.7	16.2	-13.4%

The loss of bolt tension on the shear tab is more significant than that on BFFD. The reason for this is similar to the clamping bolts on BFFD. When the connection has a large rotation, the bolts on the shear tab will start to bear on the edge of the bolt holes. The combination of moment, shear, and axial forces will significantly loosen the bolts, especially the top and bottom bolts. Test 07 and Test 15 were selected to represent the three-bolt connection and four-bolt connection,

respectively. Bolt tension histories (Figure 3-20) depict fluctuations in all bolt tension throughout the duration of the experimental evaluation. The variation and loss of bolt tension of edge bolts on the shear tab is much larger than that of middle bolts. Compared with bolts on the shear tab, the fluctuation and loss of bolt tension for the BFFD is relatively small.

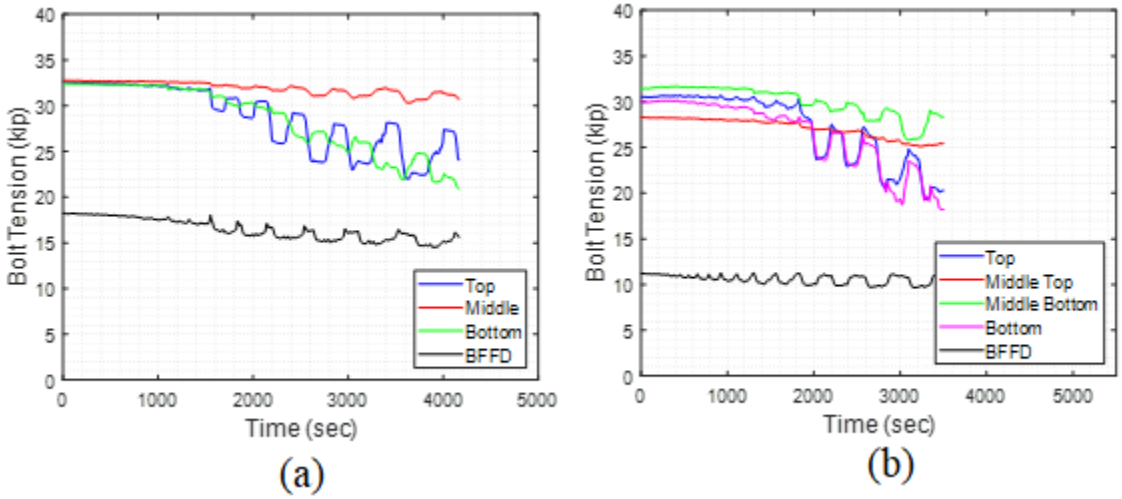

Figure 3-20. Typical history of Bolt Tension in Beam-Column Test: a) Test 07, b) Test 15

3.7 Conclusions and Future Work

This paper introduces the concept of the Bottom Flange Friction Device for supplementing energy dissipation in steel structures by including the gravity system connections in energy dissipation without any damage to the structural system. The SBFD tests demonstrated the behavior of AFC-type connections as less stable than SFC-type connections due to the inherent eccentricity. Therefore, the loss of bolt tension on AFC-type shear connection is much greater than a similar SFC-type connection. The friction coefficient between D2017 friction material and 304 stainless steel shim plate is larger than that between D2017 friction material and 1018 steel shim plate which means more energy can be dissipated using a 304 stainless steel shim plate.

The experimental testing of the shear tab connection with and without the Bottom Flange Friction Device showed that the connection with the BFFD dissipated greater amounts of energy

and had a higher strength than the bare shear tab connection. It also showed that the initiation of slip of the BFFD occurred before the shear tab indicating that the BFFD activated early in the deformation pattern to dissipate energy. The lower the slip force of the BFFD, the earlier the slip occurred, although even the higher BFFD slip force still occurred before the bare shear tab. The results did show that the BFFD did not negatively impact the performance of the shear tab as the connection experienced significant rotation without failure of the shear tab or bearing of the friction device bolt. From a percentage point of view, for three-bolt shear tab connections, the impact of activation force of BFFD is significant. For four-bolt shear tab connection, the impact of activation force was not as significant due to the base moment strength (moment strength of bare simple shear tab connection) being larger and the damage of the shim plate. However, the increase in moment strength can be estimated by 75% the friction force in the BFFD times the distance between center of shear tab and the BFFD clamping bolt. Fluctuation and loss of bolt tension happened to all the bolts during the tests, especially the edge bolts on the shear tab. These results indicate the behavior of the BFFD is as expected with initiation of slip prior to full inelastic response.

The results from these tests will be critical for the full assessment of the impact of enhanced energy dissipation in the gravity system. The experimental results from these tests will be used to validate high fidelity finite element models that will be used to explore the important parameters to response and develop backbone curves that will be used in case study structural analysis models. These case study buildings will be analyzed under a suite of earthquake ground motions of various levels to assess the impact of enhanced energy dissipation on system response.

References

ATC. (2007). *Interim Testing Protocols for Determining the Seismic Performance Characteristics of Structural and Nonstructural Components.* Redwood City, California: FEMA.

Clifton, G. C. (2005). *Semi-rigid joints for moment-resisting steel framed seismic-resisting systems.* PhD Dissertation, The University of Auckland New Zealand, Auckland, New Zealand.

Crocker, J. P., & Chambers, J. J. (2004). Single Plate Shear Connection Response to Rotation Demands Imposed by Frames Undergoing Cyclic Lateral Displacements. *Journal of Structural Engineering*, 934-941.

Erochko, J. A. (2013). *Improvements to the Design and Use of Post-Tensioned Self-Centering Energy-Dissipative (SCED) Braces.* Toronto, Canada: University of Toronto.

Flores, F. X., Charney, F. A., & Lopez-Garcia, D. (2016). The influence of gravity column continuity on the seismic performance of special steel moment frame structures. *Journal of Constructional Steel Research*, 217-230.

Francavilla, A., Latour, M., Piluso, V., & Rizzano, G. (2020). Design criteria for beam-to-column connections equipped with friction devices. *Journal of Constructional Steel Research*.

Golondrino, J. C., MacRae, G. A., Chase, J. G., Rodgers, G. W., & Clifton, C. G. (2012). *Behavior of Asymmetrical Friction Connections Using Different Shim Materials.* Christchurch, New Zealand: New Zealand Society for Earthquake Engineering.

Golondrino, J. C., MacRae, G. A., Chase, J. G., Rodgers, G. W., & Clifton, C. G. (2013). *Application of Brake Pads on Asymmetrical Friction Connection (AFC).* Wellington, New Zealand: New Zealand Society for Earthquake Engineering.

Grigorian, C. E., & Popov, E. P. (1994). *Energy Dissipation with Slotted Bolted Connections (Report UCB/EERC-94/02).* Berkeley, CA: Earthquake Engineering Research Center.

Guo, T., Song, L., & Zhang, G. (2011). Numerical simulation for the seismic behavior of self centering steel beam-column connections with bottom flange friction devices. *Earthquake Engineering and Engineering Vibration*, 229-238.

Khoo, H.-H. (2013). *Development of the low damage self-centering Sliding Hinge Joint.* PhD Dissertation, The University of Auckland New Zealand, Auckland.

Khoo, H.-H., Clifton, C., Butterworth, J., MacRae, G., & Ferguson, G. (2012). Influence of Steel Shim Hardness on the Sliding Hinge Joint Performance. *Journal of Construction Steel Research*, 119-129.

Latour, M., Aniello, M. D., Zimbru, M., Rizzano, G., Piluso, V., & Landolfo, R. (2018). Removable friction dampers for low-damage steel beam-to-column joints. *Soil Dynamics and Earthquake Engineering*, 66-81.

Liu, J., & Astaneh-Asl, A. (2000). *Cyclic Tests on Simple Connections, Including Effects of the Slab.* Berkeley, CA: SAC Joint Venture.

Schnorr Corporation. (2003). Handbook for Disc Springs. Ann Arbor, Michigan, United States.

Tsai, K., Chou, C., Lin, C., Chen, P., & Jhang, S. (2008). Seismic self-centering steel beam-to-column moment connections. *Earthquake Engineering and Structural Dynamics*, 627-644.

Wolski, M., Ricles, J. M., & Sause, R. (2006). Seismic resistant self-centering steel momentresisting frame with bottom flange friction devices. *Proceedings of the 5th international conference on behavior of steel structuresin seismic areas* (pp. 481-487). STESSA.

Wolski, M., Ricles, J. M., & Sause, R. (2009). Experimental Study of a Self-Centering Beam–Column Connection with Bottom Flange Friction Device. *Journal of Structural Engineering*, 479-488.

Yeung, S., Zhou, H., Khoo, H., Clifton, G., & MacRae, G. (2013). Sliding shear capacities of the Asymmetric Friction Connection. *Proceedings of the 2013 NZSEE Conference.* Wellington, NZ: New Zealand Society for Earthquake Engineering.

Zhang, A., Zhang, Y., Li, R., & Wang, Z. (2016). Cyclic behavior of a prefabricated self-centering beam-column connection with a bolted web friction device. *Engineering Structures*, 185-198.

Chapter 4 Numerical Evaluation of Strength and Energy Dissipation of Modified Shear Tab Connections

Hongyang Wu, Graduate Research Assistant, Department of Civil and Environmental Engineering, 238 Harbert Engineering Center, Auburn University, Auburn, AL 36849, hzw0035@auburn.edu

Justin D. Marshall, Associate Professor of Civil and Environmental Engineering, 238 Harbert Engineering Center, Auburn University, Auburn, AL 36849, jdmarshall@auburn.edu

Abstract

Based on current design criteria, lateral loads are resisted only by the lateral force resisting system. The energy generated by seismic events is designed to be dissipated through plastic deformation in specific ductile components to meet life-safety requirements. Shear tab connections designed as part of gravity load system are assumed as pinned and ignored as contributors to the lateral load resisting system. Previous research has shown that simple connections can dissipate energy during significant events. Enhancing the energy dissipation of these connections could provide improved performance for seismic events as well as for significant windstorms. This paper reports the second phase of a research project focused on enhancing the energy dissipation of simple connections to improve performance of steel frame structures. The proposed connection modifications include adding a Bottom Flange Friction Device (BFFD) and increasing the connection depth. Previous experimental testing is validated with rigorous finite element modeling to enable further evaluation of important parameters of the baseline and enhanced simple connections. A suite of numerical shear tab connection models with different configurations were built based on the same modelling method used in the test validation models. A series of 31 pushover analyses were used to investigate the engineering characteristics of the suite of shear tab

connections. The results were also compared with a previously generated simplified moment-rotation model. In the end, a prediction model for simplified moment-rotation curves for shear tab connections with different configurations is proposed based on the previous model and the parametric study results. The simplified moment-rotation curves can be utilized for analyzing the impact of shear tab connections on the lateral response of steel structures.

Keywords: Shear tab connection, Energy dissipation, Bottom flange friction device, Finite element simulation

4.1 Introduction

In seismic design of steel structures, moment frames and braced frames are the most common lateral load resisting systems. The shear tab connection which is the most common beam-column joint in the gravity load system is often designed to carry gravity load only without any contribution to the lateral load resisting system. Bolted shear tab connections can sustain bending moment as the beam end rotates relative to the support. A series of cyclic tests on simple shear connections with and without the concrete slab performed by Liu and Astaneh (2000) proved that simple shear tab connections have reliable moment strength and ductility capacity while maintaining gravity load capacity. Although the moment strength of shear tab connections is much less than that of moment and braced frames, it can still dissipate energy during earthquakes and windstorms, especially as the number of shear tab connections is much greater than that of the lateral load resisting components. Therefore, it would be beneficial to account for these shear tab connections as supplemental energy dissipators in performance-based design or when assessing functional recovery. Several modifications to shear tab connections can be made to increase the positive effect on dynamic response of steel structures. In this paper, two low-cost modifications are considered and analyzed. One modification is the addition of a Bottom Flange Friction Device

(BFFD). The other is increasing the bolt spacing on the shear tab or alternatively worded, increasing the connection depth without increasing the number of bolts. Both modifications increase the moment strength and energy dissipation capacity of shear tab connections. Although including the shear tab connections in the model seems to have a promising positive influence as supplemental energy dissipator in steel structures, they are often neglected in lateral load design and assessment due to the lack of information regarding the expected connection behavior (Flores, Charney, & Lopez-Garcia, 2016).

The overall research objective is to improve the energy dissipation capacity of steel frames by supplementing the lateral system with the gravity system. The energy dissipation from the gravity system can be activated in small and moderate earthquakes which would result in energy dissipation without damage to the structure. Enhancing energy dissipation would serve to decrease demands on the structure and improve performance of steel structures in small, moderate and severe earthquakes as well as significant wind events. A previous paper (Wu & Marshall, 2022) reported the experimental results of shear tab connections with and without a Bottom Flange Friction Device. This paper continues the research effort by utilizing the experimental test results in rigorous numerical models that investigate the important parameters of baseline shear tab models as well as shear tabs with the BFFD and with wider bolt spacing. The simple shear tab connection itself is considered as the baseline model.

Liu and Astaneh (2000) conducted a series of experimental tests on shear tab connections. A shear tab moment-rotation prediction model was proposed based on their experimental results. However, two modifications discussed in this paper have not been evaluated. Using numerical simulation results, shear tab connection behavior can be investigated in detail. The concept of traditional seismic force resisting systems for steel structures is to dissipate energy through plastic

deformation of certain structure elements in lateral system, for instance, reduced beam section (RBS) moment connections and buckling-restrained braces (BRB). The plastic deformation of these elements might require large repair costs in the aftermath of a seismic event. Therefore, it will be valuable to determine the impact of modifying shear tab energy dissipation on the response of the structural system. The intent of this paper is numerical evaluation of the shear tab connections as supplemental dissipators. Figure 4-1 shows the shear tab connection with different configurations. The conventional bolt space on the shear tab is 76 mm. If sufficient space exists to expand the distance between bolts on the shear tab (i.e., increase the connection depth), it is a low-cost method to increase the connection moment strength and energy dissipation capacity. Adding a BFFD is another method to achieve the same goal. To evaluate energy dissipation capacity of shear tab connections with different configurations, this paper is organized in three main parts as follows: i) validating a finite element model based on experimental results; ii) conducting a parametric study on shear tab connections; iii) evaluating Liu and Astaneh's simple shear tab moment-rotation prediction model and proposing an updated prediction model of moment-rotation curves for shear tab connections with different configurations. The proposed moment-rotation model of enhanced simple connections can be used in nonlinear analysis models as part of a performance-based design procedure for steel frame structures. The last research phase will assess the impact of including the gravity system with enhanced shear tabs on the response of case study steel frame buildings. The research presented in this paper provides the foundation for the future structural modeling efforts.

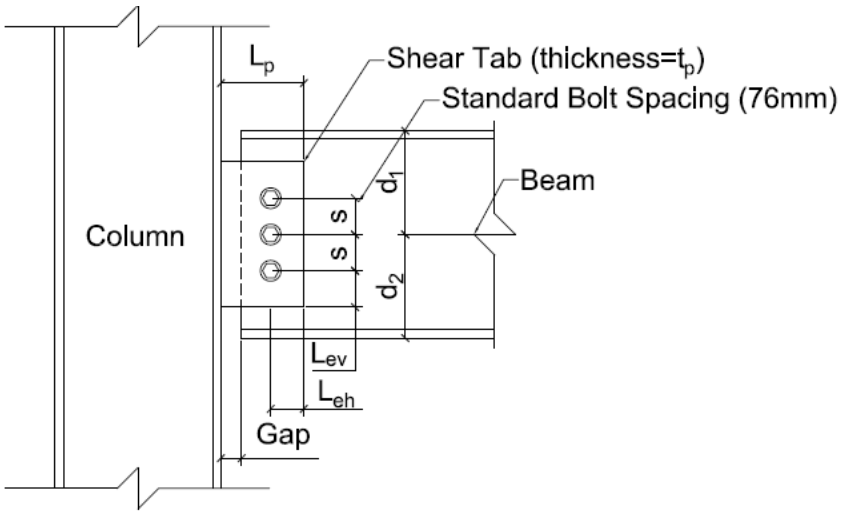

a) Standard Shear Tab Connection

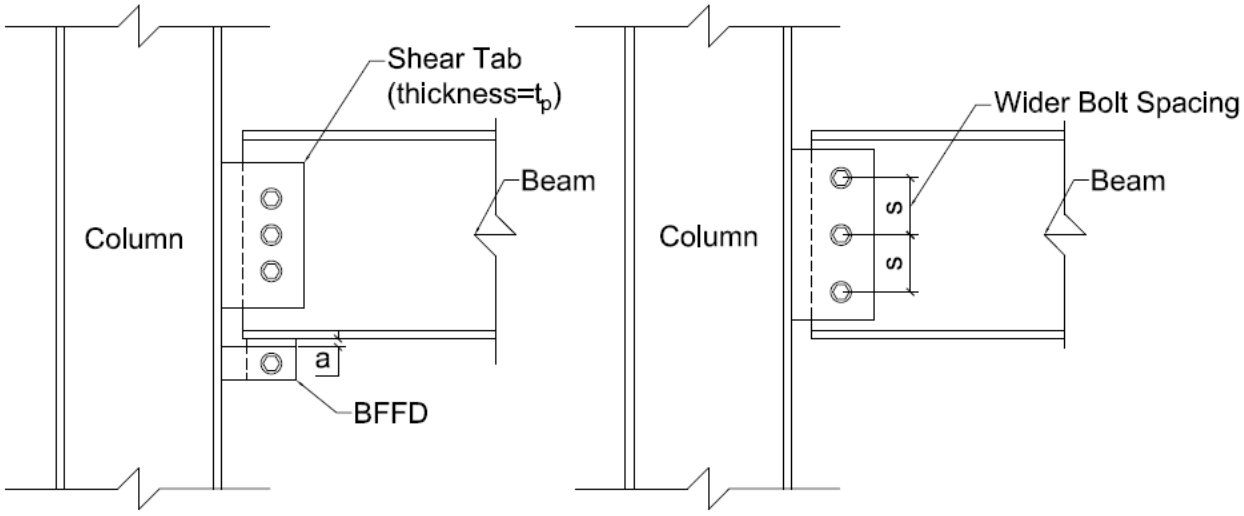

b) Shear Tab Connection with BFFD **c) Shear Tab Connection with Wider Bolt Spacing**

Figure 4-1. Sketch of Shear Tab Connection with Different Configurations

4.2 Literature Review

During an earthquake, lateral displacement occurs in both gravity load frames and lateral resisting frames. The rotational demand on shear tab connections due to lateral load is much larger than that due to gravity loads alone which means the shear tab response will be different during a seismic event compared with gravity load only situation. If there is only gravity load on the structure, the moment generated at the connection is a result of a rather small eccentricity relative to the bolt line. Based on previous research, if the shear force is far away from the bolt line which

means the distance between shear force and bolt line is larger than the height of bolt line, the relation between connection rotation and moment is insensitive to connection shear (Richard, Gillett, Kriegh, & Lewis, 1980). The connection plate is experiencing a nearly rigid body plate rotation under cyclic load. Therefore, predicting the behavior of these shear tab connections is important in predicting the structure seismic performance (Crocker & Chambers, 2004). Shear tab connections (Liu & Astaneh-Asl, 2000) have been shown to have rotational stiffness and resistance to lateral load. During cyclic tests, yield lines began to appear at the top and bottom bolts of the shear tabs followed by slip between shear tab and beam webs, bolt hole deformation and other mechanisms leading to connection failure. Typically, the first of these mechanisms is yielding of the shear tab followed by bearing of the bolt holes and out-of-plane warping of the plate and beam web (Liu & Astaneh-Asl, 2000). Limit states observed in shear tab connections include yielding of the shear tab, fracture of the shear tab net section, bearing failure of the bolt holes, bolt fracture, and fracture of the weld (Liu & Astaneh-Asl, 2000). The typical shear tab moment rotation model was proposed based on the test results demonstrated in Figure 4-2. All the variables in this model can be calculated based on Figure 4-3. The bolts on the shear tab would slip first. θ_{slip} is equal to 0.0042 radians which is an empirical value derived from previous test data. M_{slip} is calculated by the friction force provided by each bolt. When positive moment is generated (beam moves up), the bolts above the centerline of the bolt group provide the compressive component while the bolts below the centerline provide the tensile component based on the "bolt element assumption" (Liu & Astaneh-Asl, 2000). Eventually, the bolts will start to contact with bolt holes on the shear tab and beam web until it reaches bearing failure. θ_{max} is equal to 0.05 radians which is also an empirical number for bare simple shear tab connections. M_{max} is calculated by the bearing

capacity for each bolt. θ_{ult} represents the theoretical rotation before the binding of beam flange and column which can be calculated as gap/d_1 for positive rotation.

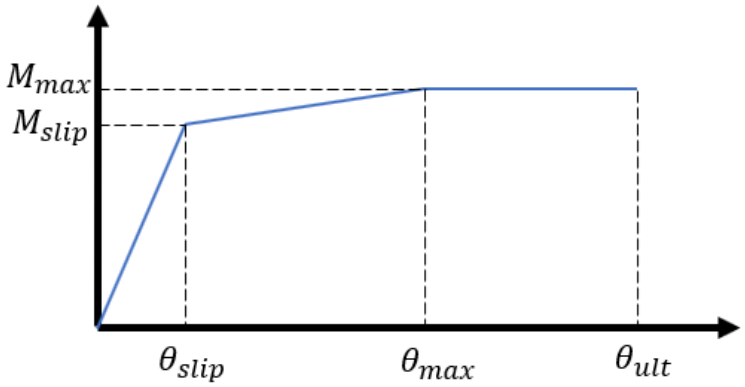

Figure 4-2. Typical Bare Shear Tab Moment-Rotation Model

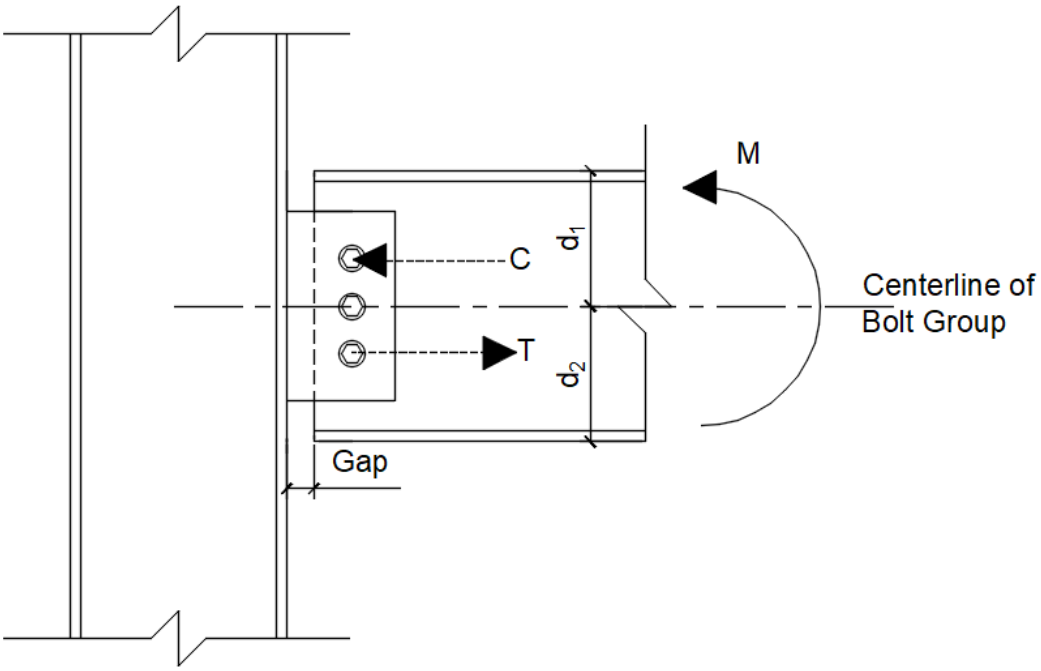

Figure 4-3. Shear Tab Connection Properties and Force Distribution for Positive Moment

The mechanism of energy dissipation in shear tab connections is friction between the beam web and the shear plate. Friction is also used in other applications to moment frames and has been demonstrated as a reliable system to dissipate energy. A post-tension friction damped connection for steel moment frames was introduced by Rojas et. al. (2005). The friction device was installed

on the top and bottom beam flanges while high-strength post-tensioning strands were installed parallel to the corresponding beams. Since the floor system is on the top of the moment frame in steel structures, installing a friction device at that location will cause interference with the slab system. Therefore, a new type of post-tension friction damped connection was introduced (Wolski, Ricles, & Sause, 2009). The friction device was installed on the bottom beam flange called the Bottom Flange Friction Device while the post-tension high strength strands were installed parallel to the corresponding beams through the column flange. A 22-degree slot hole was adopted in the friction device to have a better fit for rotational behavior in the test. The test results show that the bottom flange friction device provides reliable energy dissipation, and that the connection remains damage-free under the design earthquake (Wolski, Ricles, & Sause, 2009). A removable friction device for low damage steel beam-column joints was introduced by Latour et al. (2018). The results show that even without the self-centering system, the beam-column joint with a friction device can still dissipate energy efficiently. The previous research focused on investigating the effect of friction device as the lateral load resisting system and the primary energy dissipation component. The clamping force of bolts in the friction device must be calculated to achieve the required strength and the damage free response under the design earthquake.

In this research, the BFFDs are installed below the shear tab connections. The clamping force of bolts in the friction devices is only required to reach the minimum pretension load (AISC, 2010). Wu and Marshall (Wu & Marshall, 2022) have shown that adding a BFFD to the shear tab connection significantly improves the strength and energy dissipation. The numerical study of shear tab connections in this paper followed Wu and Marshall's experiments. Multiple friction devices and shear tab connections with different configurations are modeled and analyzed to establish a simplified moment-rotation model that can be used in performance-based design.

4.3 FEM Modelling and Validation

The first step is establishing a finite element model that is shown to be consistent with the prior experimental testing (Wu & Marshall, 2022). The finite element model was developed by using the commercial software ABAQUS 2020 (2020). The importance of the finite element model validation is to demonstrate the behavior of the connection and the limit states observed is captured in the analysis models. Modeling of shear tab connections using rigorous finite element models has been completed by other researchers. A finite element model of bare simple shear tab connection established by Wen et al. (2013) provides more information related to the shear tab connection in the micro level including stress distribution in the shear tab connection zone, change of the neutral axis along the beam sections, and the distribution of normal stress along the shear tab connection. Weigand (2017) developed a new component-based model for shear tab connections. Although the force-displacement behaviors of the individual connection component are aggregated, the model can still approximately capture the behavior of shear tab connections.

4.3.1 Geometry

The geometry of a typical shear tab connection with and without BFFD is shown in Figure 4-1. In this paper, the width of the shear tab L_p is 114 mm while the depth of shear tab varies based on the number of bolts, N, and bolt spacing, s. Bolt edge distances, L_{eh} and L_{ev}, are 38 mm and 32 mm, respectively. The gap between beam and column flange, *gap*, is 13 mm. Figure 4-4. shows the detailed geometry of the tested BFFD. The length, width, and location of the bolt hole of the column flange component and the shim plate are the same. However, the thickness of the bottom flange component and the column flange component is 6 mm while the thickness of the shim plate is 3 mm. The 3 mm thick friction material (Ferotec Friction D2017) was placed in the recesses with half the thickness of the friction material protruding above the plate surface. A 16 mm

diameter bolt was modelled with different bolt tensions corresponding to the experimental set up (Wu & Marshall, 2022). The BFFD was attached to the bottom of the beam flange. The gap between the column flange component and the beam flange, *a*, is 13 mm. The details of the specimens are presented in Table 4-1 where the geometry for shear tab connections can be identified from Figure 4-1. *N* represents the number of bolts in the shear tab. The bolt diameter for the shear tab is 19 mm in this table. The W16X61 steel section was modelled as column while the W14×26 and W16×31 steel sections were modelled as beams for the numerical verification. The column and beam length are 2.1m and 0.72m, respectively. A standard three-bolt shear tab served as connection for the W14×26 section while the W16×31 beam was connected with a four-bolt shear tab. Figure 4-5 depicts the example ABAQUS model.

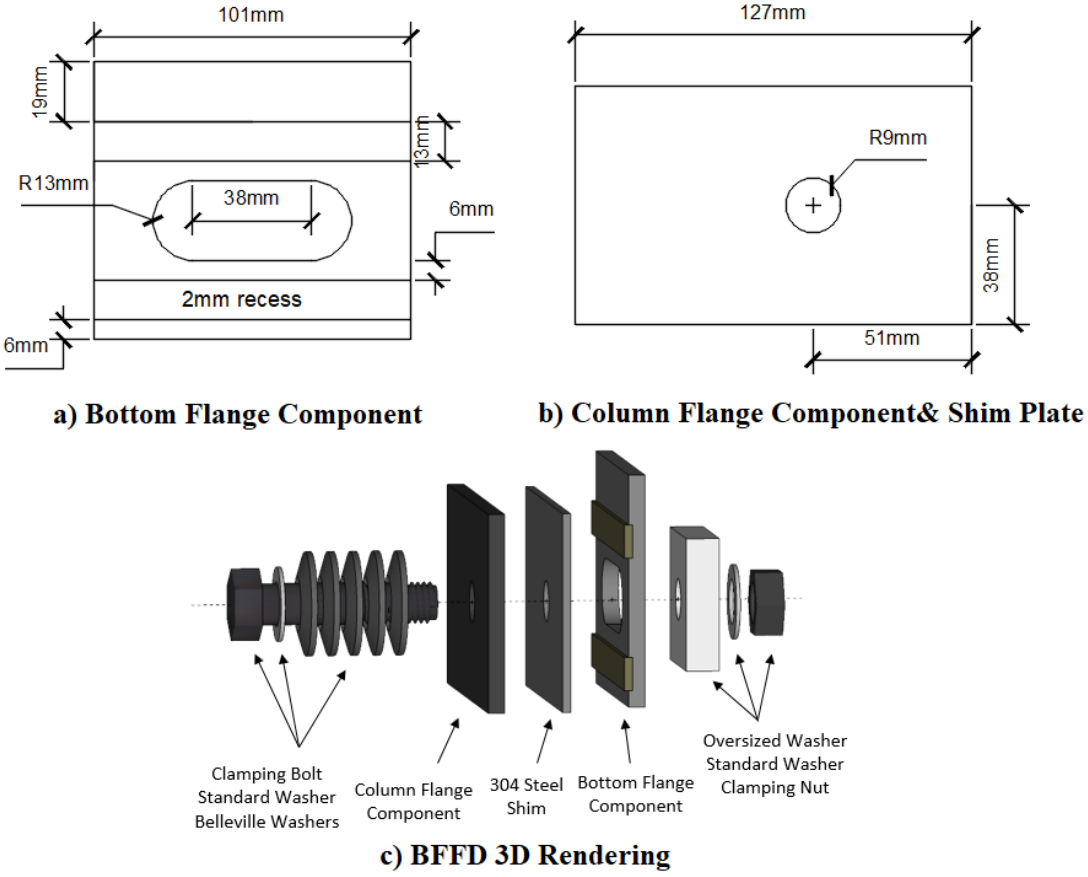

Figure 4-4. Detailed Geometry of Tested BFFD

Table 4-1. Numerical Simulation Tests for Verification with Experimental Results

Test	Beam	N	s	d_1	d_2	t_p	Bolt Tension
			mm	mm	mm	mm	kN
1	W14X26	3	76	177	177	6	0
2	W14X26	3	76	177	177	6	45
3	W14X26	3	76	177	177	6	82
4	W16X31	4	76	203	203	6	0
5	W16X31	4	76	203	203	6	45

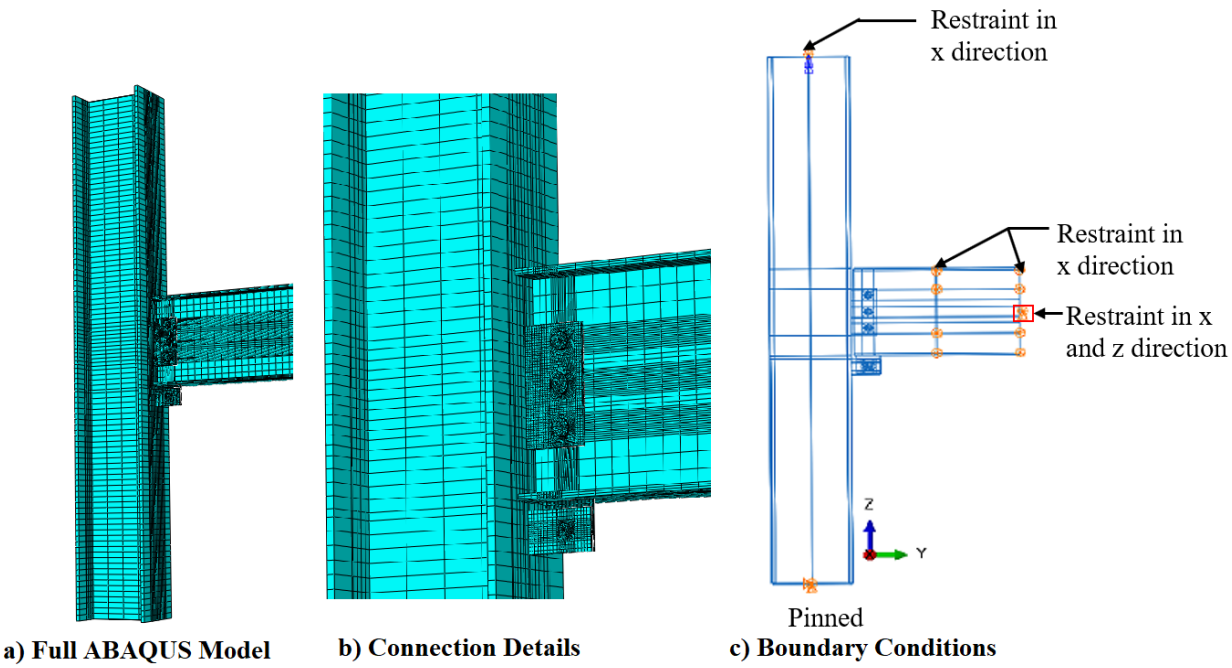

Figure 4-5. Example ABAQUS Model of Shear Tab Connection with BFFD

4.3.2 Element Type and Mesh

There are numerous elements available in the ABAQUS program library. In this numerical simulation, all the parts including the beam, column, shear tab, bolts and BFFD are modelled by using C3D8R elements. This is an eight-node solid element. Each node has three translational degrees of freedom. Hex-structured meshes are used to simulate the column, beam, shear tab,

friction material and steel plates in the BFFD while hex-structured and wedge-sweep meshes are used to simulate the bolts. Mesh density was carefully selected to capture the localized behavior of the shear tab connection. Different mesh sizes between 3 mm and 30 mm were applied to different components of shear tab connection in the ABAQUS models to balance the numerical model. The goal of the analysis balance is to use as large mesh size as possible to achieve convergence and accuracy with reasonable mesh sizes. For the shear tab and all the BFFD components, a 5 mm mesh size was chosen for all the models to balance the computational time and the acceptable accuracy level. The bolt, bolt head and nut were modeled as one solid body. The mesh size of the bolt was the same as the tab to ensure consistent contact between the bolt shank and the holes in both the shear tab and the beam web. The diameter of bolt holes on the shear tab and beam web were 2 mm larger than the bolts. The slot hole on the bottom flange component was large enough to prevent to contact with BFFD clamping bolt. Two mesh sizes were implemented for the beam and column. Appropriate partitions were made in the beam and column first. The mesh size of partitions related with shear tab, BFFD and bolts was 5 mm while the mesh size of remaining beam and column was increased to 13 mm.

4.3.3 Material Properties and Contact

Several materials were used in this numerical simulation, including steel materials (ASTM F3125, ASTM A992, ASTM A36 and 304 stainless steel) and friction material (Ferotec Friction D2017). All the steel materials contain both elastic and plastic behavior. The elastic material behavior for steel in this paper was defined by using two parameters, Young's modulus and Poisson's ratio. The Young's Modulus is 200GPa and the Poisson's ratio is 0.3. The plastic material behavior of ASTM A992 and ASTM A36 were defined based on the default corresponding steel material property in SAP2000 (CSI., 2011) while ASTM F3125 was

determined by the experimental result of Raham et al. (2007). 304 stainless steel was defined based on the minimum requirements of manufacturer specifications where a yield and an ultimate strength of 205 and 520Mpa, respectively were assumed. The true stress-strain relationship was used for all steel material as shown in Figure 4-6. The D2017 friction material only has elastic material behavior. The modulus of elasticity and Poisson's ratio are 7.7GPa and 0.3, respectively.

The model parts in contact, such as the bolts and plates, were assigned with interactions modelling both the Normal Behavior to avoid overclosure (by means of the "Hard Contact" option) and Tangential behavior to define the relative sliding (by employing the Coulomb friction law). The friction coefficient is 0.3 for the contact between two steel uncoated faying surfaces (AISC, 2010). The friction coefficient between 304 stainless steel and D2017 friction material is 0.19 as determined by Wu and Marshall (2022). Since no plastic deformation is expected in the welded connections (shear tab, column flange component and bottom flange component), tie constraints linking together surfaces in contact have been used to replicate the welds in a simplified manner.

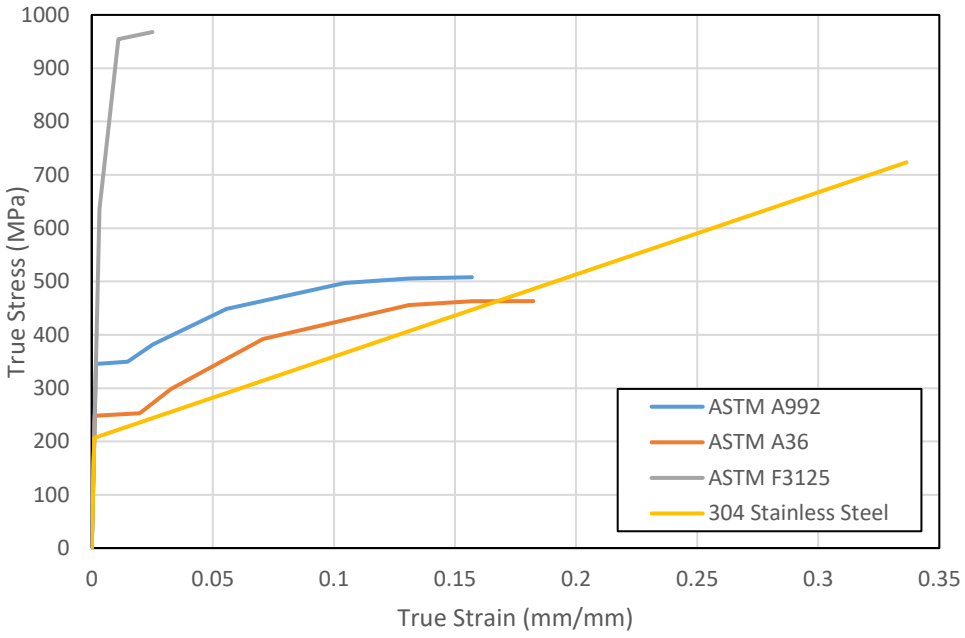

Figure 4-6. True Stress-Strain Curve for Steel Materials

4.3.4 Loading and Boundary Condition

The boundary conditions shown in Figure 4-5 were simulated based on the experimental set up (Wu & Marshall, 2022). A pinned support was applied at the column base. Restraint in the x-direction (out-of-plane) was applied on the top of the column, the beam midspan, and the beam free end to prevent the twisting behavior. An additional restraint in the z-direction was applied on a small portion of the cross section at the beam free end to ensure the beam can only move horizontally. This additional restraint cannot be applied on the whole cross section because it would prevent the beam flexure behavior which would generate an additional moment.

A general static analysis with the Newton-Raphson method was performed. The 'NLgeom' option was selected in ABAQUS to capture the large displacement effect. The analysis was conducted in two loading steps: i) apply the bolt pretension load and ii) apply the displacement history. The first step is to simulate the bolt tightening behavior. The pretension load for the bolts on the shear tab is 133kN while the pretension load for the BFFD clamping bolt is shown in Table 1. The first step establishes firm contact between adjacent surfaces. For example, the contact between the shear tab plate and the beam web, and the bolt head and the shear tab provided the initial friction to be overcome in the connection. The bolt length will be fixed after the first step to maintain the bolt tension during the simulation. Since displacement-controlled analysis was used in the simulations, the second step is to apply a displacement protocol to the top of the column consistent with the experimental testing. The loading protocol was the interim protocol I-quasi-static cyclic testing from FEMA 461 (ATC, 2007). For the three-bolt shear tab, the initial amplitude is 1 mm, and the final target amplitude is 76 mm. The initial amplitude is 1 mm, and the final target amplitude is 64 mm for the four-bolt shear tab. Figure 4-7 shows the displacement protocol applied to the top of column in the verification simulation.

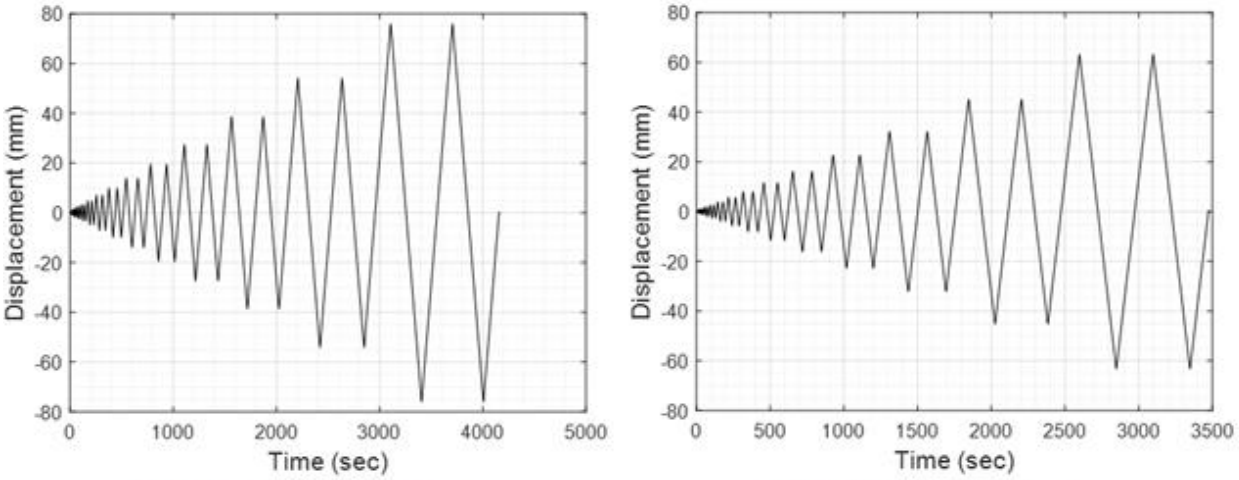

a) Three-Bolt Connection b) Four-Bolt Connection

Figure 4-7. Displacement Protocol

4.3.5 Validation of the Finite Element Model

The finite element model was verified using the experimental results obtained by Wu and Marshall (2022). The shear tab connection details for verification purpose are shown in Table 4-1. Figure 4-8 shows the comparison of moment-rotation curves between experimental and numerical results. The numerical results agree reasonably well with the experimental results. First, a cluster of loops were formed at the center of the hysteresis plots before significant slipping occurs in the connection. Then slip behavior becomes obvious. The slip moment in the numerical simulation is very close to the experimental result in the positive direction while it was not as consistent in the negative direction. Based on the displacement protocol, symmetrical behavior is expected. However, asymmetric behavior was observed throughout all the experimental test results due to fabrication defects, such as the shear tab not being welded plum with the column, and imperfect positioning of bolts during erection (Wu & Marshall, 2022). The bolts in the shear tab connection come into bearing with the edge of the holes at higher levels of deformation. This type of behavior resulted a significant moment increase in the connections. The localized deformation at the bolt hole edges on the shear tab were observed in both experiments and numerical

simulations. The elastic stiffness of the moment rotation curves is very similar between experimental and simulation results in all the tests. The consistency between the moment rotation curves generated by numerical models were good enough to match the results from the experimental tests. This provides confidence that using this modeling strategy is viable to conduct a parametric study of shear tab connections with and without bottom flange friction devices.

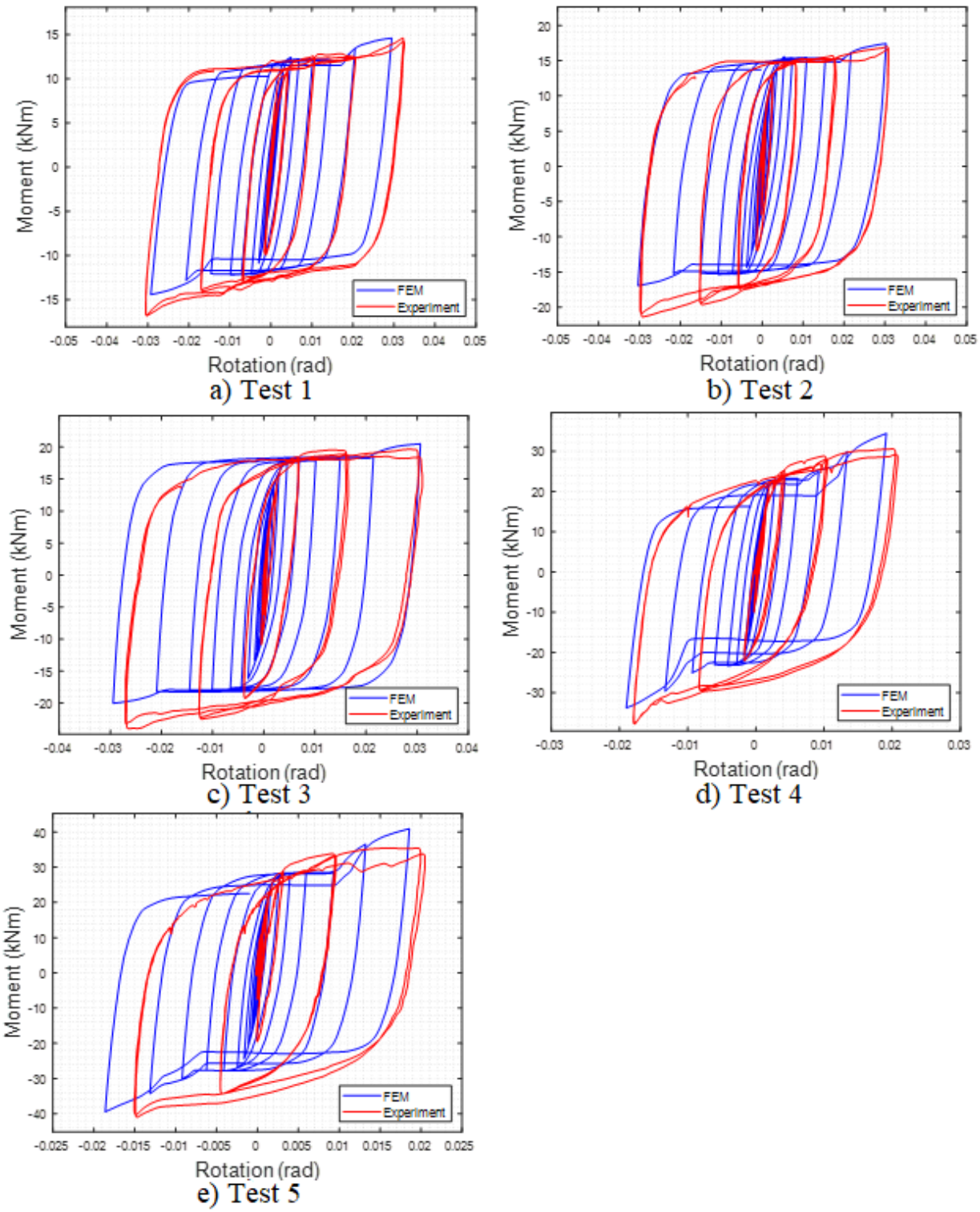

Figure 4-8. Comparison of Experimental versus Numerical Results

4.4 Parametric Study

The validated numerical models were used in a parametric study to further assess the performance of the different variations of the shear tab connection. Three different cases are considered in this study. The baseline case is the bare shear tab. The second case is a shear tab with a BFFD. This second case can also have the shear tab shifted up from the center of the beam towards the top of the beam which increases the overall depth of the connection and hence the strength and energy dissipation. The last case considered is a bare shear tab connection with a wider bolt spacing.

First, ABAQUS models of shear tab connections with different configurations based on considered parameters were built. The difference between the ABAQUS model used in the parametric study and the validated ABAQUS model in Section 3 is the material of the shear tab. ASTM A572 Grade 50 instead of ASTM A36 was used in the parametric study. The elastic material behavior of ASTM A572 Grade 50 was also defined using two parameters, Young's modulus and Poisson's ratio. The Young's Modulus is 200GPa and the Poisson's ratio is 0.3. The plastic material behavior of ASTM A572 Grade 50 was defined based on the default corresponding steel material property in SAP2000 (CSI., 2011).

Parameters investigated in this paper include the beam depth, BFFD bolt tension, shear tab plate thickness, number of bolts, shear tab location, bolt spacing and the direction of displacement at the top of the column. The reason the direction of displacement at the top of column is included is because the rotation in the positive and negative direction before the binding of beam flange and column are different when the shear tab is moved up since the centerline of beam and the shear tab are not coincident. Pushover analysis instead of a cyclic displacement protocol was selected to conduct the parametric study since it shortens the analysis time and provides the detailed results

of shear tab connections. In addition, the results of pushover analysis are more straightforward to be evaluated and used to establish the prediction model for a simplified moment-rotation curve for shear tab connections with different configurations. The pushover curve (moment-rotation curve) was collected for each parametric study model. A method for simplifying the moment-rotation curve based on the pushover curve from ABAQUS models is proposed. The simplified moment-rotation curves were generated for all the models. In the end, comparisons of moment-rotation curves among the numerical models in the parametric study were conducted by using both ABAQUS and simplified moment-rotation curves qualitatively and quantitatively.

4.4.1 Geometry of Parametric Study Models

A series of 31 pushover analysis were performed on the shear tab connections with different configurations. The detailed information of the shear tab connection parametric models is shown in Table 4-2. The nomenclature of the models starts with the beam section. Each name also shows that these are shear tab connections (ST) followed by the number of bolts on the shear tab. These two terms represent the simple shear tab connections without modification. If bolt spacing was increased, “S” with increased bolt spacing would be added. “FD” and “tp” represent the BFFD clamping bolt tension and the thickness of shear tab plate, respectively. Clamping bolt tension values of 49kN and 85kN were selected to investigate the influence of clamping force on shear tab connections. 49 KN is the pretension bolt load on the BFFD in the experimental test (Wu & Marshall, 2022). The higher value, 85kN, is the minimum full pretension load based on AISC for the given bolt diameter (AISC, 2010). “U” shows the distance the shear tab was moved up from the mid-height of the beam. “Rev” means the pushover analysis went to the opposite direction (beam moves down) to generate a negative rotation in the connection. The geometric characteristics which are not mentioned here are the same as the verification models in Section 3.

Table 4-2. Summary of Numerical Models in Parametric Study

Test	Name	Beam	N	s	d_1	d_2	t_p	Bolt Tension
				mm	mm	mm	mm	kN
1	W14-ST3	W14X26	3	76	177	177	6	0
2	W14-ST3-FD49	W14X26	3	76	177	177	6	49
3	W14-ST3-FD85	W14X26	3	76	177	177	6	85
4	W14-ST3-FD85-U25	W14X26	3	76	152	202	6	85
5	W14-ST3-FD85-U25-Rev	W14X26	3	76	152	202	6	85
6	W14-ST3-S102	W14X26	3	102	177	177	6	0
7	W16-ST3	W16X31	3	76	203	203	6	0
8	W16-ST3-FD85	W16X31	3	76	203	203	6	85
9	W16-ST3-FD85-U50	W16X31	3	76	153	253	6	85
10	W16-ST3-FD85-U50-Rev	W16X31	3	76	153	253	6	85
11	W16-ST3-S127	W16X31	3	127	203	203	6	0
12	W16-ST3-tp10	W16X31	3	76	203	203	10	0
13	W16-ST3-FD85-tp10	W16X31	3	76	203	203	10	85
14	W16-ST3-FD85-U50-tp10	W16X31	3	76	153	253	10	85
15	W16-ST3-FD85-U50-tp10-Rev	W16X31	3	76	153	253	10	85
16	W16-ST3-S127-tp10	W16X31	3	127	203	203	10	0
17	W16-ST4	W16X31	4	76	203	203	6	0
18	W16-ST4-FD49	W16X31	4	76	203	203	6	49
19	W16-ST4-FD85	W16X31	4	76	203	203	6	85
20	W16-ST4-FD85-U25	W16X31	4	76	178	228	6	85
21	W16-ST4-FD85-U25-Rev	W16X31	4	76	178	228	6	85
22	W18-ST4	W18X35	4	76	225	225	6	0
23	W18-ST4-FD85	W18X35	4	76	225	225	6	85
24	W18-ST4-FD85-U50	W18X35	4	76	175	275	6	85
25	W18-ST4-FD85-U50-Rev	W18X35	4	76	175	275	6	85
26	W18-ST4-S102	W18X35	4	102	225	225	6	0
27	W27-ST6	W27X84	6	76	339	339	6	0
28	W27-ST6-FD85	W27X84	6	76	339	339	6	85
29	W27-ST6-FD85-U76	W27X84	6	76	263	415	6	85
30	W27-ST6-FD85-U76-Rev	W27X84	6	76	263	415	6	85
31	W27-ST6-S102	W27X84	6	102	339	339	6	0

4.4.2 ABAQUS Results and Simplified Pushover Curves

Compared with the results from cyclic test from Section 4.3, the numerical pushover analysis can show more detailed behavior of shear tab connections that can be used as a

backbone curve for an analysis model. A pushover curve (Test 21) from numerical simulation is shown in Figure 4-9(a) (blue line). Figure 4-10 shows the deformed shape of the shear tab connection for Test 21 (W16-ST4-FD85-U25-Rev). There are four phases observed from the ABAQUS pushover analysis result which are listed on the bottom of Figure 4-9(a). The connection behavior with and without BFFD are similar. First, before the bolts slip, the moment increases substantially with a very small rotation in the "Pre-slip" phase. In the "Sliding" phase, all the bolts began to move, the moment remains approximately same since the diameter of bolt holes on the shear tab were 2 mm larger than the bolts so that there was tiny space for bolts to move freely. Then, the connection went into the "Bolt Hole Bearing" phase, as the bolts on the shear tab started to contact with the bolt holes on the shear tab and beam web. The moment increases gradually as the connection continues rotating. The inelastic deformation can be observed on the shear tab shown in Figure 4-10. Finally, in the "Beam and Column Flange Binding" phase, the beam bottom flange contacts the column surface. The moment increases dramatically since bearing between the beam and column flange was resisting the increase in rotation as well which would generate a significant amount of moment. In this paper, the "Beam and Column Flange binding" phase will not be further discussed since significant inelastic behavior will occur in the "Beam and Column Flange Binding" phase. The performance of shear tab connections will significantly change due the binding of the beam flange and column, and this occurs beyond the valid range of modeling for many other components of the structural analysis model.

A simplified pushover curve was developed based on the pushover curve from the ABAQUS model shown in Figure 4-9(a) (orange line). There are only two phases in the simplified pushover curve, including "Pre-slip" and "Post-slip" as shown on the top of Figure 4-

9(a). The “Pre-slip” phase in the simplified pushover curve is a straight line representing the initial stiffness of the connection. Since there is not a well-defined yield point, calculation of the initial stiffness and the slip rotation was not trivial. The connection stiffness gradually decreased before it fully slipped. Therefore, “Segment 1” and “Segment 2” were defined to locate the “Slip point” in the simplified pushover curve shown in Figure 4-9(b). For each displacement increment of response, both the previous stiffness and the current stiffness were calculated. If the current stiffness is less than 85% of the previous stiffness, the corresponding point was defined as “Point 1”. If the current stiffness is less than 70% of previous stiffness, the corresponding point was defined as “Point 2”. The corresponding moment at “Point 2” was defined as slip moment. The origin and “Point 1” were connected as “Segment 1” while “Point 1” and “Point 2” were connected as “Segment 2”. An iterative approach was utilized to identify the 85% and 70% values that were used to capture the “Pre-slip” phase. The selected values provided the best qualitative and quantitative representation of the nonlinear response that occurred in this phase. The average slope of “Segment 1” and “Segment 2” was calculated as the initial stiffness of the connection. The slip rotation was calculated as the slip moment divided by the initial stiffness. The “Post-slip” phase combines the “Sliding” and “Bolt Hole Bearing” phase of the pushover curve from the ABAQUS model. This is because the “Sliding” phase is not obvious in the experimental results ((Liu & Astaneh-Asl, 2000), (Wu & Marshall, 2022)). A rotation of 0.05 radians was defined as maximum rotation in the “Post-slip” phase since nonlinear analysis of steel frame structures can become unrealistic when the story drift reaches this range of drift. In addition, the experimental tests (Wu & Marshall, 2022) were not able to push the column far enough to reach a rotation of 0.05 radians to fully validate the connection behavior with large rotations. The “Post-slip” phase was defined based on the energy dissipation in this section.

When the binding rotation is smaller than 0.05 radians, the energy dissipated between slip rotation and binding rotation in the ABAQUS pushover curve will be calculated first. The "Post-slip" phase in the simplified pushover curve will be defined to dissipate the same amount of energy between slip rotation and binding rotation. Then the moment will remain the same until it reaches 0.05 radians. If the binding moment is larger than 0.05 radians, the energy dissipated between slip rotation and 0.05 radians will be the same between the ABAQUS pushover curve and simplified pushover curve. Figure 4-9(a) shows the pushover curve of model (Test 21) with binding rotation less than 0.05. The pushover curve of model (Test 4) with binding rotation larger than 0.05 is shown in Figure 4-11. A simplified pushover curve is helpful to analyze the behavior of shear tab connections quantitatively and develop the prediction model of moment-rotation curve.

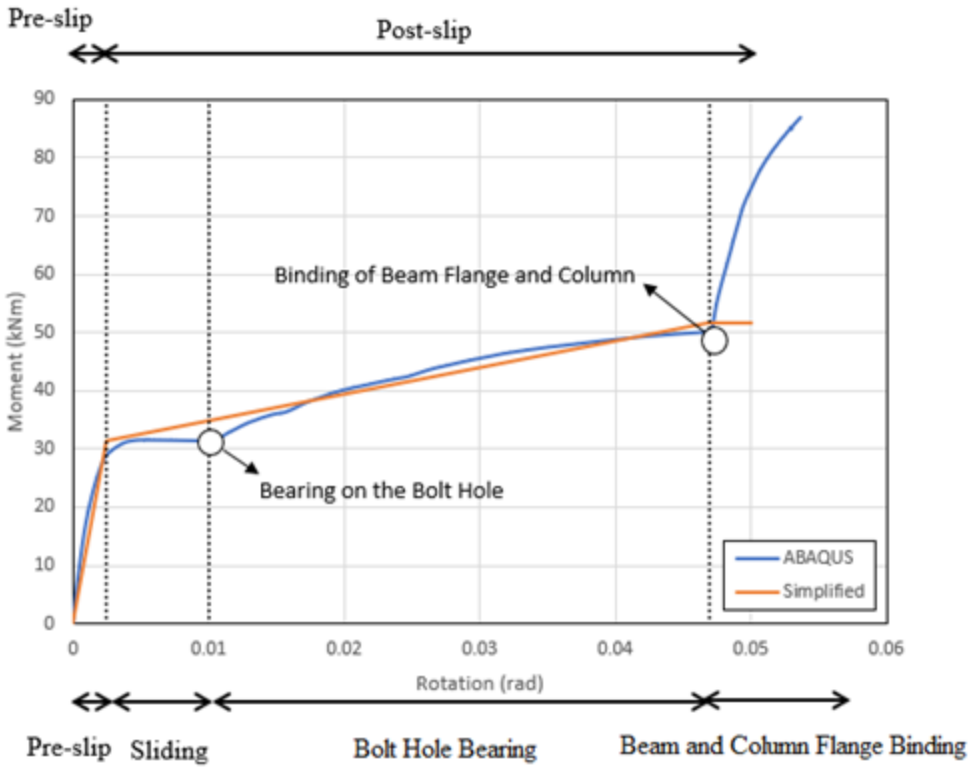

a) Typical Pushover Curve for Shear Tab Connection

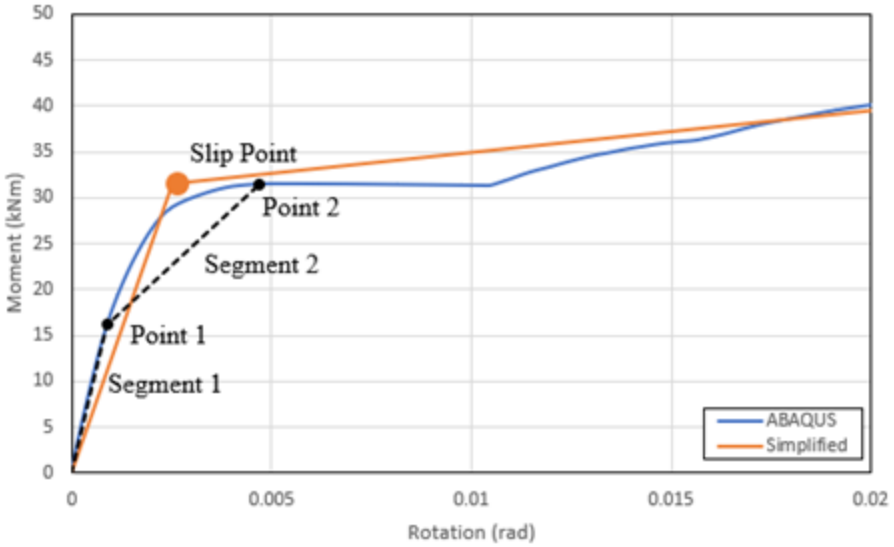

b) Pushover Curve focusing on "Pre-Slip" Phase

Figure 4-9. Pushover Curve for Test 21 (W16-ST4-FD85-U25-Rev)

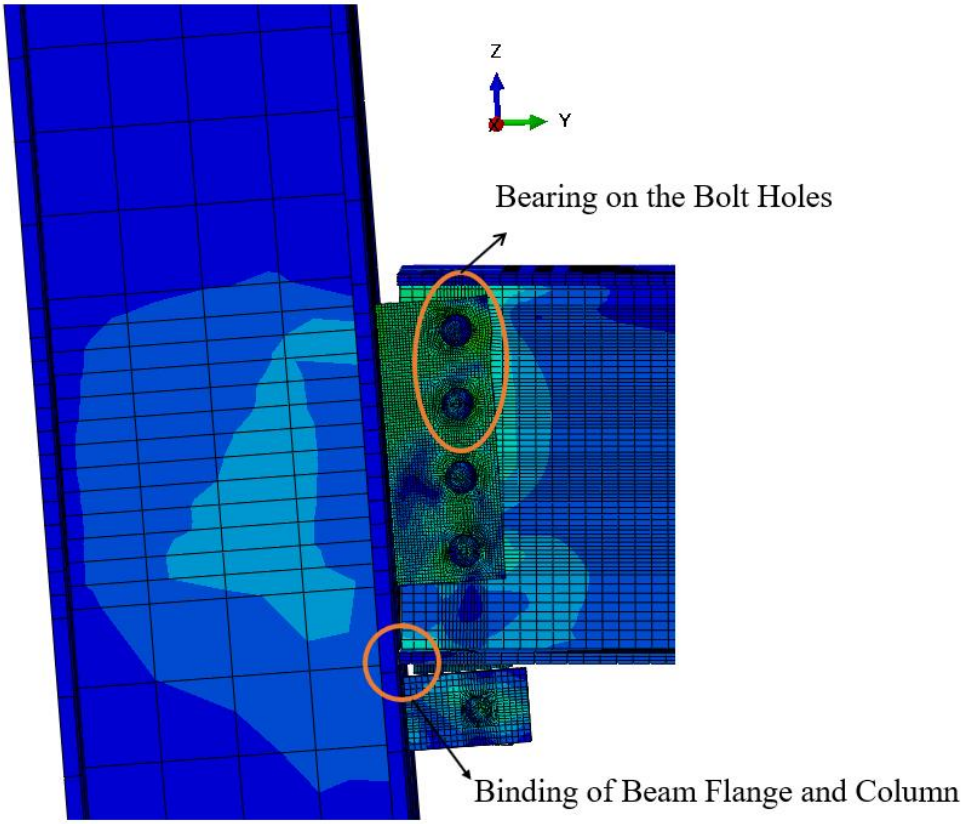

Figure 4-10. Deformed Shape of Shear Tab Connection for Test 21 (W16-ST4-FD85-U25-Rev)

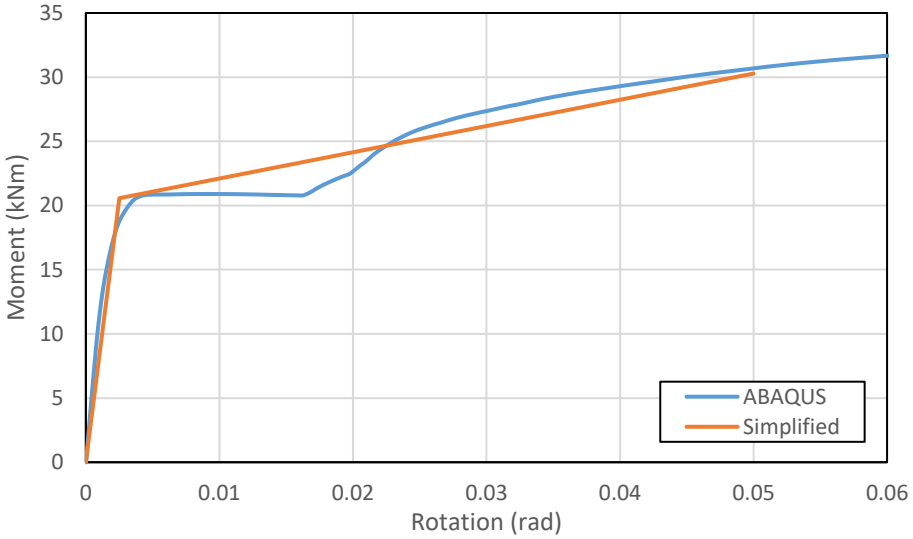

Figure 4-11. Pushover Curve for Test 4 (W14-ST3-FD85-U25)

4.4.3 Parametric Study Results and Discussion

Figure 4-12 and Figure 4-13 show the comparison of the ABAQUS and simplified pushover curves in the parametric study, respectively. Figure 4-12(a) and Figure 4-13(a) show the impact of the BFFD on the shear tab connections. W14-ST3 represents shear tab connection without BFFD while W14-ST3-FD49, W14-ST3-FD85 and W14-ST3-FD85-U25 represent shear tab connections with a BFFD. The result of ABAQUS and simplified pushover curve are similar with each other. In the "Pre-slip" phase, slip moment increases significantly as the BFFD is added. Clamping bolt tension and distance between the center of the shear tab and the BFFD clamping bolt have a significant impact on the slip moment as expected. The slip rotation of connections with a BFFD is smaller than the connections without a BFFD. Once the connection transitions to the "Sliding" and "Bolt Hole Bearing" phases, the slopes in these phases are very similar among the connections with and without a BFFD for both the ABAQUS and the simplified curves. Adding the BFFD results in additional moment strength for the shear tab connections. Based on the ABAQUS pushover result (Figure 4-12(a)), the rotation of shear tab bolt bearing without a BFFD is slightly larger than that of the connection with a BFFD. The influence of beam depth is shown in Figure 4-12(b) and Figure 4-13(b). The ABAQUS pushover curve agrees with the simplified pushover curve. Based on W16-ST4 and W18-ST4, the beam depth has no effect on the connection in the "Pre-slip" phase while the post-slip stiffness of W18-ST4 is slightly larger than that of W16-ST4 since the web thickness the W18X35 is larger than that of the W16X31. For the connections with a BFFD, W18-ST4-FD85 has a larger increase in moment due to the BFFD since the distance between the clamping bolt and center of the shear tab is larger.

The impact of the number of bolts on the shear tab is obvious as shown in Figure 4-12(c) and Figure 4-13(c). W16-ST3 and W16-ST3-FD85 have three bolts on the shear tab while W16-

ST4 and W16-ST4-FD85 have four bolts. The slip moment and pre-slip stiffness increases significantly as the number of shear tab bolts increases. Similarly, the slope of the pushover curves in the "Sliding" and "Bolt Hole Bearing" for connections with more bolts on the shear tab also increases significantly. The impact of bolt spacing is like the impact of number of bolts on the shear tab. The improved behavior of the shear tab connections occurs in both "Pre-slip" and the "Sliding" and "Bolt Hole Bearing" phases. Figure 4-12(d) and Figure 4-13(d) show the slip moment, pre-slip stiffness and the pushover curve slopes in the "Sliding" and "Bolt Hole Bearing" phases increase significantly when the shear tab bolt spacing increases. W14-ST3-S102 and W18-ST4-S102 represent the shear tab connections with larger bolt spacing. This is an economical and practical way to improve the behavior of shear tab connections without adding any additional components if there is sufficient beam web depth.

The impact of shear tab thickness was also investigated in this paper as shown in Figure 4-12(e) and Figure 4-13(e). W16-ST3 and W16-ST3-FD85 have a 6 mm shear tab while W16-ST3-tp10 and W16-ST3-FD85-tp10 have a 10 mm shear tab. In the "Pre-slip" phase, the effect of shear tab thickness is insignificant since the friction force in the connection dominates the performance. When the connection transitions to the "Sliding" and "Bolt Hole Bearing" phase, the slope of the pushover curves is significantly related with the thickness of the shear tab. A shear tab connection with a thicker shear tab plate will provide a lager post-slip stiffness. Overall, the results of simplified pushover curves are comparable to the ABAQUS pushover curves and adequately reflect the performance of shear tab connections. Therefore, the simplified pushover curves were used to assess the parametric study quantitively. The detailed parametric study results in the "Pre-slip" and "Post-slip" phases are shown in Tables 4-3 and 4-4, respectively.

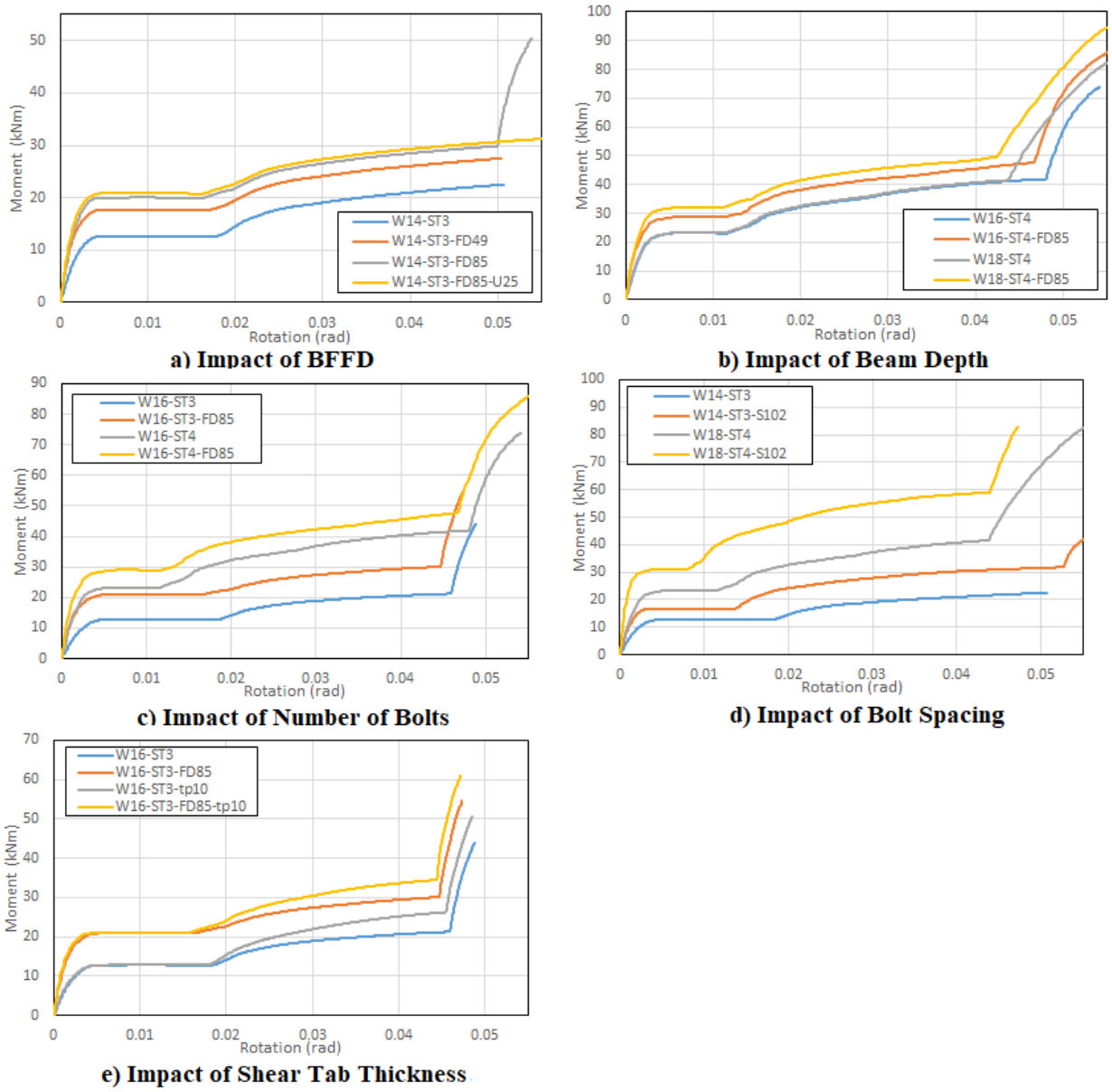

Figure 4-12. Comparison of ABAQUS Pushover Analysis Results in Parametric Study

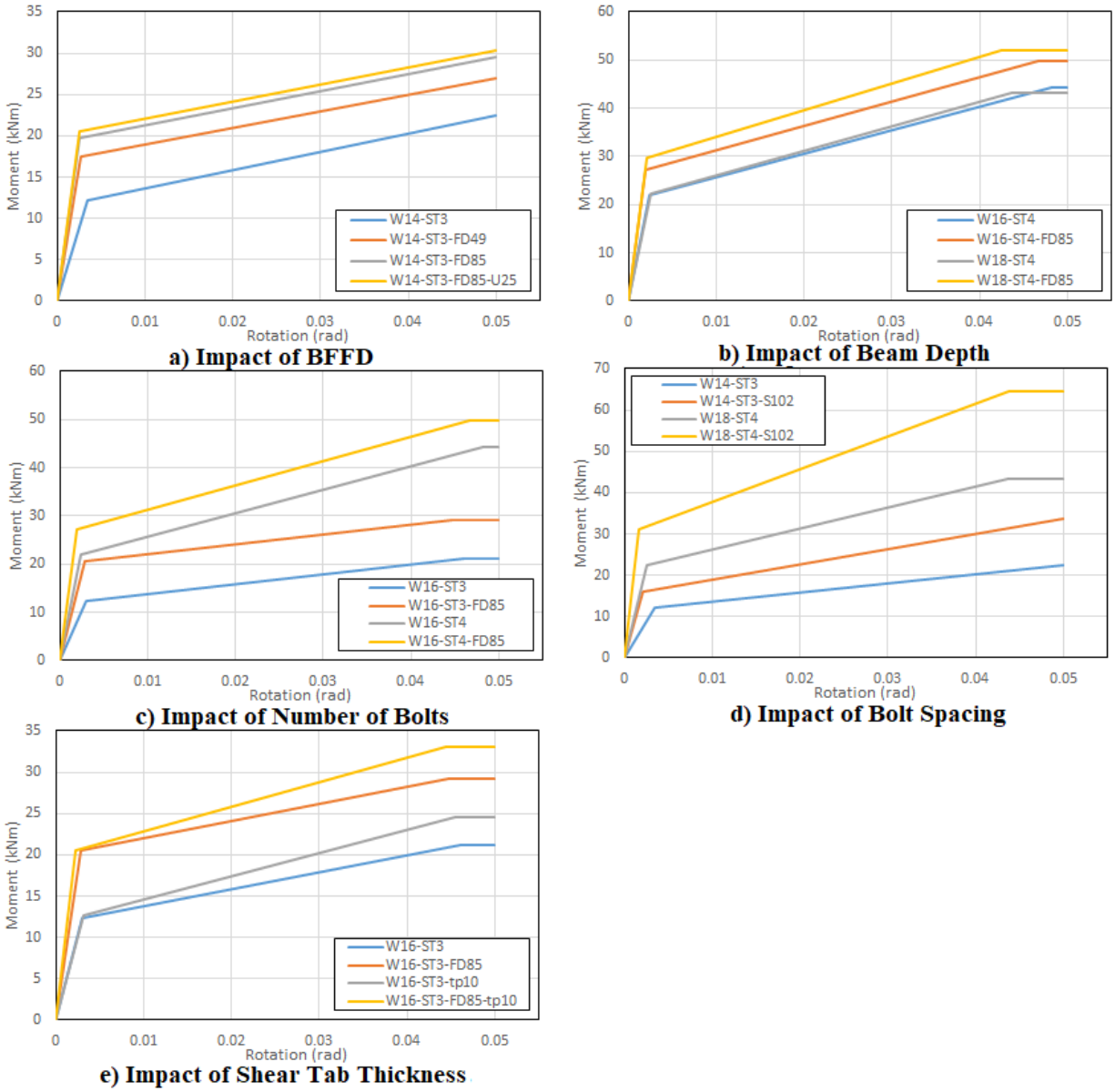

Figure 4-13. Comparison of Simplified Pushover Analysis Results in Parametric Study

Table 4-3. Summary of Parametric Study Results in "Pre-slip" Phase

Test	Name	Slip Rotation	Slip Moment	Pre-slip Stiffness	Expected Increased Moment	Increased Moment Ratio
		radians	kNm	kNm/rad	kNm	-
1	W14-ST3	0.00350	12.7	3,616	-	-
2	W14-ST3-FD49	0.00270	17.5	6,487	5.5	0.88
3	W14-ST3-FD85	0.00260	19.8	7,606	9.5	0.75
4	W14-ST3-FD85-U25	0.00250	20.6	8,226	10.6	0.75
5	W14-ST3-FD85-U25-Rev	0.00250	20.8	8,317	10.6	0.77
6	W14-ST3-S102	0.00200	15.9	7,967	-	-
7	W16-ST3	0.00300	12.4	4,143	-	-
8	W16-ST3-FD85	0.00280	20.6	7,345	10.6	0.77
9	W16-ST3-FD85-U50	0.00270	22.1	8,203	12.7	0.77
10	W16-ST3-FD85-U50-Rev	0.00190	22.5	11,835	12.7	0.79
11	W16-ST3-S127	0.00170	19.8	11,632	-	-
12	W16-ST3-tp10	0.00310	12.7	4,083	-	-
13	W16-ST3-FD85-tp10	0.00220	20.6	9,348	10.6	0.74
14	W16-ST3-FD85-U50-tp10	0.00210	22.1	10,547	12.7	0.75
15	W16-ST3-FD85-U50-tp10-Rev	0.00210	22.1	10,547	12.7	0.75
16	W16-ST3-S127-tp10	0.00130	20.1	15,472	-	-
17	W16-ST4	0.00240	22.0	9,181	-	-
18	W16-ST4-FD49	0.00240	26.9	11,206	6.1	0.79
19	W16-ST4-FD85	0.00250	29.0	11,616	10.6	0.66
20	W16-ST4-FD85-U25	0.00210	30.5	14,529	11.7	0.73
21	W16-ST4-FD85-U25-Rev	0.00250	31.5	12,611	11.7	0.81
22	W18-ST4	0.00250	21.9	8,769	-	-
23	W18-ST4-FD85	0.00210	29.8	14,206	11.5	0.69
24	W18-ST4-FD85-U50	0.00190	31.6	16,653	13.6	0.71
25	W18-ST4-FD85-U50-Rev	0.00190	31.6	16,653	13.6	0.71
26	W18-ST4-S102	0.00180	31.1	17,264	-	-
27	W27-ST6	0.00170	48.6	28,582	-	-
28	W27-ST6-FD85	0.00140	59.9	42,779	16.3	0.69
29	W27-ST6-FD85-U76	0.00086	62.5	72,662	19.5	0.71
30	W27-ST6-FD85-U76-Rev	0.00086	62.5	72,662	19.5	0.71
31	W27-ST6-S102	0.00120	68.3	56,877	-	-

Table 4-4. Summary of Parametric Study Results in "Post-slip" Phase

Test	Name	Post-slip Stiffness	Post/Pre-slip	Binding Rotation	Expected Binding Rotation	Binding Rotation Ratio
		kNm/rad	-	radians	radians	-
1	W14-ST3	211	0.06	-	0.073	-
2	W14-ST3-FD49	201	0.03	-	0.073	-
3	W14-ST3-FD85	205	0.03	-	0.073	-
4	W14-ST3-FD85-U25	205	0.02	-	0.086	-
5	W14-ST3-FD85-U25-Rev	171	0.02	-	0.064	-
6	W14-ST3-S102	370	0.05	-	0.073	-
7	W16-ST3	205	0.05	0.046	0.064	0.72
8	W16-ST3-FD85	208	0.03	0.045	0.064	0.70
9	W16-ST3-FD85-U50	208	0.03	-	0.085	-
10	W16-ST3-FD85-U50-Rev	154	0.01	0.040	0.051	0.78
11	W16-ST3-S127	565	0.05	0.047	0.064	0.73
12	W16-ST3-tp10	283	0.07	0.046	0.064	0.71
13	W16-ST3-FD85-tp10	295	0.03	0.044	0.064	0.69
14	W16-ST3-FD85-U50-tp10	300	0.03	-	0.085	-
15	W16-ST3-FD85-U50-tp10-Rev	285	0.03	0.039	0.051	0.77
16	W16-ST3-S127-tp10	748	0.05	0.045	0.064	0.71
17	W16-ST4	490	0.05	0.048	0.064	0.75
18	W16-ST4-FD49	424	0.04	0.047	0.064	0.74
19	W16-ST4-FD85	430	0.04	0.047	0.064	0.73
20	W16-ST4-FD85-U25	500	0.03	-	0.073	-
21	W16-ST4-FD85-U25-Rev	454	0.04	0.047	0.057	0.82
22	W18-ST4	520	0.06	0.044	0.058	0.75
23	W18-ST4-FD85	550	0.04	0.042	0.058	0.73
24	W18-ST4-FD85-U50	529	0.03	-	0.074	-
25	W18-ST4-FD85-U50-Rev	515	0.03	0.039	0.047	0.83
26	W18-ST4-S102	799	0.05	0.044	0.058	0.76
27	W27-ST6	1905	0.07	0.029	0.038	0.77
28	W27-ST6-FD85	1758	0.04	0.029	0.038	0.76
29	W27-ST6-FD85-U76	1741	0.02	0.038	0.049	0.77
30	W27-ST6-FD85-U76-Rev	1720	0.02	0.025	0.031	0.79
31	W27-ST6-S102	2943	0.05	0.029	0.038	0.74

Based on Table 4-3, all the slip rotations in this parametric study are less than 0.0044 radians which is smaller than the assumption made by Liu and Astaneh (2000). Both adding the BFFD and increasing the bolt spacing on the shear tab increases the slip moment and pre-slip stiffness. The slip rotation reduced slightly when the BFFD was attached. The initiation of slip of the BFFD occurred before the shear tab indicating that the BFFD activated early in the deformation pattern to dissipate energy. The impact of shear tab thickness is insignificant on the slip moment. The "Expected Increased Moment" in Table 4-3 represents the expected increase in moment strength in the shear tab connection when adding a BFFD. This can be calculated by using the BFFD friction force multiplied by the distance between the center of shear tab and BFFD clamping bolt. The actual increased moment strength due to the BFFD is calculated based on the slip moment from the numerical model. The "Increased Moment Ratio" in Table 4-3 represents the ratio of the actual increased moment strength to the expected increased moment strength. It shows that the "Increased Moment Ratio" slightly decreases as the size of beam and number of bolts on the shear tab increases. The actual increased moment strength reaches at least 70% of the expected value due to the BFFD.

The post-slip stiffness and ratio of post-slip stiffness to pre-slip stiffness for the tests are shown in Table 4-4. The impact of the BFFD on the post-slip stiffness is not significant. The post-slip stiffness did not significantly change when a BFFD was added to a shear tab connection. However, the bolt spacing, and the thickness of the shear tab plate have a significant influence on the post-slip stiffness. As the bolt spacing, and the thickness of shear tab plate increases, the connection post-slip stiffness increases significantly. Based on Tests 1, 6, 7, 11, 12, 16, 17, 22, 26, 27 and 31, the post-slip stiffness of a bare shear tab connection typically reaches at least 5% of the pre-slip stiffness. For binding rotation, only the models with binding rotation less than 0.05 radians

were shown in Table 4-4 since 0.05 radians is the considered maximum rotation in the shear tab connection model. The "Expected Binding Rotation" in Table 4-4 represents the theoretical binding rotation in the model which can be calculated by using the *Gap* dimension (Figure 4-1) divided by d_1 or d_2 depending on the direction of rotation. The actual binding rotations were always smaller than the expected value since the beam and column also experience a small amount of flexural deformation in the pushover analysis. The actual binding rotation is approximately 75% of the theoretical binding rotation. The information provided in Tables 4-3 and 4-4 is helpful to evaluate and improve the moment-rotation prediction model for shear tab connections in Section 4.5.

4.5 Liu and Astaneh's Moment-Rotation Model

Liu and Astaneh (2000) developed a moment-rotation model for standard simple shear tab connections based on experimental results. The basis of the calculation is shown in Figure 4-2. The slip moment is calculated using the friction force provided by each bolt while the maximum moment is calculated by using the bearing capacity for each bolt. The slip rotation and maximum rotation were determined as two empirical rotations which are 0.0044 and 0.05 radians, respectively.

4.5.1 Evaluation of Liu and Astaneh's Moment-Rotation Model

Table 4-5 shows the slip moment, maximum moment, and the ratio of the result of the Liu and Astaneh model to the simplified models for all the shear tab connections without a BFFD. The predictions of slip moment by Liu and Astaneh's model are consistently less than the simplified model for both standard shear tab connection models and shear tab connection models with larger bolt spacing. A scale factor of 1.5 was recommended by Liu and Astaneh. Based on the results from numerical analysis, the ratio of maximum moment between the prediction of Liu and

Astaneh's model and the ABAQUS results is between 0.72 and 0.85 which is a relatively small range. Therefore, a scale factor of 1.7 instead of 1.5 is proposed to estimate the slip moment of a bare shear tab connection. Similarly, the predictions of maximum moment by Liu and Astaneh's model are less than the simplified model for both standard shear tab connections and shear tab connections with larger bolt spacing. However, the ratio of maximum moment between the prediction of Liu and Astaneh's model and the simplified model results have greater variability. The ratio of maximum moment of Test 11 (W16-ST3-S127) is 0.66 while that of Test 27 (W27-ST6) is 0.98. Therefore, it could be unconservative to add any scale factor to it in certain conditions. Based on the discussion in Section 4, the post-slip stiffness should be at least 5% of the pre-slip stiffness. If the post-slip stiffness does not reach 5% of pre-slip stiffness in the estimated moment-rotation model, the maximum moment needs to be increased to meet the 5% minimum requirement. In other words, it is recommended to use the Liu and Astaneh calculation for the maximum strength of the connection unless this does not provide at least a 5% post-yield stiffness. In this case, the maximum strength should be based on a 5% post-yield stiffness, the slip moment, and the initial stiffness.

Table 4-5 shows the comparison of pre-slip and post-slip stiffness between Liu and Astaneh's model and the simplified model for all the shear tab connection models without a BFFD. The pre-slip stiffness predicted by Liu and Astaneh's model is significantly less than for the simplified model for both standard shear tab connection models and shear tab connection models with larger bolt spacing since the slip moment used in Liu and Astaneh's model is an empirical value of 0.0044 radians which significantly overestimates the actual slip value. The slip rotation is related to the depth of the bolt group on the shear tab as shown in Figure 4-14. As the bolt group depth increases, the slip rotation decreases. Based on the parametric study results, a new method

to estimate the slip moment is proposed in this paper. When the depth of bolt group is less than 200 mm, between 200 mm and 400 mm and larger than 400 mm, the slip rotation is equal to 0.0035 radians, 0.0025 radians, and 0.0015 radians, respectively.

The post-slip stiffness predicted by Liu and Astaneh's model is also less than the simplified model for both standard and wide bolt spacing shear tab connection models due to the overestimation of maximum rotation. Even with Test 27 (W27-ST6), the estimation of maximum moment is very close to the simplified model. The post-slip stiffness predicted by Liu and Astaneh's model is only 67% of the simplified model. In Liu and Astaneh's model, the maximum rotation is also an empirical value which is 0.05 radians for bare shear tab connection. It should be noted that for the Liu and Astaneh tests used a 25 mm gap between the end of the beam and the column. This results in a larger deformation before the beam flange bears on the column. However, for some large beams, the theoretical binding rotation is smaller than 0.05 radians which means these connections cannot reach 0.05 radians before the beam flange contacts the column. Based on the results from Section 4, the actual binding rotation is approximately 75% of the theoretical binding rotation. Therefore, if 75% of the theoretical binding rotation is less than 0.05 radians, the maximum rotation is equal to 75% of the theoretical binding rotation and ultimate rotation is equal to 0.05 radians. Otherwise, both maximum and ultimate rotation are equal to 0.05 radians.

Table 4-5. Comparison of Slip Moment and Maximum Moment between Liu et al. Model and ABAQUS Result

Test	Name	Slip Moment		Slip Moment Ratio	Max Moment		Max Moment Ratio
		Liu et al.	Simplified		Liu et al.	Simplified	
		kNm	kNm	-	kNm	kNm	-
1	W14-ST3	9.2	12.7	0.72	16.7	22.5	0.74
6	W14-ST3-S102	12.2	15.9	0.77	22.3	33.7	0.66
7	W16-ST3	9.2	12.4	0.74	17.4	21.2	0.82
11	W16-ST3-S127	15.3	19.8	0.77	28.9	45.1	0.64
12	W16-ST3-tp10	9.2	12.7	0.72	21.5	24.6	0.87
16	W16-ST3-S127-tp10	15.3	20.1	0.76	35.8	53.1	0.67
17	W16-ST4	18.3	22.0	0.83	30.4	44.4	0.68
22	W18-ST4	18.3	21.9	0.84	31.8	43.3	0.74
26	W18-ST4-S102	24.4	31.1	0.79	42.4	64.6	0.66
27	W27-ST6	41.2	48.6	0.85	99.7	101.4	0.98
31	W27-ST6-S102	54.9	68.3	0.80	133.0	149.8	0.89

Table 4-6. Comparison of Pre-slip and Post-slip Stiffness between Liu et al. Model and ABAQUS Result

Test	Name	Pre-slip Stiffness		Pre-slip Ratio	Post-slip Stiffness		Post-slip Ratio
		Liu et al.	Simplified		Liu et al.	Simplified	
		kNm/rad	kNm/rad	-	kNm/rad	kNm/rad	-
1	W14-ST3	2,080	3,616	0.58	165	211	0.78
6	W14-ST3-S102	2,774	7,967	0.35	220	370	0.60
7	W16-ST3	2,080	4,143	0.50	180	205	0.88
11	W16-ST3-S127	3,467	11,632	0.30	300	565	0.53
12	W16-ST3-tp10	2,080	4,083	0.51	270	283	0.96
16	W16-ST3-S127-tp10	3,467	15,472	0.22	451	748	0.60
17	W16-ST4	4,160	9,181	0.45	264	490	0.54
22	W18-ST4	4,160	8,769	0.47	296	520	0.57
26	W18-ST4-S102	5,547	19,422	0.29	395	795	0.50
27	W27-ST6	9,361	28,582	0.33	1,284	1,905	0.67
31	W27-ST6-S102	12,481	56,877	0.22	1,712	2,943	0.58

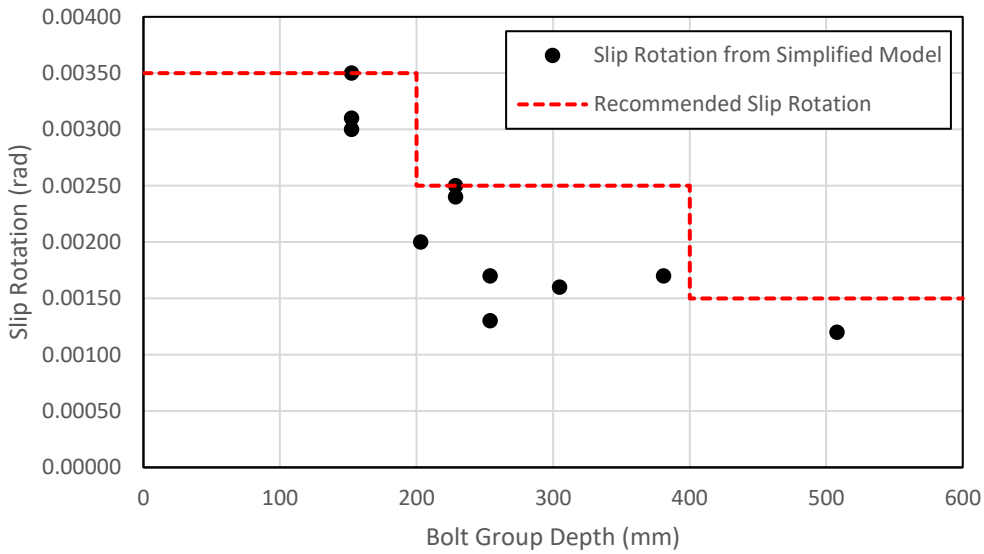

Figure 4-14. Relationship between Bolt Group Depth and Slip Rotation

4.5.2 Modified Moment-Rotation Model for Shear tab connections

A modified version of the moment-rotation model for shear tab connections with and without a BFFD is proposed in this paper based on Liu and Astaneh's moment-rotation model for bare shear tab connections. For the shear tab connection without BFFD, the overall shape of the moment-rotation curve is similar to Liu and Astaneh's model shown in Figure 4-2 which is a bilinear or a trilinear curve depending on the value of binding rotation. M_{slip} is calculated by the friction force provided by each bolt. A scale factor of 1.7 needs to be used in place of 1.5 to have a better estimation. θ_{slip} is defined as 0.0035, 0.0025 or 0.0015 radians based on the depth of bolt group. M_{max} is calculated by the bearing capacity for each bolt as part of a moment resisting couple. θ_{max} is equal to 75% of the theoretical binding rotation while θ_{ult} is equal to 0.05 radians, if 75% of the theoretical binding rotation is less than 0.05 radians. If 75% of the theoretical binding rotation is larger than 0.05 radians, both maximum and ultimate rotation are equal to 0.05 radians. The pre-slip and post-slip stiffness need to be checked as well. The pre-slip stiffness is based on

the slip moment and the slip rotation. If the post-slip stiffness is less than 5% of pre-slip stiffness, the calculated value of M_{max} needs to be increased to meet the 5% requirement.

For the shear tab connection with a BFFD, a moment-rotation model of corresponding shear tab connection without BFFD should be created first. Then, the additional moment strength needs to be added to both M_{slip} and M_{max} for the shear tab connection without a BFFD. The additional moment is calculated as 70% of the BFFD slip force is multiplied by the distance between the center of the shear tab and the BFFD clamping bolt. In the parametric study, the slip rotation and binding rotation of a shear tab connection with BFFD is negligibly smaller than that of the corresponding shear tab connection without BFFD. Therefore, θ_{slip}, θ_{max} and θ_{ult} of shear tab connections with a BFFD remain the same.

4.6 Conclusions

The overall research objective of this effort is to improve the response of steel frames by enhancing energy dissipation in the gravity connections. Previous work included experimental testing of shear tabs with and without a BFFD. This paper extends the experimental work by developing a finite element model using ABAQUS to simulate the experimental response of the shear tab connections with different configurations. The ABAQUS model was validated by the experimental results. Using the validated model, the effects of several parameters of the shear tab connections were investigated numerically. A simplified pushover curve was generated from the results of the ABAQUS analyses. The numerical results were used to assess the validity of Liu and Astaneh's moment-rotation model for bare shear tab connections. In the end, a modified moment-rotation model for shear tab connections with and without a BFFD is proposed. The conclusions drawn from this study are listed as follows.

- The effect of beam depth is negligible in the “Pre-slip” phase while an increase in thickness of beam web results in an increase of maximum moment and post-slip stiffness since the maximum moment is related with the bearing capacity for each bolt on the shear tab. The influence of shear tab plate thickness is the same as the beam depth.
- Both number of bolts and bolt spacing have a significant impact on the shear tab connections in both “Pre-slip” and “Post-slip” phases. An increased number of bolts or a larger bolt spacing results in an increase in slip moment, pre-slip stiffness, and post-slip stiffness.
- An increased number of bolts or a larger bolt spacing results in a decreased slip rotation. Increasing the bolt spacing is an economical and simple way to improve the behavior of shear tab connections if there is sufficient beam depth.
- For the bare shear tab connection with a 6 mm shear tab plate, the ratio of post-slip to pre-slip stiffness is at least 5%. An increase of shear tab plate or web thickness results in an increase of the stiffness ratio.
- A BFFD has a significant impact on the shear tab connections in both “Pre-slip” and “Post-slip” phases. In the “Pre-slip” phase, slip moment increases significantly as BFFD is added. Clamping bolt tension and distance between the center of the shear tab and the BFFD clamping bolt have a significant impact on the slip moment. Adding the BFFD results in additional moment strength. The actual moment strength increase can be estimated by 70% of the expected increase of moment strength due to the BFFD bolt slip.
- The slip rotation of connections with a BFFD is slightly smaller than the connections without BFFD. These results indicate the behavior of the BFFD is as expected with initiation of slip prior to full inelastic response of the shear tab connection.

- The actual binding rotation for shear tab connections with different configurations is approximately 75% of the theoretical binding rotation which can be calculated by the connection geometry.
- Liu and Astaneh's moment-rotation model for bare shear tab connections has a reasonable estimate of the slip moment and maximum moment while the estimation of slip rotation and maximum rotation are too large.
- The proposed modifications to the Liu and Astaneh model provide a simplified backbone curve that can be used to include the nonlinear response of shear tab connections in a structural analysis model.

In conclusion, the numerical simulation of the shear tab connection with and without the Bottom Flange Friction Device showed that both the connection with the BFFD and the larger bolt spacing had a higher moment strength and stiffness than the bare shear tab connection with standard bolt spacing (76 mm). It also showed that the initiation of slip of the BFFD occurred before the shear tab indicating that the BFFD activated early in the deformation pattern to dissipate energy. Maximizing the bolt spacing on the shear tab is the simplest and most economical way to improve the performance of shear tab connections in seismic analysis as it had similar improvements to adding a BFFD. The moment-rotation model for shear tab connections could be applied to nonlinear dynamic building models (including moment and braced frames) subjected to earthquake records to further investigate the impact of the modified shear tab connections on system response.

References

ABAQUS. (2020). *ABAQUS Analysis User's Guide.* Palo Alto, CA: ABAQUS Inc.

AISC. (2010). *Manual of Steel Construction, 14th Edition.* Chicago: American Institute of Steel Construction.

ATC. (2007). *Interim Testing Protocols for Determining the Seismic Performance Characteristics of Structural and Nonstructural Components.* Redwood City, California: FEMA.

Crocker, J. P., & Chambers, J. J. (2004). Single Plate Shear Connection Response to Rotation Demands Imposed by Frames Undergoing Cyclic Lateral Displacements. *Journal of Structural Engineering*, 934-941.

CSI. (2011). *CSI Analysis Reference Manual for SAP2000®, ETABS®, SAFE® and CSiBridge®.* Berkely, CA: Computers and Structures Inc.

Flores, F. X., Charney, F. A., & Lopez-Garcia, D. (2016). The influence of gravity column continuity on the seismic performance of special steel moment frame structures. *Journal of Constructional Steel Research*, 217-230.

Latour, M., Aniello, M. D., Zimbru, M., Rizzano, G., Piluso, V., & Landolfo, R. (2018). Removable friction dampers for low-damage steel beam-to-column joints. *Soil Dynamics and Earthquake Engineering*, 66-81.

Liu, J., & Astaneh-Asl, A. (2000). *Cyclic Tests on Simple Connections, Including Effects of the Slab.* Berkeley, CA: SAC Joint Venture.

Rahman, A., Mahamid, M., Amro, A., & Ghorbanpoor, A. (2007). The analyses of extended shear tab steel connections, part I: the unstiffened connections. *Eng J Am Inst Steel Constr, Vol. 44 (No. 2)*.

Richard, R., Gillett, P., Kriegh, J., & Lewis, B. (1980). The analysis and design of single plate framing connections. *Engineering Journal*, Quarter 2, 38-52.

Rojas, P., Ricles, J. M., & Sause, R. (2005). Seismic Performance of Post-tensioned Steel Moment Resisting Frames With Friction Devices. *Journal of Structural Engineering*, 529-540.

Weigand, J. M. (2017). Component-Based Model for Single-Plate Shear Connections with Pretension and Pinched Hysteresis. *J. Struct. Eng.*

Wen, R., Akbas, B., Sutchiewcharn, N., & Shen, J. (2013). Inelastic behaviors of steel shear tab connections. *Structural Design of Tall and Special Buildings Volume 23, Issue 12*, 929-946.

Wolski, M., Ricles, J. M., & Sause, R. (2009). Experimental Study of a Self-Centering Beam–Column Connection with Bottom Flange Friction Device. *Journal of Structural Engineering*, 479-488.

Wu, H., & Marshall, J. (2022). Experimental Evaluation of a Shear Tab Connection with a Bottom Flange Friction Device. *Engineering Journal, (Under Review)*.

Chapter 5 Impact of Shear Tab Connections on the Seismic Response of Steel Structures

Hongyang Wu, Graduate Research Assistant, Department of Civil and Environmental Engineering, 238 Harbert Engineering Center, Auburn University, Auburn, AL 36849, hzw0035@auburn.edu

Humam Hussein Mohammed Al-Ghabawi, Assistant Lecturer, Department of Civil Engineering, University of Technology, Baghdad, Iraq, humam.h.m.1993@gmail.com

Justin D. Marshall, Associate Professor of Civil and Environmental Engineering, 238 Harbert Engineering Center, Auburn University, Auburn, AL 36849, jdmarshall@auburn.edu

Abstract

Current structural design practice assumes seismic demands are resisted only by the seismic force resisting system while the contribution of the gravity load system to seismic resistance is negligible. The shear tab, one of the most common gravity connections, is usually designed assuming a pinned condition which does not provide moment capacity and cannot dissipate any seismic energy. However, previous research showed that shear tab connections are not truly pinned. The modeled simple connections developed moments prior to slipping which resulted in frictional energy dissipation and a positive effect on steel structures in earthquakes. This paper reports the results of the third phase of a research effort focused on enhancing the energy dissipation of shear tab connections to improve response of steel frame structures. Shear tab connections with and without modifications were considered. The modifications include adding a Bottom Flange Friction Device and increasing the connection depth. The impact of enhancing shear tab connections on the seismic response of three buildings (4-, 8-, and 16-story buildings) with two different lateral force resisting systems was evaluated through 3-D nonlinear

response history analysis in OpenSeesPy. Each building has one direction with a Reduced Beam Section special moment frame and an orthogonal Buckling Restrained Braced frame. Nonlinear response history analysis was performed in both directions of each building with a suite of 11 scaled earthquake records at each hazard level. In general, the impact of shear tab connections on the seismic response of steel structures is significant. Adding a BFFD and increasing the connection depth dissipate energy and improve the response of steel structures in earthquakes.

Keywords: steel structures, shear tab connection, energy dissipation, Bottom Flange Friction Device, finite element simulation

5.1 Introduction

In structural design practice, the gravity load and lateral load resisting system are typically designed separately. In steel structures this is clearly seen through the assumption of simple connections in the gravity system. Although it has been suggested that the strength and stiffness of gravity load system improves the behavior of steel structures when they are subjected to high intensity ground motions, the contribution of the gravity load system is typically ignored in design and subsequent performance assessment of the steel structures (Flores, Charney, & Lopez-Garcia, 2016). This is due to the strength and stiffness of a moment frame or braced frame being significantly larger than the gravity load system. In addition, the lack of information on modelling the connections makes it simpler to ignore the gravity system contribution. The shear tab connection is the most common simple connection used on beam-column joints in the gravity load system. It is typically modelled as a pinned connection in seismic analysis for simplicity and conservatism. However, Liu and Astaneh (2000) showed the standard shear tab connection could sustain bending moment as the beam end rotates. Both moment strength and ductility were observed in the experimental tests on shear tab connections with and without a concrete slab. Shear

tab connections performing as supplemental energy dissipators improve the structural response to earthquakes. The results were validated by numerical analysis in ABAQUS by Rou Wen et al (2013). In addition to a standard shear tab connection, two modified versions are discussed in this paper. One is a shear tab connection with a Bottom Flange Friction Device (BFFD), the other is a shear tab connection with the same number of bolts but a wider bolt spacing. Figure 5-1 shows a sketch of a standard shear tab connection and the modified versions. Both modifications provide increased strength and energy dissipation. The BFFD has been assessed both experimentally and numerically to understand the mechanics and modeling((Wu & Marshall, 2022a), (Wu & Marshall, 2022b)).

In this research, the BFFDs are installed on the shear tab connections in the gravity load system. Only one 16 mm bolt was used in the BFFD. The bolt pretension force was the minimum pretension defined by the AISC steel manual (2010). Increasing the bolt spacing on the shear tab is another way to increase moment strength with very low-cost impact. The conventional bolt space on shear tabs is 76 mm. The increase in shear tab moment strength depends on the depth of the beam relative to the number of bolts. Compared with adding a BFFD, increasing the bolt spacing is more convenient and economical. Both modified shear tab connections have larger moment strength and stiffness compared with the standard configuration (Wu & Marshall, 2022b).

There is little research assessing the impact of shear tab connections on seismic response of steel structures. Wen et al. modeled the shear tab connections on buildings from the SAC report (Liu & Astaneh-Asl, 2000) in a seismic analysis of the three-story non-ductile concentrically braced frames (Wen, Akbas, & Shen, 2013). A 2-D seismic analysis with one ground motion record was conducted. The results show that including the shear tab connections in the model enhances the stability and delays the collapse for non-ductile concentrically braced frames.

Investigating the impact shear tab connections with different configurations on the seismic response of other steel lateral has beneficial outcomes as it relates to design and retrofit of steel structures for both strength and functional recovery.

There are three phases in this research project to accomplish this goal and provide reliable results and conclusions. The first phase is to evaluate the shear tab connection with and without the BFFD experimentally (Wu & Marshall, 2022a). A series of 27 component level tests were used to investigate the performance of a Slotted Bolted Friction Device (SBFD). Then, a series of 18 large-scale tests were performed to investigate the performance of a Bottom Flange Friction Device on a shear tab beam-column connection. The hysteretic response, energy dissipation, bolt tension, friction coefficient and initial connection stiffness were evaluated. The second phase of the research numerically evaluated shear tab connections with different configurations at the component level (Wu & Marshall, 2022b). ABAQUS (2020) models were developed to validate the experimental results from the first phase. A series of 31 pushover analyses with the same modelling scheme were used to investigate the engineering characteristics of the suite of shear tab connections. This paper is the third phase of the research project. This paper evaluates the impact of enhanced shear tab connections on steel structures. The buildings utilized are based on the information from (Harris & Speicher, 2015) and (Harris & Speicher, 2018). The primary difference is the beam-column gravity connections will be included in the model. The OpenSeesPy models of the shear tab connections are developed based on the previous work (Wu & Marshall, 2022b).The shear tab connections will be applied to 3-D models of 4-, 8-, and 16-story buildings with Reduced Beam Section (RBS) special moment frames (SMF) and Buckling Restrained Braced Frames (BRBF) in the two orthogonal directions. Seismic analysis at the Design Earthquake (DE) and Service Level Earthquake (SLE) hazard levels were used to assess the

response. The results presented and discussed include drift and acceleration for each story, base shear, and energy dissipation in the shear tab connections, the RBS connections, and Buckling Restrained Braces (BRB).

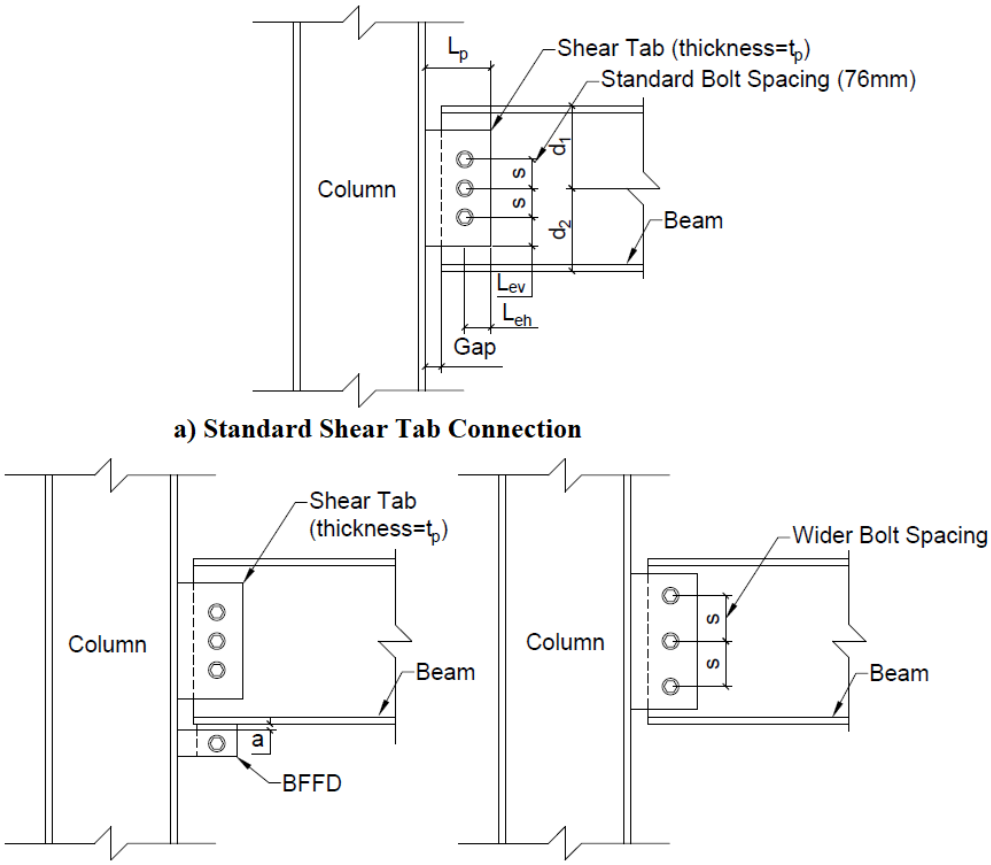

a) Standard Shear Tab Connection

b) Shear Tab Connection with BFFD **c) Shear Tab Connection with Wider Bolt Spacing**

Figure 5-1. Sketch of Shear Connection with and without BFFD

5.2 Basic Information about the Buildings

The 4-, 8-, and 16-story buildings were designed according to the 2012 International Building Code (Harris & Speicher, 2018). Figure 5-2 and Figure 5-3 show the typical floor flaming plan of the 4- and 8-story buildings and the 16-story building, respectively. The office buildings have a first-floor story height of 5.5m while the remaining story heights are 4.3m. Both floor flaming plans show a 30.5 m dimension of the north-south direction is 30.5m and a 45.5m

dimension of the east-west direction. The secondary beams are not shown in the floor flaming plan since they will not be included in the model.

The beam depth in the gravity load system was increased to allow for the proposed connection modifications. The beam section framing into the corner column and those between grid lines C and D were changed from W16X26 to W18X35. The remaining gravity beam sections running from east to west used a W16x31 in place of a W14X22. The column size in the gravity load system was designed by the gravity load information since they are not provided (Harris & Speicher, 2015). Table 5-1 shows the gravity column cross sections for all the buildings. The slab is lightweight concrete on steel decking with a total thickness of 83 mm.

The exterior frames are designed for seismic resistance. The east-west direction utilizes an RBS SMF (Grid Lines A and F) while the north-south direction uses a BRBF (Grid Lines 1 and 6). The location of the SMF is same for all the buildings. However, the location of the BRBF for the 16-story building is different from the 4- and 8-story buildings. The brace configuration in these three buildings is also different. The 4-story building has chevron (inverted-V) bracing while the 8- and 16-story buildings have a two-story X-bracing pattern. Detailed information for the SMF is described in (Harris & Speicher, 2015). The information related to the BRBF is provided by Harris and Speicher (2018).

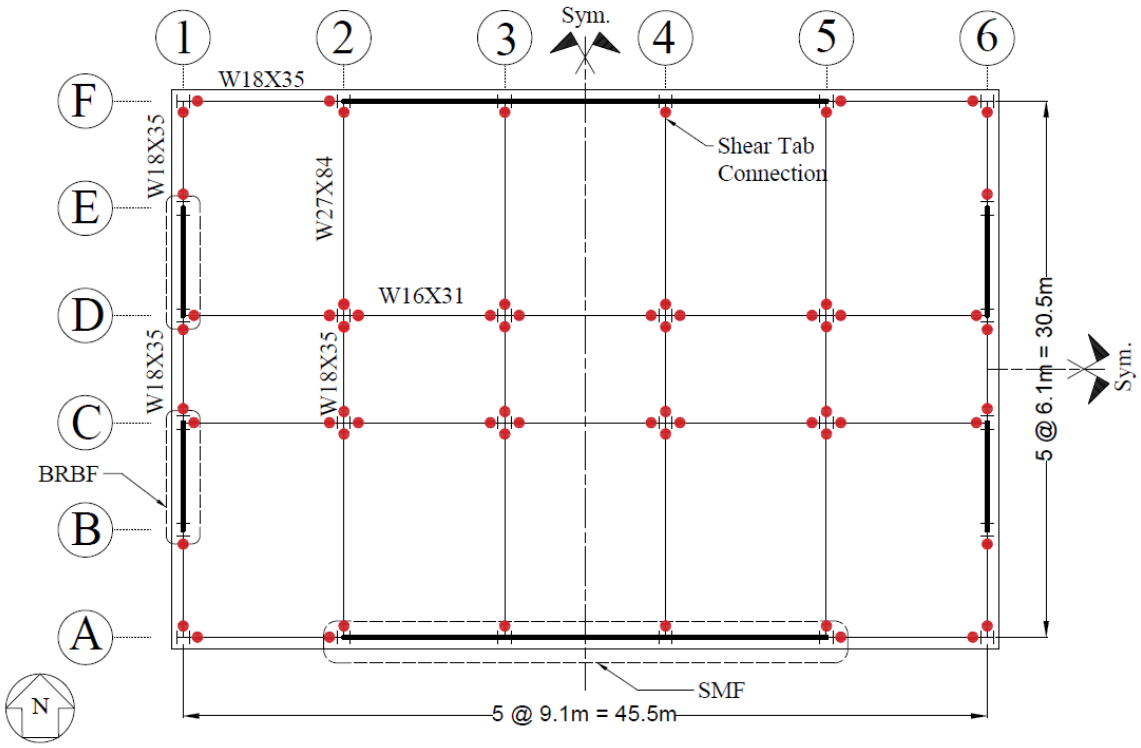

Figure 5-2. Typical Floor Framing Plan for 4- and 8-story Buildings

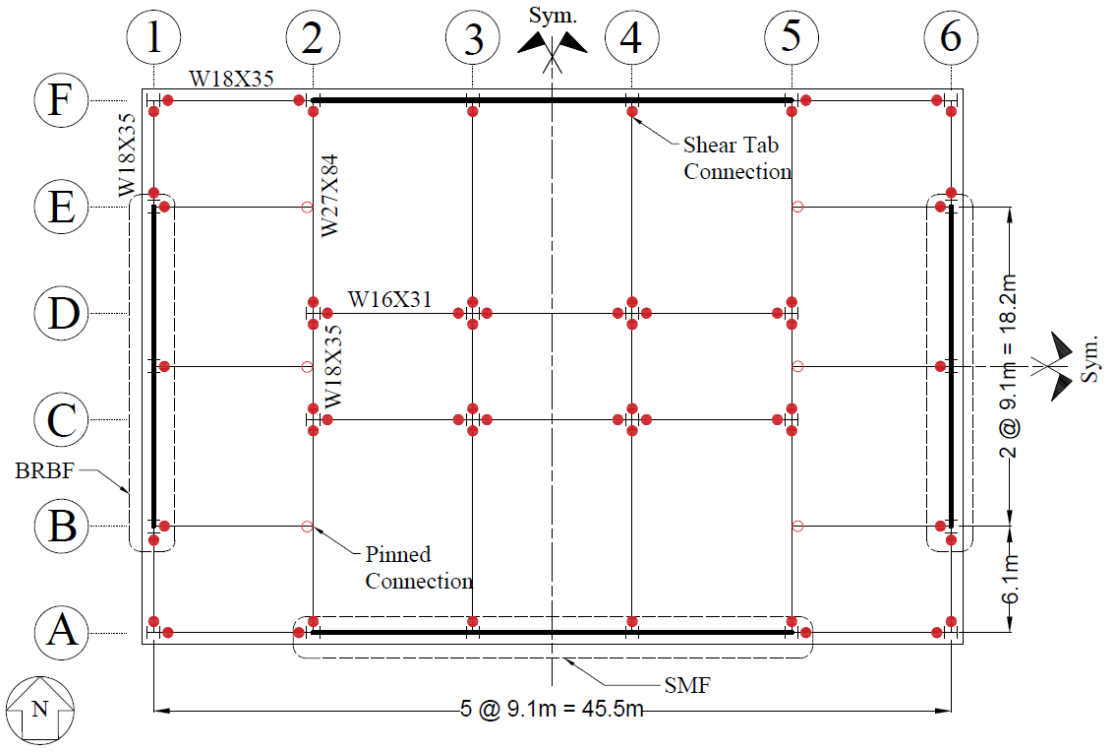

Figure 5-3. Typical Floor Framing Plan for 16-story Buildings

Table 5-1. Column Cross Sections for all the Buildings

<table>
<tr><td rowspan="2">Story</td><td colspan="2">4-story Building</td><td colspan="2">8-story Building</td><td colspan="2">16-story Building</td></tr>
<tr><td>Corner</td><td>Interior</td><td>Corner</td><td>Interior</td><td>Corner</td><td>Interior</td></tr>
<tr><td>1</td><td rowspan="4">W14X53</td><td rowspan="4">W14X61</td><td rowspan="4">W14X61</td><td rowspan="4">W14X90</td><td rowspan="4">W14X68</td><td rowspan="4">W14X159</td></tr>
<tr><td>2</td></tr>
<tr><td>3</td></tr>
<tr><td>4</td></tr>
<tr><td>5</td><td rowspan="12">-</td><td rowspan="4">W14X53</td><td rowspan="4">W14X61</td><td rowspan="4">W14X53</td><td rowspan="4">W14X109</td></tr>
<tr><td>6</td></tr>
<tr><td>7</td></tr>
<tr><td>8</td></tr>
<tr><td>9</td><td rowspan="8">-</td><td rowspan="4">W14X53</td><td rowspan="4">W14X90</td></tr>
<tr><td>10</td></tr>
<tr><td>11</td></tr>
<tr><td>12</td></tr>
<tr><td>13</td><td rowspan="4">W14X53</td><td rowspan="4">W14X61</td></tr>
<tr><td>14</td></tr>
<tr><td>15</td></tr>
<tr><td>16</td></tr>
</table>

All these buildings are located on the west coast of United States. The importance factor for all the structures is 1. Both site class and seismic design category is D. The maximum considered earthquake spectral response for short period, S_S, is 1.5g while it is 0.6g for the one second period, S_1. The design spectral response acceleration is 1.0g for short period, S_{DS}, and 0.6g for long period, S_{D1}. All other hazard information is provided in (Harris & Speicher, 2015).

5.3 FEM Modelling

Three-dimensional building models were created in OpenSeesPy. The RBS connections, the panel zone, and the columns' distributed plasticity (fiber section) were added to capture the inelastic behavior of SMFs. The nonlinear properties of the BRBs were applied to simulate the inelastic behavior of BRBFs. The shear tab connections with different configurations were added

on each floor in gravity load system for all the buildings. The shear tab locations are shown in Figures 5-2 and 5-3 by solid red dots. The details of modeling these nonlinear components will be discussed later. The interior beams and columns in the gravity load system were modeled by elastic beam elements (ForceBeamColumn3D). The gravity load columns will be rotated by 90 degrees aligning the strong axis with the BRBF direction to conduct the seismic analysis in the BRBF direction. The interior beam-beam connection (Figure 5-3) and the BRBF beam-column connections were modeled as pinned. The SMF beam-column connections were modeled including panel zone effects. The beams connected with BRBs at the midspan were modeled as continuous beams. The BRBs were modeled as a truss element with modified stiffness. The modified stiffness is equal to the BRB core elastic stiffness (E_s) times the modification factor (KF). The average modification factor (KF) is 1.48 based on Harris and Speicher's research (2018).

5.3.1 Shear Tab Connections

The geometry of a standard shear tab connection is shown in Figure 5-1(a). In this paper, the width of the shear tab L_p is 114 mm while the depth varies based on the number of bolts, N, and bolt spacing, s. Bolt edge distances, L_{eh} and L_{ev}, are 38 mm and 32 mm, respectively. The gap between the beam and the column flange, *gap*, is 13 mm. The gap between the BFFD and the beam flange, a, is 13 mm. The BFFD component are shown in Figure 5-4. The component dimensions are the same as the BFFD in Wu and Marshall (2022b). The shear tab connections are designed based on the beam gravity loads. All the shear tab bolts are fully pretensioned. Table 5-2 shows the details of the shear tab connections with different configurations that are utilized in the buildings. In the table, Bolt Tension represents the clamping force in the BFFD. 85kN is the minimum full pretension load based on AISC (2010) for a 16 mm ASTM F3125 Grade A325 bolt.

The pushover analysis on these connections to develop the backbone modeling curves for each connection variation was conducted using the commercial software ABAQUS 2020 (ABAQUS, 2020) shown in Figure 5-5(a). The ABAQUS model was validated by the experimental results (Wu & Marshall, 2022b). Moment-rotation pushover curves were generated for all the connections in Table 5-2.

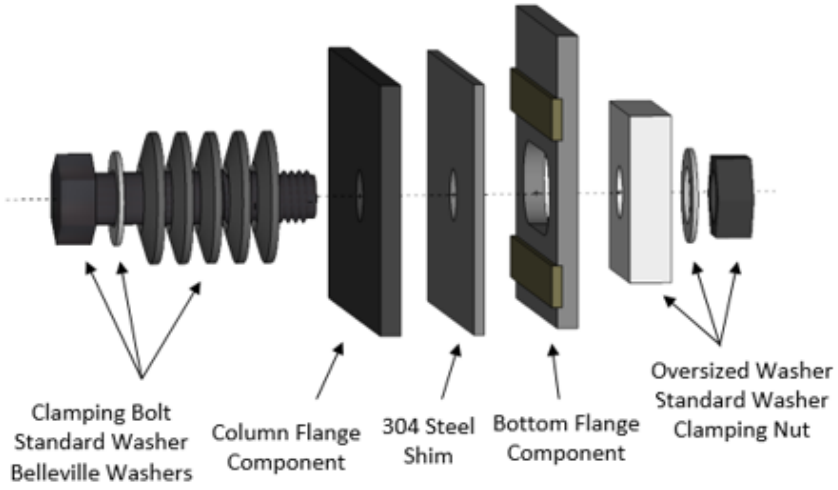

Figure 5-4. Details of Components of BFFD

Table 5-2. Details of Shear Tab Connection with different Configurations

Test	Beam	Column	N	s	d_1	d_2	t_p	Bolt Tension
				mm	mm	mm	mm	kN
1	W16X31	W14X61	3	76	203	203	6	0
2	W16X31	W14X90	3	76	203	203	6	0
3	W16X31	W14X145	3	76	203	203	6	0
4	W16X31	W14X61	3	76	203	203	10	0
5	W18X35	W14X61	4	76	225	225	6	0
6	W27X84	W14X61	6	76	339	339	6	0
7	W16X31	W14X61	3	76	203	203	10	85
8	W18X35	W14X61	4	76	225	225	6	85
9	W27X84	W14X61	6	76	339	339	6	85
10-1	W16X31	W14X61	3	76	153	253	10	85
10-2	W16X31	W14X61	3	76	153	253	10	85
11-1	W18X35	W14X61	4	76	175	275	6	85
11-2	W18X35	W14X61	4	76	175	275	6	85
12-1	W27X84	W14X61	6	76	263	415	6	85
12-2	W27X84	W14X61	6	76	263	415	6	85
13	W16X31	W14X61	3	127	203	203	10	0
14	W18X35	W14X61	4	102	225	225	6	0
15	W27X84	W14X61	6	102	339	339	6	0

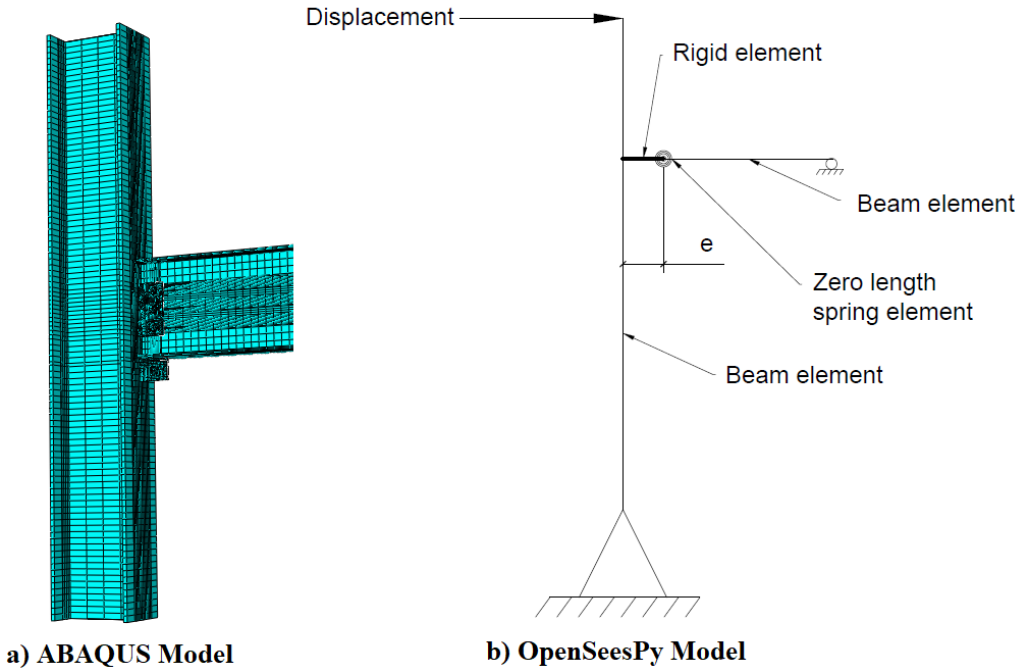

Figure 5-5. Numerical Models of Shear Tab Connection

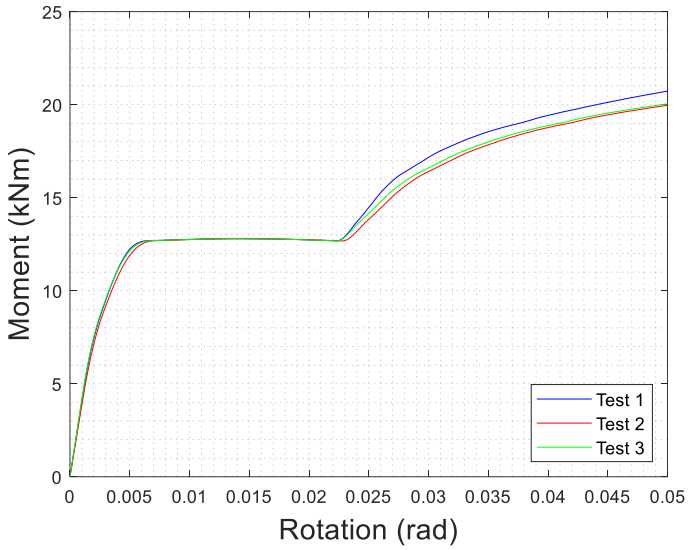

Figure 5-6. Result of Pushover Analysis for Test 1, 2 and 3

The shear tab connections in Tests 4, 5 and 6 are standard shear tab connections. The shear tab connections in Tests 7, 8 and 9 are shear tab connections with a BFFD. The connections in Tests 10-1, 10-2, 11-1, 11-2, 12-1 and 12-2 are modified shear tab connections with a BFFD. The shear tab on the beam was moved up to increase the connection moment strength. The adjusted shear tab position means the centerline of the beam and the shear tab are not coincident. The connections were pushed in both directions since rotation in the positive (beam moves up) and negative direction before the binding of beam flange and column are different. For Tests 10-1 and 10-2, the connections are same with the opposite direction of rotation. The shear tab connections in Tests 13, 14 and 15 have a wider bolt spacing.

The pushover analyses in Figure 5-6 (Connections 1 – 3) have the same shear tab connection with different column cross sections. The purpose of these three tests is to investigate the influence of column size on the shear tab connections. The results shown in Figure 5-6 indicate that the difference among these pushover analyses is negligible. Therefore, the column influence on shear tab connection is not considered further.

The OpenSeesPy shear tab connection models were developed based on the simplified moment-rotation pushover curve which is a modified form of the pushover curves generated from ABAQUS. The shear tab connection behavior after binding of the beam flange and column is not considered. Detailed information on the simplified shear tab pushover curve development is presented in Wu and Marshall (2022b). The typical OpenSeespy model of shear tab connection is shown in Figure 5-5(b). The beam and column are modeled using line elements with the insertion point being the cross section mid-height. The shear tab connection is modelled as a spring using the Steel4 material. The distance between the column and spring, *e*, is the distance between the column centerline and shear tab bolt line. The element connecting these points is modeled as rigid. The Steel4 material parameters are calibrated in OpenSeesPy to fit the simplified ABAQUS results. Figure 5-7 shows a comparison between the ABAQUS results and OpenSeesPy results for Test 4. The difference between the ABAQUS (simplified) and OpenSeesPy results is minimal (Figure 5-7(a)). Figure 5-7(b) shows that the shear tab behavior under cyclic response is reasonably captured by the OpenSeesPy model.

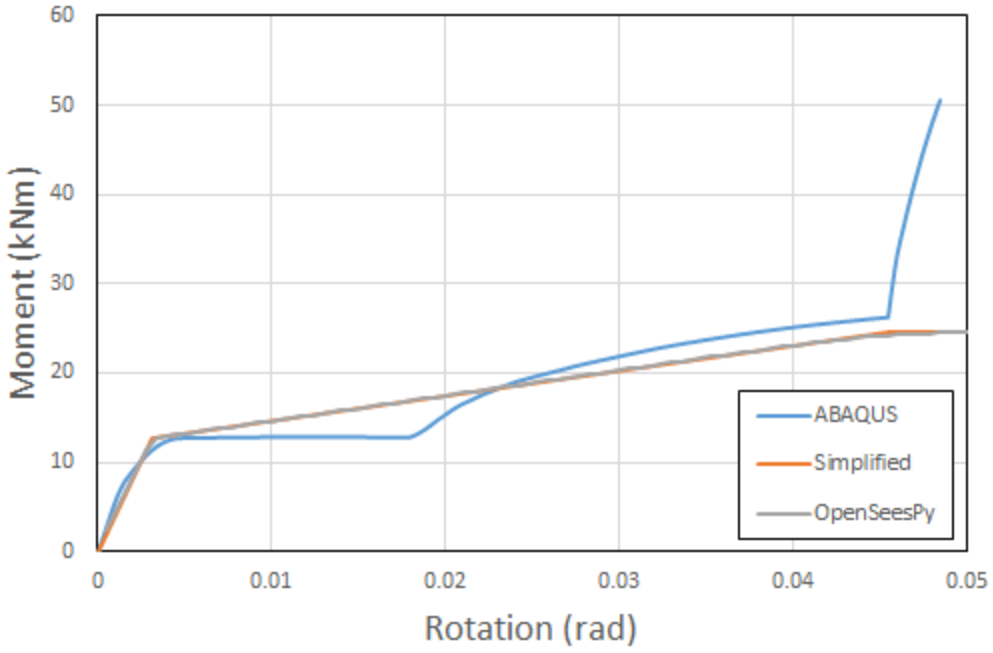

a) Comparison of Pushover Test

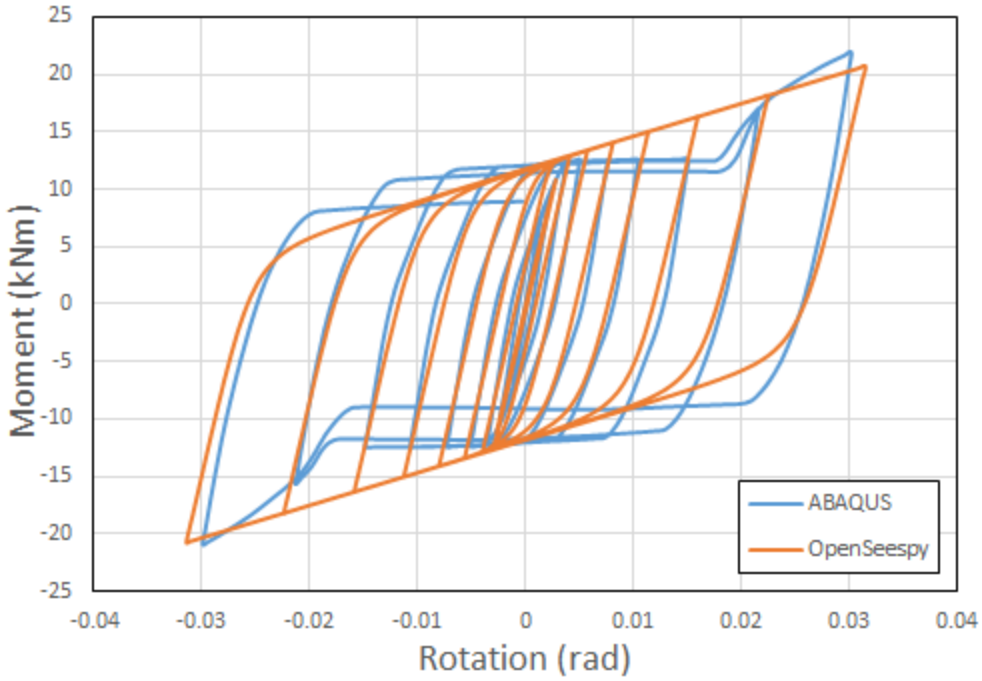

b) Comparison of Cyclic Test

Figure 5-7. Comparison of Results between ABAQUS and OpenSeesPy for Test 4

5.3.2 Reduced Beam Section and Column Distributed Plasticity

A spring element with modified Ibarra-Krawinkler deterioration model (Ibarra & Krawinkler, 2005) was used to model the RBS in the special moment frames. The spring element was located at the center of the RBS. The moment capacity of the spring was calculated based on the reduced beam cross section with a factor of 1.07 to account for strain hardening (Lignos, 2008). The stiffnesses of the RBS and the beam segment between the two RBS connections were modeled based on Gupta and Krawinkler's research (1999). The rotational stiffness of the spring was n (n=10) times higher than the rotational stiffness of the beam segment.

The modelling scheme using distributed plasticity (fiber section) along the column to capture potential column inelasticity. The cross sections of columns were divided into multiple fibers which are enough to reasonably match with the cross section exact integration curve. Material property of ASTM A992 steel was applied on the fibers.

5.3.3 Panel Zone

The panel zone was modeled by the Gupta and Krawinkler approach (1999). The width and height of panel zone are equal to the depth of column and beam, respectively. Figure 5-8 shows the OpenSeesPy panel zone model. The model uses eight beam elements with very large moments of inertia ($I=10^9$ mm^4). All the corner joints except the top right joint were modelled as an ideal hinge. A rotational spring element was modelled at top right corner to represent the nonlinear force-deformation response of the panel zone. Elements 1 and 2 were modelled to connect the beam and column in the out of plane direction. For element 1, both axial and flexural stiffnesses are very large. However, for element 2, the flexural stiffness is large while the axial stiffness is approximately zero. Moment releases were applied to the joints of element 1, 2 and beam element

framing into the panel zone in the orthogonal direction. The SMF OpenSeesPy model is validated with the experimental results (Popov, Blondet, & Stepanov, 1997)by Al-Ghabawi (2021).

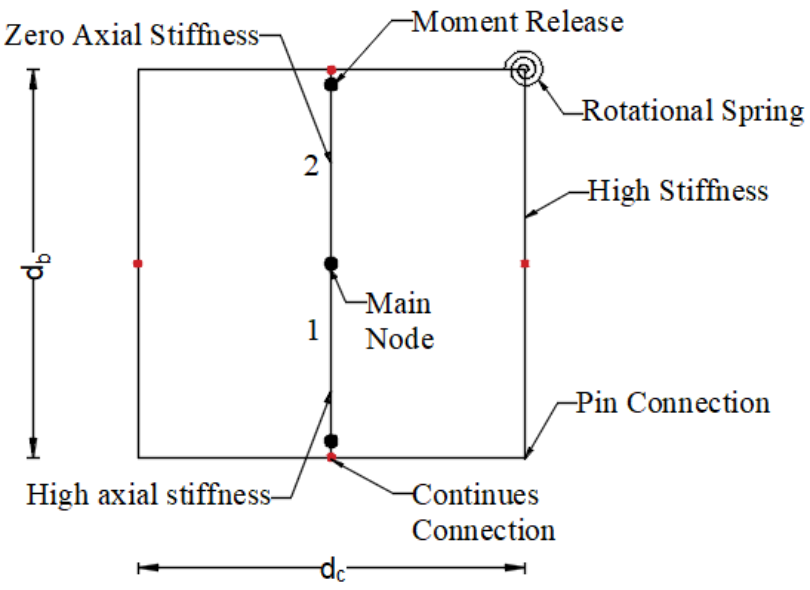

Figure 5-8. OpenSeesPy Panel Zone Model

5.3.4 Buckling Restrained Brace

The OpenSeesPy model of the BRB elements were modelled as truss elements with Steel02 and Pinching4 materials. The Pinching4 material was applied in parallel with Steel02. The tensile strength of the Pinching4 was zero while the compressive strength is defined based on experimental data (Upadhyay, Pantelides, & Ibarra, 2019). The additional compressive force is based on the friction developed between the BRB steel core and surrounding mortar which results in the BRB compression strength being higher than the tension strength. The modelling scheme of the BRB and the adjacent beam and column is shown in Figure 5-9. To account for the influence of the gusset plate, the stiffness of the beam and column in the gusset plate region is multiplied by 2 (Speicher & Harris, 2019). The BRB OpenSeesPy model is validated with the experimental

results ((Merritt, Uang, & Benzoni, 2003), (Newell, Uang, & Benzoni, 2006)) by Al-Ghabawi (2021).

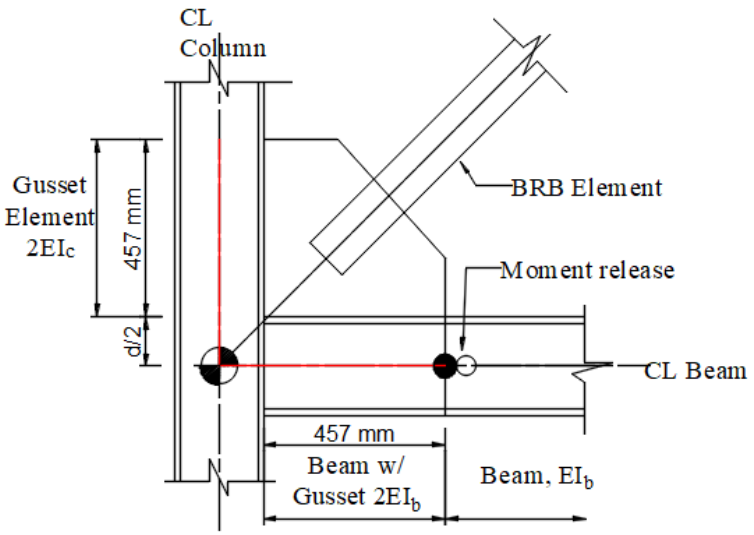

Figure 5-9. OpenSeesPy model of BRB with Adjacent Beam and Column

5.3.5 Base Fixity

Base restraint has a significant effect on steel moment frame behavior under earthquake loads. The assumption that the column bases are pinned will overestimate the column flexibility while the assumption that the column bases are fixed will underestimate the column flexibility. This can have a large effect on the first story drift. It is assumed that all the columns in the moment frames are fixed at the base while the columns in the braced frames and gravity load system are assumed to be pinned at the base.

5.3.6 Mass and Damping

The lumped mass method is used in this paper. The lumped mass is calculated based on the weight information from (Harris & Speicher, 2015). Each beam-column joint had the mass applied based on the associated tributary area.

For the nonlinear dynamic response history analysis, Rayleigh damping of 2.5% is assigned to the first modal period as well as all the period that captured at least 95% of the effective modal mass for all the structures. The modal properties for the structures without shear tab connections are shown in Table 5-3. The modification of adding the shear tab connections with different configurations had little impact on the modal properties.

Table 5-3. Period of Vibration for Modal Analysis in OpenSeesPy

Mode	4-story Building	8-story Building	16-story Building
	Period (sec)	Period (sec)	Period (sec)
1	1.752	2.726	4.013
2	0.809	2.024	2.419
3	0.587	1.352	1.698
4	0.516	0.944	1.454
5	0.310	0.678	0.860
6	0.243	0.519	0.830

5.3.7 Ground Motion Selection and Scaling

The ground motions for seismic analysis were selected from the Far Field record set from FEMA P695 (2009). Eleven ground motions were selected, and amplitude scaled based on the SLE and DE acceleration response spectrum and the modal analysis results. Maximum Considered Earthquake (MCE), DE and SLE are seismic design parameters for building code design. They are derived based on statistical analysis of past seismicity data. MCE, DE and SLE are defined as the ground shaking level at building site with 2% probability of exceedance in 50 years, 10% probability of exceedance in 50 years and 50% probability of exceedance in 30 years. The DE is taken as 2/3 times the MCE. The scaling was done in accordance with ASCE 7 ensuring that over the range of periods considered important, the mean did not fall below 10 percent of the spectrum. Tables 5-4, 5-5 and 5-6 show the selected ground motions and the

corresponding scale factors. Note that for the 16-story building the difference in the period range between the SMF and BRBF required a different suite of scaled earthquakes.

Table 5-4. Selected Ground Motions and Scale Factors for 4-Story Building

PEER Number	Event	Station	Scale Factor (SLE)	Scale Factor (DE)
FF02-1	Northridge-1994	Canyon Country-West Lost Canyon	0.72	1.13
FF04-1	Hector Mine-1999	Hector	1.19	1.87
FF05-1	Imperial Valley-1979	Delta	1.17	1.76
FF06-1	Imperial Valley-1979	El Centro Array #11	0.75	1.23
FF08-1	Kobe, Japan-1995	Shin-Osaka	1.22	2.18
FF09-1	Kocaeli, Turkey-1999	Duzce	1.11	1.68
FF10-2	Kocaeli, Turkey-1999	Arcelik	2.14	3.34
FF11-2	Landers-1992	Yermo Fire Station	1.50	2.36
FF16-1	Superstition Hills-1987	El Centro Imp. Co. Center	0.96	1.47
FF19-2	ChiChi, Taiwan-1999	CHY101-N	0.71	1.04
FF21-1	San Fernando-1971	LA-Hollywood Stor Lot	1.57	2.52

Table 5-5. Selected Ground Motions and Scale Factors for 8-Story Building

PEER Number	Event	Station	Scale Factor (SLE)	Scale Factor (DE)
FF04-1	Hector Mine-1999	Hector	1.77	3.49
FF05-1	Imperial Valley-1979	Delta	0.98	1.90
FF06-1	Imperial Valley-1979	El Centro Array #11	0.79	1.54
FF09-1	Kocaeli, Turkey-1999	Duzce	0.68	1.35
FF10-2	Kocaeli, Turkey-1999	Arcelik	2.17	4.19
FF11-2	Landers-1992	Yermo Fire Station	1.44	2.82
FF15-2	Manjil, Iran-1990	Manjil-Transverse	0.49	0.93
FF16-1	Superstition Hills-1987	El Centro Imp. Co. Center	1.11	2.15
FF17-2	Superstition Hills-1987	Poe Road	0.91	1.79
FF19-2	ChiChi, Taiwan-1999	CHY101-N	0.77	0.91
FF21-2	San Fernando-1971	LA-Hollywood Stor Lot	2.38	4.61

Table 5-6. Selected Ground Motions and Scale Factors for 16-Story Building

SMF Direction				
PEER Number	Event	Station	Scale Factor (SLE)	Scale Factor (DE)
FF05-2	Imperial Valley-1979	Delta	1.24	1.83
FF06-2	Imperial Valley-1979	El Centro Array #11	0.85	1.62
FF09-1	Kocaeli, Turkey-1999	Duzce	0.45	0.82
FF10-2	Kocaeli, Turkey-1999	Arcelik	1.87	2.76
FF11-2	Landers-1992	Yermo Fire Station	1.05	1.94
FF12-1	Landers-1992	Coolwater-LN	1.24	2.40
FF15-2	Manjil, Iran-1990	Manjil-Transverse	0.72	1.36
FF16-1	Superstition Hills-1987	El Centro Imp. Co. Center	0.86	1.57
FF19-1	ChiChi, Taiwan-1999	CHY101-E	0.70	1.23
FF20-1	ChiChi, Taiwan-1999	TCU045 E	0.88	1.72
FF21-1	San Fernando-1971	LA-Hollywood Stor Lot	1.54	2.92
BRBF Direction				
PEER Number	Event	Station	Scale Factor (SLE)	Scale Factor (DE)
FF05-1	Imperial Valley-1979	Delta	1.04	1.73
FF06-2	Imperial Valley-1979	El Centro Array #11	0.95	1.66
FF08-2	Kobe, Japan-1995	Shin-Osaka	1.41	2.41
FF09-1	Kocaeli, Turkey-1999	Duzce	0.67	1.11
FF10-2	Kocaeli, Turkey-1999	Arcelik	1.84	2.94
FF11-2	Landers-1992	Yermo Fire Station	1.47	2.43
FF15-2	Manjil, Iran-1990	Manjil-Transverse	0.59	1.00
FF16-1	Superstition Hills-1987	El Centro Imp. Co. Center	1.15	1.94
FF17-2	Superstition Hills-1987	Poe Road	1.13	1.95
FF19-1	ChiChi, Taiwan-1999	CHY101-E	0.71	1.12
FF21-1	San Fernando-1971	LA-Hollywood Stor Lot	1.48	2.51

5.4 Result and Discussion

In this section, the results of pushover analysis for 4-, 8-, and 16-story buildings in SMF and BRBF direction with shear tab connections with different configurations are presented first. The total base shear versus building drift was plotted to have a general understanding of the impact of shear tab connections on steel structures. Then, the results of seismic response of the buildings

including story drift, total acceleration, base shear, and energy dissipation in the moment connections, buckling restrained braces and shear tab connections are presented and discussed to investigate the influence of shear tab connections on response.

5.4.1 Results of Pushover Analysis

Pushover analysis was conducted on the 4-, 8-, and 16-story buildings in the SMF and BRBF direction. Figures 5-10, 5-11 and 5-12 show the pushover curves of the 4-, 8-, and 16-story buildings in SMF direction, respectively while the pushover curves of 4-, 8-, and 16-story buildings in BRBF direction were shown in Figure 5-13, 5-14 and 5-15, respectively. The "Baseline" case means the shear tab connections were modelled as pinned connections. The pushover curve for "Baseline" models were compared with the pushover curves in the NIST Reports ((Harris & Speicher, 2015), (Harris & Speicher, 2018)). All the" Baseline" models generated similar pushover curves when compared with the corresponding models in the NIST Reports. The "Shear Tab" models represent the buildings with standard shear tab connections. The results show that the strength and stiffness of buildings increased in both the SMF and BRBF directions for all the buildings. The increasements of base shear between "Baseline" and "Shear Tab" are 4%, 3% and 2% for the 4-, 8-, and 16-story buildings in SMF direction while 20%, 18% and 10% for the 4-, 8-, and 16-story buildings in BRBF direction, respectively. The impact of shear tab connections on BRBFs is larger than that on SMFs. The influence of shear tab connection decreases when the height of building increases. Both adding a BFFD ("BFFD") and increasing the bolt spacing ("Wider Spacing") on the shear tab demonstrated an increase in strength and stiffness, but the change was smaller as compared to the change from the Baseline to the Shear Tab models. The "BFFD_Offset" represents the modified shear tab connections with BFFD. The shear tab was moved up to increase the distance between BFFD and the center of the shear tab bolt group.

However, the difference between “BFFD” and “BFFD_Offset” models for all the buildings is not significant. Therefore, the nonlinear response history analysis will not be applied for the “BFFD_Offset” models.

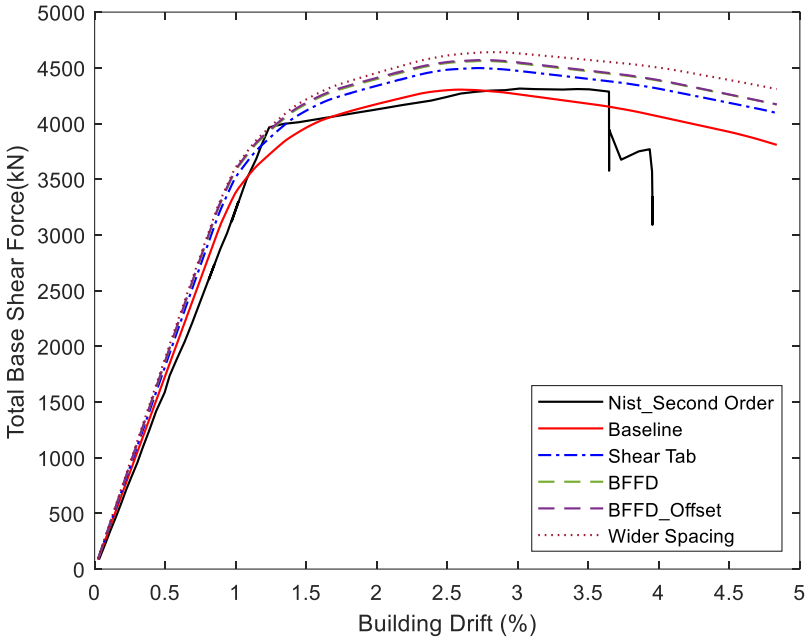

Figure 5-10. Pushover Curve for the 4-Story Building in the SMF Direction

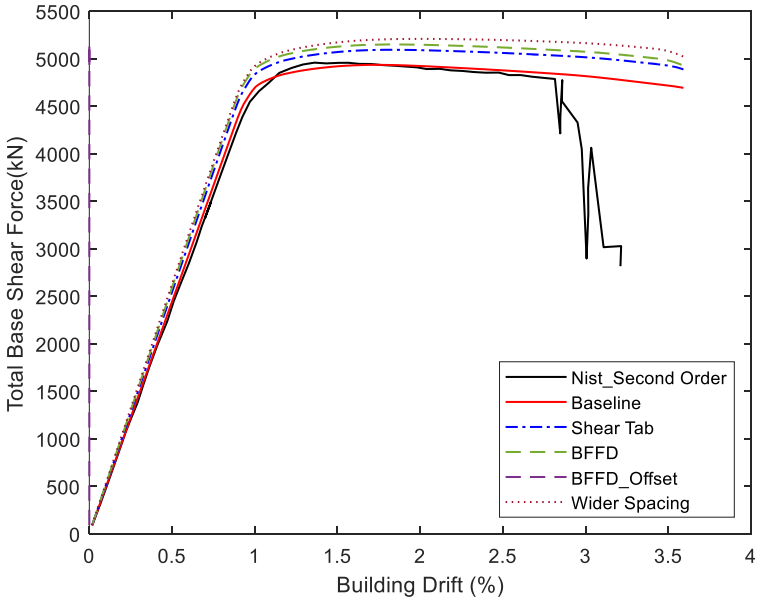

Figure 5-11. Pushover Curve for the 8-Story Building in the SMF Direction

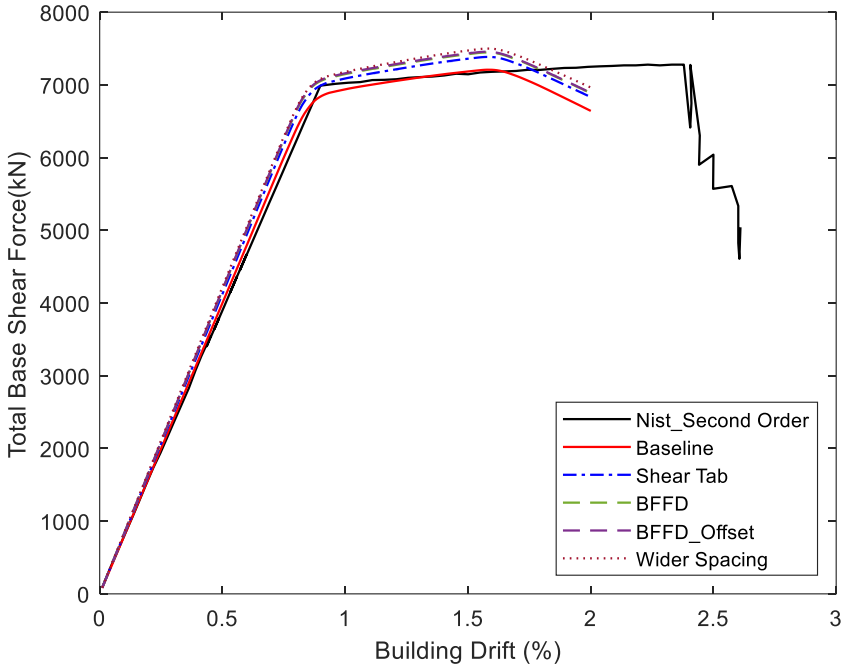

Figure 5-12. Pushover Curve for the 16-Story Building in the SMF Direction

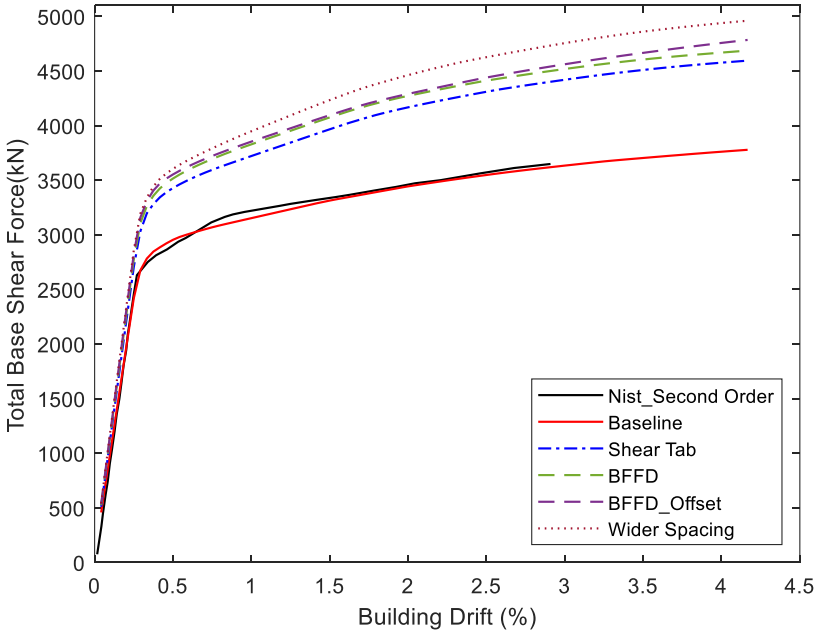

Figure 5-13. Pushover Curve for the 4-Story Building in the BRBF Direction

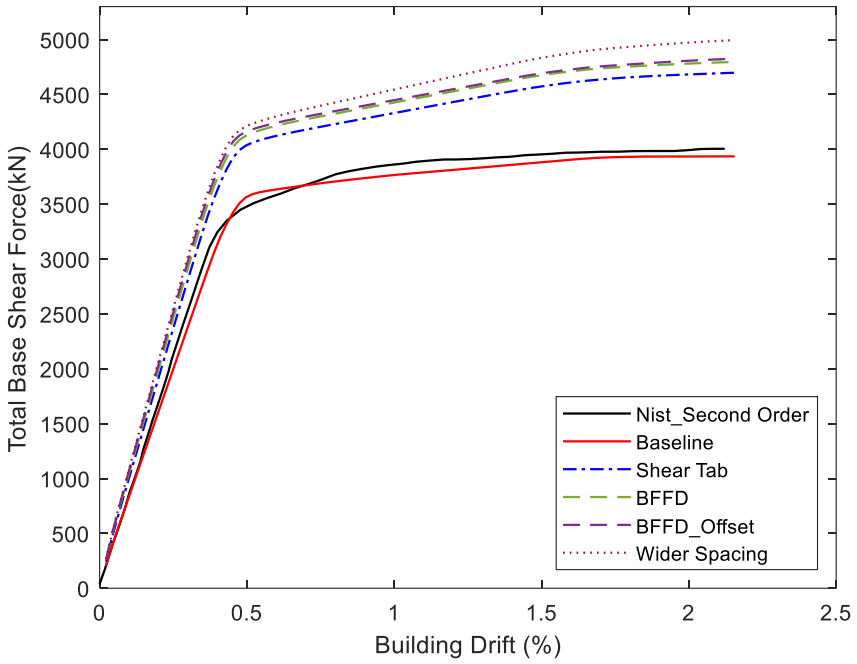

Figure 5-14. Pushover Curve for the 8-Story Building in the BRBF Direction

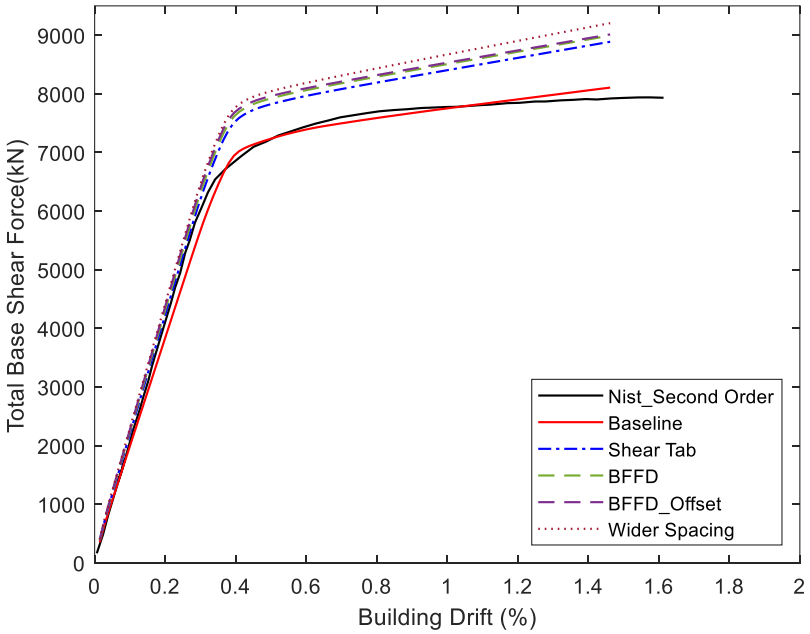

Figure 5-15. Pushover Curve for the 16-Story Building in the BRBF Direction

5.4.2 Results of Nonlinear Response History Analysis

5.4.2.1 Story Drift

Story drift is defined as the difference in lateral displacement between two adjacent stories divided by the story height. During a strong ground motion, large lateral demands are imposed on structures. If the drift of the structure becomes too large, P-delta effects can cause instability of the structure and potentially collapse. In this research, maximum relative drift for each story was calculated for the buildings in both directions under the corresponding ground motion suite. The average value of maximum relative drift for each story in the corresponding ground motion suite will be called average maximum drift.

Figures 5-16 through 5-21 show the average maximum drift for 4-, 8- and 16-story buildings in the SMF direction at SLE and DE. The summary of the average maximum drift and the drift ratio (BL, ST) for 4-, 8- and 16-story buildings in the SMF direction at SLE and DE are shown from Tables 5-7 to 5-12. The drift ratio is defined as the average maximum drift of models with shear tabs with different configurations ("Shear Tab", "BFFD" and "Wider Spacing" models) divided by the average maximum drift of the "Baseline" model (BL) or the "Shear Tab" model (ST). The results show that there is a beneficial impact of adding shear tab connections. This is particularly true for the upper stories in the SMF direction, especially the top story. The average maximum drift decreases for each story after adding the shear tab connections. For instance, the 8-story SMF building at SLE, the average maximum drift on the top story reduced by 14% after including the standard shear tab connections. The influence of the magnitude of ground motions is not significant. The influence of shear tab connections for the buildings at SLE is a little bit larger than that for the buildings at DE which indicates the shear tab connections have larger impact in the small-scale earthquakes. In addition, the modifications of shear tab connections slightly decreased the average maximum drift for each story for all the buildings. Top stories received

larger impact compared with the remaining stories. For the 8-story SMF building at DE, the average maximum drift on the top story reduced by 7% after adding the BFFD and 9% after increasing the shear tab bolt spacing. The model with wider bolt spacing on the shear tab has 16% less average maximum drift on the top story compared to the baseline model.

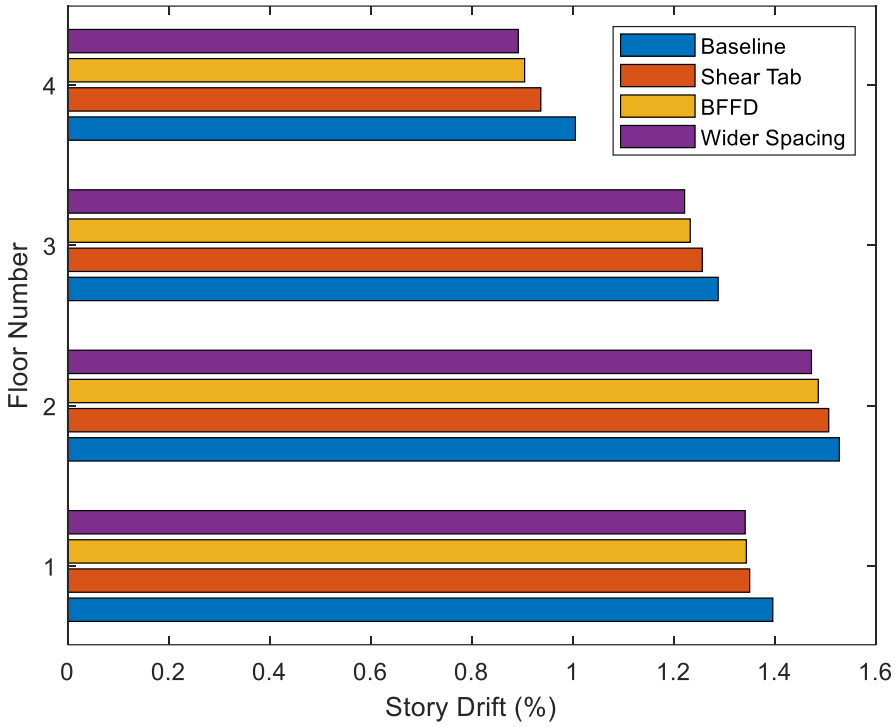

Figure 5-16. Average Maximum Drift for the 4-Story Building in the SMF Direction at SLE

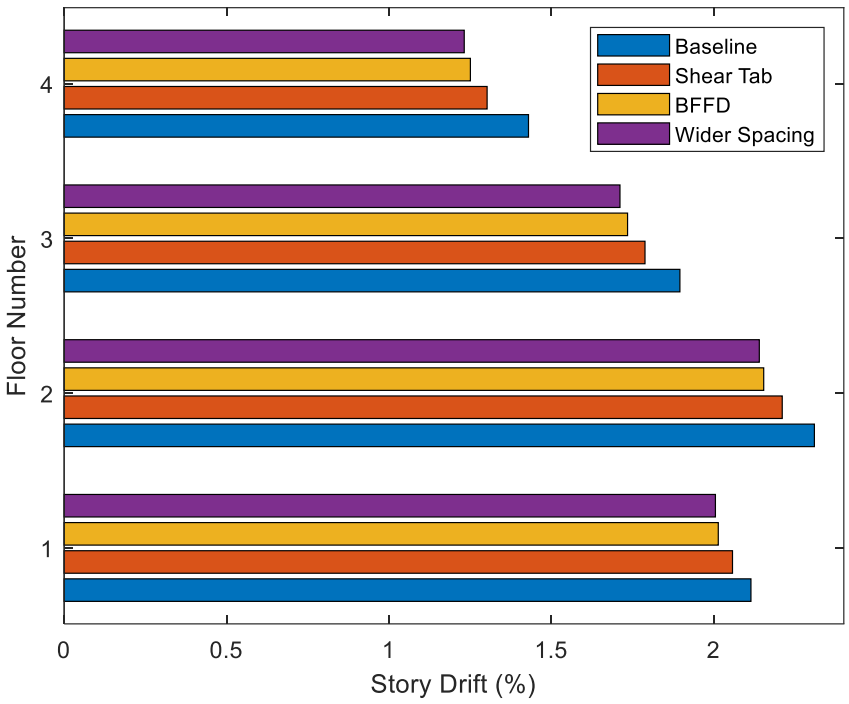

Figure 5-17. Average Maximum Drift for the 4-Story Building in the SMF Direction at DE

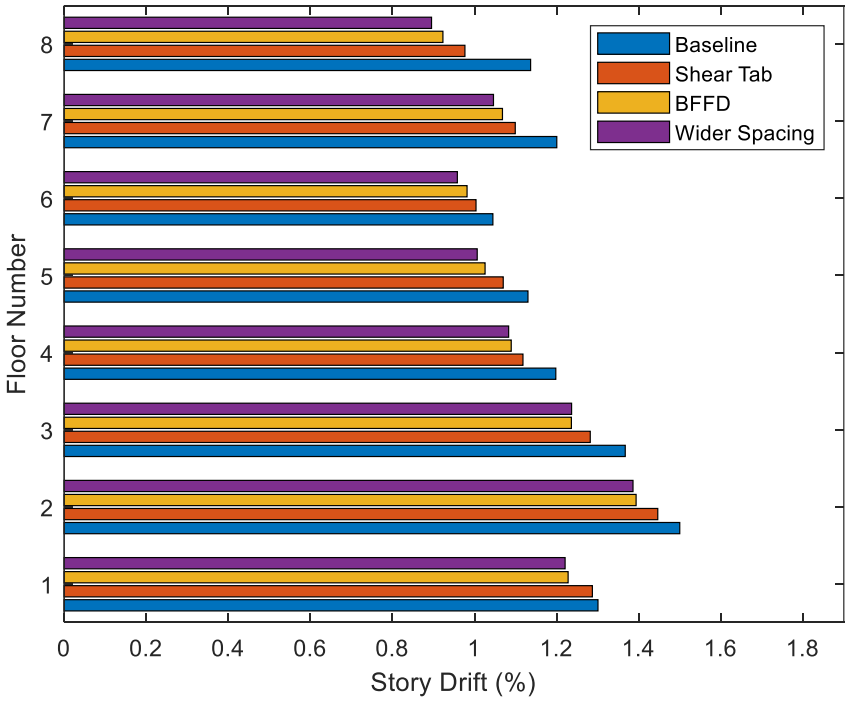

Figure 5-18. Average Maximum Drift for the 8-Story Building in the SMF Direction at SLE

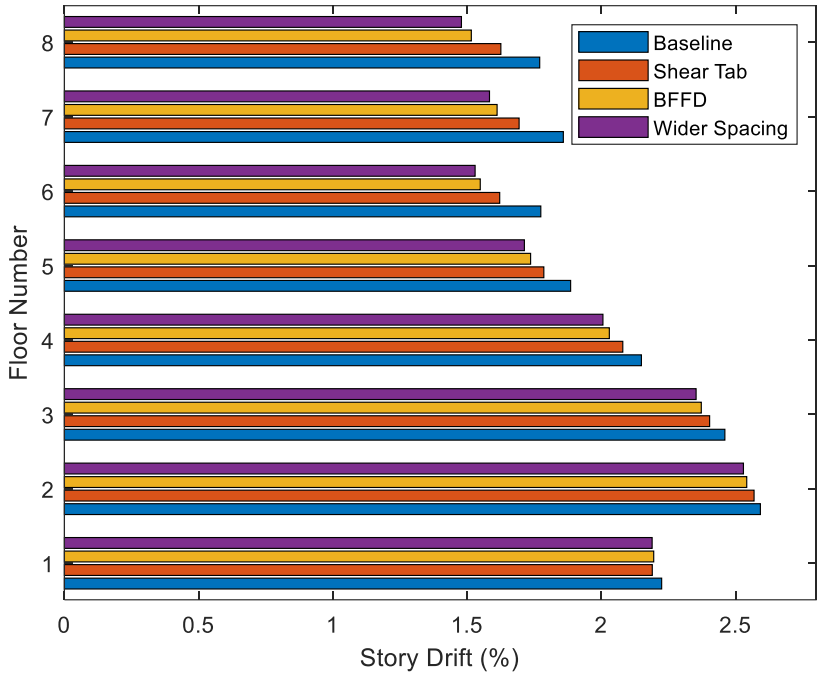

Figure 5-19. Average Maximum Drift for the 8-Story Building in the SMF Direction at DE

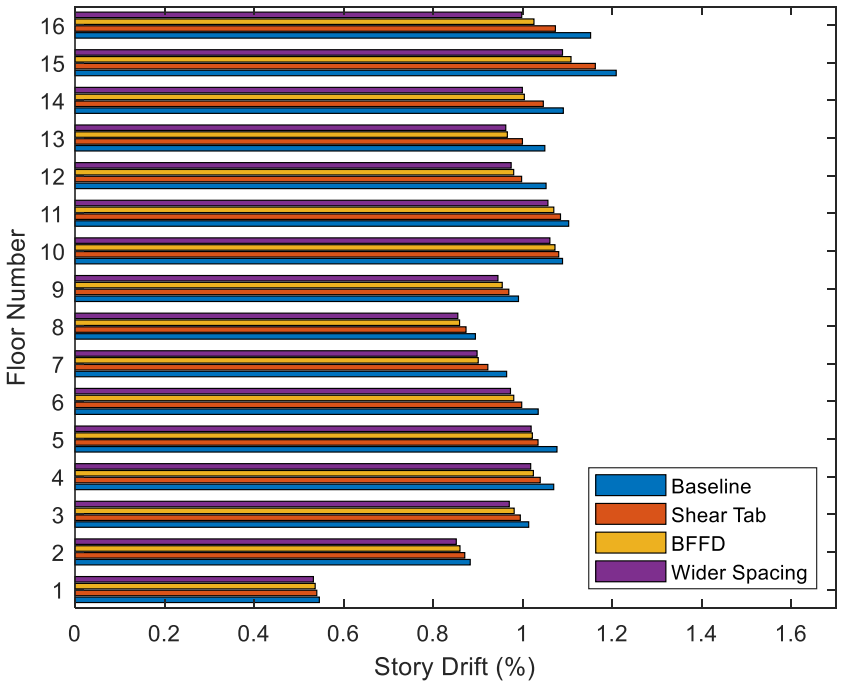

Figure 5-20. Average Maximum Drift for the 16-Story Building in the SMF Direction at SLE

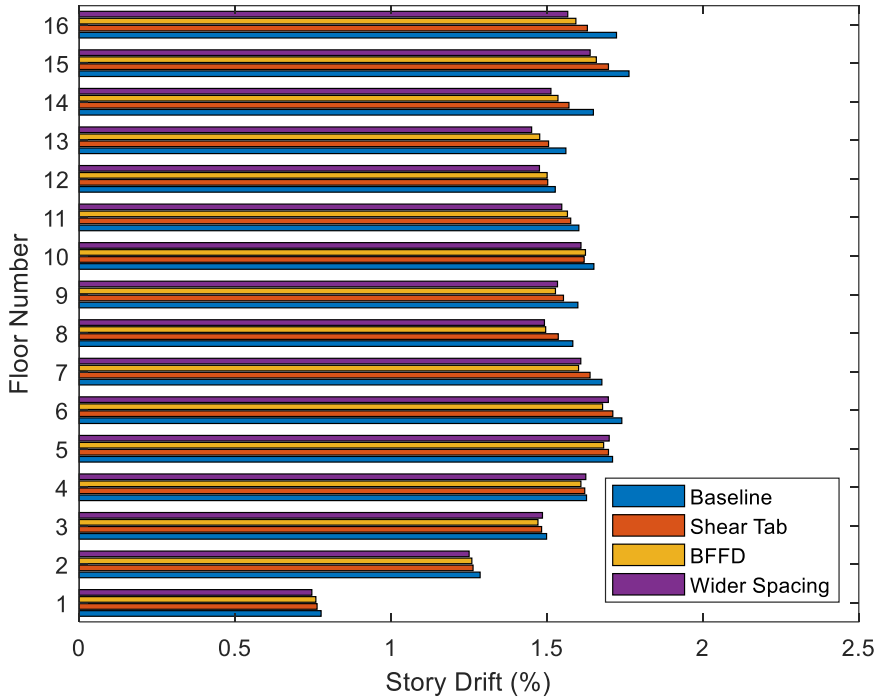

Figure 5-21. Average Maximum Drift for the 16-Story Building in the SMF Direction at DE

Table 5-7. Story Drift for the 4-Story Building in the SMF Direction at SLE

Story	Baseline	Shear Tab		BFFD		Wider Spacing	
	AVG MAX Drift (%)	AVG MAX Drift (%)	Drift Ratio (BL)	AVG MAX Drift (%)	Drift Ratio (BL) Drift Ratio (ST)	AVG MAX Drift (%)	Drift Ratio (BL) Drift Ratio (ST)
1	1.40	1.35	0.97	1.34	0.96 1.00	1.34	0.96 0.99
2	1.53	1.51	0.99	1.49	0.97 0.99	1.47	0.96 0.98
3	1.29	1.26	0.98	1.23	0.96 0.98	1.22	0.95 0.97
4	1.01	0.94	0.93	0.90	0.90 0.97	0.89	0.89 0.95

Table 5-8. Story Drift for the 4-Story Building in the SMF Direction at DE

Story	Baseline	Shear Tab		BFFD		Wider Spacing	
	AVG MAX Drift (%)	AVG MAX Drift (%)	Drift Ratio (BL)	AVG MAX Drift (%)	Drift Ratio (BL)	AVG MAX Drift (%)	Drift Ratio (BL)
					Drift Ratio (ST)		Drift Ratio (ST)
1	2.11	2.06	0.97	2.01	0.95	2.00	0.95
					0.98		0.97
2	2.31	2.21	0.96	2.15	0.93	2.14	0.93
					0.97		0.97
3	1.90	1.79	0.94	1.73	0.92	1.71	0.90
					0.97		0.96
4	1.43	1.30	0.91	1.25	0.87	1.23	0.86
					0.96		0.95

Table 5-9. Story Drift for the 8-Story Building in the SMF Direction at SLE

Story	Baseline	Shear Tab		BFFD		Wider Spacing	
	AVG MAX Drift (%)	AVG MAX Drift (%)	Drift Ratio (BL)	AVG MAX Drift (%)	Drift Ratio (BL)	AVG MAX Drift (%)	Drift Ratio (BL)
					Drift Ratio (ST)		Drift Ratio (ST)
1	1.30	1.29	0.99	1.23	0.94	1.22	0.94
					0.95		0.95
2	1.50	1.45	0.96	1.39	0.93	1.39	0.92
					0.96		0.96
3	1.37	1.28	0.94	1.24	0.90	1.24	0.90
					0.96		0.96
4	1.20	1.12	0.93	1.09	0.91	1.08	0.90
					0.97		0.97
5	1.13	1.07	0.95	1.03	0.91	1.01	0.89
					0.96		0.94
6	1.04	1.00	0.96	0.98	0.94	0.96	0.92
					0.98		0.95
7	1.20	1.10	0.92	1.07	0.89	1.05	0.87
					0.97		0.95
8	1.14	0.98	0.86	0.92	0.81	0.90	0.79
					0.95		0.92

Table 5-10 Story Drift for the 8-Story Building in the SMF Direction at DE

Story	Baseline	Shear Tab		BFFD		Wider Spacing	
	AVG MAX Drift (%)	AVG MAX Drift (%)	Drift Ratio (BL)	AVG MAX Drift (%)	Drift Ratio (BL)	AVG MAX Drift (%)	Drift Ratio (BL)
					Drift Ratio (ST)		Drift Ratio (ST)
1	2.22	2.19	0.98	2.20	0.99	2.19	0.98
					1.00		1.00
2	2.59	2.57	0.99	2.54	0.98	2.53	0.98
					0.99		0.98
3	2.46	2.40	0.98	2.37	0.96	2.35	0.96
					0.99		0.98
4	2.15	2.08	0.97	2.03	0.94	2.01	0.93
					0.98		0.96
5	1.89	1.79	0.95	1.74	0.92	1.71	0.91
					0.97		0.96
6	1.77	1.62	0.91	1.55	0.87	1.53	0.86
					0.96		0.94
7	1.86	1.69	0.91	1.61	0.87	1.58	0.85
					0.95		0.93
8	1.77	1.63	0.92	1.52	0.86	1.48	0.84
					0.93		0.91

Table 5-11. Story Drift for the 16-Story Building in the SMF Direction at SLE

Story	Baseline	Shear Tab		BFFD		Wider Spacing	
	AVG MAX Drift (%)	AVG MAX Drift (%)	Drift Ratio (BL)	AVG MAX Drift (%)	Drift Ratio (BL)	AVG MAX Drift (%)	Drift Ratio (BL)
					Drift Ratio (ST)		Drift Ratio (ST)
1	0.55	0.54	0.99	0.54	0.98	0.53	0.98
					0.99		0.99
2	0.88	0.87	0.99	0.86	0.98	0.85	0.96
					0.99		0.98
3	1.01	0.99	0.98	0.98	0.97	0.97	0.96
					0.99		0.98
4	1.07	1.04	0.97	1.03	0.96	1.02	0.95
					0.99		0.98
5	1.08	1.03	0.96	1.03	0.96	1.02	0.95
					0.99		0.99
6	1.03	1.00	0.96	0.99	0.95	0.97	0.94
					0.99		0.97
7	0.96	0.92	0.96	0.91	0.94	0.90	0.93
					0.98		0.97
8	0.89	0.87	0.98	0.86	0.96	0.86	0.96
					0.99		0.98
9	0.99	0.97	0.98	0.95	0.96	0.94	0.95
					0.98		0.97
10	1.09	1.08	0.99	1.07	0.98	1.06	0.97
					0.99		0.98
11	1.10	1.08	0.98	1.06	0.96	1.06	0.96
					0.98		0.97
12	1.05	1.00	0.95	0.97	0.92	0.97	0.93
					0.97		0.98
13	1.05	1.00	0.95	0.97	0.93	0.96	0.92
					0.97		0.96
14	1.09	1.05	0.96	1.01	0.92	1.00	0.92
					0.96		0.96
15	1.21	1.16	0.96	1.11	0.92	1.09	0.90
					0.96		0.94
16	1.15	1.07	0.93	1.02	0.89	1.00	0.87
					0.95		0.93

Table 5-12. Story Drift for the 16-Story Building in the SMF Direction at DE

Story	Baseline	Shear Tab		BFFD		Wider Spacing	
	AVG MAX Drift (%)	AVG MAX Drift (%)	Drift Ratio (BL)	AVG MAX Drift (%)	Drift Ratio (BL)	AVG MAX Drift (%)	Drift Ratio (BL)
					Drift Ratio (ST)		Drift Ratio (ST)
1	0.78	0.76	0.98	0.76	0.98	0.75	0.96
					0.99		0.98
2	1.29	1.26	0.98	1.26	0.98	1.25	0.97
					1.00		0.99
3	1.50	1.48	0.99	1.47	0.98	1.49	0.99
					0.99		1.00
4	1.63	1.62	1.00	1.61	0.99	1.62	1.00
					0.99		1.00
5	1.71	1.70	0.99	1.68	0.98	1.70	0.99
					0.99		1.00
6	1.74	1.71	0.98	1.68	0.96	1.70	0.98
					0.98		0.99
7	1.68	1.64	0.98	1.60	0.96	1.61	0.96
					0.98		0.98
8	1.58	1.54	0.97	1.50	0.95	1.49	0.94
					0.97		0.97
9	1.60	1.55	0.97	1.53	0.96	1.53	0.96
					0.98		0.99
10	1.65	1.62	0.98	1.62	0.98	1.61	0.97
					1.00		0.99
11	1.60	1.58	0.98	1.57	0.98	1.55	0.97
					0.99		0.98
12	1.53	1.50	0.98	1.50	0.98	1.48	0.97
					1.00		0.98
13	1.56	1.51	0.96	1.48	0.95	1.45	0.93
					0.98		0.96
14	1.65	1.57	0.95	1.54	0.93	1.51	0.92
					0.98		0.96
15	1.76	1.70	0.96	1.66	0.94	1.64	0.93
					0.98		0.97
16	1.72	1.63	0.95	1.59	0.92	1.57	0.91
					0.98		0.96

Figure 5-22 through 5-27 show the average maximum drift for 4-, 8- and 16-story buildings in the BRBF direction at SLE and DE. The summary of the average maximum drift and the drift ratio (BL, ST) for 4-, 8- and 16-story buildings in the BRBF direction at SLE and DE are shown from Tables 5-13 to 5-18. The results show that the impact of shear tab connections on the BRBF buildings is similar to the SMF direction but more significant. There is a significant impact of adding a shear tab connection on the average maximum drift on the upper stories in the BRBF direction, especially for the top two stories. The average maximum drift decreases for upper stories when adding the shear tab connections. For example, the 4-story BRBF at SLE has the average maximum drift on the top two stories reduced by 49% and 24% after including the standard shear tab connections. However, for the lower stories, especially the first story, the average maximum drift increases when including the standard shear tab connections. For the 4-story building in the BRBF direction at DE, the average maximum drift on the top first story increased by 20% after including the standard shear tab connections. The influence of the hazard level is not significant in the results.

The modified shear tab connections decreased the average maximum drift for upper stories, especially the top two stories, for all the buildings. For the 4-story building in the SMF direction at SLE, the average maximum drift on the top two stories reduced by 12% and 5% after adding the BFFD and 20% and 8% after increasing the shear tab bolt spacing. The model with wider bolt spacing on the shear tab has 59% less average maximum drift on the top story compared to the baseline model. Overall, the impact of shear tab connections is larger for the 4-story BRBF than for the 16-story BRBF.

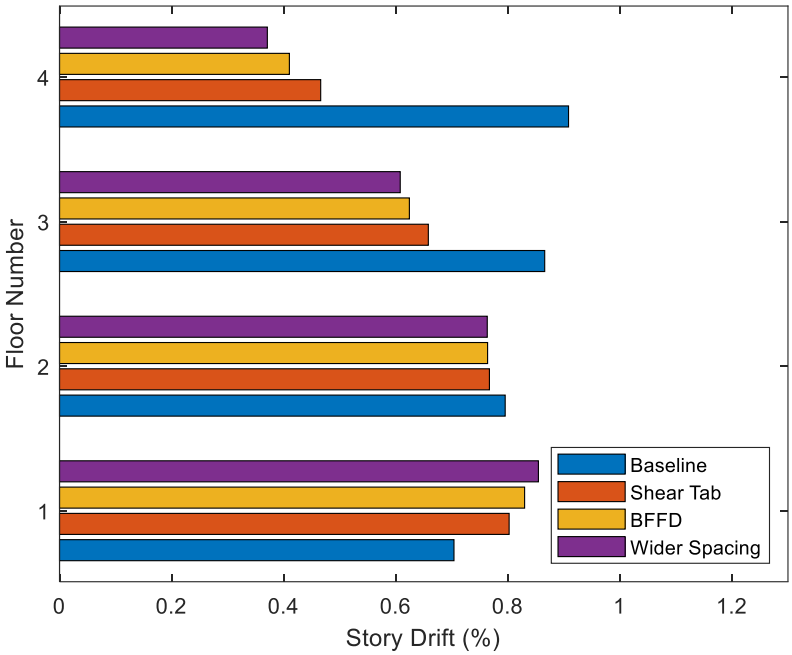

Figure 5-22. Average Maximum Drift for the 4-Story Building in the BRBF Direction at SLE

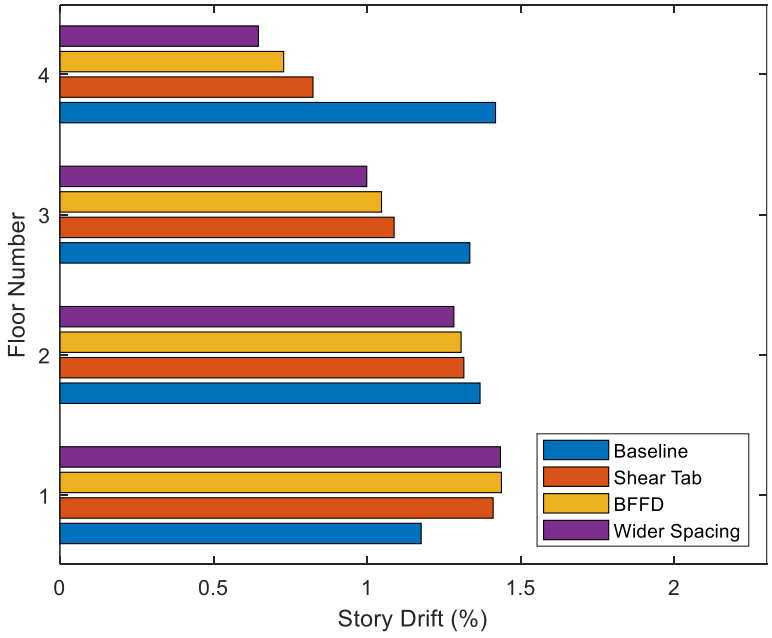

Figure 5-23. Average Maximum Drift for the 4-Story Building in the BRBF Direction at DE

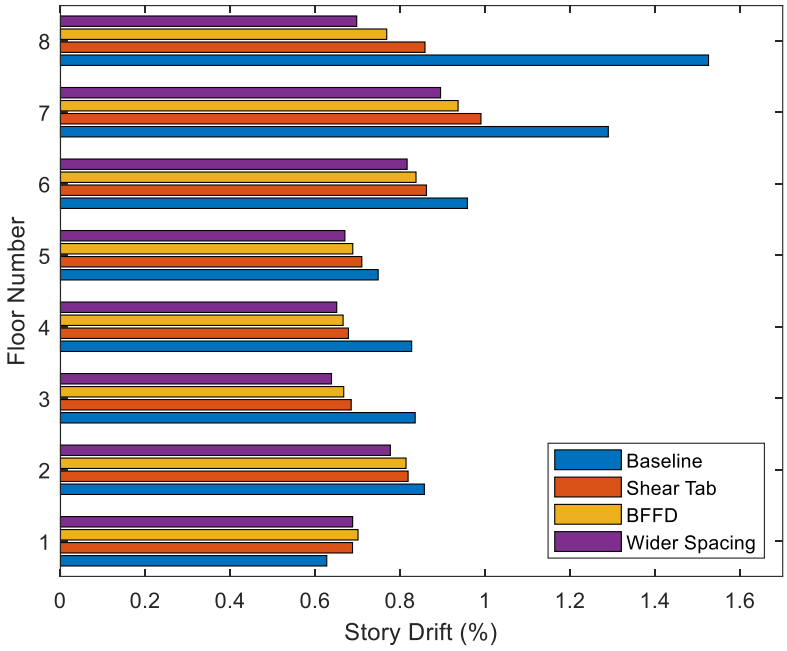

Figure 5-24. Average Maximum Drift for the 8-Story Building in the BRBF Direction at SLE

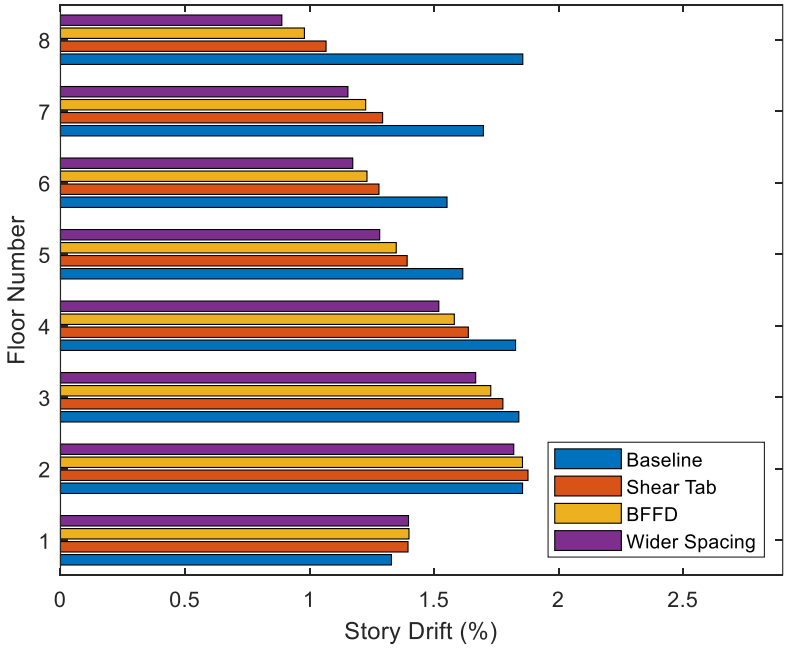

Figure 5-25. Average Maximum Drift for the 8-Story Building in the BRBF Direction at DE

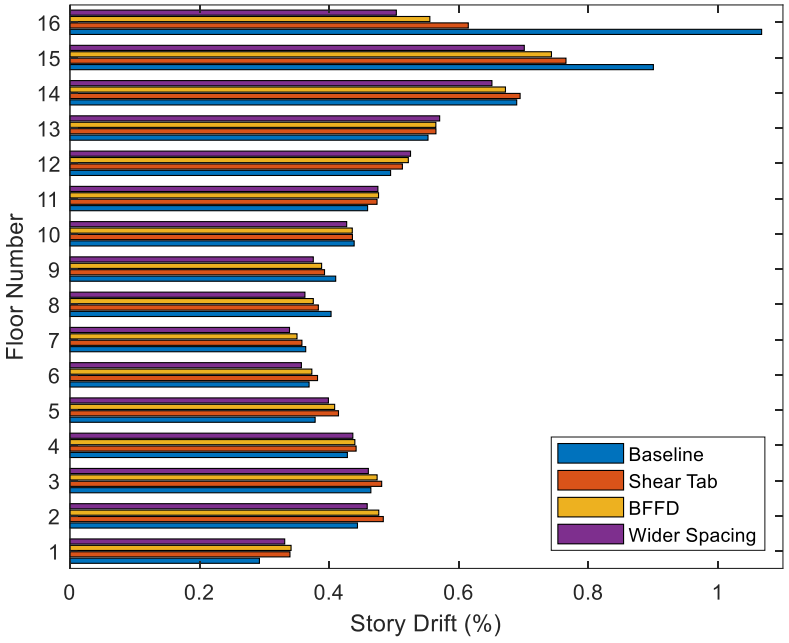

Figure 5-26. Average Maximum Drift for the 16-Story Building in the BRBF Direction at SLE

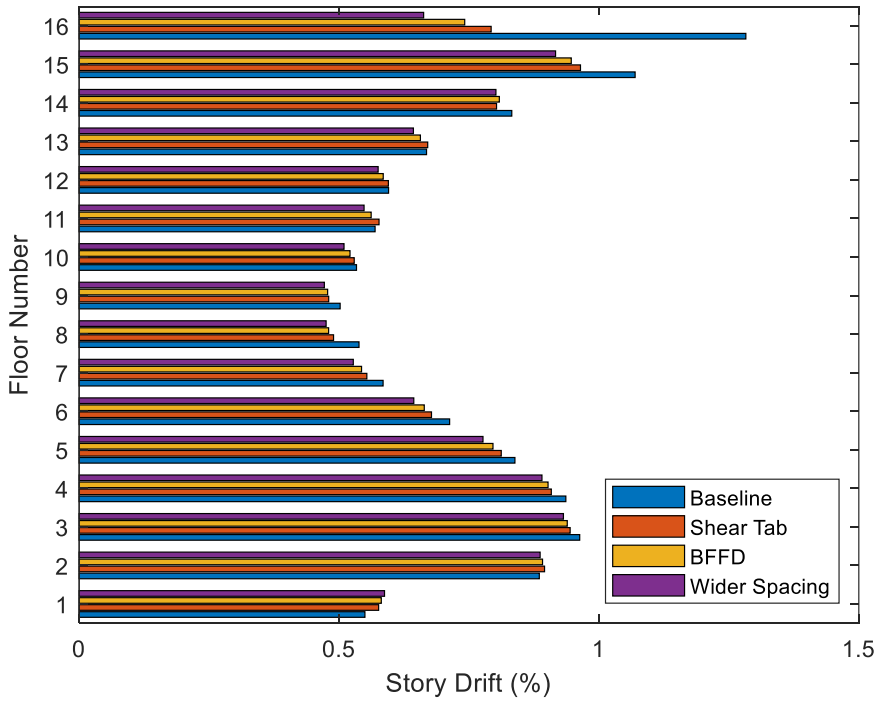

Figure 5-27. Average Maximum Drift for the 16-Story Building in the BRBF Direction at DE

Table 5-13. Story Drift for the 4-Story Building in the BRBF Direction at SLE

Story	Baseline	Shear Tab		BFFD		Wider Spacing	
	AVG MAX Drift (%)	AVG MAX Drift (%)	Drift Ratio (BL)	AVG MAX Drift (%)	Drift Ratio (BL)	AVG MAX Drift (%)	Drift Ratio (BL)
					Drift Ratio (ST)		Drift Ratio (ST)
1	0.70	0.80	1.14	0.83	1.18	0.85	1.21
					1.03		1.07
2	0.80	0.77	0.96	0.76	0.96	0.76	0.96
					1.00		0.99
3	0.87	0.66	0.76	0.62	0.72	0.61	0.70
					0.95		0.92
4	0.91	0.47	0.51	0.41	0.45	0.37	0.41
					0.88		0.80

Table 5-14. Story Drift for the 4-Story Building in the BRBF Direction at DE

Story	Baseline	Shear Tab		BFFD		Wider Spacing	
	AVG MAX Drift (%)	AVG MAX Drift (%)	Drift Ratio (BL)	AVG MAX Drift (%)	Drift Ratio (BL)	AVG MAX Drift (%)	Drift Ratio (BL)
					Drift Ratio (ST)		Drift Ratio (ST)
1	1.18	1.41	1.20	1.44	1.22	1.43	1.22
					1.02		1.02
2	1.37	1.31	0.96	1.31	0.95	1.28	0.94
					0.99		0.98
3	1.33	1.09	0.82	1.05	0.78	1.00	0.75
					0.96		0.92
4	1.42	0.82	0.58	0.73	0.51	0.65	0.46
					0.88		0.78

Table 5-15. Story Drift for the 8-Story Building in the BRBF Direction at SLE

Story	Baseline	Shear Tab		BFFD		Wider Spacing	
	AVG MAX Drift (%)	AVG MAX Drift (%)	Drift Ratio (BL)	AVG MAX Drift (%)	Drift Ratio (BL)	AVG MAX Drift (%)	Drift Ratio (BL)
					Drift Ratio (ST)		Drift Ratio (ST)
1	0.63	0.69	1.10	0.70	1.12	0.69	1.10
					1.02		1.00
2	0.86	0.82	0.96	0.81	0.95	0.78	0.91
					0.99		0.95
3	0.83	0.68	0.82	0.67	0.80	0.64	0.76
					0.97		0.93
4	0.83	0.68	0.82	0.67	0.80	0.65	0.79
					0.98		0.96
5	0.75	0.71	0.95	0.69	0.92	0.67	0.90
					0.97		0.94
6	0.96	0.86	0.90	0.84	0.87	0.82	0.85
					0.97		0.95
7	1.29	0.99	0.77	0.94	0.73	0.89	0.69
					0.95		0.90
8	1.53	0.86	0.56	0.77	0.50	0.70	0.46
					0.89		0.81

Table 5-16. Story Drift for the 8-Story Building in the BRBF Direction at DE

Story	Baseline	Shear Tab		BFFD		Wider Spacing	
	AVG MAX Drift (%)	AVG MAX Drift (%)	Drift Ratio (BL)	AVG MAX Drift (%)	Drift Ratio (BL)	AVG MAX Drift (%)	Drift Ratio (BL)
					Drift Ratio (ST)		Drift Ratio (ST)
1	1.33	1.40	1.05	1.40	1.05	1.40	1.05
					1.00		1.00
2	1.86	1.88	1.01	1.86	1.00	1.82	0.98
					0.99		0.97
3	1.84	1.78	0.97	1.73	0.94	1.67	0.91
					0.97		0.94
4	1.83	1.64	0.90	1.58	0.87	1.52	0.83
					0.97		0.93
5	1.62	1.39	0.86	1.35	0.83	1.28	0.79
					0.97		0.92
6	1.55	1.28	0.82	1.23	0.79	1.17	0.76
					0.96		0.92
7	1.70	1.29	0.76	1.23	0.72	1.15	0.68
					0.95		0.89
8	1.86	1.07	0.57	0.98	0.53	0.89	0.48
					0.92		0.83

Table 5-17. Story Drift for the 16-Story Building in the BRBF Direction at SLE

Story	Baseline	Shear Tab		BFFD		Wider Spacing	
	AVG MAX Drift (%)	AVG MAX Drift (%)	Drift Ratio (BL)	AVG MAX Drift (%)	Drift Ratio (BL)	AVG MAX Drift (%)	Drift Ratio (BL)
					Drift Ratio (ST)		Drift Ratio (ST)
1	0.29	0.34	1.16	0.34	1.17	0.33	1.13
					1.01		0.98
2	0.44	0.48	1.09	0.48	1.07	0.46	1.03
					0.99		0.95
3	0.46	0.48	1.04	0.47	1.02	0.46	0.99
					0.99		0.96
4	0.43	0.44	1.03	0.44	1.03	0.44	1.02
					1.00		0.99
5	0.38	0.41	1.10	0.41	1.08	0.40	1.05
					0.99		0.96
6	0.37	0.38	1.04	0.37	1.01	0.36	0.97
					0.98		0.93
7	0.36	0.36	0.98	0.35	0.96	0.34	0.93
					0.98		0.95
8	0.40	0.38	0.95	0.38	0.93	0.36	0.90
					0.98		0.95
9	0.41	0.39	0.96	0.39	0.95	0.38	0.92
					0.99		0.96
10	0.44	0.44	0.99	0.44	0.99	0.43	0.97
					1.00		0.98
11	0.46	0.47	1.03	0.48	1.04	0.48	1.03
					1.00		1.00
12	0.49	0.51	1.04	0.52	1.06	0.53	1.06
					1.02		1.02
13	0.55	0.56	1.02	0.56	1.02	0.57	1.03
					1.00		1.01
14	0.69	0.69	1.01	0.67	0.97	0.65	0.94
					0.97		0.94
15	0.90	0.77	0.85	0.74	0.83	0.70	0.78
					0.97		0.92
16	1.07	0.61	0.58	0.56	0.52	0.50	0.47
					0.90		0.82

Table 5-18. Story Drift for the 16-Story Building in the BRBF Direction at DE

Story	Baseline	Shear Tab		BFFD		Wider Spacing	
	AVG MAX Drift (%)	AVG MAX Drift (%)	Drift Ratio (BL)	AVG MAX Drift (%)	Drift Ratio (BL)	AVG MAX Drift (%)	Drift Ratio (BL)
					Drift Ratio (ST)		Drift Ratio (ST)
1	0.55	0.58	1.05	0.58	1.06	0.59	1.07
					1.01		1.02
2	0.89	0.90	1.01	0.89	1.01	0.89	1.00
					1.00		0.99
3	0.96	0.94	0.98	0.94	0.98	0.93	0.97
					0.99		0.99
4	0.94	0.91	0.97	0.90	0.96	0.89	0.95
					0.99		0.98
5	0.84	0.81	0.97	0.80	0.95	0.78	0.93
					0.98		0.96
6	0.71	0.68	0.95	0.66	0.93	0.64	0.90
					0.98		0.95
7	0.58	0.55	0.95	0.54	0.93	0.53	0.90
					0.98		0.95
8	0.54	0.49	0.91	0.48	0.89	0.48	0.88
					0.98		0.97
9	0.50	0.48	0.96	0.48	0.95	0.47	0.94
					1.00		0.98
10	0.53	0.53	0.99	0.52	0.98	0.51	0.96
					0.98		0.96
11	0.57	0.58	1.01	0.56	0.99	0.55	0.96
					0.97		0.95
12	0.60	0.59	1.00	0.59	0.98	0.58	0.97
					0.98		0.97
13	0.67	0.67	1.00	0.66	0.98	0.64	0.96
					0.98		0.96
14	0.83	0.80	0.96	0.81	0.97	0.80	0.96
					1.01		1.00
15	1.07	0.96	0.90	0.95	0.89	0.92	0.86
					0.98		0.95
16	1.28	0.79	0.62	0.74	0.58	0.66	0.52
					0.94		0.84

5.4.2.2 Total Acceleration

The seismic body and surface waves create inertial forces within the building. The acceleration, or the rate of change of the velocity of the waves setting the building in motion, determines the percentage of the building mass or weight that must be dealt with as a horizontal force. All acceleration in this study is measured in terms of the acceleration due to gravity or g. In this research, maximum absolute total acceleration for each story is presented for the buildings in both SMF and BRBF direction under the corresponding suite of scaled ground motions for each earthquake record. The average value of maximum absolute total acceleration for each story in the corresponding ground motion suite is called average maximum total acceleration.

Tables 5-19 through 5-24 show the average maximum total acceleration for the 4-, 8- and 16-story buildings in the SMF and BRBF directions. The results show that the impact of shear tab connections on the average maximum total acceleration is insignificant in the SMF and BRBF direction. In the SMF direction, the average maximum total acceleration decreases slightly due to the shear tab connections. For example, the 4-story building in the SMF direction at SLE, the average maximum total acceleration on the top story is 0.03g (6%) less for the "Wider Spacing" models compared with the "Baseline" model. In the BRBF direction, a small increase is observed on the top story for all the buildings. For the 8-story BRBF at DE, the average maximum total acceleration on the top story is 0.05g (15%) larger for the "Wider Spacing" models compared with the "Baseline" model. The influence of modifications of shear tab connections is negligible in both SMF and BRBF direction for all the buildings.

Table 5-19. Total Acceleration for the 4-Story Building in the SMF Direction

Story	Service Level Earthquake (SLE)				Design Level Earthquake (DE)			
	Baseline	Shear Tab	BFFD	Wider Spacing	Baseline	Shear Tab	BFFD	Wider Spacing
1	0.31	0.30	0.29	0.29	0.44	0.42	0.42	0.41
2	0.33	0.32	0.32	0.31	0.44	0.43	0.43	0.42
3	0.30	0.30	0.30	0.30	0.40	0.39	0.39	0.39
4	0.46	0.44	0.43	0.43	0.57	0.57	0.56	0.56

Table 5-20. Total Acceleration for the 8-Story Building in the SMF Direction

Story	Service Level Earthquake (SLE)				Design Level Earthquake (DE)			
	Baseline	Shear Tab	BFFD	Wider Spacing	Baseline	Shear Tab	BFFD	Wider Spacing
1	0.26	0.26	0.26	0.26	0.46	0.46	0.46	0.45
2	0.32	0.29	0.28	0.27	0.49	0.48	0.47	0.46
3	0.28	0.27	0.26	0.25	0.46	0.44	0.43	0.43
4	0.27	0.25	0.26	0.25	0.42	0.41	0.41	0.40
5	0.26	0.27	0.26	0.25	0.42	0.41	0.40	0.39
6	0.29	0.28	0.27	0.27	0.48	0.46	0.45	0.45
7	0.28	0.28	0.28	0.28	0.42	0.43	0.43	0.43
8	0.45	0.43	0.42	0.42	0.62	0.63	0.63	0.63

Table 5-21. Total Acceleration for the 16-Story Building in the SMF Direction

Story	Service Level Earthquake (SLE)				Design Level Earthquake (DE)			
	Baseline	Shear Tab	BFFD	Wider Spacing	Baseline	Shear Tab	BFFD	Wider Spacing
1	0.28	0.27	0.27	0.27	0.49	0.48	0.47	0.46
2	0.31	0.31	0.31	0.30	0.52	0.51	0.51	0.50
3	0.34	0.33	0.33	0.32	0.54	0.52	0.52	0.51
4	0.31	0.31	0.30	0.29	0.48	0.46	0.46	0.45
5	0.30	0.29	0.29	0.28	0.47	0.47	0.46	0.45
6	0.29	0.29	0.29	0.29	0.47	0.47	0.47	0.46
7	0.30	0.29	0.29	0.29	0.48	0.47	0.46	0.46
8	0.32	0.32	0.31	0.31	0.51	0.50	0.49	0.48
9	0.32	0.31	0.31	0.30	0.50	0.49	0.49	0.49
10	0.31	0.29	0.28	0.27	0.49	0.47	0.46	0.45
11	0.30	0.29	0.28	0.28	0.49	0.47	0.47	0.46
12	0.30	0.29	0.29	0.28	0.48	0.46	0.46	0.45
13	0.32	0.31	0.31	0.30	0.50	0.49	0.48	0.48
14	0.33	0.32	0.32	0.31	0.53	0.51	0.49	0.49
15	0.32	0.31	0.30	0.30	0.46	0.46	0.46	0.45
16	0.54	0.54	0.52	0.52	0.75	0.75	0.75	0.75

Table 5-22. Total Acceleration for the 4-Story Building in the BRBF Direction

Story	Service Level Earthquake (SLE)				Design Level Earthquake (DE)			
	Baseline	Shear Tab	BFFD	Wider Spacing	Baseline	Shear Tab	BFFD	Wider Spacing
1	0.30	0.30	0.30	0.29	0.44	0.38	0.38	0.38
2	0.28	0.30	0.29	0.29	0.38	0.38	0.37	0.36
3	0.30	0.31	0.31	0.30	0.40	0.37	0.37	0.37
4	0.35	0.37	0.38	0.38	0.43	0.42	0.42	0.42

Table 5-23. Total Acceleration for the 8-Story Building in the BRBF Direction

Story	Service Level Earthquake (SLE)				Design Level Earthquake (DE)			
	Baseline	Shear Tab	BFFD	Wider Spacing	Baseline	Shear Tab	BFFD	Wider Spacing
1	0.28	0.28	0.28	0.29	0.48	0.47	0.48	0.47
2	0.29	0.30	0.30	0.30	0.46	0.47	0.48	0.49
3	0.30	0.29	0.29	0.28	0.46	0.47	0.46	0.46
4	0.28	0.26	0.27	0.28	0.45	0.42	0.42	0.41
5	0.29	0.29	0.29	0.29	0.45	0.43	0.44	0.43
6	0.29	0.30	0.29	0.29	0.42	0.41	0.41	0.40
7	0.32	0.31	0.32	0.31	0.40	0.38	0.37	0.37
8	0.31	0.34	0.34	0.35	0.34	0.38	0.39	0.39

Table 5-24. Total Acceleration for the 16-Story Building in the BRBF Direction

Story	Service Level Earthquake (SLE)				Design Level Earthquake (DE)			
	Baseline	Shear Tab	BFFD	Wider Spacing	Baseline	Shear Tab	BFFD	Wider Spacing
1	0.29	0.28	0.29	0.30	0.46	0.46	0.46	0.45
2	0.31	0.31	0.32	0.32	0.47	0.47	0.48	0.47
3	0.32	0.32	0.32	0.32	0.48	0.47	0.47	0.47
4	0.33	0.32	0.32	0.32	0.46	0.48	0.48	0.48
5	0.32	0.32	0.32	0.32	0.48	0.48	0.49	0.49
6	0.32	0.32	0.32	0.32	0.46	0.48	0.48	0.47
7	0.35	0.33	0.34	0.34	0.47	0.48	0.48	0.48
8	0.32	0.34	0.34	0.35	0.50	0.48	0.49	0.48
9	0.36	0.37	0.37	0.36	0.49	0.51	0.51	0.49
10	0.35	0.34	0.35	0.35	0.50	0.49	0.49	0.47
11	0.37	0.35	0.35	0.34	0.49	0.50	0.50	0.49
12	0.37	0.36	0.35	0.34	0.50	0.50	0.49	0.47
13	0.38	0.34	0.35	0.34	0.51	0.50	0.51	0.50
14	0.37	0.36	0.36	0.35	0.50	0.50	0.50	0.49
15	0.39	0.38	0.38	0.37	0.51	0.48	0.46	0.46
16	0.37	0.39	0.40	0.41	0.40	0.43	0.44	0.45

5.4.2.3 Base Shear

When seismic activity occurs, the base of the structure experiences a lateral force as the results of the imposed demands, whose maximum value is termed as base shear. In this research, the base shear is defined as the sum of the shear force on the bottom of columns on the first floor.

Figures 5-28 through 5-30 show the boxplot of maximum base shear for the 4-, 8- and 16-story buildings in the SMF direction. Boxplot is a standardized way of displaying the distribution of data based on a five number summary including “minimum”, “first quartile (Q1)”, “median”, “third quartile (Q3)” and “maximum”. “Median” is the middle value of the data set. “First quartile” represents the middle value between the smallest value and the “median” while “third quartile” represents the middle value between the largest value and the “median”. The difference between Q1 and Q3 is called interquartile range (IQR). “Minimum” is equal to Q1 minus 1.5 times IQR while “maximum” is equal to Q3 plus 1.5 times IQR. All the data samples which are smaller than “minimum” or larger than “maximum” is called as outliers represented by the open circles in the boxplots. The summary of the average maximum base shear and the shear ratio (BL, ST) for 4-, 8- and 16-story buildings in the SMF direction are shown in Table 5-25. The definition of shear ratio (BL, ST) is the same with the drift ratio (BL, ST) replacing the average maximum drift by the average maximum base shear. The results show that the impact of shear tab connection on the base shear is insignificant in the SMF direction for all buildings. The largest difference occurred in the 8-story building at SLE, the average maximum base shear is 4% more in the “Wider Spacing” model than the “Baseline” model.

Figures 5-31 through 5-33 show the boxplot of maximum base shear for 4-, 8- and 16-story buildings in the BRBF direction, respectively. The summary of the average maximum base shear and the shear ratio (BL, ST) for 4-, 8- and 16-story buildings in the SMF direction are shown in Table 5-26. The results show there is an impact of adding shear tab connection on the average

maximum base shear in the BRBF direction. The average maximum base shear increases after adding the shear tab connections. For example, the 4-story BRBF at DE average maximum base shear increased by 11% after including the standard shear tab connections. The influence of the magnitude of ground motions is insignificant on the base shear. Similarly, the impact of modifications on shear tab connections is insignificant as well. The modifications on the shear tab slightly increases the base shear in the buildings. Overall, the impact of shear tab connections is larger for the 4-story BRBF as compared to the 16-story.

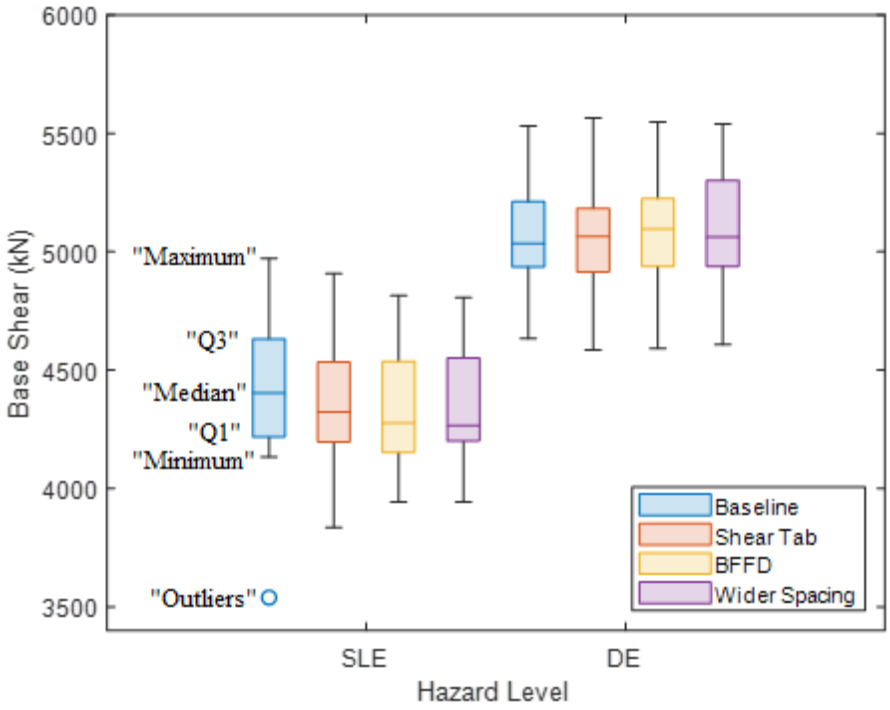

Figure 5-28. Maximum Base Shear for the 4-Story Building in the SMF Direction

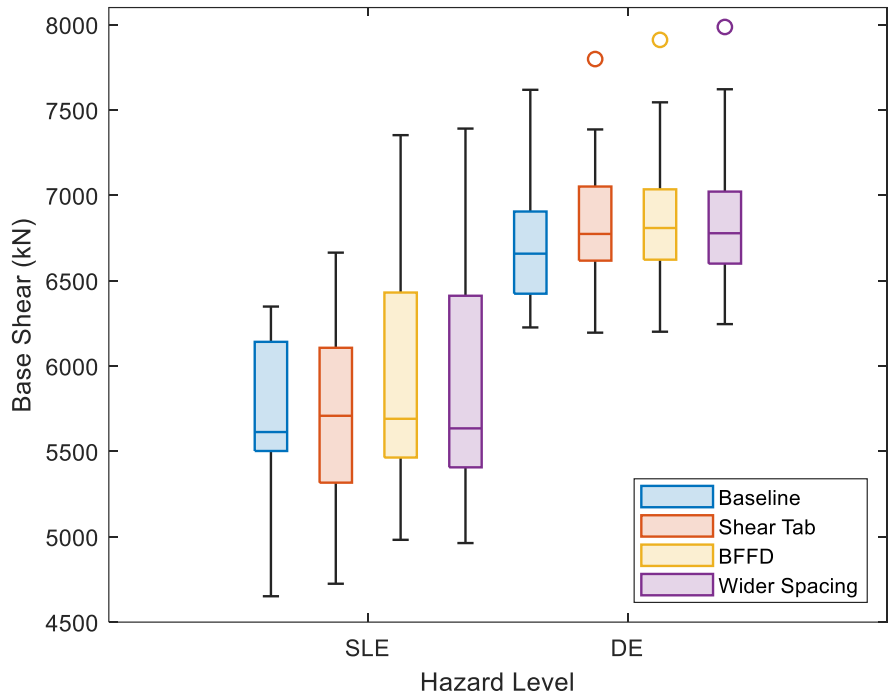

Figure 5-29. Maximum Base Shear for the 8-Story Building in the SMF Direction

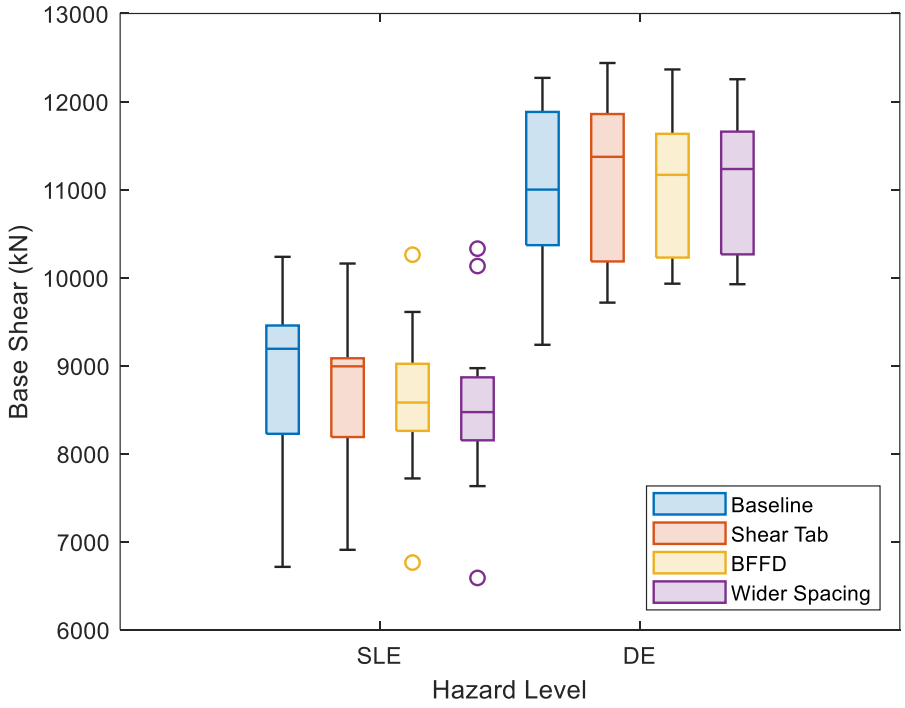

Figure 5-30. Maximum Base Shear for the 16-Story Building in the SMF Direction

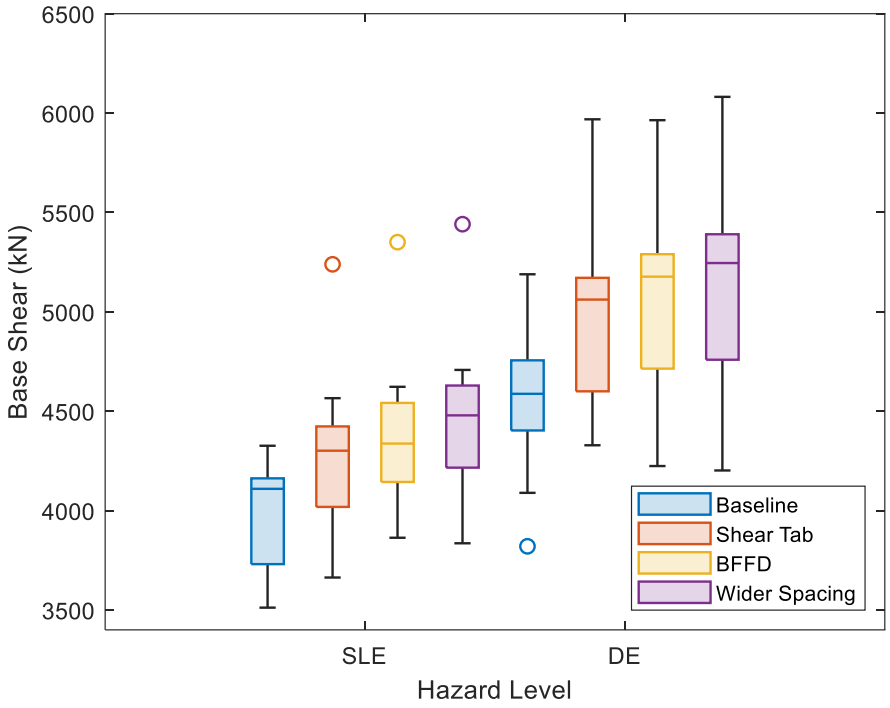

Figure 5-31. Maximum Base Shear for the 4-Story Building in the BRBF Direction

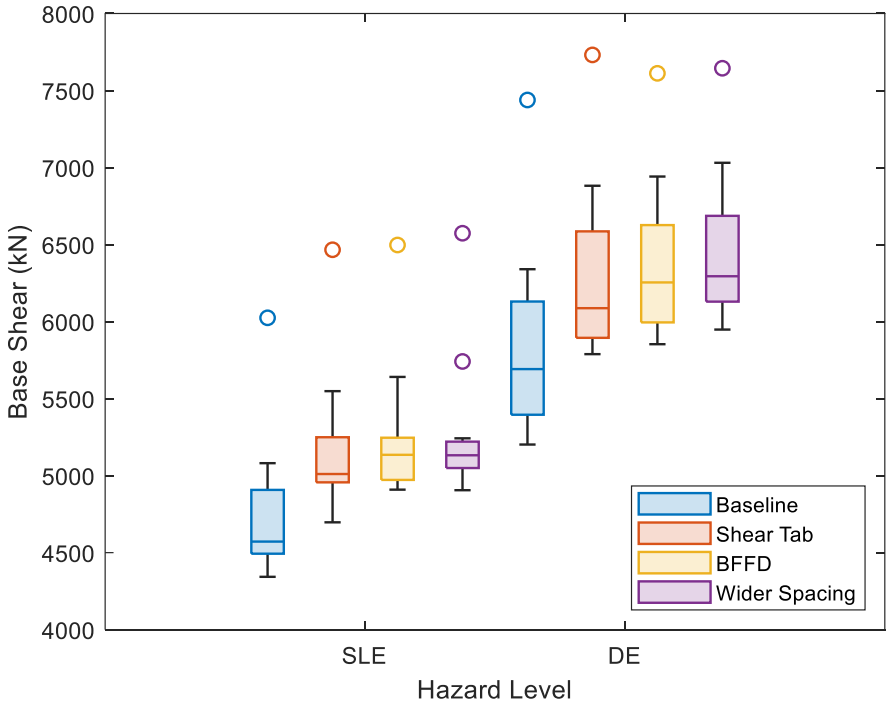

Figure 5-32. Maximum Base Shear for the 8-Story Building in the BRBF Direction

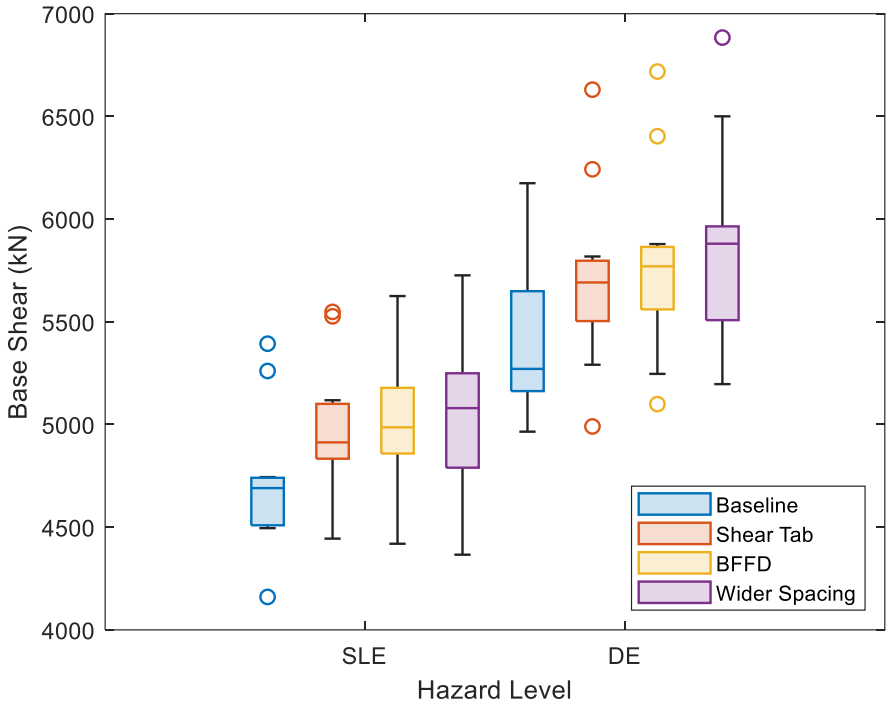

Figure 5-33. Maximum Base Shear for the 16-Story Building in the BRBF Direction

Table 5-25. Base Shear for the Building in the SMF Direction

	Service Level Earthquake (SLE)				Design Level Earthquake (DE)			
	Baseline	Shear Tab	BFFD	Wider Spacing	Baseline	Shear Tab	BFFD	Wider Spacing
	4-Story Building							
AVG Max Base Shear (kN)	4387	4375	4356	4366	5067	5088	5098	5106
Shear Ratio (BL)	-	1.00	0.99	1.00	-	1.00	1.01	1.01
Shear Ratio (ST)	-	-	1.00	1.00	-	-	1.00	1.00
	8-Story Building							
AVG Max Base Shear (kN)	5700	5723	5905	5872	6699	6856	6890	6895
Shear Ratio (BL)	-	1.00	1.04	1.03	-	1.02	1.03	1.03
Shear Ratio (ST)	-	-	1.03	1.03	-	-	1.00	1.01
	16-Story Building							
AVG Max Base Shear (kN)	8872	8743	8592	8555	11038	11131	11077	11053
Shear Ratio (BL)	-	0.99	0.97	0.96	-	1.01	1.00	1.00
Shear Ratio (ST)	-	-	0.98	0.98	-	-	1.00	0.99

Table 5-26. Base Shear for the Building in the BRBF Direction

	Service Level Earthquake (SLE)				Design Level Earthquake (DE)			
	Baseline	Shear Tab	BFFD	Wider Spacing	Baseline	Shear Tab	BFFD	Wider Spacing
	4-Story Building							
AVG Max Base Shear (kN)	3978	4291	4378	4459	4552	5040	5136	5193
Shear Ratio (BL)	-	1.08	1.10	1.12	-	1.11	1.13	1.14
Shear Ratio (ST)	-	-	1.02	1.04	-	-	1.02	1.03
	8-Story Building							
AVG Max Base Shear (kN)	4769	5190	5257	5278	5874	6304	6381	6462
Shear Ratio (BL)	-	1.09	1.10	1.11	-	1.07	1.09	1.10
Shear Ratio (ST)	-	-	1.01	1.02	-	-	1.01	1.03
	16-Story Building							
AVG Max Base Shear (kN)	4713	4967	5013	5029	5430	5710	5782	5864
Shear Ratio (BL)	-	1.05	1.06	1.07	-	1.05	1.06	1.08
Shear Ratio (ST)	-	-	1.01	1.01	-	-	1.01	1.03

5.4.2.4 Energy Dissipation

One of the important aspects of ductility-based design is the ability of a structure to absorb and dissipate energy. It is valuable to investigate the impact of shear tab connections on RBS, BRB and shear tab connections. Including the shear tab connections in the models can be beneficial if they can help major energy dissipation components (RBS and BRB) in the lateral load systems to dissipate energy from the seismic events.

Figures 5-34 through 5-36 show the boxplot of the energy dissipated by RBS connections for 4-, 8- and 16-story buildings in the SMF direction. The summary of the average energy

dissipated by RBS and the energy ratio (BL, ST) for 4-, 8- and 16-story buildings in the SMF direction are shown in Table 5-27. Figures 5-40, 5-41 and 5-42 show the boxplot of the energy dissipated by shear tab connections for 4-, 8- and 16-story buildings in the SMF direction, respectively. The summary of the average energy dissipated by shear tab connections and the energy ratio (ST) for 4-, 8- and 16-story buildings in the SMF direction are shown in Table 5-28. The definition of energy ratio (BL, ST) is the same with the drift ratio (BL, ST) replacing the average maximum drift by the average energy. The results show the impact of adding shear tab connections on energy dissipated by RBS is significant in the SMF direction. The average energy dissipated by RBS decreased by 23%, 17% and 18% for the 4-, 8- and 16-story buildings at SLE, respectively. For 4-, 8- and 16-story buildings at DE, the average energy dissipated by RBS reduced by 13%, 12% and 9%. The influence of shear tab connections for the buildings at SLE is larger than that for the buildings at DE. The modified shear tab connections decreased the average energy dissipated by RBS for all the buildings in the SMF direction compared with the standard shear tab connection. For the 4-story building in the SMF direction at SLE, the average energy dissipated by RBS reduced by 16% after adding the BFFD and 21% after increasing bolt spacing on the shear tab. The RBS in the model with wider bolt spacing on the shear tab averagely dissipated 40% less energy compared to the baseline model. In addition, the modified shear tab connections increased the energy dissipated by shear tab connections significantly. For the 8-story SMF at DE, the average energy dissipated by shear tab connections increased by 34% after adding the BFFD and 39% after increasing bolt spacing on the shear tab.

Figures 5-37 through 5-39 show the boxplot of the energy dissipated by BRBs for 4-, 8- and 16-story buildings. The summary of the average energy dissipated by BRB and the energy ratio (BL, ST) for 4-, 8- and 16-story buildings in the BRBF direction are shown in Table 5-29.

Figures 5-43, 5-44 and 5-45 show the boxplot of the energy dissipated by shear tab connections for 4-, 8- and 16-story buildings in the BRBF direction, respectively. The summary of the average energy dissipated by shear tab connections and the energy ratio (ST) for 4-, 8- and 16-story buildings in the BRBF direction are shown in Table 5-30. The results show the impact of adding shear tab connections on energy dissipated for the BRBF is less significant than for the SMF. The change of average energy dissipation by BRBs is the same for the buildings at SLE and DE. The average energy dissipated by BRBs decreased by 3%, 11% and 5% for the 4-, 8- and 16-story buildings, respectively. The modifications of shear tab connections slightly decreased the average energy dissipated by BRBs for all the buildings in the BRBF direction compared with the standard shear tab connection. For the 4-story building in the SMF direction at SLE, the average energy dissipated by BRBs reduced by 4% after adding the BFFD and 9% after increasing bolt spacing on the shear tab. The BRB in the model with wider shear tab bolt spacing had an average of 12% less energy compared to the baseline model. Similarly, the impact of the modifications of shear tab connection is less significant in the BRBF direction than that in the SMF direction. For the 8-story building in the BRBF direction at DE, the average energy dissipated by shear tab connections increased by 11% after adding the BFFD and 15% after increasing bolt spacing on the shear tab.

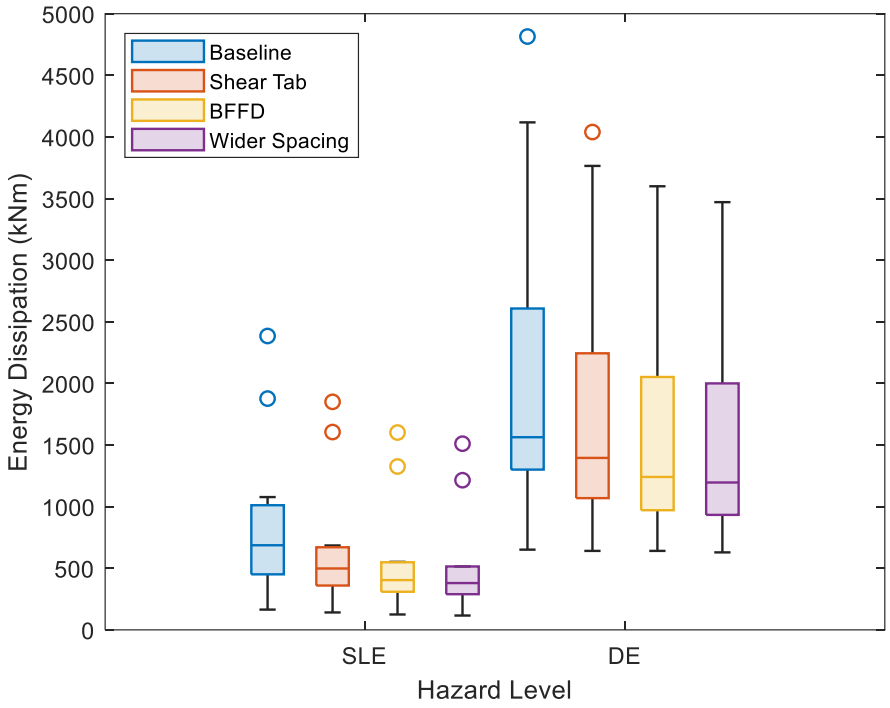

Figure 5-34. Energy Dissipated by RBS in the 4-Story Building in the SMF Direction

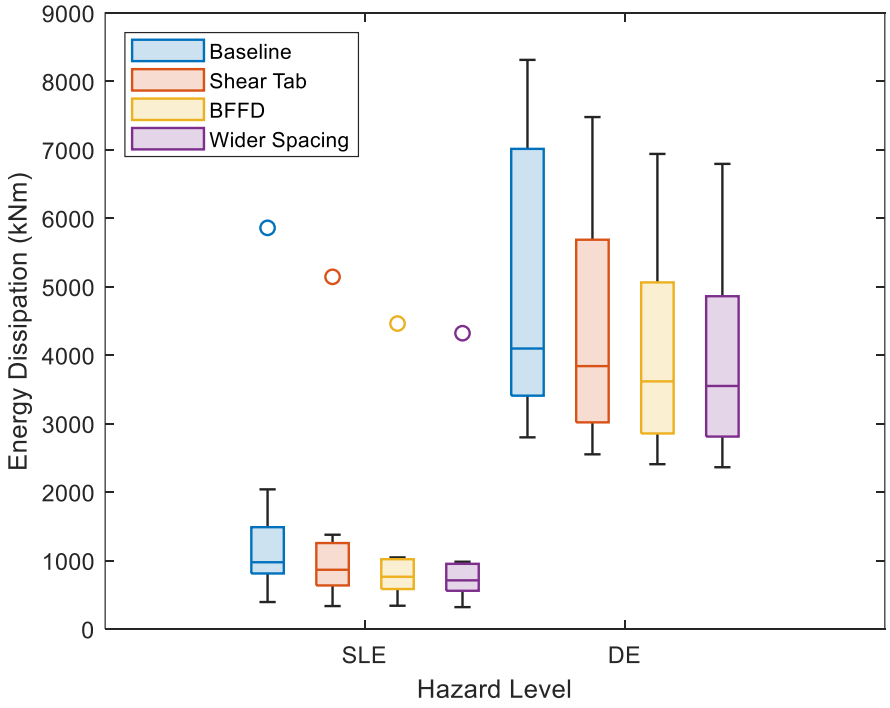

Figure 5-35. Energy Dissipated by RBS in the 8-Story Building in the SMF Direction

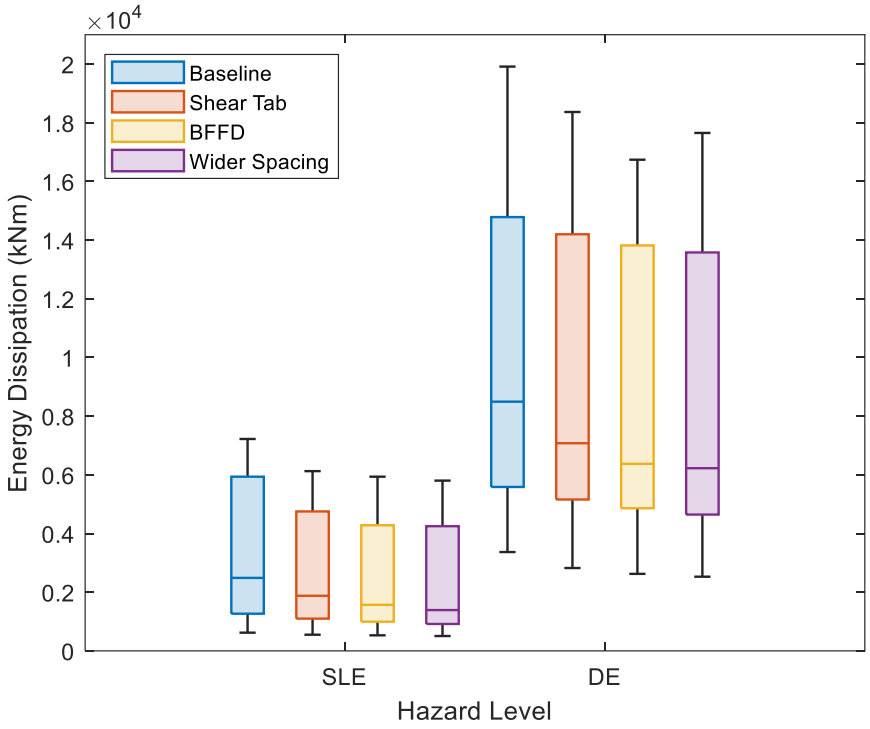

Figure 5-36. Energy Dissipated by RBS in the 16-Story Building in the SMF Direction

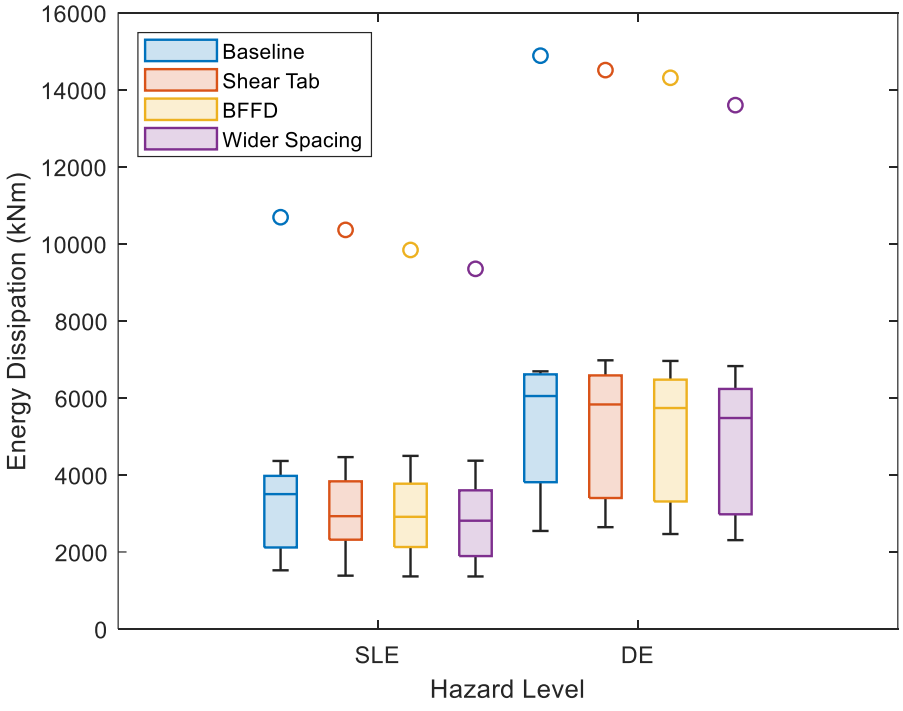

Figure 5-37. Energy Dissipated by BRB in the 4-Story Building in the BRBF Direction

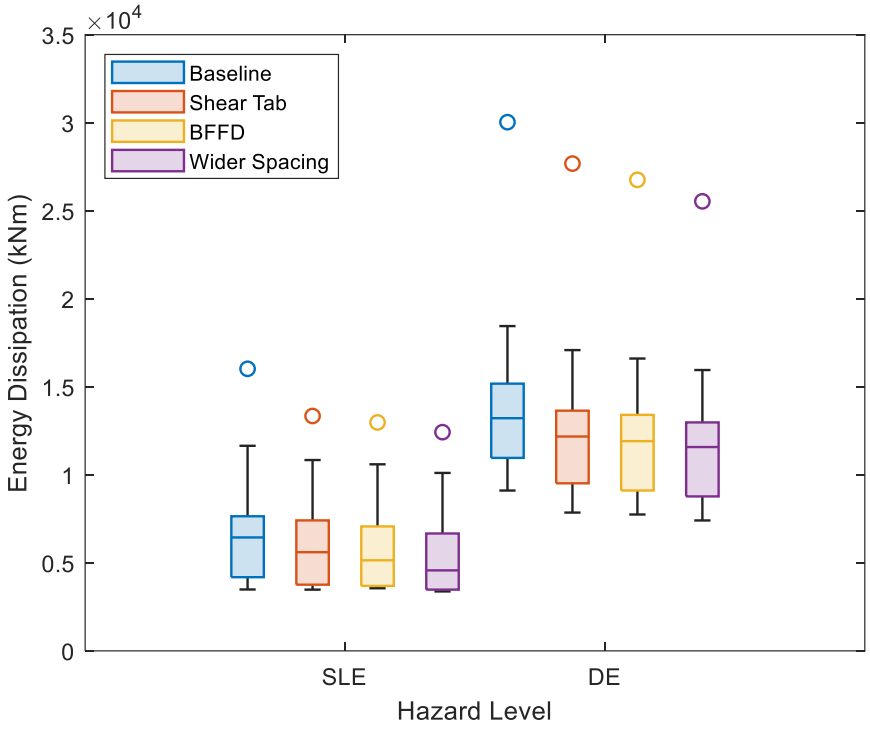

Figure 5-38. Energy Dissipated by BRB in the 8-Story Building in the BRBF Direction

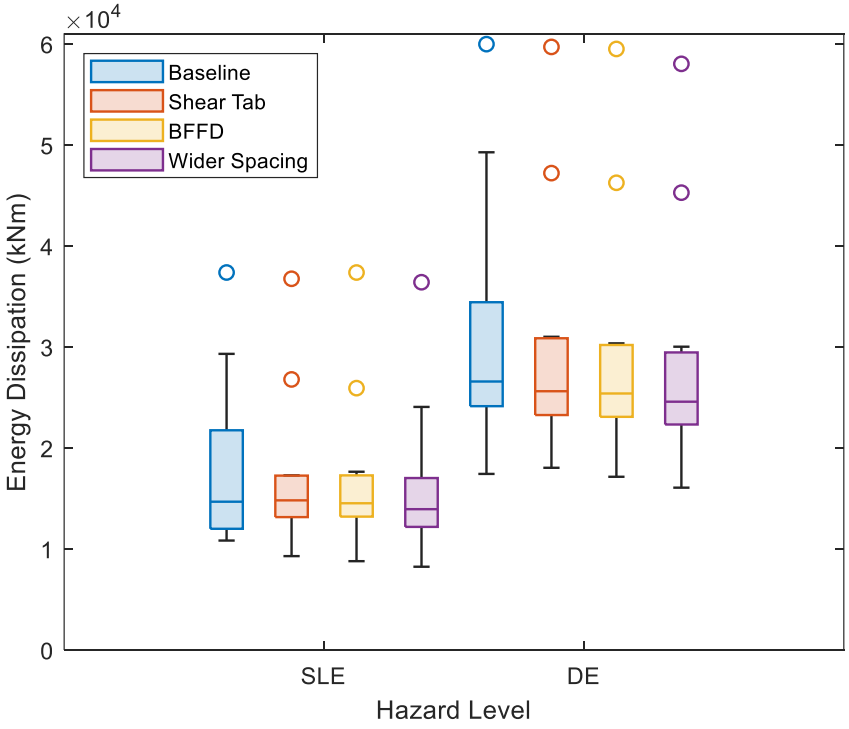

Figure 5-39. Energy Dissipated by BRB in the 16-Story Building in the BRBF Direction

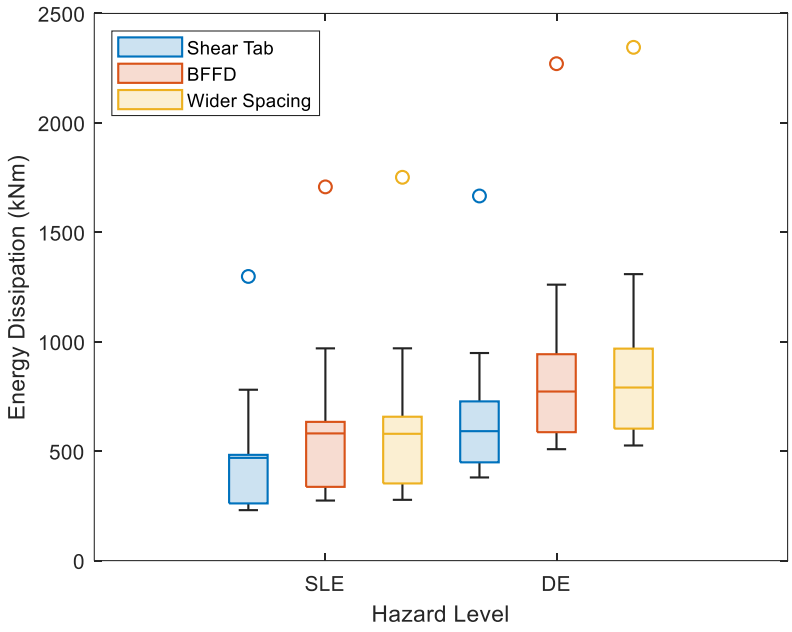

Figure 5-40. Energy Dissipated by Shear Tab Connection in the 4-Story Building in the SMF Direction

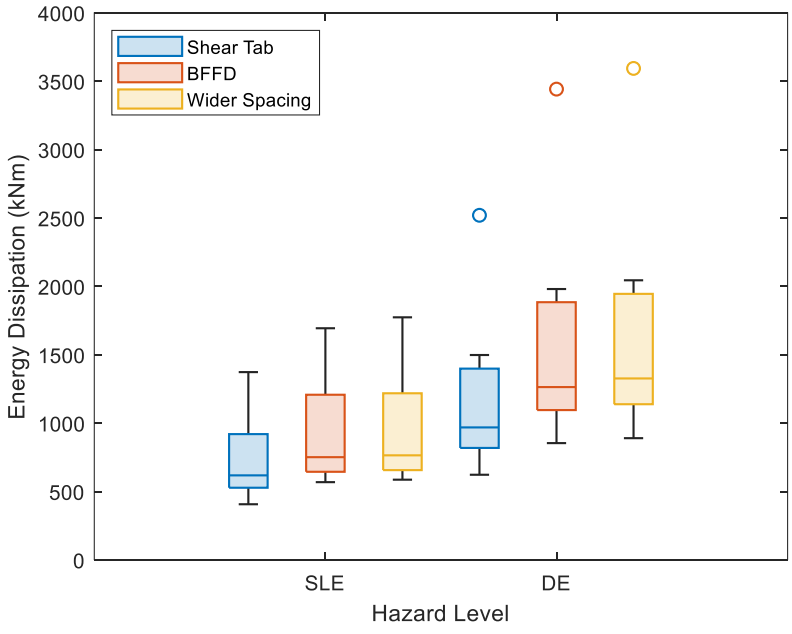

Figure 5-41. Energy Dissipated by Shear Tab Connection in the 8-Story Building in the SMF Direction

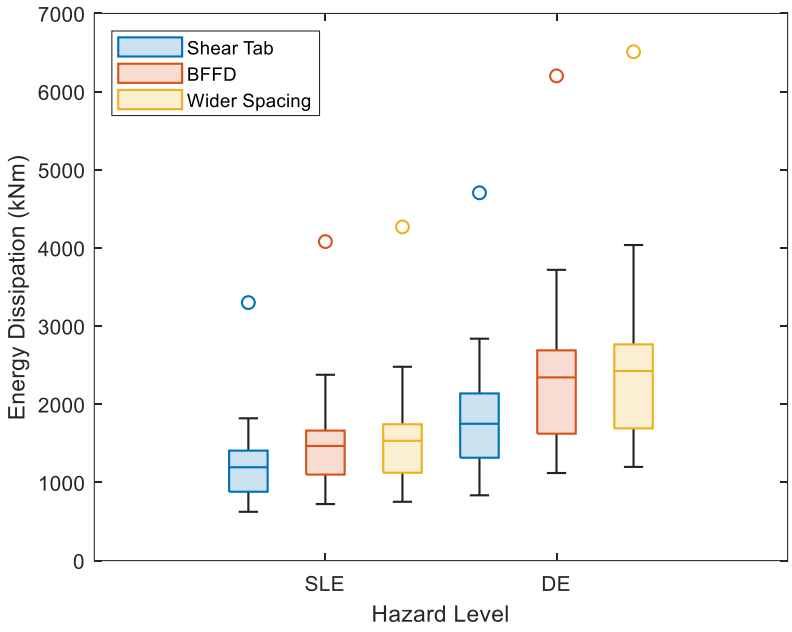

Figure 5-42. Energy Dissipated by Shear Tab Connection in the 16-Story Building in the SMF Direction

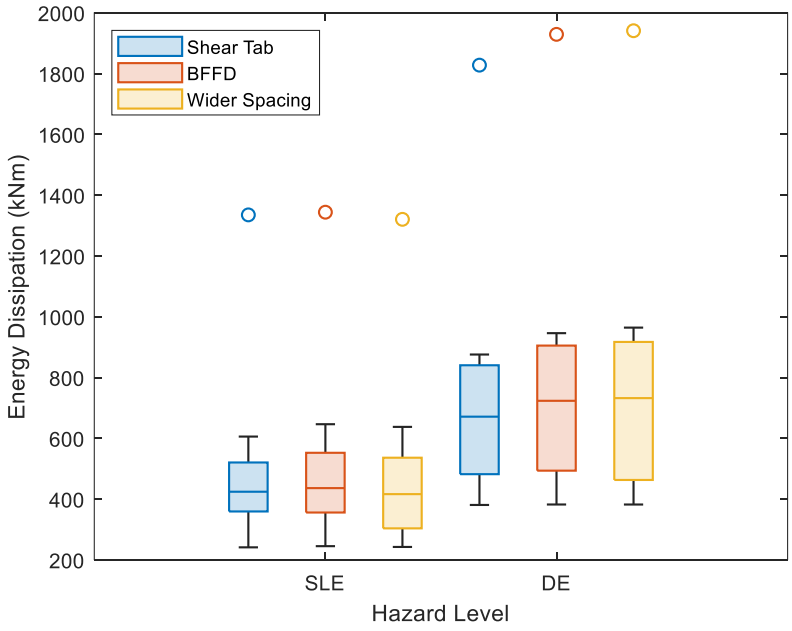

Figure 5-43. Energy Dissipated by Shear Tab Connection in the 4-Story Building in the BRBF Direction

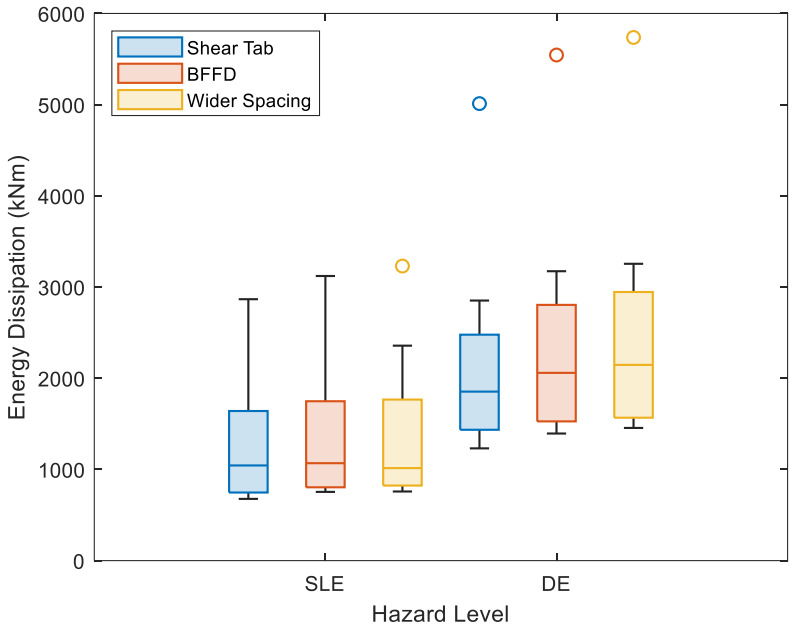

Figure 5-44. Energy Dissipated by Shear Tab Connection in the 8-Story Building in the BRBF Direction

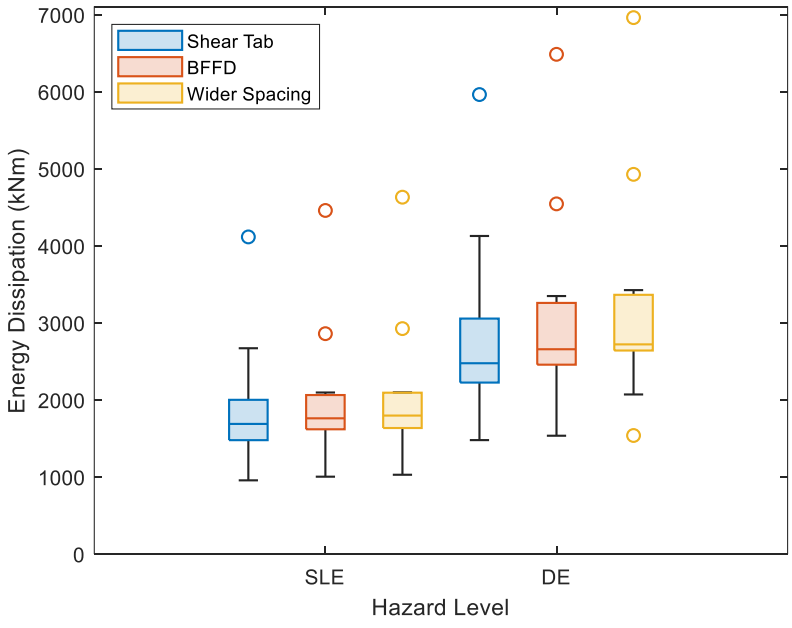

Figure 5-45. Energy Dissipated by Shear Tab Connection in the 16-Story Building in the BRBF Direction

Table 5-27. Energy Dissipated by RBS for the Building in the SMF Direction

	Service Level Earthquake (SLE)				Design Level Earthquake (DE)			
	Baseline	Shear Tab	BFFD	Wider Spacing	Baseline	Shear Tab	BFFD	Wider Spacing
	4-Story Building							
AVG Dissipated Energy (kNm)	862	664	558	522	2093	1819	1663	1613
Energy Ratio (BL)	-	0.77	0.65	0.60	-	0.87	0.79	0.77
Energy Ratio (ST)	-	-	0.84	0.79	-	-	0.91	0.89
	8-Story Building							
AVG Dissipated Energy (kNm)	1506	1246	1067	1011	5011	4426	4124	4021
Energy Ratio (BL)	-	0.83	0.71	0.67	-	0.88	0.82	0.80
Energy Ratio (ST)	-	-	0.86	0.81	-	-	0.93	0.91
	16-Story Building							
AVG Dissipated Energy (kNm)	3368	2764	2521	2413	10151	9231	8611	8447
Energy Ratio (BL)	-	0.82	0.75	0.72	-	0.91	0.85	0.83
Energy Ratio (ST)	-	-	0.91	0.87	-	-	0.93	0.91

Table 5-28. Energy Dissipated by Shear Tab Connection for the Building in the SMF Direction

	Service Level Earthquake (SLE)			Design Level Earthquake (DE)		
	Shear Tab	BFFD	Wider Spacing	Shear Tab	BFFD	Wider Spacing
	4-Story Building					
AVG Dissipated Energy (kNm)	487	619	631	672	892	916
Energy Ratio (ST)	-	1.27	1.30	-	1.33	1.36
	8-Story Building					
AVG Dissipated Energy (kNm)	738	943	968	1164	1557	1617
Energy Ratio (ST)	-	1.28	1.31	-	1.34	1.39
	16-Story Building					
AVG Dissipated Energy (kNm)	1318	1634	1695	1960	2552	2674
Energy Ratio (ST)	-	1.24	1.29	-	1.30	1.36

Table 5-29. Energy Dissipated by BRB for the Building in the BRBF Direction

	Service Level Earthquake (SLE)				Design Level Earthquake (DE)			
	Baseline	Shear Tab	BFFD	Wider Spacing	Baseline	Shear Tab	BFFD	Wider Spacing
	4-Story Building							
AVG Dissipated Energy (kNm)	3708	3585	3457	3255	6006	5819	5702	5456
Energy Ratio (BL)	-	0.97	0.93	0.88	-	0.97	0.95	0.91
Energy Ratio (ST)	-	-	0.96	0.91	-	-	0.98	0.94
	8-Story Building							
AVG Dissipated Energy (kNm)	7084	6283	6085	5736	14471	12929	12561	12082
Energy Ratio (BL)	-	0.89	0.86	0.81	-	0.89	0.87	0.83
Energy Ratio (ST)	-	-	0.97	0.91	-	-	0.97	0.93
	16-Story Building							
AVG Dissipated Energy (kNm)	18257	17430	17284	16453	31507	29991	29560	28635
Energy Ratio (BL)	-	0.95	0.95	0.90	-	0.95	0.94	0.91
Energy Ratio (ST)	-	-	0.99	0.94	-	-	0.99	0.95

Table 5-30. Energy Dissipated by Shear Tab Connection for the Building in the BRBF Direction

	Service Level Earthquake (SLE)			Design Level Earthquake (DE)		
	Shear Tab	BFFD	Wider Spacing	Shear Tab	BFFD	Wider Spacing
	4-Story Building					
AVG Dissipated Energy (kNm)	496	507	489	743	787	792
Energy Ratio (ST)	-	1.02	0.99	-	1.06	1.07
	8-Story Building					
AVG Dissipated Energy (kNm)	1291	1402	1418	2163	2397	2484
Energy Ratio (ST)	-	1.09	1.10	-	1.11	1.15
	16-Story Building					
AVG Dissipated Energy (kNm)	1905	2041	2087	2814	3063	3248
Energy Ratio (ST)	-	1.07	1.10	-	1.09	1.15

5.5 Conclusions

The overall research objective of this effort is to investigate the impact of shear tab connections on seismic response of steel structures, including SMF and BRBF. OpenSeesPy models including the hysteretic response of shear tab connections were developed based on previous work including experimental tests and numerical simulations. This paper extends the previous work from component level to building level by applying the shear tab connections to building models. In order to get a better understanding of the impact of shear tab connections, 4-, 8- and 16-story buildings with different configurations of shear tab connections were designed and modeled in OpenSeesPy. A suite of 11 ground motion records with different scale factors were applied on the building model to investigate the behavior of buildings at SLE and DE. Story drift, total acceleration, base shear and energy dissipation were presented and discussed. The conclusions drawn from this study are listed as follows.

- The impact of shear tab connections is significant on the story drift, especially in upper stories. For SMF, the story drift decreases for each story after including shear tab connections in the model. The BRBF experienced more significant effect than the SMF on story drift. The upper story drifts decreased significantly, especially the top two stories, while the lower story drifts increased, especially the first story.
- The impact of shear tab connections on the total acceleration on each story is negligible. Very small differences were observed between the building models with shear tab connections and the baseline models.
- The impact of shear tab connections on the base shear is different between the SMF and BRBF. There is no influence of the shear tab connections on the base shear in the SMF

direction. However, base shear increases in the BRBF direction after including the shear tab connections in the models.

- Adding the model of shear tab connections significantly decreases the energy dissipated by RBS and BRB in the lateral load resisting system. The modifications to the shear tab connection resulted in additional reduction in the energy dissipated by RBS connections and BRBs. The modifications to the shear tab connections significantly increased the energy dissipated by the shear tab connections compared to the standard shear tab connection.

In conclusion, the seismic analysis of the 4-, 8- and 16-story building with different configurations of shear tab connections showed that the impact of shear tab connection is significant on the seismic response of steel structures. Including shear tab connection hysteresis in the model improves the behavior of building models in the earthquakes. The influence of the shear tab connections is more significant on the low-rise buildings at SLE than the high-rise buildings at DE. The modifications of shear tab connections included adding BFFD and increasing the bolt group length on the shear tab can improve the seismic behavior of buildings with a low cost at SLE and DE. Larger improvement of seismic behavior of buildings at SLE compared with DE was observed in the analysis. Compared with adding BFFD, maximizing the bolt spacing on the shear tab is simpler and more economical to improve the performance of steel buildings in seismic analysis since it doesn't require additional machining work. The BFFD can be more useful if more and bigger bolts are used to generate larger friction force in the device.

References

ABAQUS. (2020). *Abaqus Analysis User's Guide.* Palo Alto, CA: ABAQUS Inc.

AISC. (2010). *Manual of Steel Construction, 14th Edition.* Chicago: American Institute of Steel Construction.

Al-Ghabawi, H. (2021). *Soil-Structure Interaction Effects on the Seismic Response of Steel Structures.* Auburn University.

ATC. (2007). *Interim Testing Protocols for Determining the Seismic Performance Characteristics of Structural and Nonstructural Components.* Redwood City, California: FEMA.

Crocker, J. P., & Chambers, J. J. (2004). Single Plate Shear Connection Response to Rotation Demands Imposed by Frames Undergoing Cyclic Lateral Displacements. *Journal of Structural Engineering*, 934-941.

CSI. (2011). *CSI Analysis Reference Manual for SAP2000®, ETABS®, SAFE® and CSiBridge®.* Berkely, CA: Computers and Structures Inc.

FEMA. (2009). *Evaluation of the FEMA P-695 Methodology for Quantification of Building Seismic Performance Factors.* Gaithersburg: National Institute of Standards and Technology.

Flores, F. X., Charney, F. A., & Lopez-Garcia, D. (2016). The influence of gravity column continuity on the seismic performance of special steel moment frame structures. *Journal of Constructional Steel Research*, 217-230.

Guo, T., Song, L., & Zhang, G. (2011). Numerical simulation of the seismic behavior of self-centering steel beam-column connections with bottom fl ange friction devices. *EARTHQUAKE ENGINEERING AND ENGINEERING VIBRATION*, 229-238.

Gupta, A., & Krawinkler, H. (1998). *Seismic demands for the performance evaluation of steel moment resisting frame structures.* Stanford University.

Gupta, A., & Krawinkler, H. (1999). *Seismic demands for the performance evaluation of steel moment resisting frame structures.* Stanford University.

Harris, J., & Speicher, M. (2015). *Assessment of First Generation Performance-Based Seismic Design Methods for New Steel Buildings Volume 1: Special Moment Frames.* National Institute of Standards and Technology.

Harris, J., & Speicher, M. (2018). Collapse Prevention seismic performance assessment of new buckling-restrained braced frames using ASCE 41. *Engineering Structures, 164*, 274-289.

Ibarra, L. F., & Krawinkler, H. (2005). *Global Collapse of Frame Structures under Seismic Excitations. John A. Blume Earthquake Engineering Center Technical Report 152.* Stanford Digital Repository.

Khoo, H.-H., Clifton, C., Butterworth, J., MacRae, G., Ferguson, G., & . (2012). Influence of Steel Shim Hardness on the Sliding Hinge Joint Performance. *Journal of Construction Steel Research*, 119-129.

Latour, M., Aniello, M. D., Zimbru, M., Rizzano, G., Piluso, V., & Landolfo, R. (2018). Removable friction dampers for low-damage steel beam-to-column joints. *Soil Dynamics and Earthquake Engineering*, 66-81.

Lignos, D. (2008). *Sideway collapes of deteriorating structure systems under seismic excitations.* Stanford University.

Liu, J., & Astaneh-Asl, A. (2000). *Cyclic Tests on Simple Connections, Including Effects of the Slab.* Berkeley, CA: SAC Joint Venture.

Merritt, S., Uang, C., & Benzoni, G. (2003). *Subassemblage testing of Star Seismic buckling-restrained braces.* University of California, San Diego.

Newell, J., Uang, C. M., & Benzoni, G. (2006). *Subassemblage testing of CoreBrace buckling-restrained braces (G Series).* University of California, San Diego.

Popov, E. P., Blondet, M., & Stepanov, L. (1997). *Cyclic Testing of Four Full-Scale Steel Beam-Volumn Connections with "DOGBONES"*. University of California, Berkeley.

Rahman, A., Mahamid, M., Amro, A., & Ghorbanpoor, A. (2007). The analyses of extended shear tab steel connections, part I: the unstiffened connections. *Eng J Am Inst Steel Constr, Vol. 44 (No. 2)*.

Richard, R., Gillett, P., Kriegh, J., & Lewis, B. (1980). The analysis and design of single plate framing connections. *Engineering Journal*, Quarter 2, 38-52.

Rojas, P., Ricles, J. M., & Sause, R. (2005). Seismic Performance of Post-tensioned Steel Moment Resisting Frames With Friction Devices. *Journal of Structural Engineering*, 529-540.

Speicher, M., & Harris, J. (2019). *Assessment of First Generation PerformanceBased Seismic Design Methods for New Steel Buildings, volume 4: Buckling-Restrained Braced Frames.* National Institute of Standards and Technology.

Tsai, K.-C., Chou, C.-C., Lin, C.-L., Chen, P.-C., & Jhang, S.-J. (2008). Seismic self-centering steel beam-to-column moment connections. *EARTHQUAKE ENGINEERING AND STRUCTURAL DYNAMICS*, 627-644.

Upadhyay, A., Pantelides, C. P., & Ibarra, L. (2019). Residual drift mitigation for bridges retrofitted with buckling restrained braces or self centering energy dissipation devices. *Engineering Structures, 199*.

Wen, R., Akbas, B., & Shen, J. (2013). Practical moment–rotation relations of steel shear tab connections. *Journal of Constructional Steel Research*, 296-308.

Wen, R., Akbas, B., Sutchiewcharn, N., & Shen, J. (2013). Inelastic behaviors of steel shear tab connections. *Structural Design of Tall and Special Buildings Volume 23, Issue 12*, 929-946.

Wolski, M., Ricles, J. M., & Sause, R. (2009). Experimental Study of a Self-Centering Beam–Column Connection with Bottom Flange Friction Device. *Journal of Structural Engineering*, 479-488.

Wu, H., & Marshall, J. (2022a). Experimental Evaluation of a Shear Tab Connection with a Bottom Flange Friction Device. *Engineering Journal, (Under Review)*.

Wu, H., & Marshall, J. (2022b). Numerical Evaluation of Energy Dissipation Capacity of Modified Shear Tab Connections. *Journal of Constructional Steel Research, (Under Review)*.

Chapter 6 Conclusions and Future Work

6.1 Summary

The overall research objective of this effort is to investigate and improve the response of steel frames by enhancing energy dissipation in the gravity connections.

The first phase of the research project introduced the concept of the Bottom Flange Friction Device for supplementing energy dissipation in steel structures by including the gravity system connections in energy dissipation without any damage to the structural system. The experimental testing of the shear tab connection with and without the Bottom Flange Friction Device showed that the connection with the BFFD dissipated greater amounts of energy and had a higher strength than the bare shear tab connection. It also showed that the initiation of slip of the BFFD occurred before the shear tab indicating that the BFFD activated at a lower rotation to dissipate energy before the lateral system yields.

The second phase of the research project extended the experimental work by developing a finite element model using ABAQUS to simulate the experimental response of the shear tab connections with different configurations. The ABAQUS model was validated by the experimental results. The numerical results showed that both the connection with the BFFD and the larger bolt spacing had a higher moment strength and stiffness than the bare shear tab connection with standard bolt spacing (76 mm). It also showed that the initiation of slip of the BFFD occurred before the shear tab indicating that the BFFD activated early in the deformation response to dissipate energy. A modified moment-rotation model for shear tab connections with and without a BFFD is proposed based on the results of numerical analysis.

The third phase of the research project investigated the impact of shear tab connections on seismic response of steel structures, including SMF and BRBF. An OpenSeesPy model with shear

tab connections was developed based on the previous work. It extended the previous work from component level to building level by applying the shear tab connections and the associated modifications to the building models. The results showed that the impact of shear tab connections is significant on the seismic response of steel structures. Including the effect of shear tab connections improves the behavior of buildings in earthquakes. The shear tab influence is more significant for low-rise buildings at SLE than the high-rise buildings at DE. The shear tab connection modifications included adding a BFFD and increasing the bolt group length on the further improves the seismic behavior of buildings without adding significant cost. Maximizing the bolt spacing on the shear tab is the simplest and most economical way to improve the performance of steel buildings in earthquakes. The BFFD can be more efficient if more and larger bolts are used to increase the device friction force.

6.2 Important Conlusions

The findings of the work presented in this dissertation are a contribution to advance the understanding of shear tab connections in seimic analysis in both component and building level. The important conclusions drawn from this study are listed as follows.

- Both the connection with the BFFD and the larger bolt spacing dissipated greater amounts of energy and had a higher strength than the standard bare shear tab connection.
- The initiation of slip of the BFFD occurred before the shear tab indicating that the BFFD activated early in the deformation pattern to dissipate energy.
- The impact of shear tab connection is significant on the seismic response of steel structures. Including shear tab connection hysteresis in the model improves the behavior of buildings in the earthquakes.

- The influence of the shear tab connections is more significant on the low-rise buildings at SLE than the high-rise buildings at DE.
- Compared with adding BFFD, maximizing the bolt spacing on the shear tab is simpler and more economical to improve the performance of steel buildings in seismic analysis since it doesn't require additional machining work.

These results are expected to be useful for performance-based design of steel structures and for code developers.

6.3 Future Work

The results indicate a beneficial effect of shear tab connection on the seismic response of buildings, especially in low-rise buildings at SLE. More research is needed to have a further understanding of shear tab connections.

The impact of BFFD can be more significant if larger friction force can be obtained in the device. Future efforts should include an investigation of the effect of larger BFFDs on the seismic response of steel structures.

The slab is an important part in the beam-column connection. Future efforts should include an investigation of the effect of the slab on the behavior of the shear tab connection. The shear tab connection with slab system needs to be investigated in both component and building level. The impact of BFFD can be more significant if larger friction force can be obtained in the device.

In this study, SMF and BRBF are selected to conduct the seismic analysis. It will be valuable to investigate the impact of shear tab connections on the seismic response of steel structures with ordinary moment frame (OMF), ordinary concentrically braced frame (OCBF), special concentrically braced frame (SCBF) and eccentrically braced frame (EBF).